



HAL
open science

Renal Cysts formation: study on the organization and dynamics of 3D biomimetic cellular models for polycystic disease

Brice Lapin

► **To cite this version:**

Brice Lapin. Renal Cysts formation: study on the organization and dynamics of 3D biomimetic cellular models for polycystic disease. Biotechnology. Université Paris sciences et lettres, 2023. English. NNT: 2023UPSL066 . tel-04639358

HAL Id: tel-04639358

<https://theses.hal.science/tel-04639358>

Submitted on 9 Jul 2024

HAL is a multi-disciplinary open access archive for the deposit and dissemination of scientific research documents, whether they are published or not. The documents may come from teaching and research institutions in France or abroad, or from public or private research centers.

L'archive ouverte pluridisciplinaire **HAL**, est destinée au dépôt et à la diffusion de documents scientifiques de niveau recherche, publiés ou non, émanant des établissements d'enseignement et de recherche français ou étrangers, des laboratoires publics ou privés.



THÈSE DE DOCTORAT
DE L'UNIVERSITÉ PSL

Préparée à l'Institut Curie – UMR 168 « Physique des cellules et cancer »

Renal Cysts formation: study on the organization and dynamics of 3D biomimetic cellular models for polycystic disease

Formation de kystes rénaux : étude de l'organisation et de la dynamique de modèles cellulaires de polykystose dans les environnements 3D biomimétiques

Soutenue par

Brice Lapin

Le 9 novembre 2023

Ecole doctorale n° 474

**Frontières de l'Innovation en
Recherche et Éducation
(FIRE)**

Spécialité

**FRONTIERES DU VIVANT-
SCIENCES DU VIVANT
APPLIQUEES, BIOTECHNOLOGIE
ET INGENIERIES DES
BIOSYSTEMES MOLECULAIRES**



Composition du jury :

Sophie, DEMOLOMBE Directrice de Recherche, Université Côte d'Azur	<i>Présidente</i>
Abdul, BARAKAT Directeur de Recherche, Ecole Polytechnique	<i>Rapporteur</i>
Bénédicte, DELAVAL Directrice de Recherche, Université de Montpellier	<i>Rapporteuse</i>
Frank, BIENAIME MCUPH, INEP-Université Paris Cité	<i>Examineur</i>
Jacques, FATTACCIOLI Maître de conférences, ENS-Université PSL	<i>Examineur</i>
Sylvie, COSCOY Chargée de recherche, Institut Curie	<i>Directrice de thèse</i>
Stéphanie, DESCROIX Directrice de recherche, Institut Curie	<i>Codirectrice de thèse</i>

Preamble

Ultrafiltration is a process wherein a membrane filters out particles down to the nanometer from a solution through reverse osmosis. Research on membrane and processes for ultrafiltration is a hot topic for water treatment, either for consumption in processes like desalination or for water depollution, especially in places where fresh water can be a scarce resource. In the case of desalination, minerals need to be added back in a controlled way for the water to be suitable for consumption. The kidney is a fantastic machine responsible for keeping the homeostasis of the blood plasma through a similar process: balancing the ion concentration, the pH, eliminating potentially detrimental small molecules through excretion. This process is the result of tightly regulated flows, pressures, reabsorption and secretions confined in tubular units with tightly regulated geometries. From the blood, the kidney extracts 150L of filtrate per day from which only 1 or 2 L is lost in excretion. The heart pushing the blood through the kidney and the kidney itself consumes 360 Wh every day on average, this gives a rough estimate of 2.4 kWh/m³ of filtrate. On average a desalination plant using ultrafiltration will consume twice as much energy per m³ than this 10 cm organ.

Polycystic kidney diseases are a family of kidney pathologies that profoundly alter the tubular unit geometry through localized balloon-shaped distensions called cysts. Those cysts result in a cascade of processes that dysregulate the geometry and flow within the tubular units of kidney. This can ultimately render the organ ineffective, and renal function would need to be artificially performed by dialysis as no curative treatment is available beyond transplantation. Autosomal Dominant Polycystic Kidney Disease or ADPKD is the most common inherited form of polycystic kidney disease, with a conservative estimate of 1 out of 1000 people carrying a mutation responsible for the disease. In France, it represented almost 6% of the patients with kidney failure in 2016. Among those patients, many will need a kidney transplant. Per the French "Haute Autorité de Santé" it is the solution to terminal kidney failure that presents the most advantages in terms of cost, life expectancy and life quality. However, there is a constant disequilibrium between need for kidneys and availabilities, therefore patients need to go through possibly several years of dialysis before being transplanted. During this time, their overall health can decline. Nevertheless, organ transplant recipients need lifelong treatments to prevent rejection of the organ that comes with possible serious side effects such as high blood pressure, increased risk of infections and cancer. For all these reasons, finding an efficient curative treatment for ADPKD is still an important endeavor for patients and public health in general. Unfortunately, despite an identification of the principal genes behind ADPKD, *PKD1* and *PKD2*, almost 30 years ago, the pathogenesis is still not clear. Although a genetic disease, ADPKD has a slow development followed by a rapid exponential onset of cysts late in life. The widely accepted theory to explain this particular pattern is that cyst formations follow a three-hit mechanism process. First, there is a heterozygous germline mutation on *PKD1* or *PKD2*. Second, somatic mutations lead to total loss of a functioning gene in some cells. These cells with the right microenvironment may then initially form cysts that do not initially impair the organ function. Disruptions in the kidney microenvironment favoring cyst formation are a third hit. They are likely favored by the first cysts that then fuel the additional and terminal formation of cysts leading to kidney failure. What are the processes and mechanisms necessary to initiate cyst formation? What proteins and what unbalanced signaling pathways are involved? Getting better answers to these questions would offer new opportunities to find a treatment.

In our lab, thanks to our technological expertise, we want to address these questions with a kidney-on-chip. Kidney-on-chips are microphysiological systems that are essentially cell cultures mimicking *in vitro* the microenvironment of the kidney tubular units. These systems offer similar modularity and control as classical cultures in dishes while incorporating essential elements for the tubular unit function. In a previous work, our group developed one of the most faithful reported kidney-on-chip in terms of geometry to study the dynamics of tubular dilation in ADPKD. We focused on the gene *PKD1* because it is by far the most involved in cases of ADPKD (85% of cases). **The first object of this thesis was to develop a new kidney-on-chip that would mimic the tubular geometries found in the kidney as faithfully while integrating the physiological hydrodynamic constraints due to the kidney function and the pathological hydrodynamic constraints due to the presence of cysts.**

The second object of this thesis was to expand our previous work on tubular dilation due to the absence of *PKD1* to other segments of the kidney tubules and decipher the mechanism behind these tubular dilations. After successfully integrating hydrodynamic constraints to our system, **our third objective was to assess how flow and pressure could modulate the tubular dilations that we had previously observed without them in relation to *PKD1* and if they could be involved in the third hit.** Finally, **our last objective was to recapitulate the somatic mutation behind the second hit in our tubular system and to study cell competition that could lead to localized tubular distention resulting in cysts.**

In the first chapter of this thesis, I delve into the kidney tubules and their microenvironment, giving a description and discussing how geometries and resulting hydrodynamic constraints in the kidney are essential for the organ function and homeostasis. After I review the literature around the pathogenesis of ADPKD and discuss how loss of *PKD1* and *PKD2* disrupts key features of the kidney tubules and leads to ADPKD. Then I briefly review how researchers have modeled ADPKD so far and which questions could and could not be answered by these models.

In the second chapter, I briefly review the preexisting kidney-on-chip described in the literature. Then I describe and explain the development of the kidney on chip we developed to meet criteria of faithful geometry, as well as controlled and stable perfusion, but also of reproducibility, notably regarding seeding of cells in the system. I will explain how we were able to decouple flow shear stress from intraluminal pressure in our system to study separately the influence of these mechanical cues.

In the third chapter, I present and discuss the results of experiments that we performed on tubular dilation with cell lines derived from murine collecting ducts in static condition depending on their expression of *Pkd1* and present my hypothesis on mechanisms explaining the increased tubular dilation seen with cells without *Pkd1*.

In the fourth chapter, I present and discuss the results of similar experiment in tubules under physiological flow shear stress only and flow shear stress with intraluminal pressure and discuss once more how flow shear stress may protect tubule from dilation and how loss of *Pkd1* leads to increased tubular dilation when adding intratubular pressure.

Finally in the fifth chapter, I present how we modelled somatic mutations in ADPKD by mixing cells expressing and not expressing *Pkd1* in our tubules and discuss resulting cell competitions.

Table of contents

1. Introduction: the kidney microenvironment and the Autosomal Dominant Polycystic Kidney Disease

1.1	The kidney and its microenvironment.....	8
1.1.1	General description of the organ and its functions: <i>Geometries and permeabilities throughout the nephrons are linked to the filtration and reabsorption functions.</i>	9
1.1.2	A description of the physical microenvironment in the nephrons	13
	Geometries, shear stress and pressure	13
	Basement membrane and extracellular matrix.....	16
1.1.3	How does the kidney physical microenvironment regulate kidney cells fate and the nephrons homeostasis?	17
	How does the tubular shape influence epithelial cell behavior? How is curvature important for polarization, migration, proliferation?	17
	The importance of hydrodynamic cues:	18
1.2.1	ADPKD as a health issue	21
1.2.2	Polycystin-1 and Polycystin-2, two proteins involved in mechanosensation essential for the kidney epithelium homeostasis	23
	The role of polycystins in maintaining the kidney epithelium.	23
	Polycystins as mechanosensory proteins	25
1.2.3.	Mosaicism in ADPKD, first triggering event for cyst formation:	29
1.2.3.1.	Somatic mutation as an event leading to cyst formation.....	29
1.2.3.2.	Competition in mosaicism disrupting homeostasis: What we know from ADPKD models and what we can learn from differently fated mosaic epithelium.	29
1.2.3.3.	How does a cyst form?	31
1.2.4.	A third hit is necessary to explain how cyst formation explodes at intermediate stages. 34	
1.2.4.1.	The hypothesis of a snowball effect.....	34
1.2.4.2.	The role of kidney injuries and how they could be part of the snowball effect. ..	35
1.2.4.3.	Evidence of pro-cyst chemical signaling	36
1.2.4.4.	A mechanical origin for the snowball effect: how abnormal mechanical constraints could trigger and accelerate cystogenesis	37
1.3.	Preexisting models of ADPKD or more generally polycystic kidney diseases, advantages and limitations	40
1.3.1.	Mouse models and their limitations: to what extent do they allow to capture what happens in human ADPKD?	40
	Spontaneous murine models	41
	Orthologous deletion murine models	41
1.3.2.	<i>In vitro</i> models	43
1.3.2.1.	Cell cultures in hydrogel	43

1.3.2.2.	Kidney organoids as a promising platform: pros and cons	46
2.	A multitube and perfused kidney-on-chip	
2.1.	Overview of preexisting kidney-on-chip: why they are not enough for our question....	50
2.2.	A previously developed solution in the lab	56
2.2.1	A multitubular chip design and fabrication	56
2.2.2.	Lowering the spacing of the channels in this chip may promote tubule deformation in an ADPKD model.....	57
2.2.3	A compromise between a design achieving faithful geometry and poor fluidic control?	58
The problem of multiplexing		58
The problem of seeding.....		59
2.3.	My solution: the next generation of kidney on chip.....	61
2.3.1.	The concept and principles behind the first design to decouple fluidically parallel channels.	61
2.3.2.	A resistive chip and a new seeding technique for a dense reproducible seeding and multiplexing.....	62
Playing with wires to increase seeding density.		62
Increasing the chip resistivity, solution to allow multiplexing.		63
2.4.	Chip perfusion to decouple flow from pressure.	64
2.4.1	Perfusion using hydrostatic pressure.	64
2.4.2.	How to apply shear stress with limited intraluminal pressure?.....	66
2.4.3.	In practice, two main issues and how to solve them.....	68
How to limit channel clogging to stabilize channel perfusion?.....		68
How to strongly attach collagen to PDMS to prevent leakage?.....		71
2.5	Conclusion.....	74
3.	The importance of <i>Pkd1</i> for the maintenance of the tubular geometry	
3.1.	Introduction.....	75
3.2.	Results	77
3.2.1.	Loss of <i>Pkd1</i> leads to tubular dilation with cells derived from the collecting duct.	77
3.2.2.	This increased dilation is not due to increased proliferation but is rather correlated to cell spreading.....	79
3.2.3.	ECM remodeling appears critical for this tube dilation.	80
3.3	Discussion, perspectives, and conclusion.....	83
3.3.1.	Loss of <i>Pkd1</i> , difference in cell morphology and curvature.....	83
3.3.2.	The importance of the ECM properties.....	84
3.3.3.	A generalized kidney tubular dilation due to loss of <i>Pkd1</i> but cell type dependent mechanisms	85
3.3.4	Conclusion	86

4. The importance of flow shear stress and intraluminal pressure for the tubule homeostasis with or without Pkd1

4.1. Introduction.....	87
4.2. Results	89
4.2.1. Flow shear stress helps to maintain the homeostasis of tubules	89
4.2.2. Addition of intraluminal pressure leads to important tubular dilations favored by loss of <i>Pkd1</i>	91
4.2.3. Dilatation under luminal pressure is very sensitive to extracellular matrix density.	94
4.2.4 Loss of <i>Pkd1</i> in cells from the proximal convoluted tubules may also favor dilation under pressure as flow shear stress only partially thwarted its effects.	95
4.3 Discussion.....	97
4.3.1. On the importance of flow shear stress to maintain the tubule homeostasis.....	97
4.3.2. On the importance of intraluminal pressure to maintain the tubule homeostasis	98
4.3.3 On the different response of tubules to intraluminal pressure due to <i>Pkd1</i>	99
4.4. Conclusion and significance for ADPKD	101

5. Modelling mosaicism in APDKD

5.1. Cell mosaicism and competition	102
5.2. Results	104
5.2.1 Modelling cell mosaicism in the proximal tubule	104
Experiment design and cell validation.....	104
The importance of the substrate: how the geometry and stiffness of the surface can impact the outcome of cell competition.....	105
The predominance of <i>Pkd1</i> ^{-/-} cells is followed by luminal growth and homogeneous channel dilation.	107
A proliferation driven competition	108
The impact of flow shear stress and pressure	109
5.2.2 Modelling cell mosaicism in the collecting duct.....	110
Experiment design and cell validation.....	110
Strong tissue surveillance mechanisms from wild-type cells?	111
The impact of flow shear stress and pressure	112
5.3 Discussion and conclusion	114
On the fundamental differences of behavior of PCTs and mIMCD-3.....	114
On the absence of cyst-like differential tubular dilation.....	116

6. Conclusion and perspectives

6.1. Overall conclusion	118
6.2. Towards mimicking cyst-tubule interactions.....	120
6.3. Extending the model to the stromal compartment	122

Methods

Chip fabrication	124
Construction of a Multitubular Perfusable Kidney-on-Chip for the Study of Renal diseases	124
Chip optimized for syringe perfusion	147
Chip made with PDMS-PEG	147
2D flat collagen surfaces.....	148
Cell culture	148
Cell culture in chips with perfusion.....	148
Immunostaining	149
Image analysis	149
Tubule diameter	149
Nuclei segmentation for internuclear distance and Ki-67 ratio computation.....	149
Segmentation of GFP and mCherry/mScarlet fluorescent cells in the mosaic tubules.....	150
Measure of flow rate in channels.....	150
Glossary	151
References	152
Appendix	163
Résumé en Français	169

1.Introduction: the kidney microenvironment and the Autosomal Dominant Polycystic Kidney Disease

1.1 The kidney and its microenvironment

Animals who possess an excretory organ are called nephrozoan and constitute a vast majority of the animal kingdom. The function of excretory systems is to maintain a chemical balance and homeostasis in body fluids, controlling pH and osmolarity, while excreting unwanted or harmful chemical species. These excretory systems possess a variability reflecting that of the animal kingdom, but overall key structures are conserved in the form of a network of tubular structures. A set of essential transcription factors and structural proteins is conserved throughout all nephrozoan main excretory organs suggesting that they all come from a common ultrafiltration-based, ciliated excretory organ (**figure 1.1**) (Gąsiorowski *et al.*, 2021). Planarian animals such as planarian flatworms possess protonephridia as main excretory organs. In this organ, ciliated flame cells proceed ultrafiltration. They are attached to tubular cells and generate a flow along tubular cells with their cilia. Some chemical species are then reabsorbed or secreted along this flow by the tubular cells. The cells along the flow are specialized to control the pH or the concentration of several species (Issigonis and Newmark, 2015). The main excretory organs of vertebrae are the kidneys. While these bean-shaped

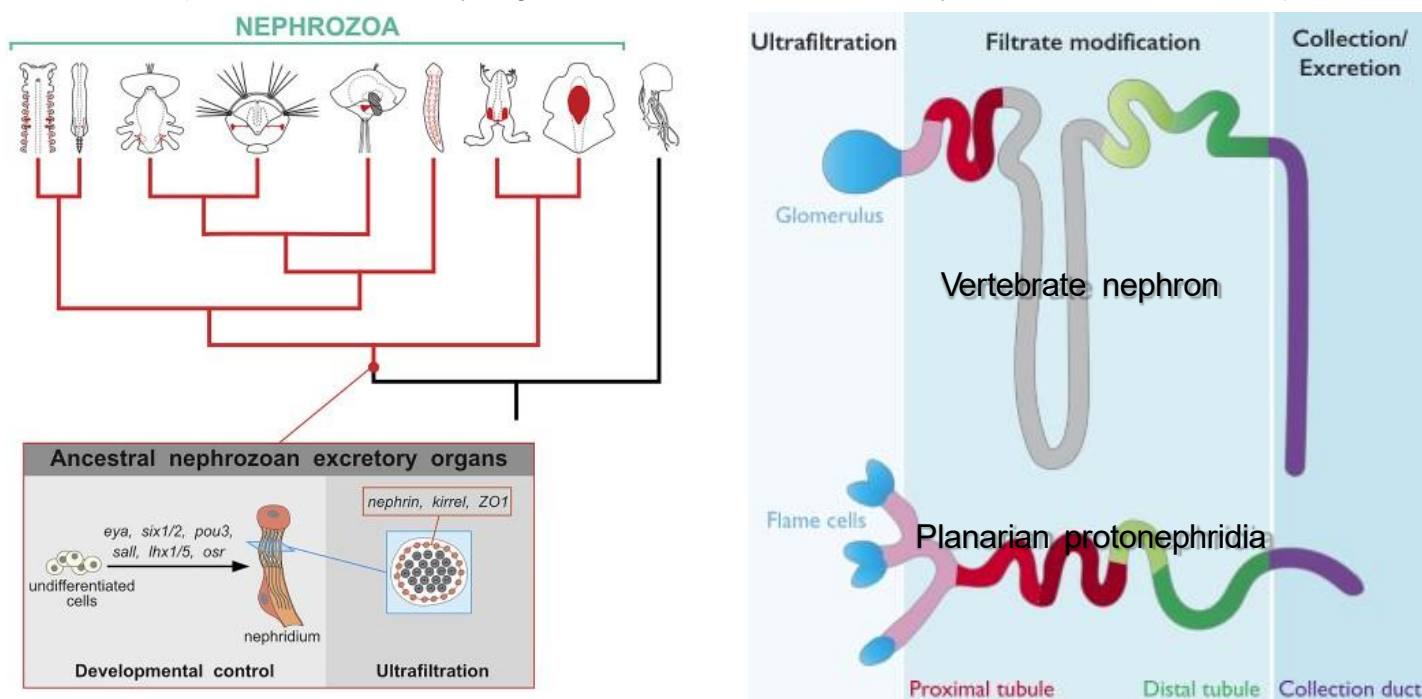


Figure 1.1: The main excretory organ tubular structure is widely conserved in the animal kingdom Nephrozoan main excretory organs originate from a common ancestor (a: from Gąsiorowski *et al.*, 2021). The vertebrate nephron is similar to the planarian protonephridia (b: adapted from Issigonis and Newmark, 2015)

organs are at first glance very different from the planarian protonephridia, they are in fact gathering at the same place where millions of very similar structures have carried very similar functions: the nephrons. In the nephrons, ultrafiltration happens at the glomeruli which are connected to a tubule formed of several specialized segments, also made of ciliated cells, each reabsorbing or secreting different species from a flow of plasma. The first main divergence comes from the generation of the flow. Kidneys are connected to pressurized circulatory system and the tubular flow in the nephrons does not come from the cilia but rather from pressure differences along the tubules.

In this chapter, we will first give a general description of the organ, then describe how ultrafiltration, reabsorption and secretion are carried out in the nephrons to maintain blood homeostasis and how these processes balance a physiological flow. We will specifically address how very well controlled geometries and different permeabilities in the nephron are tightly linked to the organ function. We will next describe the cellular microenvironment in the nephrons highlighting its different mechanical stresses and cues stemming from their geometry and extracellular matrix and the shear stress due to the physiological flow.

1.1.1 General description of the organ and its functions: *Geometries and permeabilities throughout the nephrons are linked to the filtration and reabsorption functions.*

The mammalian kidneys are made of two main regions which form the renal parenchyma; an outer region called the cortex surrounding an inner region called the medulla. Medulla are made of pyramidal structures which at its narrowest part are known as the papilla and which converge in the renal hilum. In the hilum, the renal pyramids give way to structures called minor calices that in turn join into major calyces. Calyces end up in the renal pelvis which is in turn connected to the ureter. Blood vessels irradiate the kidney from the hilum with the renal artery and the renal vein (**Figure 1.2a**).

In the renal parenchyma approximately a million nephrons are compacted parallel to each other. Nephrons are made up of two main parts: the renal corpuscle and the renal tubule (**Figure 1.2b**). The renal corpuscle is exclusively located in the cortex. The renal tubule can be divided into several segments visually characterized by their different diameters. First the proximal tubule is mostly located in the cortex, followed by the loop of Henle that elongates into the renal medulla in the shape of a trombone slide then returns into the cortex with the distal tubule then back again into the medulla where several nephrons join in the collecting ducts. Nephrons are closely intertwined with a network of renal arterioles and venules.

Blood filtration begins in the renal corpuscle. There, blood plasma is separated from the cells and from most proteins by particularly leaky capillaries that enter the corpuscle and convolute inside a structure called the Bowman's capsule. A thick basement membrane separates the Bowman's capsule from the capillaries. Facing the capillaries, in the capsule, squamous epithelial cells called podocytes cover the basement membrane. The Bowman's capsule itself surrounds this capillary bundle and is mostly constituted of a hollow space in which the filtrate enters the tubule. Endothelial cells from the capillaries, podocytes, and basement membrane in between constitute a highly selective membrane that will only allow small molecules to pass from the blood circulation to the Bowman's capsule (**Figure 1.2c**).

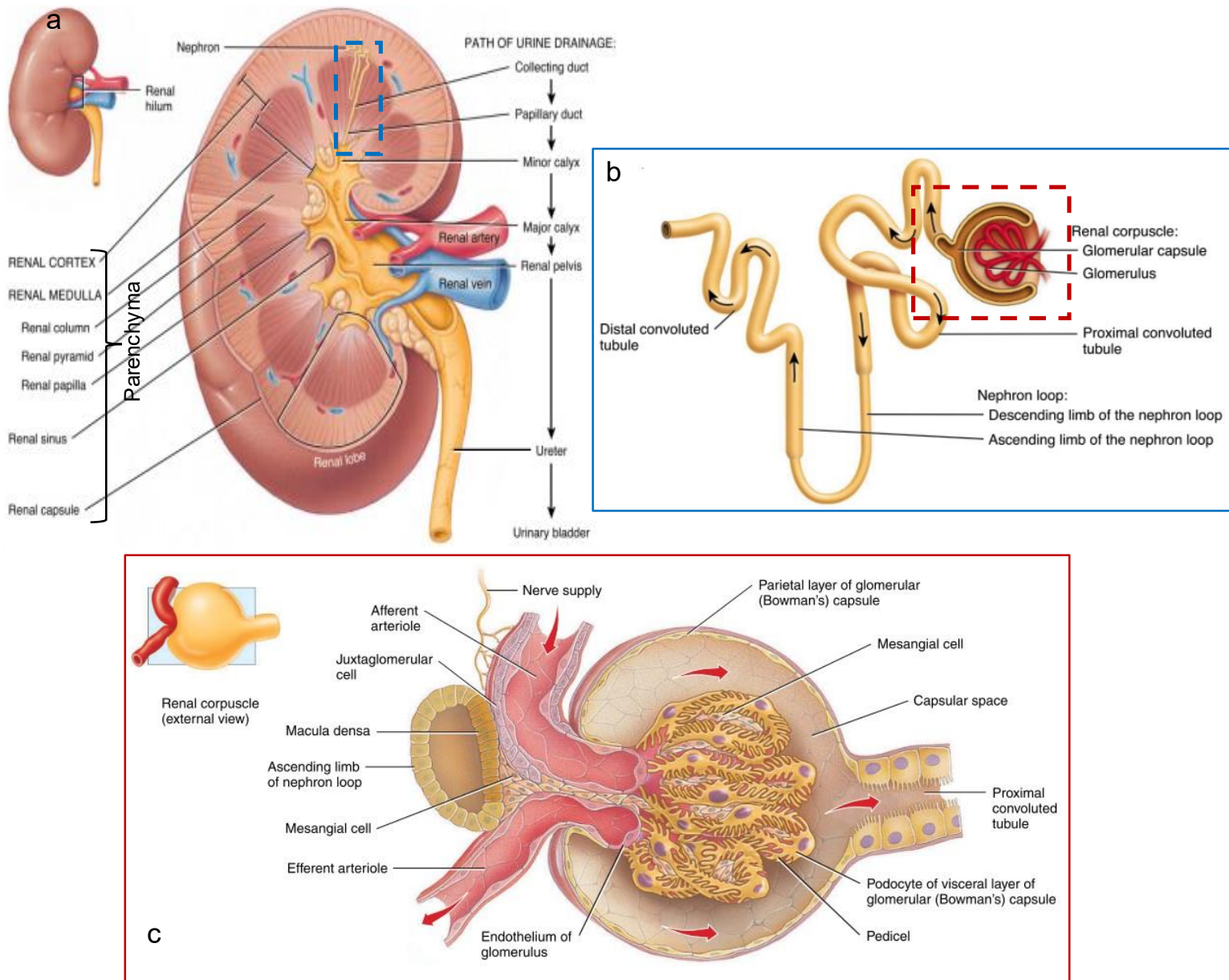


Figure 1.2: A schematic shows the kidney main regions with the path of urine production shown on the right (a) with a zoom on an individual nephron (b) and a zoom on the renal corpuscle (c) *Adapted from Tortora, Derrickson, G. J., and Bryan 2009*

Due to a local tightening of the capillaries inside the capsule, resistance to blood flow increases resulting in a locally high pressure. This positive pressure from the vessels to the capsule will generate a pressure driven flow through the capsule selective membrane, letting through only simple molecules resulting in ultrafiltration. This flow will then be injected into the renal tubules, first through the proximal convoluted tubule (PCT), then the loop of Henle and in the distal convoluted tubule (DCT) before joining other tubules filtrate into the collecting ducts (CD). Along these segment parts of the filtrate will be reabsorbed and additional chemical species will be secreted to constitute the pre-urine. The tubules are lined with epithelial cells, tightly joined with specific permeabilities, lying on a basement membrane. Those cells are mostly cuboidal and have a strong apico-basal polarity with microvilli at the apical side to increase surface exchange and a primary cilium. The thickness of cells and basement membrane, as well as cell types, vary along the segments to fulfill different functions such as exchange,

reabsorption as well as secretion, to surrounding blood vessels through the interstitium. This process is dynamically adapting to varying needs. For this purpose, cells in the DCT are composed of two main cell types, principal cells, and intercalated cells. Principal cells have Antidiuretic Hormone (ADH) and aldosterone receptors to regulate fluid flow rate through increased or decreased reabsorption.

Vessels going into the Bowman's capsule are called afferent arterioles and capillaries inside the capsule join to leave the capsule through the efferent arteriole. The efferent arteriole then goes deep into the kidney parenchyma to form peritubular capillaries that will surround the renal tubules and joined veins in the cortex then to the renal vein. Close proximity between the tubules and the peritubular capillaries allows for the exchange of fluids between them for reabsorption and secretion in the kidney tubules. Furthermore, the ascending part of the loop of Henle also goes between the afferent and efferent arteriole to help regulate blood pressure in the kidney thanks to the juxtaglomerular apparatus (**Figure 1.3**).

Nephrons can filtrate 1.2 L/min of blood into urine, which makes 150 liters of glomerular filtrate per day, also known as the glomerular filtration rate (GFR) of which only 1 or 2 liters will be excreted as urine. Therefore, most of the flow in the nephron is reabsorbed as a transepithelial flow. At the origin of this flow there is an interplay between a high hydrostatic

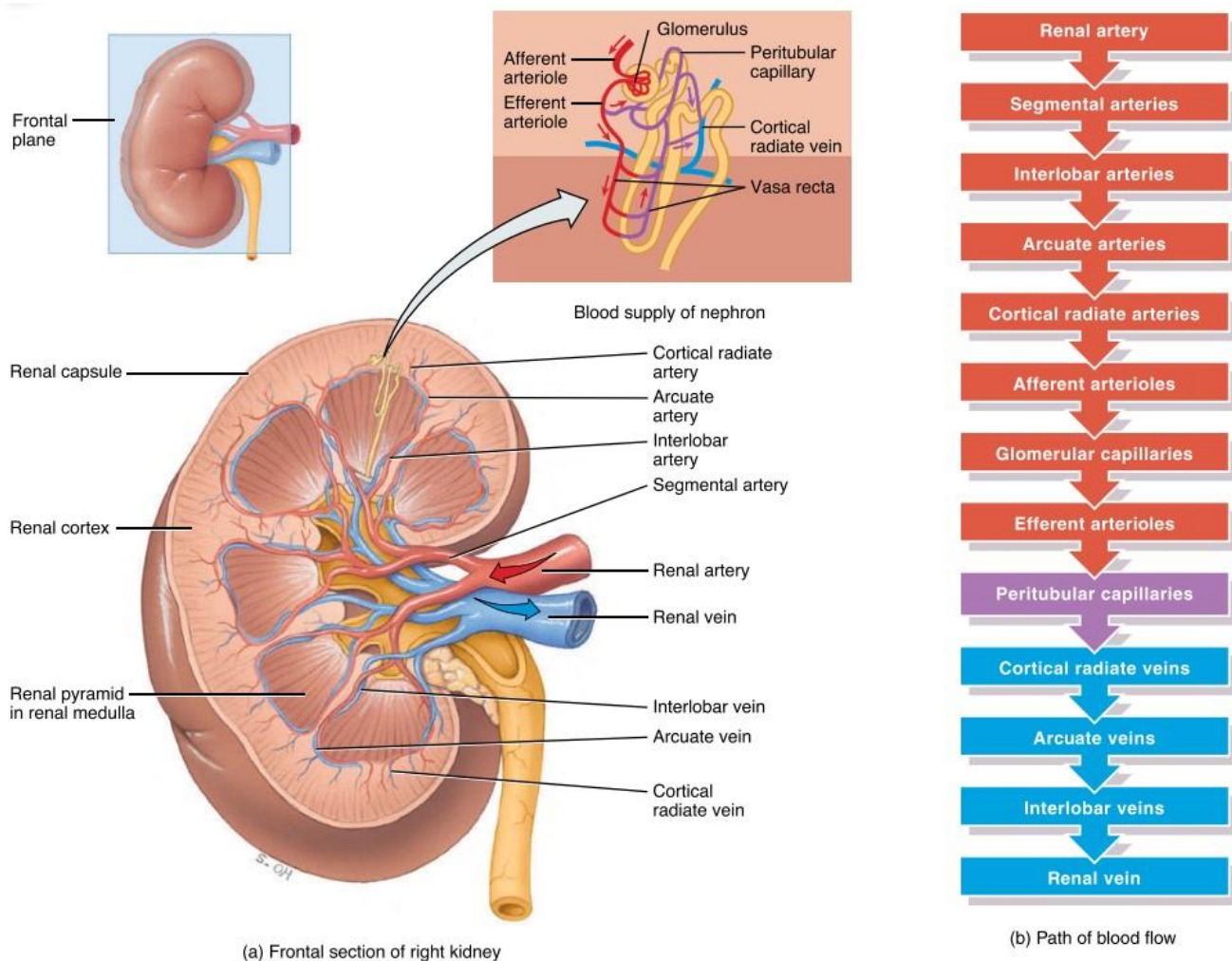
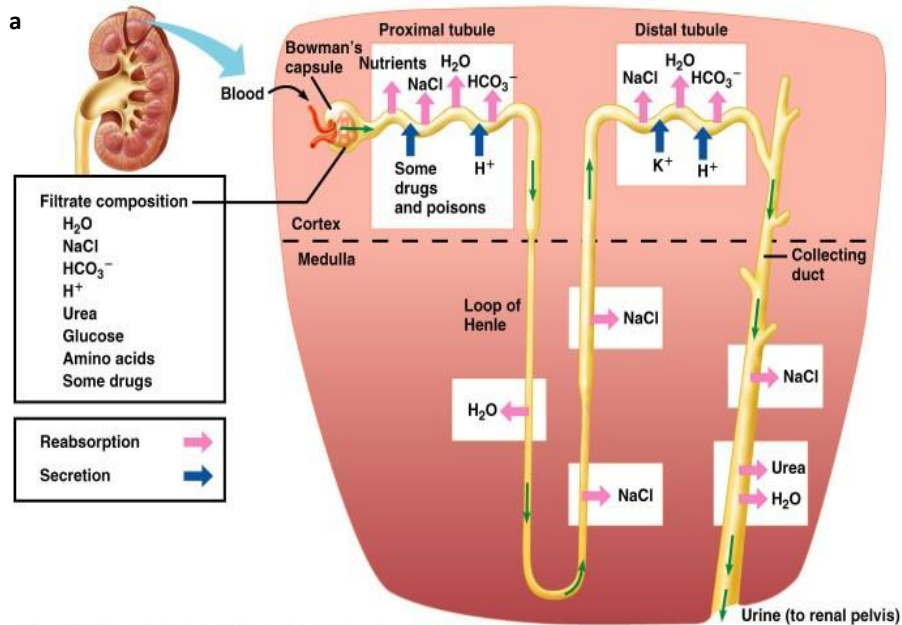


Figure 1.3 Kidney vascularization and exchanges between epithelial compartment and endothelium are integral part of the organ function Arteries are in red and veins in blue *Adapted from Tortora, Derrickson, G. J., and Bryan 2009*

pressure in the Bowman's capsule, around 50 mmHg, and the osmotic pressure resulting from the selective membrane (typically 30 mmHg). Indeed, letting only small molecules through, the membrane creates concentration gradients, concentrating bigger species such as protein on the arteriole side. The equilibrium between the two will drive the flow along the tubules. Hydrostatic pressure in the peritubular capillaries is lower while osmotic pressure is higher when leaving the efferent arteriole, this will contribute to drive transepithelial flow from the renal tubules to the capillaries. GFR thus needs to be tightly regulated as high GFR may not allow some reabsorption processes to happen efficiently and low GFR may induce accumulation of waste in the blood stream. The regulation of GFR goes upstream with constriction of afferent arterioles but also downstream with proper tubular fluid exchanges and tight regulation of tubular geometry and hydraulic resistance. Cells lining the tubules can reabsorb solutes and water through active and passive reabsorption. Passive reabsorption is due to transepithelial differences in osmotic and hydrostatic pressures while active reabsorption is a process wherein energy is used by cells to control opening of cellular pumps. The chemical species reabsorbed will depend mostly on the type of cellular pumps located on the apical and basal side of epithelial cells and on their specific permeabilities (**Figure 1.4a**). Notably all cells express Na/K ATPases on their basolateral sides to actively eject sodium, creating osmotic gradients. They can also secrete protons in the lumen or reabsorb bicarbonate to regulate the pH.

PCT are highly permeable. They notably reabsorb most of the water, glucose, and vitamins while secreting urea and ammonium as cellular activity waste. After the PCT, the osmolarity in the tubule lumen is very similar to the one in the peritubular capillaries. Due to high reabsorption in the PCT, the flow rate is highly reduced. However, in the loop of Henle, lumen diameter also consequently decreases. The main purpose of the loop of Henle is to maintain a high osmolarity into the medulla. To do that, it builds a countercurrent multiplication (**Figure 1.4b**). The loop is divided into a descending limb followed by the ascending limb facing each other. The descending limb is very water permeable while the ascending limb is not. Along the descending limb, filtrate osmolarity increases due to high levels of water reabsorption, while along the ascending limb osmolarity decreases due to ion reabsorption and water impermeability. As there is a high level of water reabsorption in the descending limb, even more solute can be reabsorbed in the ascending loop and vice-versa. This maintains an osmolarity gradient that goes from an isotonic osmolarity of 300 mOsm in the interstitium at the level of the cortex to a hypertonic osmolarity of 1200 mOsm deep in the medulla interstitium. The longer the loop of Henle, the higher the gradient. In fact, we can distinguish two types of nephrons according to their loop of Henle. Cortical nephrons (85% of nephrons) that have most of their tubule length in the cortex and juxtamedullary nephrons (15% of nephrons) that begins right at border between cortex and medulla have a longer loop of Henle that goes deeper into the medulla and whose role is to maintain this gradient more efficiently. Following the loop of Henle, in the DCT, solutes, notably urea, and water reabsorption as well as solute secretion, are modulated hormonally and with nerve impulse to follow the body needs. Furthermore, proximity of the DCT to the afferent arterioles allows feedback that will or will not favor arteriole dilation and consequently GFR. Similarly, while medulla high osmolarity leads to osmotic pressure that favors water reabsorption in the collecting ducts, hormonal and neural signals modulate the duct permeability to concentrate or not pre-urine according to levels of hydration.



Copyright © 2005 Pearson Education, Inc. Publishing as Pearson Benjamin Cummings. All rights reserved.

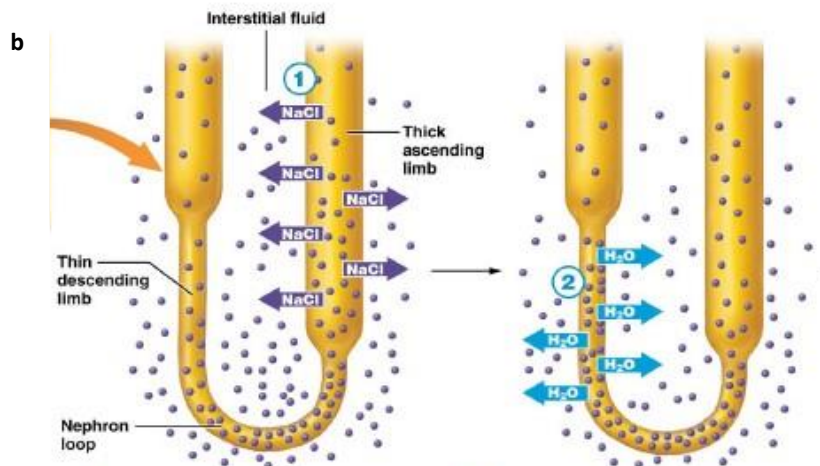


Figure 1.4: Reabsorption and secretion in the kidney Different segments of the kidney ensure different secretion, reabsorption role (a). One of these section, the loop of Henle thanks to its geometry, with counter current multiplication, ensure the remarkable ability to concentrate urine (b) *Adapted from Tortora, Derrickson, G. J., and Bryan 2009*

1.1.2 A description of the physical microenvironment in the nephrons

Geometries, shear stress and pressure

The geometry of the nephrons needs to be tightly controlled for them to correctly operate (**Figure 1.5 a-b**). When a fluid flows in a conduit like a renal tubule, flow rate is proportional to pressure gradients with a proportional coefficient given by a hydraulic resistance, wherein:

$$\Delta P = R_h Q \quad (1.1)$$

where ΔP is the pressure gradient, R_h the hydraulic resistance and Q the volumetric flow rate.

Given the average GFR of approximately 1L/min, not accounting for reabsorption, this gives a flow rate going through each nephron in the order of $\mu\text{L}/\text{min}$ at the maximum. Hence the Reynold's number of tubular flow is quite low, consequently, flows there can be considered laminar. As such they are largely dependent on the geometry of the nephron. Hydraulic resistance is then completely dependent on the tubular geometry and the filtrate viscosity following the relationship:

$$R_h = \frac{8\mu L}{\pi r^4} \quad (1.2)$$

Since flows in the kidney are mostly pressure driven, in a steady state they follow the Hagen-Poiseuille laminar equation. Thus, knowing the geometries in the kidney allows us to calculate with precision the different pressure drops along the segments:

$$\Delta P = \frac{8\mu L Q}{\pi r^4} \quad (1.3)$$

where ΔP is the pressure drop, μ is the viscosity, L is the length, Q is the volumetric flow rate per tubule, and r is the radius.

An additional difficulty comes from the fact that kidney tubules should be considered porous. As they reabsorb and secrete water, there is a net transepithelial flow. In fact, most of the flow is transepithelial because between 95 and 99% of the ultrafiltrate gets reabsorbed. To assess the actual flow rate in the tubule, it is necessary to perform directly in live micropuncture experiments. Then, by injecting a polysaccharide, inulin that is not absorbed or secreted by the tubule into the blood plasma, it is possible to evaluate with the tubular fluid/plasma (TF/P) inulin concentration ratio the percentage of fluid reabsorbed. Of course, these experiments can only be made on animal models, here we will focus on the rat. Globally, reabsorption appears to be a linear process along a tubule segment (Giebisch and Windhager, 1964). Considering tubules as rigid, calculation of pressure drops with Poiseuille equation predicts that highest pressure drops happen in the thin descending limb of the loop and in the inner medullary collecting duct (Gilmer *et al.*, 2018)(**Figure 1.5c**). These results are consistent with the fact that tubular diameter diminishes strongly at the loop of Henle and several tubules merge into one collecting duct of the same diameter (**Figure 1.5 a-b**). Interestingly, the loop of Henle that has a varying length should also vary in term of hydraulic resistance between cortical and juxtamedullary nephrons. Given the fact that the loop is one of the places of highest resistivity in the kidney, this could drastically change pressures from one type of nephron to the other. An adaptation to this would be a substantially higher diameter for long descending loops (Kriz, 1981) .

Another factor to consider is the elasticity of the tubule. Elastic tubules can be distended by intraluminal pressure. Compliance is the measure of how much a tubule diameter will increase under pressure, in that regard it can be seen as similar to the inverse of a Young modulus:

$$\frac{\Delta R}{\Delta P} = C \quad (1.4)$$

where C is the compliance, ΔR a variation in tubule radius and ΔP a variation in net pressure.

In case of diuresis state, hormonal signaling and tubuloglomerular feedback (TGF)

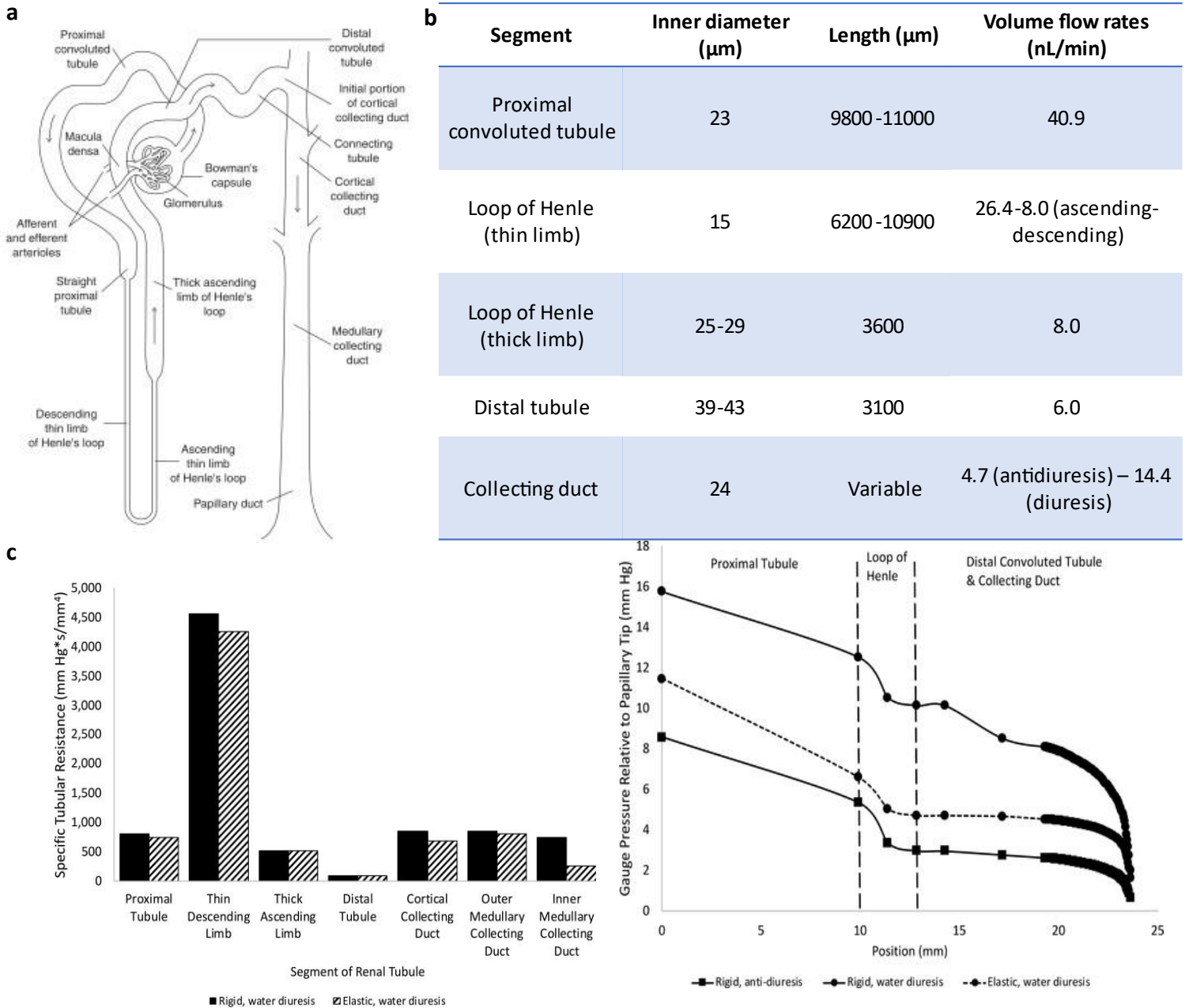


Figure 1.5: Geometries and hydraulic stresses in the nephron The different geometries of the nephron segment (a-b) lead to specific hydraulic stresses throughout the organ (b-c) due to different hydraulic resistances (c-left) unequally splitting pressure drops (c-right), Data is from rat *Source: Gilmer et al, 2018*

increase the volume filtrated in the glomerulus, leading to important increased pressures. Accounting for the tubular elasticity limits this increase in intraluminal pressures. Interestingly , a smaller diameter combined with higher compliance of the loop of Henle (**Figure 1.6b**) can be seen as a low pass filter regarding perturbation in GFR, wherein the nephron absorbs perturbation flow and pressure at high frequency largely thanks to this structure (Sakai *et al.*, 1986).

Here we mostly discuss values measured in the rat, but we can expect that overall mammalian kidneys largely follow the same patterns. The kidney epithelium function leads to constant hydrodynamic constraints. Reabsorption and secretion processes in the kidney lead to positive pressure on the apical side of the cells. On top of regulation of reabsorption and

secretion processes, we saw that good control of geometry is not only essential for the kidney function but also to maintain the equilibrium between the hydrodynamic forces and the forces maintaining the epithelium integrity that we will discuss next.

Basement membrane and extracellular matrix

We saw how the elastic properties of the tubules could be important to moderate changes of pressure due to different diuretic needs. An essential part of the kidney that we have not described so far is the extracellular matrix. Decellularizing a kidney conserves the global shape of the organ but more interestingly the microscopic tubular structures (**figure 1.6a**). Furthermore, analysis of individual tubules mechanical properties shows that their elastic properties are essentially those of their surrounding basement membrane. Indeed, in their measurement of the kidney viscoelastic properties, Grantham *et al.* showed that digesting a tubule basement membrane increased the tubules compliance greatly, almost tripling it (Grantham *et al.*, 1987). Similarly, measures of elastic moduli of decellularized kidney tubules under low strain are mostly the same as with cells (Bhave, Colon and Ferrell, 2017). We then expect the basement membrane membrane elastic properties to be main factor giving to the tubules their compliance, summarized in **figure 1.6b**.

Interestingly there is a high discrepancy between elastography measurements of kidney elastic moduli and the measurements on isolated kidney tubules, from ~10 kPa to ~1MPa (Bhave, Colon and Ferrell, 2017; Islamoglu, Gulcicek and Seyahi, 2022). As elastography measurements target the whole organ, this result can be interpreted as the sum

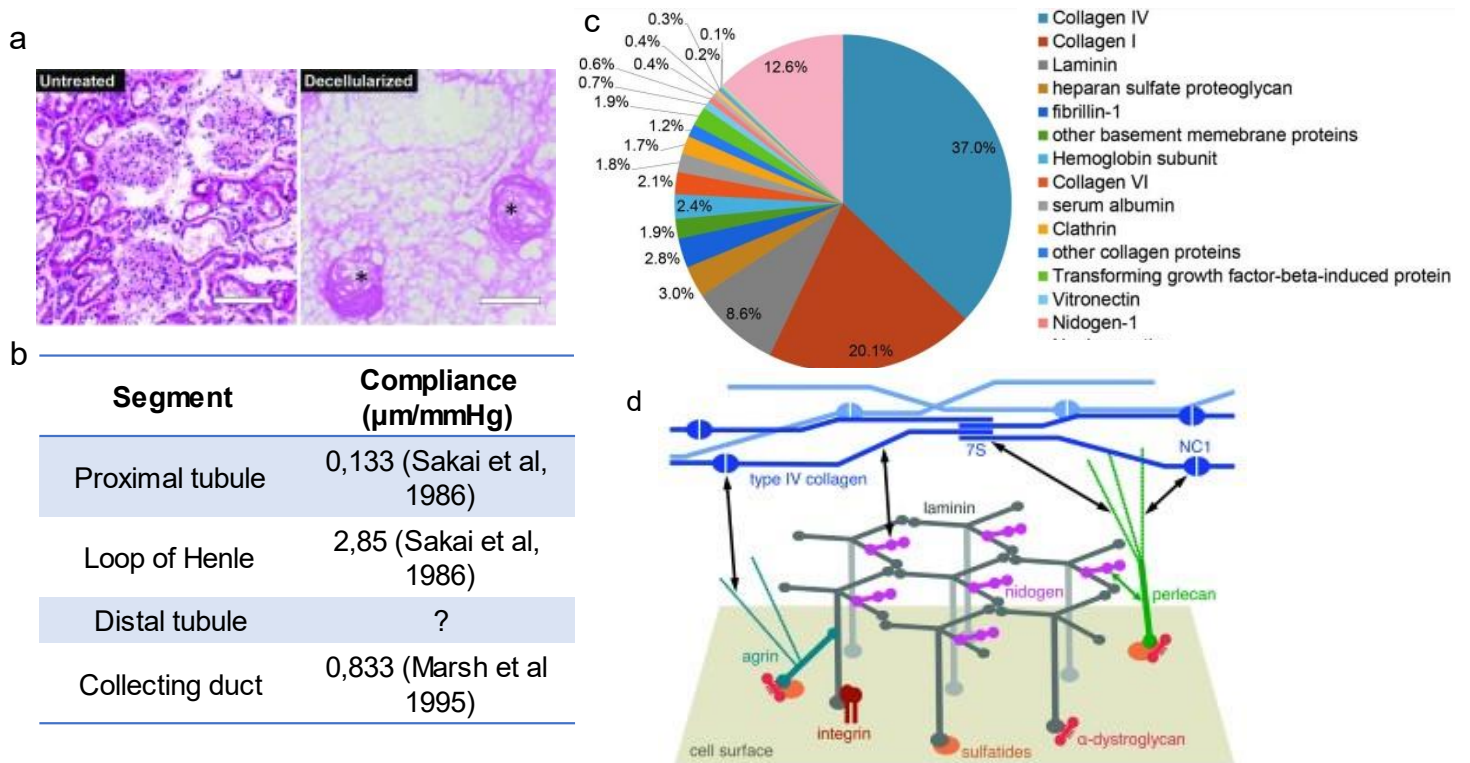


Figure 1.6: The nephron basement membrane. The basement membrane in a decellularized kidney resembles the whole organ (a, adapted from Nagao *et al.*, 2016) and is at the origin of the remarkable elastic properties of the tubules (b). Its composition (c, adapted from Nagao *et al.*, 2016) and organization provide its mechanical properties. Collagen IV assemblies, linked to laminin assemblies thanks to perlecan, nidogens and other proteins (d)

of stromal rheology with the cells and fluids. This is another indication that tubule basement membranes have a particularly important role in the maintenance of the tubule mechanical properties by providing a substrate several orders of magnitude stiffer than the cells themselves. Of note the basement membrane has a nonlinear strain-stress response, with a modulus of 0.5 MPa at low strain and up to 3 MPa at high strain (Bhave, Colon and Ferrell, 2017). This strain-stress stiffening response is typical of this type of fibrillar viscoelastic biomaterials.

The basement membrane mechanical properties are the result of a complex assembly of diverse proteins (**Figure 1.6c-d**). Collagen IV, the principal collagen and principal component in general, forms an assembly of polygonal lattices that are the backbone of the basement membrane (Mak and Mei, 2017). Without it, the integrity and the mechanical properties of the membrane can be seriously compromised (Pöschl *et al.*, 2004). Laminins are the third most abundant proteins in the basement membrane and self-assemble into polygonal lattices as well on top of the collagen IV lattice. They serve as adhesion proteins in the membrane to which integrins can preferentially bind. Both lattices are joined and stabilized by nidogen and perlecan belonging to heparan sulfate proteoglycans as intermediary proteins. The composition of the kidney basement membrane is given in the **Figure 1.6c** (Nagao *et al.*, 2016)

This composition can be dynamic and can evolve due to aging, injuries, or disease. But interestingly, aside from the short-term adaptation provided by its elasticity, basement membrane could also offer long term adaptations solutions to new stresses by change of its composition. Indeed, because they represent the main stiffness component of the tubules, basement membranes can in the end dictate the luminal diameters in an interplay with intraluminal pressures. Notably, theoretical models show that tubular tissues adopt the geometrical configurations which minimize their deformation energy involving their elasticity, the elasticity of their substrate, and the tensions within tissues (Hannezo, Prost and Joanny, 2012). By secreting or degrading their extracellular matrix, it is easy to imagine how cells from the tubules could reshape the kidney tubules, displacing this equilibrium. Surprisingly this has not been the object of extended research so far.

1.1.3 How does the kidney physical microenvironment regulate kidney cells fate and the nephrons homeostasis?

As we saw, the kidney environment can be very dynamic. Cells have many ways to actively modulate the kidney hydrodynamics by remodeling the ECM for instance, through processes such as the TGF or by tuning their shape, mechanical properties or polarities. During development cells follow a precise differentiation program, patterning and spatial reorganization that leads to a functional organ. To do that they heavily rely on complex morphogen signaling. In the adult organ, on the other hand, cells can rely on other cues to self-organize and differentiate. Geometric and hydrodynamic cues are essential because they are at the center of the organ function. In what follows we will briefly address how geometry and hydrodynamic constraints can guide cell behavior.

[How does the tubular shape influence epithelial cell behavior? How is curvature important for polarization, migration, proliferation?](#)

A kidney epithelial cell has on average a diameter between 10 and 20 μm . The typical outer diameter of a tubule is close to 50 μm . Such curvature for a kidney cell means that it must bend, leading to additional physiological stress. Furthermore, the difference of diameter between the lumen and the basal lamina creates an additional apico-basal asymmetry with a more important curvature at the apical side of cells than at the basal side. Bending the cell membrane leads to specific cytoskeletal tensions. These tensions are at the center of mechanotransduction processes. Notably through release of small GTPases, such bending can modulate the cell-cycle, actin dynamics and thus can have crucial effects on proliferation or differentiation. In that sense, the transcription factors YAP/TAZ provides another way to transduce curvature. In general curvature modulates nuclear translocation of YAP with convex surfaces promoting nuclear YAP translocation better than concave surfaces such as kidney tubules (Luciano *et al.*, 2021). Membrane curvature through membrane stretch may also induce opening of a category of ion channels called stress-activated channels (SAC), giving other pathways for mechanotransduction (Patel, Lazdunski and Honoré, 2001).

Curvature effects also translate to the tissue level. In a confluent monolayer, concave surfaces can favor high local cell densities and high tissue thickness due to an interplay between apical and baso-lateral tension (Luciano *et al.*, 2021). These changes modulate YAP nuclear translocation. Apical contractility coupled with cell-cell adhesion allows transmission of tension sensed by one cell to distant cells in the epithelium. Resulting constant tension is challenged by basal adhesion. Overall, these constraints can upregulate YAP nuclear translocation (Broaders, Cerchiari and Gartner, 2015). Curvature will also have a significant effect on collective processes such as cell migration (Venzac *et al.*, 2018). For instance, higher curvature will lower cell migration speed. In this configuration, migrations appear to be dependent on strong cell-cell adhesion (Xi *et al.*, 2017) On the other hand, curvature seems to decrease the cell density that led to jamming and disfavors forward polarization needed for guided migration. Possibly these effects may also be the result of spatial confinement induced by a closed concave tubule.

Overall, substrate long range topology, notably concave curvature long-range sensing, offers cells an important long-range cue to modulate their behavior. On another side, confinement resulting from tubular geometry can also favor exchanges between cells on the apical side.

The importance of hydrodynamic cues:

How do they influence cell differentiation?

We already saw extensively how the kidney cells could be exposed to intraluminal hydraulic pressures and shear stresses. These pressures represent another important stress for the cells and as such can be not only seen as a source of additional tension but also as another cue for the cells to orient their behavior. Indeed, it has been proposed that a mechanism through which kidney cells could sense a tubule defect would be by pressure and flow shear stress sensing (Weimbs, 2007).

The first effect of intraluminal pressure is to effectively exert a tension that wants to distort the epithelium. This tension translated to the cell membrane at equilibrium can be approached using Laplace law:

$$\Delta P = \frac{\Lambda}{R}$$

where ΔP is the pressure difference between the inside of the tubule, Δ the tension along the membrane and R the local radius.

Such tension at the cell membrane can be sensed through a plethora of mechanosensitive pathways. It can then be propagated through the cytoskeleton. Notably it can promote the formation of stress fibers, complex assemblies of F-actin and myosin. One of the processes by which cytoskeleton gets stabilized under tension is through the RhoA/ROCK pathway resulting in contractile forces. This pathway is associated with the Hippo pathway that is essential for the regulation of YAP/TAZ phosphorylation and results in YAP translocation of the nuclei. Cell membrane tension can also promote the opening of many stretch-activated ion channels (SACs) and similarly contribute to unfolding of proteins located at the membrane.

The other important hydrodynamic stress is the flow shear stress (FSS). Flow shear stress has been shown to be notably essential for the proper differentiation of certain cells such as endothelial cells (Thi *et al.*, 2004; Zhou, Li and Chien, 2014). FSS can also lead to important modifications in kidney epithelial cells. Interestingly the comparison stops here: Duan *et al* showed in fact that reorganization of cytoskeleton in kidney epithelial cells due to FSS were in fact opposite to that in endothelial cells (Duan *et al.*, 2008). Indeed, FSS favored *adherens* junction and tight junction in mouse proximal tubule cells. In their model, FSS disrupts stress fibers at the basal side of the cells by creating a strong torque between the basal membrane and the apical side of the cells. Those stress fibers reorganize in peripheral actin bands. Those actin bands, helped by the tilting of the cells, facilitate E-cadherin bonding to form *adherens* junction that in turn facilitate tight junction formations. In their model, the origin of this torque is the FSS on the apical membrane of the cells and the drag due to the

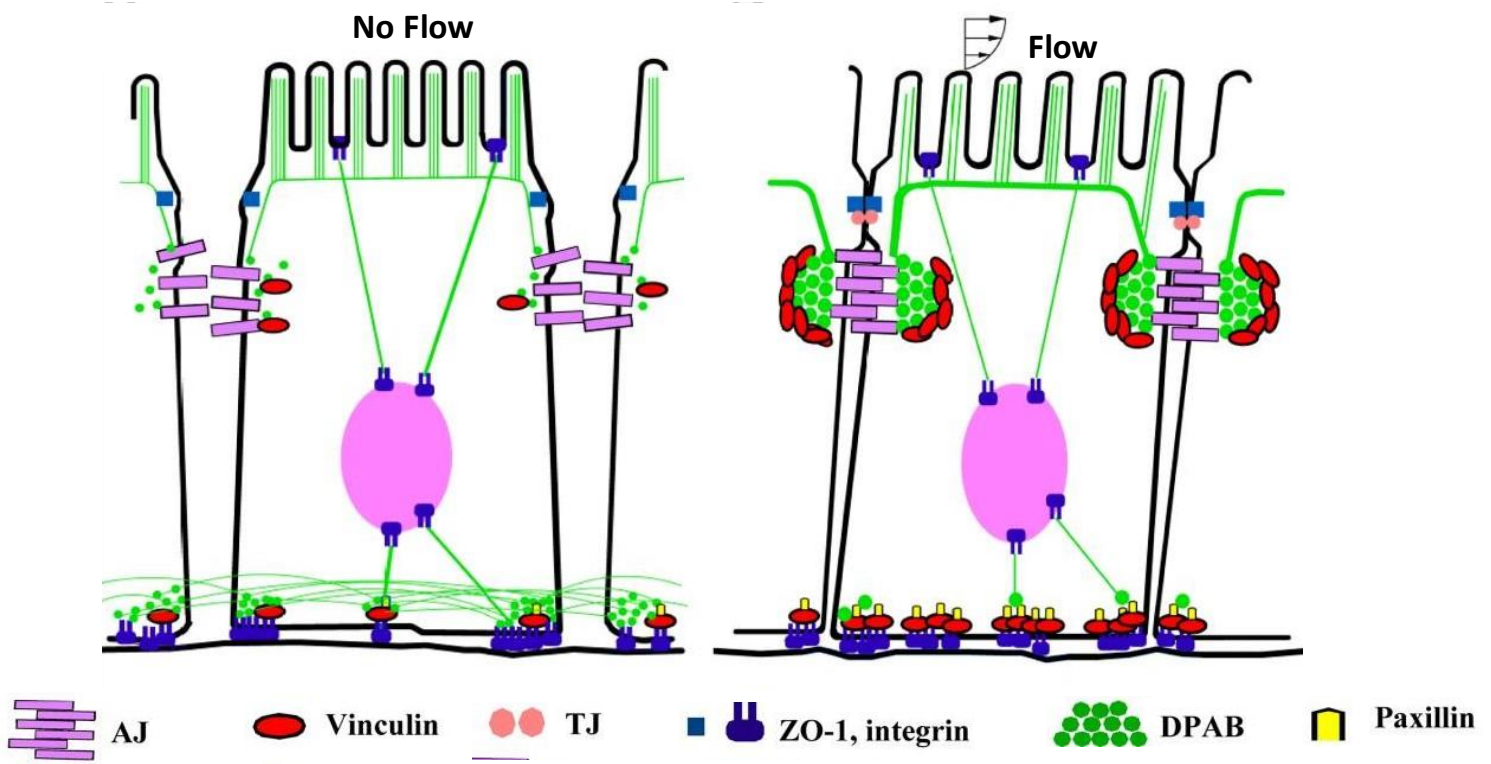


Figure 1.7: A model for FSS mechanosensing in kidney epithelial cells. In Duan *et al* model for FSS mechanosensing, under FSS a torque is created due to the tension at the base, the FSS and the drag on the microvilli. Stress fibers disappear from cell base and peripheral actin bands (DPAB), tight junctions (TJ) and *adherens* junction (AJ) are formed.

microvilli augmented by the important height of kidney epithelial cells (**Figure 1.7**). Alternatively flow stresses have been canonically associated with increased calcium cellular intake in kidney cells (Liu *et al.*, 2003). Increase of cytosol calcium concentration is in itself a signal that can have important effects on many cellular mechanisms such as proliferation, autophagy or apoptosis. The exact origin of this FSS induced calcium intake remains unclear.

There can be possibly two other candidates for FSS mechanosensory, glycocalyx and primary cilium. We will focus on the latter, as perturbation of this organite leads to a category of kidney diseases called ciliopathies that are responsible for grave disorder in the tubule homeostasis.

The primary cilium as a mechanotransduction organite

Primary cilia are flagellar structures protruding from the apical side of epithelial cell. They are essential for kidney homeostasis and cilia defects lead to serious diseases such as nephronophthisis called ciliopathies. Contrary to many flagellar cellular structures they lack active motility. Physiological FSS is enough to bend this structure. As such, attention has been set on them as potential mechanosensory organites, especially in the kidney where their absence can completely alter the organ. If their membrane is continuous with the rest of the cell membrane, they have a specific protein composition. Cilia has been largely associated with regulating intracellular Ca^{2+} through FSS mechanosensation. But recent results have put serious doubts on this mode of involvement of the primary cilium in a Ca^{2+} signaling axis (Delling *et al.*, 2016). Notably it is unclear whether increased calcium detected of FSS originates from the cilium or the cytoplasm. Many channels of the Transient receptor potential channels (TRP channels) family have been identified as ciliary proteins. These channels are non-selective cation channels which opening probabilities evolve according to stimuli. Furthermore, primary cilia are also particularly enriched in G-protein-coupled receptors. However, the function of these proteins in the cilia is still poorly identified. In addition, the mTOR pathway has also been shown to be regulated by flow shear stress in the cilium through the protein Lkb1, moderating cell size in the presence of a flow (Boehlke *et al.*, 2010). We must finally mention two important proteins that preferentially locate in the primary cilium and appear essential for its mechanosensation functions, the polycystins. The tightly linked role of polycystins and primary cilia as mechanosensors have led scientists to qualify polycystic diseases due to the absence of polycystins as ciliopathies. These two proteins are the focus of the next part of this chapter.

We have described and discussed extensively the kidney function, and how it is linked to its microenvironment, geometries and hydrodynamic constraints. We saw that to maintain a functional organ they need to be tightly regulated: the ultrafiltration and following reabsorption/secretion are vital functions that are tightly regulated by precise chemical gradients and flows and that should be responsive to the body needs in a timely manner. There appears to be feedback between the microenvironment set for these functions to be fulfilled and the cells fulfilling them so that the functional state of the kidney tubules can be maintained. Nevertheless, this equilibrium can be fragile and in the 1990s, two proteins were identified as being vital for all the processes described above, polycystin-1 and polycystin-2. Improper dosage of these proteins in the kidney cells leads to Autosomal Dominant Polycystic Kidney Disease. In the second part of this chapter, we will discuss the pathogenesis of the disease as well as the key roles of these two proteins.

1.2 A case where kidney homeostasis goes wrong: Autosomal Dominant Polycystic kidney disease (ADPKD).

1.2.1 ADPKD as a health issue

Among kidney causes of renal failure, Autosomal Dominant Polycystic Kidney Disease or ADPKD is one of the most common. This disease is characterized by a progressive loss of function of the parenchyma due to cyst formation in the kidney tubules. These cysts lead to a drastic increase of total kidney volume and decrease of glomerular filtration rate (GFR). It is the most prevalent kidney genetic disorder and is due to mutations on one allele of gene *PKD1* (85% of cases) or *PKD2* (15% of cases). These mutations are widespread and concern between 1 out 500 and 1 out 1000 people depending on ethnicities. In >70% of cases, ADPKD ends up in end stage renal disease (ESRD) with permanent kidney failure and need for dialysis for patients awaiting kidney transplant. The high disease prevalence makes it the fourth cause of kidney failure in the world and by far the first due to a genetic disorder. Patients with polycystic kidney disease in general represent 15% of total kidney transplants. In fact, kidney transplants are the preferred treatment for ADPKD as of now. There are currently no curative treatments. An approved treatment exists to slow down the onset with tolvaptan, an inhibitor of the vasopressin receptor V2R. Initial clinical trials showed a reduced increase of TKV in the first years but a loss of significant effect over time. Due to liver toxicity, side effects such as important diuresis and relative efficiency, tolvaptan is only prescribed in patients with relatively early disease with a rapid progression while transplantation remains preferable in the long run.

In ADPKD, the important kidney enlargement (**Figure 1.8a**) does not only lead to loss of function but may end up in other more systemic health issues. Abnormal kidney growth is commonly a source of pain but also of infection and hemorrhage due to tissue rupture, protein and hematuria and subsequent urinary infections. Furthermore, patients with ADPKD also experience abnormally high tension. Among manifestations outside of the urinary tract, kidney enlargement can cause abnormal compression of internal organs. Moreover, mutations at the origin of ADPKD can affect other organs and tissue. Cysts also form in the liver, although not as important. These cysts are also prone to infections and are the source of other systemic issues. ADPKD can also have deleterious consequences on blood vessels integrity, increasing chances of aneurysms notably brain aneurysms.

The disease progression has a particular pattern where cyst onset is rare and slow at the beginning of life, then shows an abrupt increase around 40-50 years old (**Figure 1.8b**). The theories about disease pathogenesis have coalesced around a progression in three phases. A first hit, due to the germline heterozygous mutations that may lead to cyst formation as soon as in utero. Then during life, a second-hit due to random somatic mutations on *PKD1* or *PKD2* lead to a few primary cyst formations. At this stage, the disease does not represent a health issue. Later in life, there is a drastic acceleration of cyst formation and cyst growth that will end up in kidney failure. This drastic acceleration is due to a third hit whose origin is still unclear. Two hypotheses for this third hit, that we will discuss later more in detail, are kidney injuries and a snowball effect. The second hypothesis stems from the fact that cysts grow in clusters and at an exponential rate in ADPKD. We will discuss later in this chapter the evidences for and against those two hypotheses and the origin for the snowball effect.

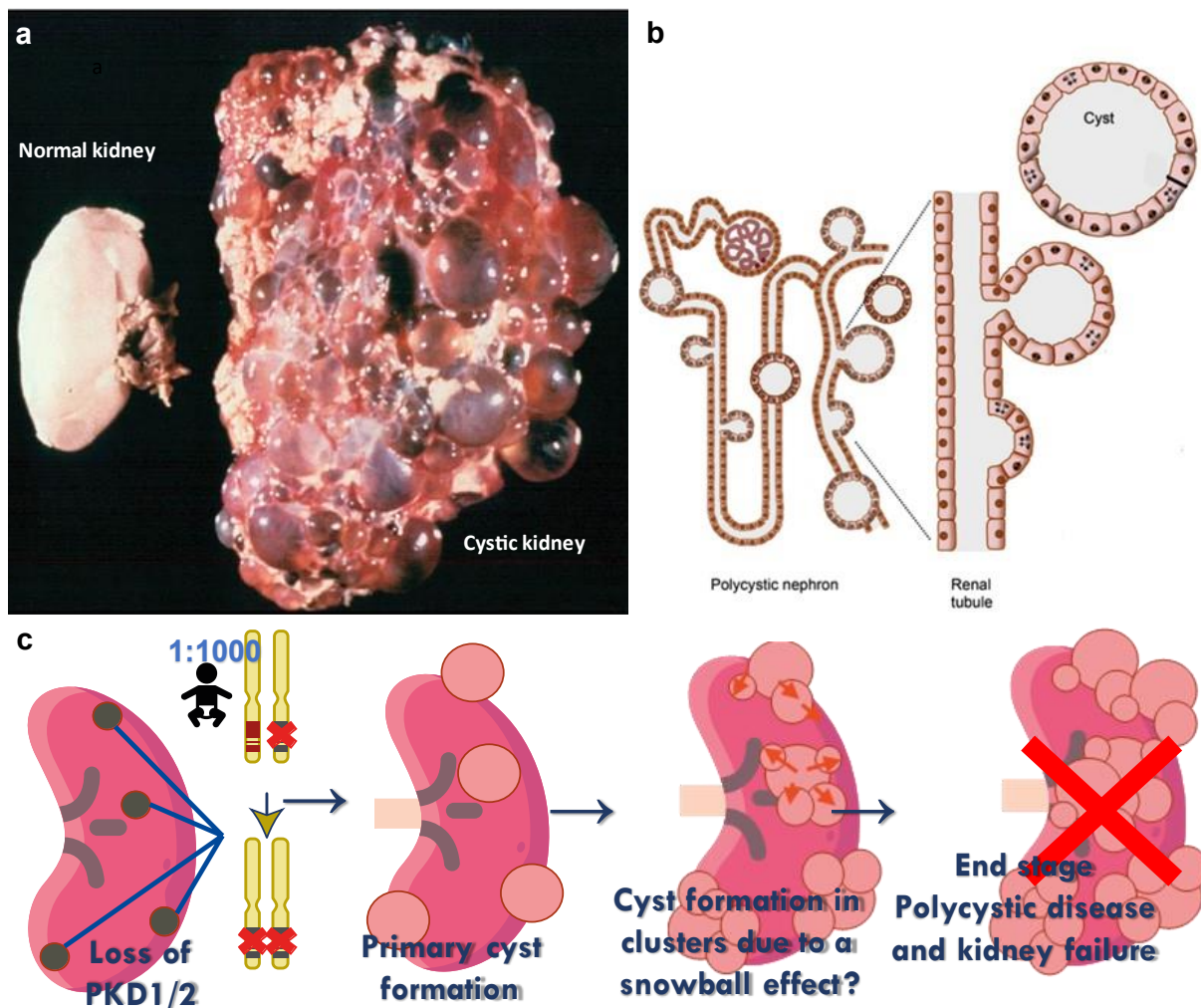


Figure 1.8: ADPKD pathogenesis. In ADPKD, cysts lead to important kidney growth (a from Calvet, James 2003). Cysts form sprouting from tubules and may separate from them (b). Cysts form following a three-hit process: first people are born with a heterozygous mutation on *PKD1/PKD2*, then somatic mutation leads to total loss of *PKD1/2* in some cells that may form primary cysts. Later in life cysts form in clusters, possibly due to a snowball effect. This third hit may lead to ESRD and kidney failure (c)

Kidney cyst formation itself remains a puzzling process raising many questions. A kidney cyst is a monolayer spherical structure that stems from a kidney tubule from which it may separate as it grows (**Figure 1.8c**). Being filled with fluid, they appear to secrete abnormal levels water and ions compared to surrounding tubules. They generally experience higher proliferation and apoptosis levels than tubules while the cells lining them are flatter and less polarized than normal kidney cells. In advanced stages they are also a source of inflammation and fibrosis which will further destroy the kidney parenchyma. In ADPKD, they originate first from the inner medullary then spread to the cortex to proximal regions. Because cyst formation involves many intricate mechanisms, it is not clear what cascade leads to their formation in the interstitium. Possibly, the field needs more relevant models to decipher the origins of cystogenesis. Such endeavors will provide precious insight on targets for curative treatment.

Next, we will first navigate through the mechanisms involved in cyst formation in ADPKD. To do so, we will first focus on the polycystins, the two proteins coded by *PKD1* and *PKD2* and assess their role. Then we will examine from the literature how localized loss of *PKD1* or *PKD2* can trigger cystogenesis in the second hit. After we will explore the arguments for and against kidney injuries and snowball effect as third hit. Lastly, we will briefly review the

main models that have been used so far to understand cyst formation and what could be improved to answer remaining questions about cystogenesis.

1.2.2 Polycystin-1 and Polycystin-2, two proteins involved in mechanosensation essential for the kidney epithelium homeostasis

In 1994 and 1996, polycystin-1 (PC1) and polycystin-2 (PC2), coded by *PKD1* and *PKD2*, respectively were identified through positional cloning as being at the origin of ADPKD. Their functions were then completely unknown. Naturally, after their discovery, subsequent research focused on characterizing the proteins from their structure (that will be introduced later) to their spatiotemporal expression and signaling, deciphering their functions. It was evident that they were critical for the nephron epithelium to maintain its functional tubular structure. Later the proteins were also found in other tissues such as liver, pancreas, and certain blood vessels, notably in the brain. In these tissues, they also seem to have an important function, as loss of *PKD1* can also lead to cysts in both liver and pancreas, as well as aggravated risk of brain aneurisms. Nonetheless, we will limit our scope to the kidney for the purpose of this discussion.

PC1 expression is at its maximum during the fetal stage, then at adult stage the protein expression drops to a level where it becomes hard to detect in many studies by immunoblotting. This suggests a particularly important role in kidney morphogenesis. Interestingly, levels are not always homogeneous during development. To summarize, studies point at a more or less uniform expression throughout segments of the nephrons at early stages, that becomes more localized to the distal part of the nephrons at later stages and after birth. These regions are the least proliferative at the late stage of development, but they are still maturing after birth, which may indicate a negative correlation between the proliferative state of cells and the levels of polycystins. Possibly as its presence weakens in the mature tissue, the protein still fulfills an important role in maintaining the mature state. Murine models have shown that inducing loss of polycystins in the adult stage still leads to polycystic disease, but cysts develop with a much slower kinetics, as if there was a switch involving polycystins role from a morphogenesis role to a maintenance role at adult stage (Lantinga-van leeuwen *et al.*, 2007; Piontek, Luis F. Menezes, *et al.*, 2007). Remarkably, a recent study demonstrated that reexpression of *Pkd1* or *Pkd2* in ADPKD mice models could reverse cystic kidneys to a pre-cystic stage. This result suggests that at adult stages, even if normally weakly expressed, the two genes are not only essential to prevent a cystic phenotype but possibly to revert any defect in the tubular structure (Dong *et al.*, 2021). Thus, it would be as if the proteins constantly ensure a constant developmental program of the nephron in their functional tubular structure.

It appears that PC1 and PC2 intervene in the kidney epithelium in many cellular processes that all together regulate tissue homeostasis, maintaining the tubule geometry. Mature epithelium like the kidney tubules are still dynamic systems that constantly renew to maintain the tissue health or in case of damage to such a degree that the adult kidney still presents a previously unsuspected plasticity (Dong *et al.*, 2021).

The role of polycystins in maintaining the kidney epithelium.

First, tight control for balanced levels of proliferation and apoptosis are necessary to maintain a stable cell density compatible with the defined geometry of nephrons. Indeed, many studies have pointed at the role of the two proteins in regulating proliferation, perhaps one of the most critical processes to maintain a functional and healthy cell density. For instance, PC1

and PC2 are thought to be upstream of many pathways that regulate the cell cycle. Both proteins have been shown to regulate intracellular calcium concentration and signaling. This can influence entrance into the cell cycle, for instance through regulation of amount of cytosolic cAMP that favors proliferation in association with MAPK pathways (Yamaguchi *et al.*, 2000, 2003, 2004, 2006). Cell-cycle arrest with PC1 in association with PC2 has also been associated to the JAK-STAT pathways and upregulation of anti-oncogene p21 (Bhunja *et al.*, 2002). PC1 has also been identified as a repressor of tumor associated signaling such as mTOR signaling (Shillingford *et al.*, 2006; Boehlke *et al.*, 2010), also linked to abnormal cell-growth and proliferation, and an upstream repressor of oncogenes associated with overproliferation such as cMyc (Cowley *et al.*, 2006; Cai *et al.*, 2018).

Simultaneously, there is also evidence for a modulatory role of PC1 in apoptosis, thus in regulation of tissue renewal and in preservation of nephron integrity. It downregulates apoptosis (Alessandra Boletta *et al.*, 2000; Boca *et al.*, 2006), and confers cells a higher resistance to mechanical stress (Peyronnet, Sharif-Naeini, Joost H.A. Folgering, et al., 2012). This property is all the more interesting considering how kidney epithelial cells are exposed to constant shear and pressure stresses. By regulating apoptosis, polycystins may as well prevent tissue overproliferation. The phenomenon of apoptosis-induced compensatory proliferation is well-described in cancer (Moreno-Celis, García-Gasca and Mejía, 2022). Likewise, in ADPKD, apoptosis may favor abnormal levels of proliferation, although it remains a topic of debate. Furthermore, limiting apoptosis may limit deleterious tissue remodeling, as cells that are healthy enough occupy the space.

Otherwise, as epithelial cells are renewed, maintaining apico-basal polarization and tissue cohesion is essential for tubule homeostasis, and critical for the epithelium stability and its function. The loss of *PKD1* reverses epithelium to a premature-like state with poorly differentiated cells (Nishio *et al.*, 2005). In addition, inducing an exogeneous expression of polycystin-1 leads to drastic changes in morphogenesis from kidney epithelial cell *in vitro*, promoting tubule like branching instead of cyst like structures (A Boletta *et al.*, 2000). Polycystins were shown to be important for cells to develop proper *adherens* junctions and cytoskeleton networks (Huan and Van Adelsberg, 1999; Sharif-Naeini, Joost H.A. Folgering, et al., 2009; Streets et al., 2009) while modulating cell shape via non-canonical Wnt pathways, size via mTOR pathways and migration abilities via Wnt pathways (Zhang *et al.*, no date; Nickel *et al.*, 2002; Nishio *et al.*, 2005; Viau *et al.*, 2020).

Interestingly these processes seem to respond to mechanical stimuli, providing the cells with a way to adapt to the interplay between the geometrical constraints and the constant hydrodynamic stresses necessary for the proper tissue function. Some of these responses are mediated by polycystins, notably PC1 modulation of the mTOR pathways allows a flow shear stress-dependent cell-size control (Boehlke *et al.*, 2010; Viau *et al.*, 2020). Furthermore, by helping preserve the right cellular differentiation and polarization, polycystins ensure proper secretion and reabsorption. Regulation of reabsorption and secretion processes is not only essential for the kidney function but also to maintain the equilibrium between the hydrodynamic forces and the forces maintaining the epithelium integrity. Finally, the basement membrane being the backbone of the kidney epithelium, the maintenance of a healthy tubular epithelium also relies on a maintenance of a healthy ECM. Defects in this ECM can not only represent a foundation for abnormal proliferation, migration or differentiation but can also break the equilibrium between intraluminal pressure and tension maintaining the tissue geometry. It is largely accepted that cysts in ADPKD are accompanied by abnormal ECM depositions, with thickened ECM and heightened levels for certain basement membrane protein, however this

phenomenon has been mostly linked to fibrosis and other phenomena such as inflammation that are at play could largely be explained by this. Nonetheless there is evidence that polycystins could be associated with regulation of ECM deposition, notably during development. In most cases, the proteins appear to downregulate ECM deposition, especially during development (Mangos *et al.*, 2010). A study however showed that polycystin-1 was required to maintain the integrity of the basement membrane, notably in stromal cells (Nie and Arend, 2017). It may also be that abnormal levels of certain protein in the basement membrane do not allow proper mechanical properties and in the end fragilize the edifice.

Polycystins as mechanosensory proteins

The two protein structures (**Figure 1.9a**) already hint at the mechanisms behind these functions. Polycystin-1 is a particularly large transmembrane protein weighing 460 kDa. It has a long N-terminal tail region (with 11 transmembrane domains) thought to be localized outside the cytoplasm and a much shorter C-terminal region inside the cytoplasm ending by coiled-coil domain like polycystin 2. Notably, many have speculated that the long N-terminal tail of PC1 could be sensitive to shear flow or could be a type of receptor. Polycystin-2 is a calcium-permeable cation channel of 110 kDa (with 6 transmembrane domains). From the TRP family, polycystin 2 is alternatively called TRPP2. Both polycystins can form a complex, binding through their coiled-coiled C-terminal tails, that is located at the membrane and mostly at the primary cilium. In fact, it seems that to be properly localized at the cilia, the polycystins need each other (Freedman *et al.*, 2013). Cryo-EM showed that PC2 can form homotetrameric channels (Wilkes *et al.*, 2017) while in the PC1-PC2 complex, one PC1 would substitute for one PC2 (**Figure 1.9b**) (Su *et al.*, 2018). Interestingly, in this configuration, the conformation of the complex should not allow a Ca^{2+} channel activity because of positively charged residues from PC1. It was speculated that a possible change of conformation could be triggered by external signaling either through ligands or through shear flow; such conformational change may then allow opening of the PC2 channel. Binding antibodies specific to the N-terminal domains showed exactly that (Delmas *et al.*, 2004), furthermore it was shown that N-terminal domains of PC1 regulates opening probability of PC2 in a PC1-PC2 complex. (Ha *et al.*, 2020). PC1 has also been hypothesized to interact with G-proteins as suggested by the protein sequence. Notably, when the protein is modified to render the G-protein region ineffective, it

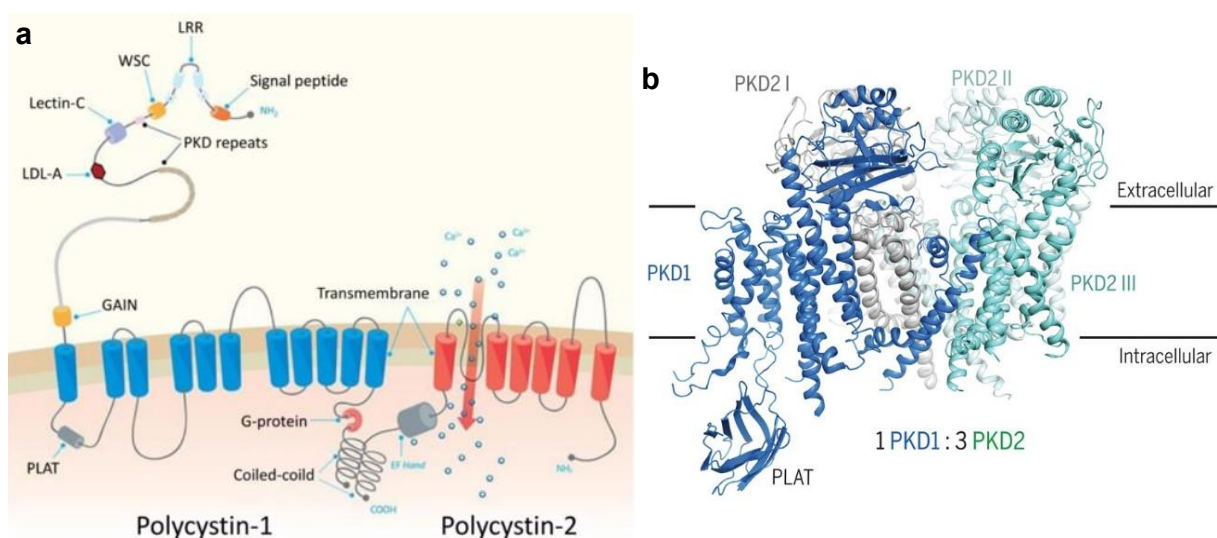


Figure 1.9: Polycystins structure. Polycystin-1 and Polycystin 2 form a complex joined by their coiled C-terminal tail (a from Adamiok-Ostrowska *et al* 2020). CryoEM showed that they form a tetrameric complex with 1 PC1 and 3 PC2 (b Cryo-EM from Su *et al* 2018)

leads to polycystic disease in mice (Parnell *et al.*, 2018) by impeding PC2 ion channel activity. Independently of PC2 it may also be that this prevents the protein to regulate G-proteins balance (Zhang, Tran and Wessely, 2018).

Because of a preferred location to the primary cilium and the shape of the PC1 extracellular tail (**Figure 1.10a**), the PC1-PC2 complex was classically thought to also be activated through shear-flow stress. However, there is still no convincing evidence of a flow conditioned channel activity from this complex in the literature. If Nauli *et al.* linked PC-1 to a flow sensor activity of the primary cilium via Ca^{2+} channels influx by PC2 (Nauli *et al.*, 2003) (Nauli *et al.*, 2008), this view was challenged a few years later when it was shown that in fact there was no calcium influx in the primary cilium triggered by shear stress (Delling *et al.*, 2016). This later result does not exclude a possible shear mechanotransduction by PC-1-PC-2 complex via other modalities than Ca^{2+} channel modulation; nor does this exclude a similar activity elsewhere that would ultimately have an impact on the primary cilium. It could also be that shear itself is not enough as, interestingly, the same group later demonstrated that the complex in primary cilium could lead to Ca^{2+} influx when exposed to soluble PC1 N-terminus. (Ha *et al.*, 2020)

If a shear sensitive Ca^{2+} channel in the primary cilium for the PC1-PC2 complex remains controversial, there is evidence for an intracellular PC2 channel activity independent from PC1. PC2 location seems to be wider than PC1 and the protein could be involved in more pathways not in the scope of our study. Notably it is now accepted that when not in a complex with PC1, PC2 forms a tetrameric channel that primarily locates at the endoplasmic reticulum (ER). PC2 channel activity at this level seems to be modulated by cytosolic Ca^{2+} concentration, and it may participate to calcium regulation in the ER and in the cytosol (Koulen *et al.*, 2002; Cai *et al.*, 2004). Interestingly, this ER location of PC2 appears not to be the most critical to prevent cystogenesis (Fu *et al.*, 2008).

Nonetheless, the examination of transcriptomics in cells subjected to shear stress highlights a distinctive alteration in the absence of *PKD1* or *PKD2* (Flores and Gusella, 2011; Kunnen *et al.*, 2018). Remarkably, this observation indicates that PC1 likely acts as a moderator, tempering the cellular response to shear stress. It is also important to note that the mechanical properties of the PC1 extracellular domain remain remarkably compatible with the hypothesis of flow-sensitive protein. Indeed, the relative difference in resistance to tensile forces of different domains in the tail suggests that shear forces could likely trigger conformational changes. (Qian *et al.*, 2005) Importantly, those forces are compatible with the shear that could be experienced in the kidney tubule. (Nag and Resnick, 2017). We could imagine then that conformational changes due to flow shear stress may allow an activation of the channel activity by PC1 N-terminus. (Ha *et al.*, 2020) To build upon this idea, under certain conditions PC1 C-terminal tail could be cleaved and translocate to the nucleus. This nuclei translocation seems to be modulated by PC2 that binds to PC1 C-terminal region. Coming back to mechanosensing, this nuclei translocation also seems to be modulated by mechanical stimuli linked to shear stress, wherein altered mechanical stimuli could be a triggering event. We should note that here loss of the primary cilium appears to be such an event. (Chauvet *et al.*, 2004a; Low, Vasanth, Claire H. Larson, *et al.*, 2006) . In the absence of flow sensed in the primary cilium, PC1 tail could translocate to the nuclei with STAT6 for instance, altering basal transcription levels in the cell (**Figure 1.10b**). Given its numerous sites of trafficking, it may as well be possible that PC1 alone or PC1-PC2 complex still have a flow sensor activity transduced elsewhere than in the primary cilium. More generally, numeral studies have shown since their discovery that PC1 and PC2 may be more ubiquitous than what was initially thought.

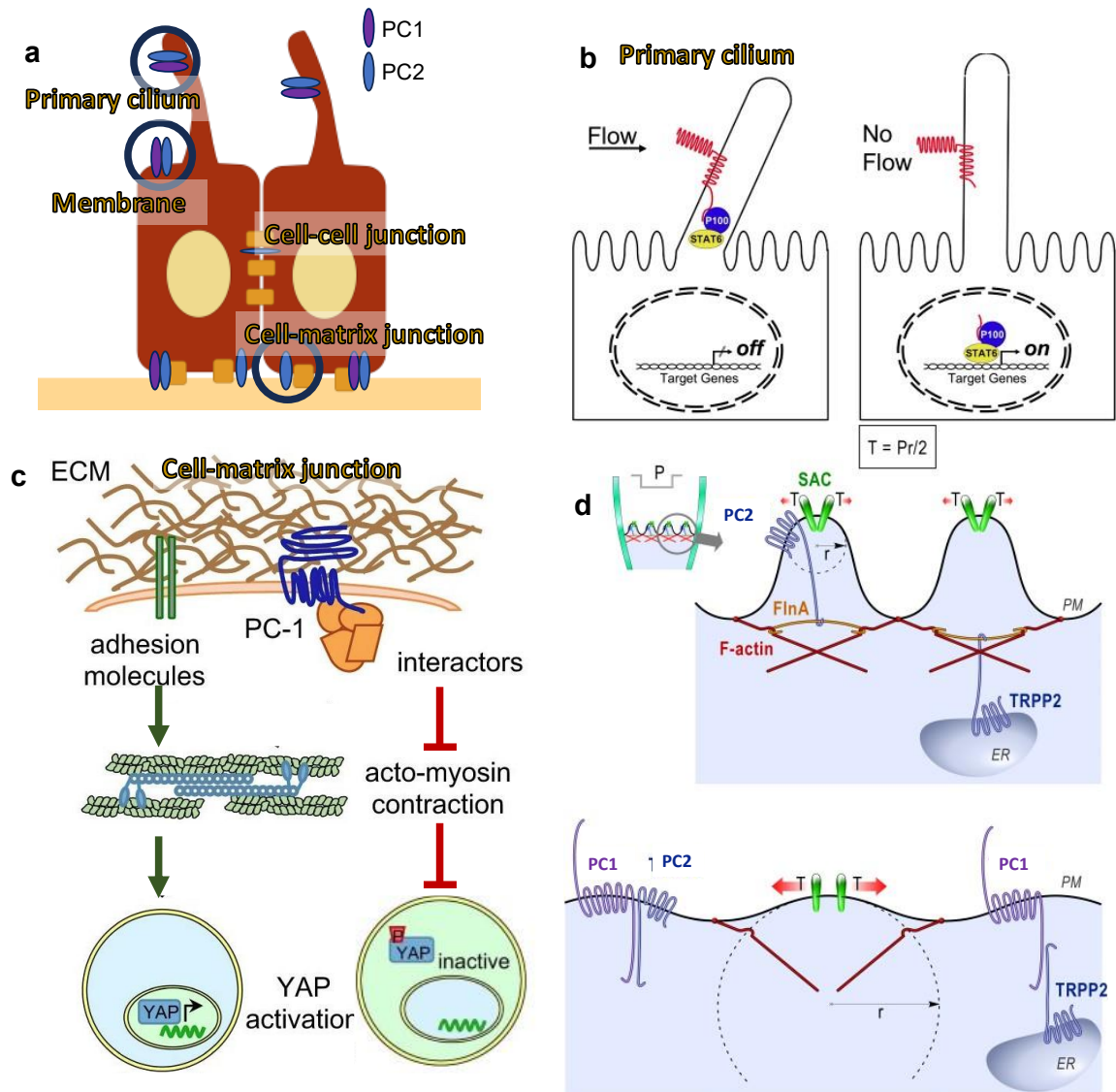


Figure 1.10: Three key polycystins functions. PC1 and PC2 are involved in mechanosensing in the primary cilium, at the membrane, in cell-cell junctions and cell-matrix adhesion(a), In the primary cilium PC1 is stable under flow but without flow may undergo cleavage at its C-terminal tail that will translocate to the nucleus, inducing gene expression (b) (adapted from Low *et al* 2006) , In the membrane in general it PC2 can downregulate the opening of SAC channels when not in complex with PC1, PC1-PC2 complex allow opening. (c) (adapted from Sharif-Naieni *et al* 2009) At junction with the matrix, PC1 will downregulate acto-myosin contractions promoted by integrins signaling, This will transduce to gene expression by promoting YAP phosphorylation and subsequent inactivation (d) (adapted from Nigro *et al*)

This might explain that in numerous staining of tissue to locate PC1 for example, the protein was shown to be located elsewhere than in the apical membrane. Notably, in Duan *et al.*, primary cilium independent shear sensing model, FSS mechanotransduction can be materialized basolaterally, where PC1 has been also found.

Indeed, PC1 and PC2 have also been observed to interact with cytoskeleton proteins complex and adhesion complex. If mechanosensing by polycystins should not be limited solely to their channel activity, it should not be limited only to flow shear stress either. As a possible pivotal actor in the formation of stable cytoskeleton structures, PC1 could dictate cell shape and migration abilities. (Yao *et al.*, 2013; Castelli *et al.*, 2015). PC1 interacts with microtubules and actin complexes to regulate focal adhesions, enhancing the cells adhesion properties,

polarization and directed migration abilities. The RhoA–YAP–c-Myc signaling axis is an example of a pathway downregulated by PC1 (Cai *et al.*, 2018) that is thought to transduce mechanical stimuli exerted on the cytoskeleton stemming from cell-matrix and cell-cell adhesion to various gene expressions (Dasgupta and McCollum, 2019). Furthermore, in connection with this same pathway, Nigro *et al.* showed that PC1 may modulate cell's reaction to stiffness and their contractility through actomyosin contractions (**Figure 1.10c**) (Nigro *et al.*, 2019). The interactions of PC2 notably with filamin-A and the actin cytoskeleton may modulate the activity of stretch activated channels by locally tuning plasma membrane topological and mechanical properties. PC1-PC2 balance would tune the opening probability of opening of these channels under stretching stresses such as intraluminal pressure. This model of a mechanosensing process is both independent of PC2 channel activity and possibly of the primary cilium (**Figure 1.10d**). (Sharif-Naeini, Joost H.A. Folgering, *et al.*, 2009)

Additionally, polycystin-1 was identified as a strong interacting partner with intermediate filaments (Xu *et al.*, 2001a). Although the function behind such interaction remains elusive, it could possibly favor long intermediate filaments network, stabilizing cell-cell adhesion and overall tissue cohesion (Xu *et al.*, 2001b). In addition, PC1 forms a complex with beta-catenin and E-cadherin in normal kidney cells and appears to be required for E-cadherin to form stable complex with b-catenin (Roitbak *et al.*, 2004). This gives another modality through which PC1 could impact adhesion properties at a cell-level and cohesiveness at a tissue level, but also proliferation, since perturbation of β -catenin/E-cadherin complex affects the Wnt-signaling pathway. The presence of the protein at cell-cell junction and cell-matrix adhesion could also be associated with other mechanosensitive pathways stemming from the cytoskeleton that have yet to be clearly characterized.

1.2.3. Mosaicism in ADPKD, first triggering event for cyst formation:

1.2.3.1. Somatic mutation as an event leading to cyst formation.

We saw that PC1 and PC2 were critical genes for the maintenance of the nephron tubular structures. Current understanding of the disease puts losses of heterozygosity (LOH), and more generally somatic mutations, at the origin of a total loss of functional PC1 or PC2, as primary events triggering cyst formation. The classical understanding further supports the notion that a cyst is monoclonal, indicating that a single cyst originates from one mutation (Qian *et al.*, 1996). However, the question may not be entirely clear as it is. In fact, early studies on the matter showed that PC1 may still be present in the epithelium lining cysts, at least in the early stages. In one study, 80% of cysts from ADPKD type 1 patients analyzed had widespread expression of *PKD1* (Ong *et al.*, 1999). This study relied on staining techniques to identify the presence of PC1. A missense mutation on the remaining allele may not be detected through these methods if it does not prevent the expression of a protein similar enough to the functional protein. Progress in sequencing made it clearer that in most cysts there were somatic mutations in ADPKD genes in cells lining cysts. In a study with a cohort of nine patients analyzing 63 kidney cysts (Tan *et al.*, 2018), 8 patients had a germline mutation on *PKD1* and 1 on *PKD2*, on par with the commonly accepted distribution between type 1 and type 2 ADPKD. Looking at somatic mutations identified in these cysts, 90% of cysts presented one on *PKD1* or *PKD2*. Only 12% of those mutations were loss of heterozygosity (LOH). In addition, only 14% were likely to conserve a protein similar enough to still be detected by immuno-assay: 10% were missense mutations and 4% were in-frame mutations likely only slightly altering the protein structure. This leaves a clear majority of mutations that would prevent the expression or lead to a completely different protein which would still be at odds with what earlier studies showed. In fact, many studies of this kind use kidneys from patients with an already advanced disease because they are the most likely to be available. This does not give an accurate picture of what happens at early stages, when cysts first appear. In fact, Ong *et al.* showed that if a substantial minority of cysts were negative for PC1 in adult kidneys, there were almost no negative cysts in infantile kidneys. To reconcile these confounding results, we can hypothesize that sporadic somatic mutations on *PKD1* or *PKD2* are a necessary primary event for large cysts to form, but cells in cyst vicinity that have not undergone such mutations participate in cyst formation. Indeed, low level of *PKD1* expression may be sufficient to trigger cystogenesis (Lantinga-van Leeuwen *et al.*, 2004). The cystic phenotype would be in fact the result of a too important imbalance between PC1 and PC2. That is how for instance, on the contrary, overexpression of *PKD1* can also cause ADPKD (Thivierge *et al.*, 2006). Thus, we can understand how *PKD1/PKD2* heterozygous cells may develop a haploinsufficiency that makes them precystic. In fact, multiple studies have shown that cysts resulting from somatic mutation events developed faster in proportion to the degree of haploinsufficiency prevailing in their vicinity (Natoli *et al.*, 2008; Takakura *et al.*, 2008; Wouter N Leonhard *et al.*, 2015). After cyst formation, *PKD1/PKD2* negative cells gain a survival advantage over *PKD1/PKD2* positive cells in cysts which make them the only cells present in the long run.

1.2.3.2. Competition in mosaicism disrupting homeostasis: What we know from ADPKD models and what we can learn from differently fated mosaic epithelium.

Let's admit that a cyst could grow only if the domain of precystic cells is large enough but constrained enough by neighboring cells (Bielmeier *et al.*, 2016). We saw that it was not clear whether precystic cells domains appear in the epithelium regardless of *PKD1/PKD2* somatic mutations. Possibly then, only cysts with a high enough burden of *PKD1/PKD2* negative cells could escape the tight control of the kidney epithelium. In fact, the cystic

phenotype regarding *PKD1/PKD2* expression appears to be more complicated than an 'on or off' response. Alternatively, cyst formation would be initiated around a single somatic mutation event. The question is then how a single isolated cell could trigger on its own the formation of a cyst, locally transforming non-cystic cells into pre-cystic ones. In both cases, cyst growth may be determined by the result of a competition between pro-cystogenesis cells and pro-tubular cells. Presumably when a cyst starts forming around a *PKD1/PKD2* negative cell there is a pressure against this cell that it would need to escape. Generally, in differently fated epithelium there are surveillance mechanisms that will tend to extrude aberrant cells. For instance, Nishio *et al.* reported that cystic cells from chimeric *Pkd1^{-/-}/Pkd1^{+/+}* were not transplantable to nude mice, letting think that they are eventually eliminated from the kidney. In their study on cell competition in a differently fated epithelium, Bielmeier *et al.* showed that aberrant epithelial cells can escape extrusion and form large enough domains end up forming cysts (**Figure 1.11a**) (Bielmeier *et al.*, 2016).

Unfortunately, the literature linking cell competition to polycystin is thin. But we can look at hallmark signaling of ADPKD and investigate those that have also been associated with cell competition more generally. In the case of ADPKD cells, overexpression of YAP has been associated with cell competition. In an *in vitro* study, MDCK cells that overexpress YAP protein tend to be extruded when surrounded by cells with lower level of YAP (Chiba *et al.*, 2016). However, this study was conducted on 2D monolayers not subjected to mechanical stress and growing on a surface much stiffer than *in vivo*, yet YAP activity is linked to mechanosensing. In other contexts, YAP activity seems on the contrary to favor cell survival over cells with a more moderate activity, notably in the context of tumorigenesis. It may be that *in vivo*, different microenvironmental stresses pertaining to curvature stresses, different cell densities or different types of substrates modulate basal YAP activity, allowing survival of *PKD1/PKD2* negative cells. Furthermore, YAP appears to be in ADPKD a promoter of the oncogene Myc (Cai *et al.*, 2018). Myc signaling has been shown to turn epithelial cells into supercompetitors in a myriad of contexts (Nagata and Igaki, 2018). Especially, in the case of ADPKD, overexpression of Myc seems necessary and sufficient for cystogenesis (Trudel, D'Agati and Costantini, 1991; Cai *et al.*, 2018; Parrot *et al.*, 2019). In the end, the ability of pre-cystic cells to locally break the tissue homeostasis may be heavily dependent on the state of surrounding cells and on the ability of these cells to turn into supercompetitors. Notably, in mouse models with a conditional knockout of *Pkd1*, it seems that the severity of cystogenesis depends on the level of haploinsufficiency of cells surrounding fully deleted *Pkd1* cells (Lantinga-van leeuwen *et al.*, 2007; Takakura *et al.*, 2008; Wouter N Leonhard *et al.*, 2015). Either mutated cells clones need to expand enough beyond a critical point to trigger cystogenesis or surrounding cells need to get to the right phenotype. In fact, in their chimeric mouse model, Nishio *et al.* showed (**Figure 1.11b**) that cells still expressing *Pkd1* participate in cyst formation. Interestingly these cells gradually disappear as the cyst grows, mostly going apoptosis and being replaced by *Pkd1⁻* cells. Thus, even after cyst initiation, mosaicism and competition are still key processes involved in cyst growth. This would explain why *Pkd1* is largely absent from analyzed human cysts given their stage of development when collected. This brings us to the second focus of this work: to have a definitive answer on the matter, more must be done to investigate the role of mosaicism in cystogenesis and more particularly on cell competition in ADPKD.

The fact that the disease severity and kinetics may be modulated by development stage for the same mutational burden is also strong indicator that its own loss of *PKD1/PKD2* is not sufficient for a group of cells to generate a cyst but is rather conditioned by the right cellular phenotypic background. It is noteworthy that the immature kidney has a more proliferative

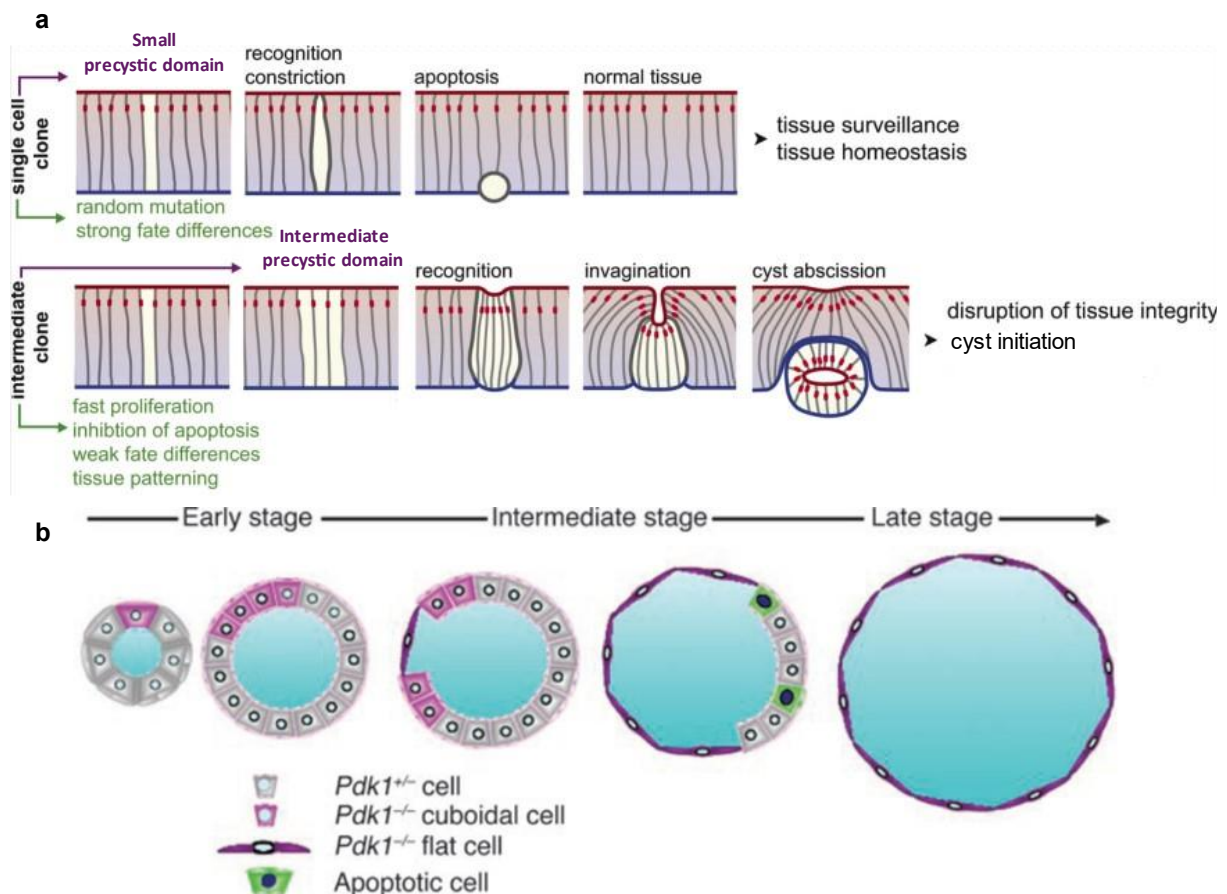


Figure 1.11: Competition and cystogenesis. There is competition at different the interface between differently fated cells in epithelium. When one or very few cells have an aberrant phenotype, they may be extruded by surrounding normal cells. When enough cells are mutated, they can form cystic structures while being pushed out from the epithelium (a) (adapted from Bielmeier *et al* 2016) Similarly competition happens in forming cysts: $PKD1^+$ cells and $PKD1^-$ are initially both present in cysts but as cysts grow, $PKD1^+$ gradually undergo apoptosis, while $PKD1^-$ cells replace them and differentiate (b) (adapted from Nishio *et al* 2005)

phenotype as nephrons are still subjected to elongation. Furthermore, cells in immature kidneys present a different cadherin profile which possibly better matches cystic cells. In human ADPKD, a germline mutation on $PKD1/PKD2$ is already present, laying the foundations for haploinsufficiency. The very slow onset of the disease is an indication that, on top of sporadic somatic mutations, the right conditions must be met so that around those mutations, the epithelium develops a state closer to the immature one. Currently the processes behind, commonly known as third hit, are still unknown.

1.2.3.3. How does a cyst form?

The hypothesis of a spatial segregation driven cystogenesis

When the right conditions are met to maintain a mosaicism between precystic cells and normal cells, the precystic domain needs then to locally disrupt the epithelium equilibrium to initiate cyst formation. Upon transformation into a cystic phenotype, cell adhesion properties are modified: β -catenin-E-cadherin complexes are no longer stable. Instead of E-cadherins, β -catenin forms a complex with N-cadherins or cadherin-8. This may result in kidney epithelial cells reverting to a more mesenchymal-like state with a different surface tension, and possibly more prone to invasion. Coincidentally, the switch to a cystic phenotype has also been associated with an increased level of proliferation (Nishio *et al.*, 2005). Upon dedifferentiation,

cytoskeleton and *adherens* junction disorganization leads to dysregulation of YAP/TAZ which may lead to loss of contact inhibition (Zhao *et al.*, 2007; Aragona *et al.*, 2013). These changes lead to interesting shifts in the equilibrium of the epithelium, where the tubular shape is locally no longer the most favorable. Belmonte *et al.* proposed a theoretical model of cyst formation in ADPKD (**Figure 1.12a**), testing at the same time the influence of cell-cell adhesion and of proliferation in cystogenesis. Interestingly, they concluded that intrinsic high proliferation levels do not lead to cystogenesis, rather decreased cell-cell adhesion and loss of contact inhibition due to switch in adhesion proteins were enough on their own to initiate cyst formation. However, both seem necessary to get the full range of cyst morphology seen in human ADPKD. Due to lower contact inhibition, an increasing number of cells requires more space. Depending on cell-cell adhesion properties, it can then be more energetically favorable for them to grow following the tubular epithelium or to grow outward. Pressure from growth in the precystic domain and a discontinuity in cell-cell adhesion at the interface between cystic cells and tubular cells will determine how the cyst will form. These differences in behavior and properties between precystic cells and tubular cells result in forces at the interface. Another way to approach this problem is then to look at these forces. In their model for cyst formation on *Drosophila*, Bielmeier *et al.* tackled cystogenesis by looking at the interface contractility resulting from cells different adhesion properties. This interface contractility can be assimilated to a surface tension between precystic and tubular domains. They observed that this interface contractility

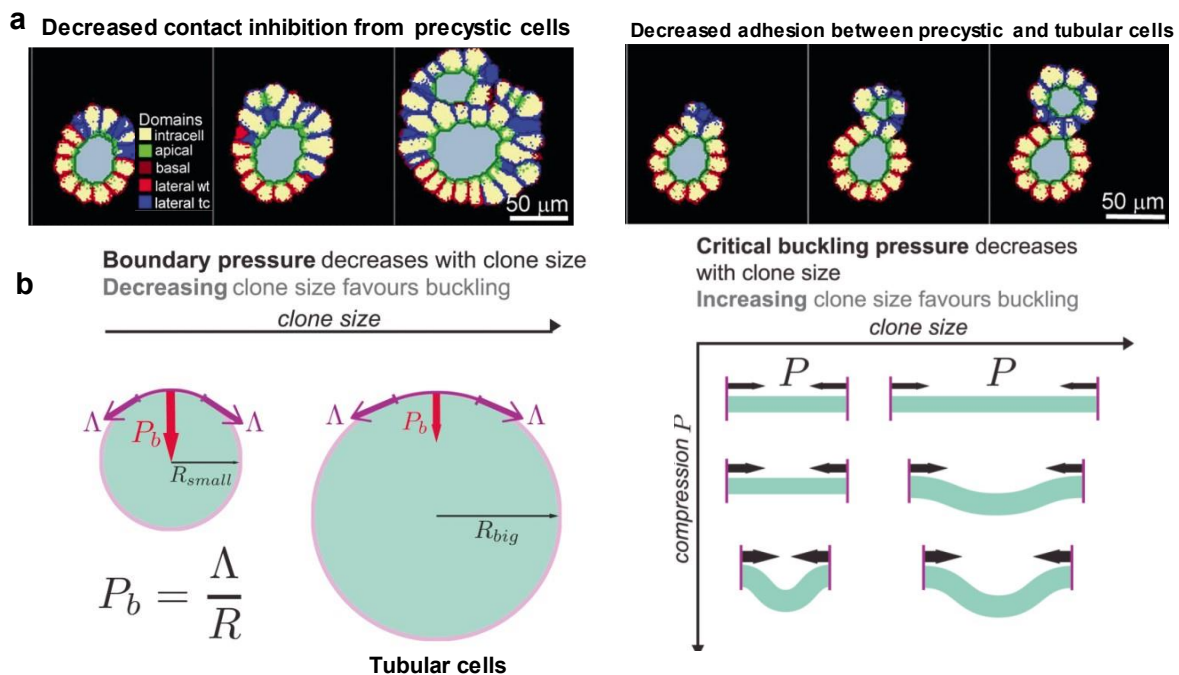


Figure 1.12: Theoretical models for forces and processes driving cystogenesis. Belmonte *et al* model showed that decreased adhesion between transformed cells (TC) and wild-type (WT) cells (creating surface tension similarly to interface contractility) leads to cyst forming growing outside the parent tubules. Loss of contact inhibition on the other hand favors cysts growing from the parent tubule. Combination of both is enough to recapitulate the range of human cyst morphology (a) (adapted from Belmonte *et al* 2018) At the interface of differently fated epithelia like precystic cells or transformed cells (TC) among tubular cells or wild type cells (WT), two phenomena are in competition: a pressure on the TC domain arise from tension due interface contractility, following Laplace law for interfaces. This pressure is greater the smaller the area of aberrant cells. On the other hand, buckling that may initiate cyst formation gets easier the larger the same area. These two effect sum up to an optimal size of TC domain for cyst formation (b) (adapted from Bielmeier *et al* 2016)

is necessary and sufficient to initiate cyst formation. They then showed that the size of the precystic domains will be highly important regarding probability of cystogenesis. If we look at cystogenesis as a buckling epithelium, on one hand, the larger the domain, the easier a buckling due to interface pressure. On the other hand, interface contractility results in a boundary pressure at the interface and this pressure will be more important the smaller the domain following Laplace's Law. Hence cysts are rendered possible with an optimal size of abnormal cells domain (**Figure 1.12b**).

If a consensus seems to appear regarding the determining role of proliferation in cystogenesis, the conclusions taken from dissection of human cystic kidneys suffer the caveat we have discussed earlier: they tend to be heavily skewed towards late stage ADPKD, hence other cellular processes such as inflammation may be at play. In mouse models, it appears that increased proliferation is only apparent as the disease worsens or has a particularly fast onset due to a high burden of mutations. Indeed, mice kidney showed elevated levels of proliferative cells when they were dissected several weeks after somatic mutations induction (Lantinga-van leeuwen *et al.*, 2007; Takakura *et al.*, 2008) in contrast to earlier stages after induction (Piontek, Luis F Menezes, *et al.*, 2007; Takakura *et al.*, 2008). Furthermore, slowing down the kinetics of the disease by decreasing the burden of somatic mutations to match human ADPKD showed that proliferation increase was not determinant in late onset of cysts (Wouter N Leonhard *et al.*, 2015). As an alternative to proliferation, a possible "steric effect" triggering cystogenesis could be fueled by changes in cell size. As we established earlier, the mTOR pathway is regulated by the polycystins and has a direct impact on cell size. It is admitted that cells lining cyst are less polarized and are much flatter than cells in tubules. It is less clear however whether this process starts with cyst formation or like increased proliferation, whether it could be a secondary process fueling the growth of cysts already forming.

The hypothesis of a mechanically driven cystogenesis

In parallel to tissue homeostasis, the equilibrium between the tension of the tubular wall, formed by the epithelium and the basal membrane, and the intraluminal pressure may also be disturbed. Notably, mispolarization and abnormal chloride secretions would lead to abnormal fluid movement from the basal to apical side of the lumen. Ensuing abnormal fluid secretion may lead to abnormal transepithelial pressure leading to additional constraints on the tubular epithelium. Many cyst models *in vitro* use abnormal apical fluid secretion to fuel cyst growth through cAMP pathway. *In vivo*, the only treatment against ADPKD to this day is an inhibitor of the vasopressin receptor V2R thought to upregulate the cAMP pathway responsible of abnormal fluid secretion in kidney cysts.

At the same time, a locally weakened basement membrane may be synonymous with a locally more compliant tissue and favor hernia-like formations leading to cystogenesis. If we follow Laplace's law at this interface, as intraluminal pressure increases, for a given luminal radius, tension in the tissue increases. When this tension increases above a certain threshold inversely proportional to the compliance of the tissue, the radius must mechanically increase. Differences in compliances, with cystic tissue having a higher compliance than surrounding tubular tissue, may then be another basis for cyst initiation. There is currently not a lot of evidence of a weakened basement membrane in early ADPKD, but mostly of many early dysregulations of many basement membrane components and metalloproteinases (Zhang, Reif and Wallace, 2020a). More research needs to be done to characterize the mechanical significance of these early abnormal modifications of the basement membrane. Unfortunately, the literature around a pure mechanical basis for cystogenesis in ADPKD is not as extensive. Early studies looking at the kidney tubules, cystic and non-cystic, viscoelastic properties show

however that expected physiological pressures in lumen are far away from the ability to locally distend the epithelium in normal condition (Grantham *et al.*, 1987). Alternatively, there is a basis for molecular communications between matrix and cells (Hu and Luo, 2013). Such communications could represent a barrier with a molecular basis and not a mechanical one, that could be disrupted and be lost in the abnormal matrix of cystic cells.

Nonetheless, many pathways involving the polycystins have been identified as important for cystogenesis, but it seems that none was deemed to be necessary and sufficient for cyst initiation in human ADPKD. Many of these pathways may be in fact redundant. Polycystins appear to be determining in structural processes maintaining the kidney functional organization and geometry. Possibly determining the nature of these processes and how they mechanically maintain a functioning organ could offer sufficient insight to be able to prevent cystogenesis altogether. Moreover, as suggested by Dong *et al.* work, these processes seem to be dynamic enough so that reverting them to normal may also be a strategy for a cure.

1.2.4. A third hit is necessary to explain how cyst formation explodes at intermediate stages.

1.2.4.1. The hypothesis of a snowball effect

The necessity of a third hit to explain cyst formation is largely a consensus. Leonhard *et al.* introduced the idea of a snowball effect to characterize this third hit: as if primary cysts lead to the formation of secondary cysts and so on (Wouter N Leonhard *et al.*, 2015). In patients it had already been observed largely how cysts growth follows largely an exponential function in respect to time (**Figure 1.13a**). It had also already been observed in murine models with late onset of cystic disease, with a similar pattern as in humans, that cysts that develop in adulthood are largely focal (Takakura *et al.*, 2008). They then quantified how cysts do not appear randomly but rather grow in clusters (**Figure 1.13b-c**). Such growth pattern bears a striking resemblance to a positive feedback loop, which could potentially fuel cystogenesis. Given the density of tubules in the kidney and the interstitial space of a few microns between tubules, it is easy to see how a cyst could interact with a healthy tubule nearby, leading to abnormal signaling in the tubules located next to cysts (**Figure 1.13c**). In fact, Takakura *et al.* showed that nephrons nearby large cysts experienced high levels of proliferation reminiscent of what was seen in cysts themselves. Furthermore, nephrons are also fluidically interconnected as several distal tubules end up in one collecting duct. Thus, a cyst past the collecting duct can

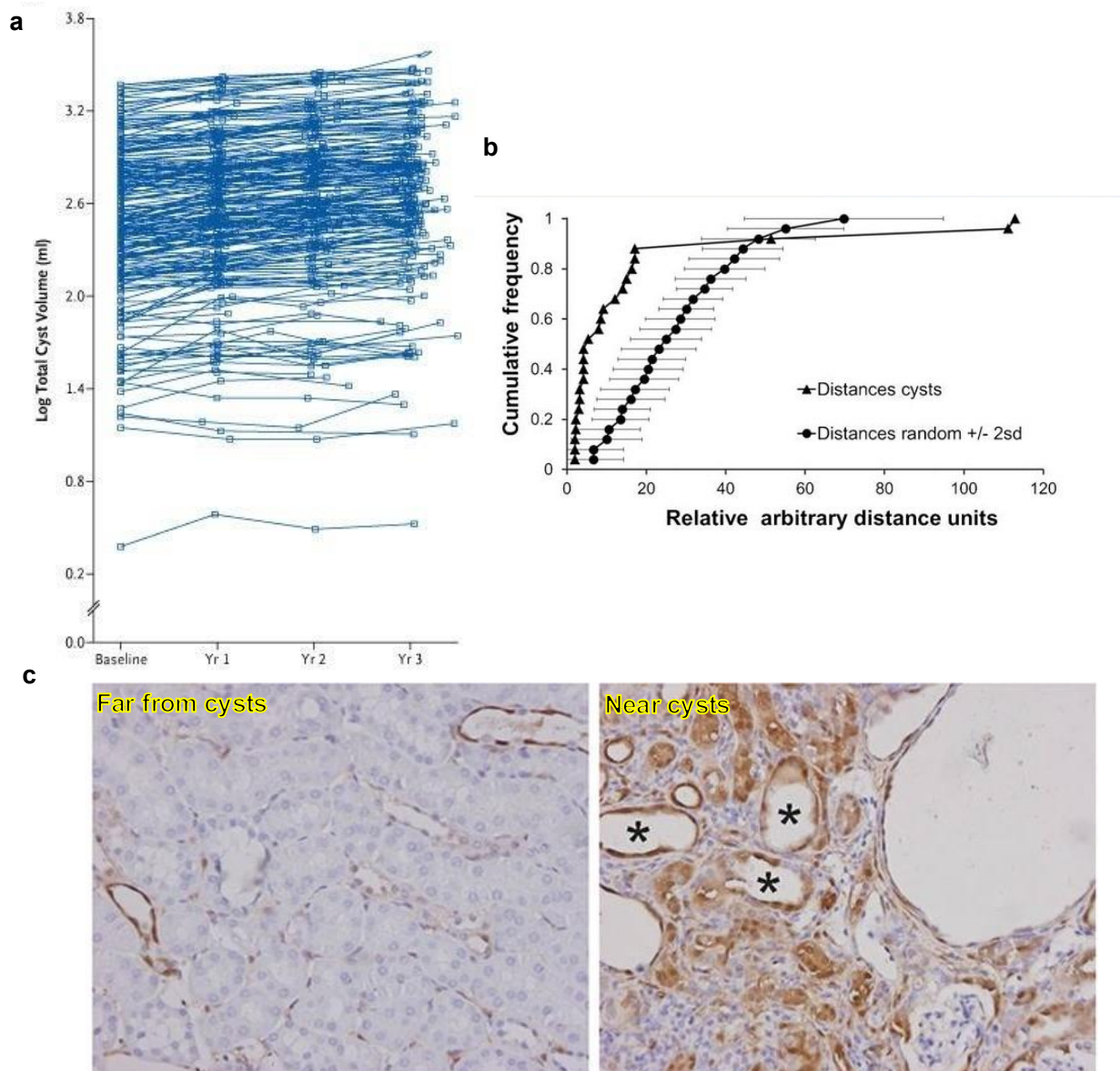


Figure 1.13: Cysts do not form randomly but may secondarily form due to a snowball effect In patients, cysts growth follow exponentials (a) (from Grantham et al 2006), Furthermore in their model Leonhard et al showed that they grow in clusters: rather than following a random pattern when forming, new cysts grow next to preexisting cysts.(b) (from Leonhard et al 2015) Histological cuts of an ADPKD mouse cystic kidney (c) shows the proximity between nephrons and growing cysts, it impact neighboring tubules by deforming or obstructing them, possibly promoting cystogenesis in these tubules. Notably we can see here more enlarged tubules next to cysts (right) than far from cyst (left). In addition, here a staining for pERK, a hallmark of cystic cells, shows clearly heightened levels of the protein in the vicinity of cysts compared to far regions (from Leonhard et al 2015)

have repercussions on several nephrons and a cyst upstream could indirectly affect an interconnected nephron.

1.2.4.2. The role of kidney injuries and how they could be part of the snowball effect.

As an alternative to a snowball effect, kidney injuries and aging have been proposed to explain the late onset of secondary cysts in ADPKD and as a third hit. For instance, Takakura *et al.* (Takakura *et al.*, 2009) showed in a *Pkd1KO* inducible mouse model, that inducing unilateral ischemia a few weeks after Cre-recombination triggered massive cystogenesis in the

injured kidney only. It appears that *in vivo*, age itself does not increase cystogenesis speed (Wouter N Leonhard et al., 2015). On the contrary, precocious disease is much faster, and the processes facilitating cystogenesis such as more proliferative phenotypes or a more plastic kidney are expected to be weakening in aged specimens. On the other hand, the number and probability of kidney injuries increases with time. Furthermore, injury repair that would ensue is at the origin of processes that would likely favor cystic phenotype: apoptosis, dedifferentiation, cell migration, proliferation. In general, there seems to be an overlap between injury repair and cystogenesis signaling (Kurbegovic and Trudel, 2016; Malas et al., 2017). All these processes can be altered in the case of haploinsufficiency for *PKD1/PKD2*. In that sense, Bastos et al. showed that *Pkd1* haploinsufficient cells are more prone to apoptosis after injury but also tend to have a more anarchic proliferation response, possibly due to an inadequate p21 expression response (Bastos et al., 2009). Yao et al. showed that migration of PC1 deficient cells was greatly impaired in term of persistency and speed (Yao et al., 2014). Additionally, many pathways usually downregulated are reactivated again for kidney injury. Notably one can argue that the damaged tissue briefly goes back to a premature state, where cystogenesis can be particularly fast (Little and Kairath, 2017). We can also take the issue through the lens of competition. Kidney injury may represent an opportunity for precystic cells that would be fitter in case of damage to proliferate and dedifferentiate to generate cystogenesis. Haploinsufficient anarchic apoptosis and proliferation response would go in that direction. Moreover, in their model, Takakura et al. notably noticed that of the cells lining cysts following injury were overwhelmingly new. In Happé et al. model on the other hand, interestingly proliferation levels came back to their baseline following injury. However, after a lagging period, proliferation went up again preceding cystogenesis. They suggested that during repair, newly formed cells, succeeding previously healthy cells probably present abnormalities that make them even more susceptible to cystogenesis after additional events (Happé et al., 2009).

If kidney injury on its own seemed to be a good candidate as third hit, there are also arguments to be made against its determinant role. Indeed, in their slow onset ADPKD model, Leonhard et al. showed that kidney injury only facilitated cyst formation for the mice with the highest burden of mutations that developed a fast disease. For the mice having a disease resembling human ADPKD, injuries did not have a significant effect in accelerating cyst formation. The main difference between their model and the model of Takakura and Happé et al. is the speed at which mouse develops cysts. In Leonhard et al. model, cystogenesis happens much slower and at a pace similar to human disease, whereas in the other models, cystogenesis is quite fast after *Pkd1*KO induction. Possibly kidney injury may be an accelerator of cystogenesis once the process is already initiated. Kidney injury, due to the proximity of nephrons, may then fuel the snowball effect through inflammation and signaling.

1.2.4.3. Evidence of pro-cyst chemical signaling

Ye et al. showed that chemical signaling may be able to promote cystogenesis (Ye et al., 1992). Indeed, they cultivated *in vitro* human kidney cells in medium supplemented with cyst fluid taken from patients. Strikingly, this fluid was enough to induce cyst-like structures in their cell cultures, compared to cells cultivated in normal medium. When they conducted their experiments, the critical composition of such signaling remained totally unknown. In urine and cystic fluid of patients with ADPKD, there is a particularly increased level of inflammatory cytokines. Provided paracrine secretion, it is very easy for these cytokines to reach neighboring tubules either through the ECM or through the lumen. Some of these inflammatory cytokines such as TNF- α have been shown to directly interact with kidney epithelial cells to favor

cystogenesis (Li *et al.*, 2008). For instance, exogenous TNF- α has been shown to be able to induce cystogenesis in developing mice. Interestingly the protein was shown to negatively impact PC2 dosage in its locations of interactions with PC1, showing a possible direct involvement in key cystogenic processes in ADPKD.

Extracellular vesicles have been recently gaining interest as one of principal vehicles of intercellular signaling. They carry a specific signature of the cell they originate from, carrying with them a picture of their membrane but also of their cytosol. When assimilated by new cells, they carry this signature with them that allows subsequent exchange with other cells of proteins and genetic materials. Ding *et al.* showed that extracellular vesicles from *PKD1* negative cells could promote cystogenesis in mice and exosomes from the urine of ADPKD patient could do the same *in vitro* (Ding *et al.*, 2021). Furthermore, inhibiting exosome production alleviated partly cyst growth, showing that endogenous exosome production in ADPKD model mice may be enough to promote cystogenesis. Investigating the origin of this effect, they highlighted the role of micro-RNAs and showed that these vesicles had the ability not only to promote procystic pathways but to also hinder PC1 expression. Finally altering *PKD1* expression also increases EVs production and half-life, feeding a possible feedback loop. A third hit through extracellular vesicles appears to be independent of kidney injury and would provide a way for the cystic phenotype to propagate not only between nephrons but we can also speculate that it could be a way for it to spread from a cell to its neighboring cells expanding a precystic cell domain, maybe enough to trigger cystogenesis.

1.2.4.4. [A mechanical origin for the snowball effect: how abnormal mechanical constraints could trigger and accelerate cystogenesis](#)

Deformation, obstruction due to cyst formation and probable consequences

Nephron proximity does not only favor signaling between them but can also mechanically have catastrophic consequences when a cyst grows. Indeed, growing cysts can deform and obstruct neighboring channels (**Figure 1.14a-b**). Deformation can lead to abnormal curvature and stretching stress. In case of maladaptation to that stress, it may lead to local injuries. When a channel gets partially obstructed, it leads to abnormal intraluminal pressures upstream of the obstruction as the local hydraulic resistivity increases. Indeed, in mouse models, intraluminal pressure measured in nephrons surrounding cysts tended to be higher and was even higher in cystic nephrons (**Figure 1.14a**) (Tanner *et al.*, 1996). Possibly these abnormally high pressures can mechanically favor hernias initiating cystogenesis as they can dangerously approach limits of wall tubular compliances (Grantham *et al.*, 1987; Tanner *et al.*, 1996).

Obstructions also greatly impair flow thus shear stress is reduced at the same time (**Figure 1.14b**). Partial or total obstruction of a nephron can have a very destructive effect on the unit. Unilateral ureteral obstruction (UUO), in which nephron flow is stopped, is characterized by injuries mostly located in the proximal tubules, by tubular atrophy and by fibrosis. Galarreta *et al.* compared them to tubules of mouse ADPKD models and showed striking similarities between the two (Galarreta *et al.*, 2014). Single nephron obstruction experiments showed similar changes in single nephron morphologies that were also accompanied by dedifferentiation of the epithelial cells and abnormal extracellular matrix (Evan *et al.*, 1986). On top of purely mechanical effect, cell mechanosensation is greatly altered.

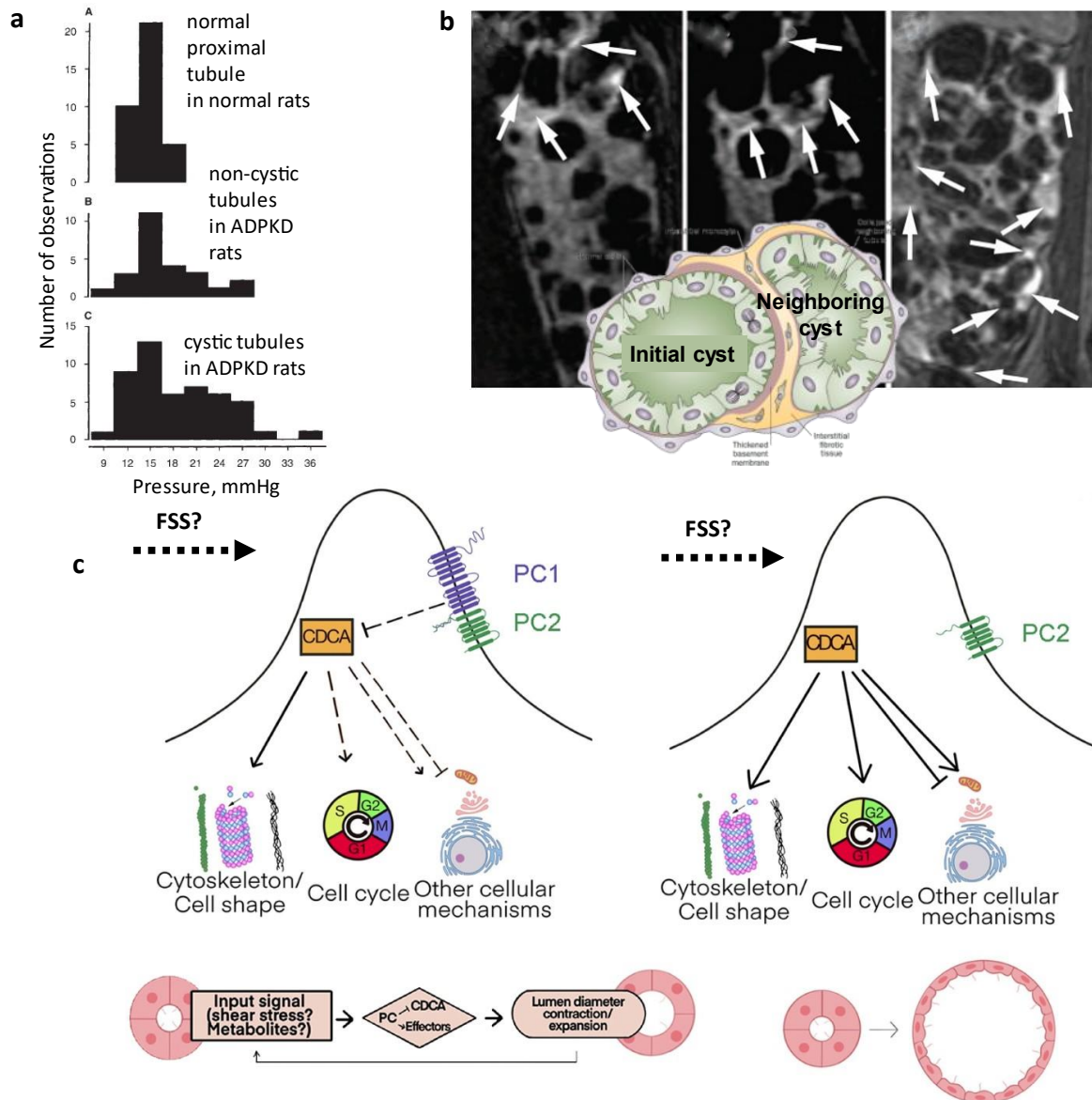


Figure 1.14: Tubule obstructions may favor secondary cystogenesis Non-cystic tubules and cystic tubules in rat models for ADPKD display higher intraluminal pressures than tubules in normal rats, probably due to cysts obstructing. (a) (from Tanner et al 1996) Similarly, in human, a contrast dye injected intravenously accumulates around cysts (white arrows), showing obstruction in kidney flow in normal tubules due to cysts (b) (adapted from Grantham et al 2011) These obstructions lead to aberrant activation of mechanosensitive pathways. For instance, a theorized CDCA, in case of challenges, through FSS input may normally help maintain a proper tubular geometry when transiently activated, modulating cell shape, cell cycle or other processes. This CDCA is regulated by PC1. In the absence of PC1, transient activations become permanent and through similar processes lead to cystogenesis (c) (adapted from Ma et al 2023)

Surely, altered mechanosensation leads to cellular response and coping mechanisms. As it appears simplistic to limit cystogenesis to a purely mechanical phenomenon, in ADPKD altered mechanosensation can become the tipping point in addition to these purely mechanical effects.

Involvement of altered mechanosensitive pathways.

As we saw previously, PC1 and PC2 are involved in multiple ways in stretch, pressure, or shear flow sensing. The mechanotransduction from polycystins intervenes in many pathways key for cell proliferation and cell fate. Some of these pathways are now classically associated with mechanosensing such as the Hippo pathway. For instance, a RhoA-YAP-c-Myc signaling axis has been shown to be essential for cystogenesis. (Cai *et al.*, 2018) Others,

like the cilium dependent cyst activation (CDCA) mechanism have been theorized precisely in the context of ADPKD (Ma, 2020).

In ADPKD, all kidney cells are already more or less subject to haploinsufficiency regarding PC1 or PC2. Altered mechanical cues may aggravate this. As we saw previously, PC1 notably undergoes modifications under shear stress. For example, PC1 C-terminal part translocates to the nucleus due to altered mechanical stimulus (Chauvet *et al.*, 2004b; Low, Vasanth, Claire H Larson, *et al.*, 2006). It may interfere with PC1-PC2 complex activity. Hence in already polycystin haploinsufficient cells, a possible normal adaptive response may lead to a pathological dosage. Another example of this is found in the CDCA. This hypothetical pathway would stem from the primary cilium. It seems that paradoxically, the primary cilium is needed for cystogenesis to happen (Ma *et al.*, 2013). In normal instances, using hydrodynamic stresses as a cue, the CDCA would be transiently activated when tubular integrity or geometry is compromised to promote repair, sensing resulting impaired flow. This pathway would be normally regulated by PC1 and PC2 complex. CDCA may be particularly solicited in the instance of kidney obstructions. Altered hydrodynamic cues such as low shear flow stress could transiently halt cell size and proliferation regulation processes through CDCA. (**Figure 1.14c**). In the case of altered levels of polycystins those processes could fail to reactivate themselves and permanently be impaired (Boehlke *et al.*, 2010; Viau *et al.*, 2020), transient activation of CDCA may fail to be properly shut down, leading to cases of futile repair. As another example, increased pressure in the lumen and deformations may lead to upregulation of the RhoA-YAP-c-Myc signaling axis, that would also fail to go back to basal level due to an haploinsufficiency of PC1. More generally, it appears that PC1 and PC2 may in fact act more as moderators of many mechanosensitive processes linked to growth and repair. In the context of ADPKD they can no longer have their moderating activity and processes necessary to maintain the tubule homeostasis become pathogenic.

In summary, cyst formation is at the origin of abnormal pressures and flow shear stress in their vicinity as a direct consequence of their growth obstructing tubular nephrons. Increased pressures and altered flows may push precystic cells over the edge to initiate cystogenesis. This process may arise from the combination of two phenomena: firstly, the precystic tubular regions might become mechanically incapable of handling the increased burden of mechanical stresses, and secondly, the normal adaptive responses to these stresses could become deleterious for the tissue homeostasis.

1.3. Preexisting models of ADPKD or more generally polycystic kidney diseases, advantages and limitations

Although ADPKD originates from a mutation on a single gene, it involves many pathways and many transduction mechanisms, making it difficult to have a model able to capture its complexity. Hence, research on ADPKD heavily focused on animal models, more specifically on murine models to be able to recapitulate as many of the phenomenon that will lead to cystogenesis. Like ADPKD, many polycystic kidney diseases are caused by a single gene mutation, such as ARPKD with the genes *PKHD1* or *PKDHD2* or many ciliopathies like nephronophthisis with NPHP genes. Although diverging from ADPKD on many points, such as ADPKD specific kinetics or organs that can be directly impacted, they share cystogenesis as the central feature leading to kidney failure. On one hand, processes transforming healthy epithelium into cystic epithelium may not exactly go through the same pathway, they can still offer some insight on how a kidney cyst mechanically forms. Notably, if the incriminated pathways are involved in similar processes and have similar endpoints phenotypically, it can be a powerful tool to assess how much of a process is necessary for cystogenesis. On the other hand, in the course for a treatment for ADPKD it is important to identify the pathways that are actually essential for cystogenesis to be able to target them.

The complexity of animal models may paradoxically transform them into an inextricable puzzle. As in ADPKD many processes may be intricate, it can become impossible to untangle causalities when two phenomena are superimposed. Furthermore, time resolution is by nature poor with animal models if we want to look at precise molecular or cellular transformations, rendering the task even harder. *In vitro* models with their simplicity allow decorrelation of several processes. If classical 2D models can provide insight on specific cellular or even tissue processes or mechanisms, they are by nature unable to recapitulate the geometries at play in ADPKD. As such, they are very limited. 3D models for ADPKD may allow to reproduce cystogenesis and with latest technical advancements become more and more sophisticated. From simple cell cultures in hydrogels to kidney organoids, they provide a range of complexity with their specific caveats. These models may fail to capture or to recapitulate necessary interactions of the epithelial cells with their environment. However, building the minimal model for a specific process in ADPKD is in itself already deciphering the mechanism behind the disease. Moreover, they allow work with live human cells, and may potentially be more precise and faithful for certain mechanisms. But in the end for clinical studies, it may be hard to prove that 3D models may be relevant enough to avoid the animal testing step.

In general, using the wrong model in a disease like ADPKD could lead to misconceptions that misdirect the focus towards irrelevant aspects. Therefore, it is important to be able to clearly identify to what degree a model is relevant. In what follows we will briefly introduce the most important models in the research for ADPKD, discuss to what aspects of ADPKD they were relevant, and show their limitations.

1.3.1. Mouse models and their limitations: to what extent do they allow to capture what happens in human ADPKD?

Murine models are the gold standard for ADPKD models. Mice share 99% of their genes with humans and have a very similar physiology. More specifically, the kidney appears to be an organ that is well preserved between the two species. On top of their fidelity to humans, their accessibility and plasticity has ensured mice are the most used model for ADPKD

research. They can be divided into two categories: spontaneous polycystic kidney disease (PKD) murine models and targeted orthologous PKD murine models.

Spontaneous murine models

The genes at the origin of ADPKDs were only identified in 1996. Before then, researchers had to rely on murine models that more largely presented similarities with human ADPKD. In fact, the genes at the origin of these congenital diseases are not always known. The murine models were selected precisely because of how they could parallel human ADPKD: cystic phenotype, altered basement membrane and extracellular matrix, altered levels of proliferation and apoptosis, dedifferentiation of epithelial cells and altered transepithelial fluid secretions.

The first model for PKD was the congenital polycystic kidney disease (*cpk*) mouse. Haploinsufficiency of the protein cystin was identified at the origin of the disease and primarily locates in the primary cilium. The phenotype is characterized by an early massive onset of cysts primarily localized in the proximal tubule, contrary to distal cysts appearing first in ADPKD. Cysts develop from the embryonic stage until death between 3 and 4 weeks, which is much faster than in ADPKD. The disease is said to be closer to ARPKD, but this model can be used as fast onset of cyst model. Similar models for ARPKD with early fast onset of cysts include *bpk*, *jcpk* and *inv* mouse models. The juvenile cystic kidney (*jck*) model on the other hand resembles more ADPKD, cysts develop focally as early as 3 days after birth, but the disease is more progressive with death at more than 4 months old. *Nek8* is the gene responsible and, similarly to *Pkd1/Pkd2* primarily affects cilia functions and cell-cell adhesion processes. The polycystic kidney disease (*pcy*) mutant is probably the spontaneous model that most resembles human ADPKD. Specimens live up to 9 months and the disease is characterized by slow, focal onset of cyst starting towards adulthood and with a location pattern close to that of human ADPKD. The mutants also develop extrarenal pathologies similar to human ADPKD like brain aneurysms. This has led this model to be one of the most used for clinical trials. However, NPHP3 was identified as the gene directly responsible for the phenotype. NPHP3 is a gene that belongs to a family of genes responsible for nephronophthisis, a ciliopathy also characterized by cystic kidneys. Unlike ADPKD, it is not characterized by abnormal sodium secretions. The Han:SPRD-Cy rat is another murine model that resembles ADPKD. Unlike the previous models this trait is dominant, similarly to ADPKD mutations. Homozygotes animals die by the early age of 3 weeks whereas heterozygous animals live well beyond adulthood, more than a year. Unlike ADPKD, the disease is characterized by cysts mostly localized in the proximal tubule. Another discrepancy is the sex dimorphism where female barely present any cyst in the kidneys and have a normal lifespan. This model was used extensively as a model for ADPKD. Notably, many studies showed the importance of the mTOR pathway in cystogenesis and benefits from using mTOR inhibitors in this rat model. However, rapamycin, an inhibitor of mTOR failed to show benefit for ADPKD in clinical trials. *Anks6* or *Pkdr1* is the gene responsible for PKD in this model. The function of this gene is unknown, but it is also associated with nephronophthisis in humans.

Orthologous deletion murine models

Identification of *PKD1* and *PKD2* as genes responsible for ADPKD coupled with the progresses in genetic engineering allowed development of mouse models orthologous for human ADPKD. In these models, *PKD1/2* can be either constitutively deactivated or conditionally via a drug thanks to construct relying on Cre-lox recombination.

The first model published by Lu *et al.* in 1999 displayed a phenotype very close to human ADPKD (Lu *et al.*, 1999). The targeted mutation was a deletion of exon 34.

Homozygous animals die at embryonic stage, presenting major PKD. Heterozygous animals were viable and developed cysts 16 months after birth essentially recapitulating human ADPKD. Similar to humans, some cysts, not all of them, presented a total absence of staining for *Pkd1* in heterozygous adult animals, consistent with the two-hit hypothesis. Cells lining cysts were more or less mispolarized and cyst presented abnormal transepithelial secretions. Interestingly different truncation of the protein followed, and even if they displayed very similar phenotypes, depending on the zone of the gene deleted, the severity of the disease varied. Moreover, total deletion of the gene *PKD1* led to the most severe phenotype. This would be consistent with the idea that ADPKD severity variations in human stems greatly from the nature of genetic mutations.

Hypomorphic models for *Pkd1* followed, testing the importance of haploinsufficiency in ADPKD. The *Pkd1-nl* mouse model, presenting a level of expression of 15-25% compared to normal, presented a variable phenotype with some mice dying at 2 months after birth with severely enlarged kidneys and others surviving more than a year with slightly enlarged kidneys. Like in human ADPKD, cysts were primarily located in the distal part of the nephrons (Lantingavan Leeuwen *et al.*, 2004). This variable phenotype was attributed to the variable genetic background of the mice.

Similarly, haploinsufficiency models for *Pkd2* were generated by creating an unstable allele, *Pkd2*^{WS25}, that has an important probability to undergo somatic mutations. *Pkd2*^{WS25/+} mouse presented a very mild disease with kidney with a few cysts at adulthood, whereas homozygous specimen presented a much more severe phenotype but also more variable, where the disease severity was correlated to level of *Pkd2* expression. Furthermore, cysts were characterized by an absence of pc2. *Pkd2*^{WS25/-} presented a more consistent severe disease and *Pkd2*^{-/-} died at embryonic stage. Overall, specimens presented cysts and lesions very similar to what can be found in human ADPKD (Wu *et al.*, 1998, 2000). Interestingly however, *Pkd2*^{+/-} did not develop a PKD. All together these results and the gradual disease severity with the gradual probability of *Pkd2* null cells further validated the second-hit hypothesis.

Latest mice models relied on inducible targeted deletions using a conditional Cre-deletion *Pkd1* inducible with tamoxifen. These models were particularly useful to study the impact of *Pkd1* deletions relative to the developmental stage and the critical role they play in cystogenesis. They further validated that a second hit, here an induced deletion in *Pkd1*^{lox/-} animals, was necessary to trigger PKD. Most importantly they provided with the first solid evidence for a third-hit mechanism, showing that the mutations were not sufficient: only when induced in adulthood *Pkd1* deletion led to a disease resembling human ADPKD in terms of kinetics, but then, there is a delay of several months between the induction and the first cysts.

If these models allow a temporal control of the second hit, they introduce two new experimental variables: time and number of deletion events. For the first Piontek *et al.* showed that to induce a disease resembling human ADPKD, it was necessary to induce deletion after a critical point in development. For the number of deletion events, typically the first inducible models display levels of deletion between 30 and 50% of total allele. Unfortunately, such a number is probably at least an order of magnitude more important than proportion of somatic mutation in human ADPKD or even in earlier *Pkd1*^{+/-} mice models. Leonhard *et al.* were among the first to point out this discrepancy (Wouter N Leonhard *et al.*, 2015). They improved the inducible deletion model by optimizing drug doses to induce a much lower number of mutations, down to 8% deleted cells. This led to a much slower onset of cyst paralleling closely the

exponential dynamics of human ADPKD. If kidney injuries in this model accelerated onset of cysts, it was never to a point comparable with the previous models and where it became decisive for the course of the disease. From these different observations compared to previous models, they hypothesized a snowball effect as the third-hit mechanism in lieu of kidney injury.

Most recent developments have offered the possibility to reinduce expression of polycystins after deletion in mice. Dong *et al.* model was then the first to provide strong evidence that processes behind cystogenesis are reversible. Such a model could provide the exciting possibility to take the problem regarding cyst formation backwards: possibly trying to see what processes are decisive to revert a cystic phenotype from a tubular one.

1.3.2. *In vitro* models

Murine models are probably the best currently available option to recapitulate the complexity of ADPKD and all the physiological and environmental factors that can be at play. Indeed, the latest models probably include all the key elements of ADPKD as they can parallel the disease faithfully, the problem is to isolate these features to assess their importance. Furthermore, they can only offer very poor time resolution. Regarding cystogenesis that follows a pattern of abrupt and rapid onset after a long period of dormancy, the difficulty is to be able to correctly grasp the chain of events. *In vivo* models provide a top-down approach when trying to decipher the mechanisms behind cystogenesis. *In vitro* models on the other hand, allow a bottom-up approach. The complexity of ADPKD is built brick by brick, key elements after another. Building the model on its own can already be identifying the key mechanisms behind cystogenesis. The approaches are multiple, but the idea is to recreate for a cell culture a microenvironment recapitulating key features of interest. For instance, in the case of ADPKD, geometry of the tissue is a central feature. Furthermore, they allow more easily to follow events dynamically with an increased time resolution. As technological advances allow to build more and more sophisticated *in vitro* models, being able to have an ADPKD in a dish becomes more and more likely. For the last decades, *in vitro* models were mostly only used as complements to *in vivo* studies to be able to isolate a cellular process. These models are typically cell cultures in a 3D environment made of a hydrogel. Offering much more complexity, organoids models were also translated to ADPKD research. They provide a powerful tool for drug testing and preclinical studies as they recapitulate elemental structures and compartments of an actual organ. Here we will briefly review classical 3D models that have been used to study cyst formation then we will explore the potential of kidney organoids applied to PKD.

1.3.2.1. Cell cultures in hydrogel

In 1987 McAteer *et al.* reported for the first time a kidney cell culture in a 3D environment (McAteer, Evan and Gardner, 1987). They seeded MDCK cells in a collagen I matrix. They observed that in this condition the MDCK cells were able to form monoclonal cysts inside the gel. The cells in the cysts were polarized, with the apical side inside of the cyst and basal side outside and cuboidal. MDCK had already demonstrated in 2D that they could form fluid-filled domes reminiscent of cysts. This experiment showed that in 3D they were able to self-organize and make a lumen filled with fluid using similar mechanisms. In this model, transepithelial fluids movement towards the lumen are one of the main mechanisms of cyst growth. Quickly after, the method was adapted from Mangoo *et al.* to culture cells isolated from ADPKD patients. These cells also demonstrated the ability to spontaneously form cysts. In this model, cyst growth was shown as being dependent cAMP mediated secretion (Wallace, Grantham and Sullivan, 1996).

Following this observation, forskolin, a cAMP agonist, started to be routinely used to induce cyst formation in similar 3D models. This type of model has notably been proposed as a drug screening platform. Booji *et al.* built such a platform using mIMCD-3 sh*Pkd1* cells, cells derived from the inner medulla collecting duct, wherein they used cyst size as a metric to assess the efficacy of a drug (**Figure 1.15a**). They tested inhibitors of pathways known to be associated with cystogenesis and observed an important diminution of cyst size (Booij *et al.*, 2017). Generally, in this model mTOR inhibitors fared the best. The use of cAMP stimulators to induce cyst formation raises several questions. Mostly, one could argue that it biases the results to a cystogenesis mechanism that may not be the most prominent one *in vivo*, possibly creating artefacts when targeting a pathway for instance. Asawa *et al.* developed an assay where they used 3D cultures of cells from a proximal tubule cell line, PN24, embryonic kidney,

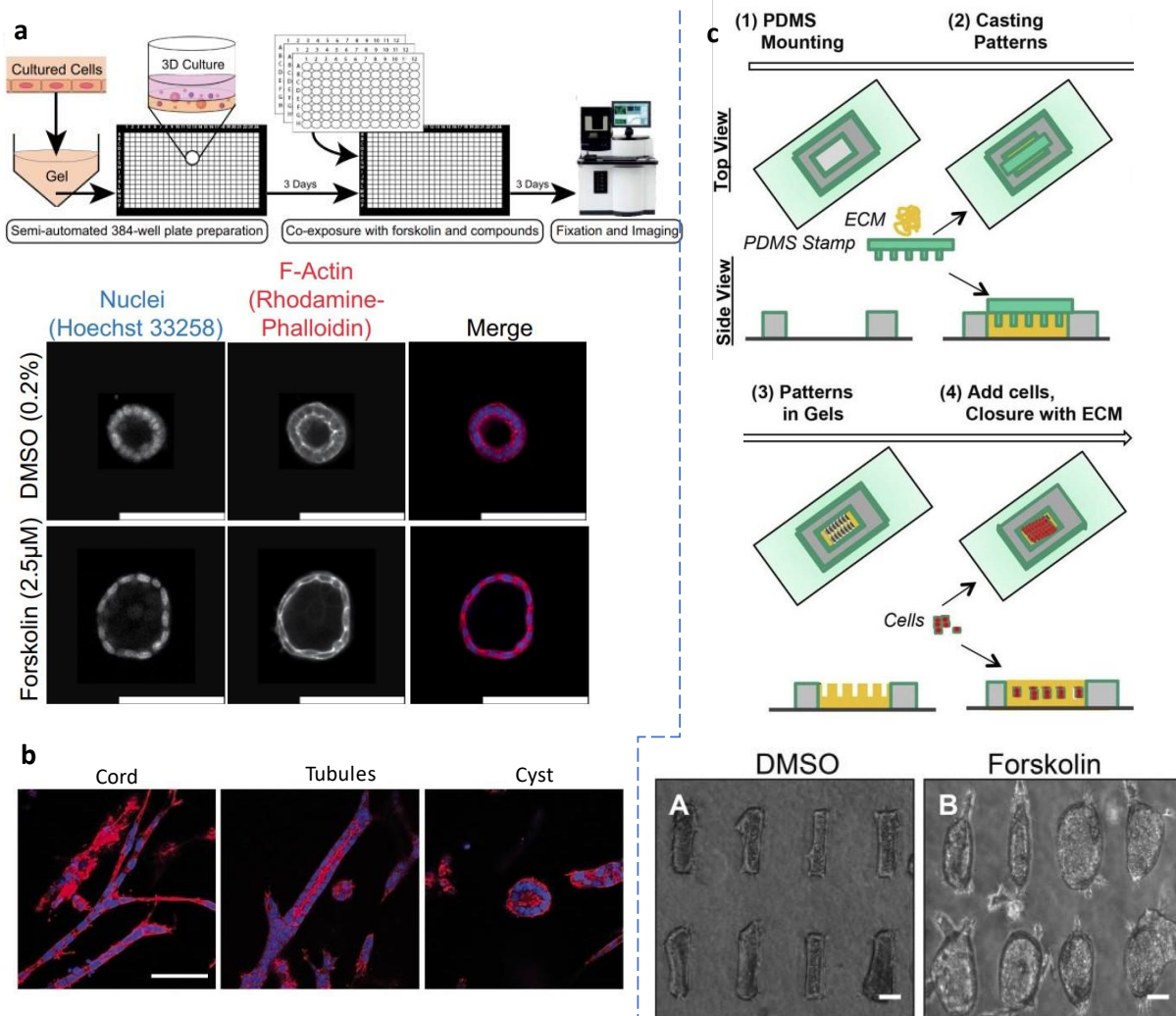


Figure 1.15: Classical in vitro models for polycystic kidney disease. In their in vitro model, Booji *et al.* use mIMCD-3 cells cultured in collagen. These cells form cystic structures in this configuration. Addition of forskolin as a cAMP promoter increases cyst volume. By measuring cyst volume upon addition of forskolin with another drug, this screening platform offer a way to evaluate the impact of the drug on cystogenesis(a) (from Booji *et al.* 2017, Scale bar: 100µm) Addition of Matrigel in the gel allow mIMCD-3 to form cord-like structures or tubules as well, offering another way to assess cystogenesis without artificially promoting it. (b) (from Cai *et al.* 2018: 100µm) It is also possible to guide the same cells in a tubular shape by growing them in a patterned gel (c). Assessing cystogenesis is done by looking at how well the cells maintain the tubular shape (c-A) For instance promoting cystogenesis with Forskolin leads to dilation of the patterned tubules (c-B) (adapted from Subramanian *et al.* 2018, scale bar: 50µm)

MEK without inducing cystogenesis with cAMP stimulator. Interestingly, MEK cells failed to make cystic structures and instead grew as filled cell masses whereas half of the structures grown from PN24 cells were cysts. They did pairwise comparison between *Pkd1* null and WT cells of cyst growth for PN24 only and viability for both as metrics for the efficacy. MEK and PN24 cells displayed very different *Pkd1* dependent sensitivity to drugs, with loss of *Pkd1* for MEK cells being much more significant. The interesting teaching from these results is that the phenotype in these 3D models is very cell dependent even when the cells are supposedly similar. Levels of protein expression linked to how well or not the cell line is differentiated, notably polycystins, may be at play.

Cai *et al.*, in their study on the role of the Hippo pathway in ADPKD, also made their own screening assay based on 3D embedded mIMCD-3 (**Figure 1.15b**). Unlike the previous assays, they did not use cyst volume as a metric but instead use a more binary measure: the ability of the cells to form cysts or tubules. Indeed, not reported by Booji *et al.*, their wild-type mIMCD-3 were able to form a mix of a few cysts with a large majority of cord and tubular structures spontaneously after several days of culture. Perhaps, this difference of behavior came from the different ECM that they used which was a mix collagen and of Matrigel. This is closer in terms of composition to the kidney ECM. Strikingly *Pkd1*KO mIMCD-3 almost exclusively form cysts. ROCK inhibitors and actomyosin contraction inhibitors recovered tubulogenesis. Due to the simplicity of the model, we can come up with a simple explanation. The cysts spherical shape minimizes the surface occupied by a cell monolayer; we can therefore expect that increasing contractility would favor this shape. Hence by moderating cell contractility, *Pkd1* may also make the tubular shape more favorable.

Returning to the disparities between analogous models able to generate tubule or not, in fact, subsequent studies showed that to promote tubulogenesis, matrix needed to have certain key properties. The matrix needs to be able to be degraded by ECM protease while promoting their expression. Furthermore, interaction with integrins seems to be essential to guide tubulogenesis (Cruz-Acuña *et al.*, 2019). In addition, cell line variability is also an important challenge adding uncertainty to this kind of model. Westermann *et al* showed that mIMCD WT cells displayed a high transcriptional variability in a polyclonal cell population. This translated into an important variability in clones extracted from that population to form tubules in collagen I- Matrigel assay (Westermann *et al.*, 2022). Notably, levels of collagen and laminin binding integrins have been shown to be essential for tubulogenesis (Chen *et al.*, 2004), echoing the need for matrices to be compatible with these integrins. Additionally, when engineering *Pkd1*KO cells to model ADPKD from these WT cells, this variability is transferred to resulting clones.

Given the possible variability of self-organization with respect to cell types or microenvironment, one approach could be to impose on the cells a predetermined shape. Subramanian *et al.* proposed a guided kidney tubule model (gKT)(**Figure 1.15c**). The model consists of 3D array with patterns of small tubules in an ECM made of a mix of collagen I and Matrigel in which are seeded the kidney cells (Subramanian *et al.*, 2018). For their proof of concept, they used mIMCD-3 cells. Interestingly the cells largely conserved the initial shape imposed on them. As a control, cells seeded in the ECM without the gKT displayed a similar distribution of cystic and tubular phenotype as reported before. However, they did not use a cell line genocopying a PKD and instead treated their gKT with forskolin. Similar to simpler unguided 3D gel models, the addition of forskolin led to important dilation of gKTs as well as the loss of the tubular shape to a more cyst like shape. To the best of our knowledge, outside of our group, this is the only model using this approach developed to model PKDs.

Because most of 3D *in vitro* models for PKDs relied on cells self-morphogenesis, they were limited by the ability of the cells to do so. If differentiated cells still have a capacity to self-organize, unfortunately, molecular cascades activate during development following a specific pattern that will eventually lead to the formation of a nephron. Cells used in these models are taken at the end of this process, thus may not fully replicate it. In addition, relying on cell self-assembly does not allow any control over resulting geometries or seriously limits the functionalization possibilities of such systems. For instance, it is hard to imagine how flow shear stress could be implemented in such systems. Microphysiological systems are constructs providing cells with the environmental instructions such as geometries or hydrodynamic stresses necessary for the cells to recapitulate one or several key features of a disease or an organ. In that respect the Subramanian *et al.* approach may fit in this category but lacks any actuation capacity.

Alternatively, recent advances in culture and differentiation of induced pluripotent stem cells (iPS) in mature tissue, allow to replicate the development process in a dish to get kidney organoids.

1.3.2.2. Kidney organoids as a promising platform: pros and cons

Before the development of kidney organoids, it was possible to culture an embryonic kidney *in vitro*. Culture of embryonic kidneys allows one to isolate a structure very close to the organ of interest from the whole organism, offering a compromise between the *in vivo* complexity and *in vitro* modularity. A developing kidney is extracted from an embryo upon reaching the metanephros state and then is cultured in an optimized medium. In these models, classically a cAMP stimulator is used to induce cystogenesis (**Figure 1.16a**). Indeed, paradoxically developing kidneys do not on their own develop cysts *in vitro* even when extracted from embryos that would die *in utero* due to a PKD. Natoli *et al.* used this type of model to develop a therapy assay for ADPKD (Natoli *et al.*, 2008) The use of embryonic kidneys allows them to follow more closely cystogenesis, notably because of faster response of the kidneys to drugs. Furthermore, because *Pkd1*^{-/-} mice die at the embryonic stage, it limits the usefulness of such animals to study cystogenesis processes. They could closely compare cyst development induced by cAMP stimulator depending on the *Pkd1* haploinsufficiency, showing that cystogenesis was *Pkd1* dose-dependent in their model. Almost simultaneously, Yang *et al.* used *in vitro* embryonic kidneys as a screening assay intermediary between screening with classical 3D cultures and *in vivo* models. They screened CTFR inhibitors with their models and demonstrated that the inhibitor that could prevent cystogenesis *in vitro* worked *in vivo* to slow cyst onset.

Freedman *et al.* established a protocol to differentiate kidney organoids from hPSCs (Cruz *et al.*, 2017). They used these organoids as models for ADPKD by deleting *PKD1* or *PKD2* with CRISPR. They could then observe spontaneous cystogenesis from PKD organoids that was absent from control. In their work, they experimented with several types of culture environment for their kidney organoids, from adherent organoids to suspended organoids to finally culture in ECM. Interestingly they observed that the microenvironment had a drastic impact on cystogenesis (**Figure 1.16b**). Indeed, substrate adhesion limited cystogenesis. Furthermore, organoids displayed very different behaviors once embedded in a suspended hydrogel. WT organoids had a better ability to migrate and remodel the ECM, but PKD organoids no longer formed cysts. Possible affinity and interactions with the ECM are dependent on PC1 and also limit cystogenesis. Interestingly cyst growth from cAMP stimulation appeared to be transient, indicating that in this case, cysts from fluid secretion are

potentially purely mechanical. Facioli *et al.* cultivated kidney organoids generated from iPSCs from ADPKD patients' erythroid cells (Facioli *et al.*, 2021). They used the same protocol as Freedman *et al.* to differentiate the iPSCs into kidney organoids, but surprisingly did not observe any spontaneous cystogenesis from ADPKD derived kidney organoids as iPSCs derived from ADPKD patients may still express *PKD1* or *PKD2* if the original cell is not fully depleted of a functional gene. They could induce cystogenesis with forskolin and showed that cyst growth was much more important in ADPKD organoids than in organoids derived from a healthy donor, similarly to what was observed with mouse embryonic kidneys.

A caveat with kidney organoids is their lack of collecting ducts; segments that happen to be the most prone to cystogenesis in human ADPKD, especially at early stages. Furthermore, both Freedman *et al.* and Facioli *et al.* reported low cyst incidence in case of adherent organoids or for organoids with an ECM. Mouse embryonic kidneys, despite being in suspension, failed to generate cysts on their own, contrary to Freedman *et al.* organoids. It is possible that embryonic kidney tubules are surrounded by their own ECM and thus oppose higher resistance to cystogenesis. Furthermore, kidney ECM has been shown to improve maturation of kidney organoids (Kim *et al.*, 2022). It may be that the Freedman *et al.* model lacks essential ECM components. In any case, kidney organoid tubular structure appears

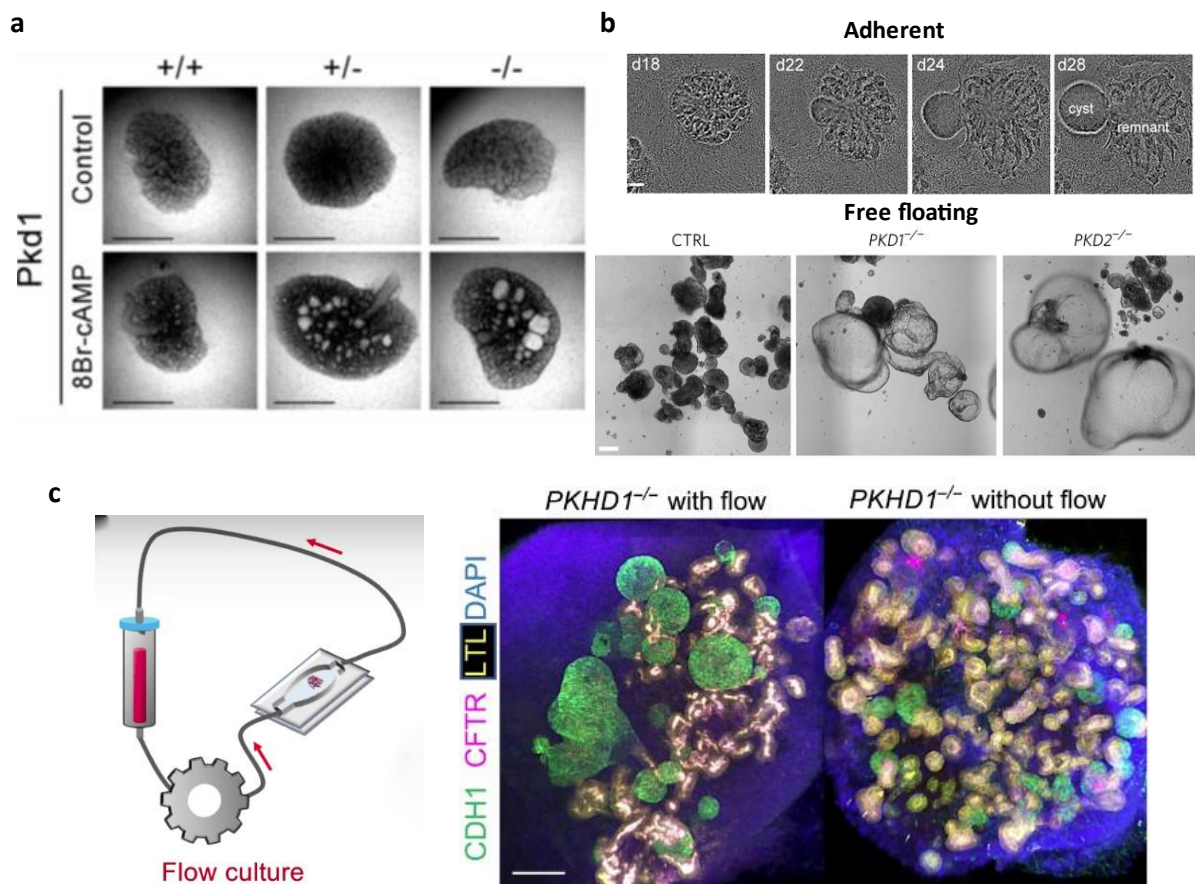


Figure 1.16: Kidney organoids for polycystic kidney disease. It is possible to grow in vitro embryonic kidneys. These kidneys do not spontaneously form cysts even in the absence of the ADPKD genes. A cAMP promoter needs to be added to promote cyst growth and assess their ability to form cyst (a)(from Natoli *et al.* 2008, scale bar: 1mm). Alternatively, it is possible to grow kidney organoids from stem cells. Depending on if they are adherent or free floating, they will generate more cyst growth when *PKD1/2*^{-/-} (b) (from Cruz *et al.* 2017, scale bar: 100µm). Culturing a kidney organoid in a flow chamber can not only improve differentiation but appears to be necessary for cystogenesis in a PKD model (*PKHD1*^{-/-})(c) (adapted from Hiratsuka *et al.* 2022, scale bar: 100µm)

determined greatly by their environment. Utilising a structure separated from the kidney presents the advantages of modularity but then is also removed from the kidney normal environment. As early as 1986, Avner *et al.* showed that when taken outside of a *cpk* mouse model, cystic embryonic kidney had a regression of the cystic phenotype towards a regular tubular structure (Avner *et al.*, 1986). This example demonstrated how in fact cystogenesis happened in response to the native environment. We also saw how mechanical cues can be important for cell differentiation and can be considered even more important in the context of ADPKD. All of the *in vitro* models we cited lack hydrodynamic stresses.

Microphysiological systems allow the artificial introduction of physiologically relevant mechanical stresses to biomimetic constructs. Flow is an example of stress that can be generated with the help of microfluidics technology. A recent system integrating kidney organoids with microfluidics to study a PKD is the Hiratsuka *et al.* platform (**Figure 1.16c**) (Hiratsuka *et al.*, 2022). They developed kidney organoids from ARPKD patients and had to use cAMP stimulation to induce cystogenesis. However, subjecting their organoids to flow rescued cystogenesis without the help of cAMP stimulation. In their system the organoid was not perfused itself but adherent to a chamber subjected to a subphysiological flow. Questions could remain over the manner shear influenced the phenotype and how it is felt by the cells. They showed that loss of the primary cilium abrogated the cystic phenotype. They also showed that flow in the lumen led to tension of the cell membrane. Unfortunately, the largest potential issue with their model is the unknown distribution of flow inside the lumens and the shear stress that is ultimately felt by the cells. Nonetheless, this model provided some precious insight on the necessity to integrate an hydrodynamic dimension to kidney models studying PKD. Embryonic kidneys, despite having the proper genotype, potentially fail to generate cysts because they lack essential hydrodynamic cues involved in cystogenesis. In certain models, such as certain kidney organoids, the lack of a proper mechanical microenvironment may compensate for the absence of hydrodynamic stresses. Yet as soon as this microenvironment is reintroduced, hydrodynamic constraints become necessary. This may denote the need to improve and modulate the models on both the ECM and the hydrodynamic side to recapitulate the subtle balance between tubular structure and cyst formation.

To summarize (**Table 1**), 3D *in vitro* models to study cystogenesis in PKDs provided a way to isolate mechanisms and environmental cues to better assess their importance. Furthermore, when applied to drug screening, these models provide the possibility of conducting high throughput assays that can be evaluated using simple metrics. However, in their simplest form, these models appear to be very cell line dependent, certainly because of different self-morphogenic potential from these cell lines. The use of different types of ECM can also markedly impact the self-organization of the cells: indeed, they provide different mechanical and biochemical environments. A decellularized kidney is mostly the same as a whole organ in terms of shape and mechanical properties. A more sophisticated approach consists of building for the cells a similar scaffold, that would orient their behavior. Such an approach has been used for kidney models but has not been widely applied to PKDs. An alternative is the organoid approach wherein the self-organization potential of stem cells is harvested to get as close as possible to kidney structures. This powerful tool offers a clear workflow and reproducible method to model a patient's kidney *in vitro*. Furthermore, kidney organoid culture is compatible with the material commonly found in biological labs and does not represent exotic technical challenges. They can be implemented into versatile culture platform from the multi-well plates to fluidic chips. By that, it could be a powerful tool for personalized medicine in PKD's. Nonetheless this approach is not clearly a bottom-up

approach. An organoid remains a complex object with a lack of control of other potentially key environmental parameters for the cell. In fact, they do not offer on their own a complete biomimetic environment, as they lack the hydrodynamic dimension of a kidney. Organ-on-chips propose to integrate in one same system modulable hydrodynamic stresses with key structural features of kidneys in a biomimetic environment. Unfortunately, this approach is currently lacking in the field. Because ADPKD is a disease that encompasses problems including the control of geometry and mechanical stresses, we think kidney-on-chips could greatly benefit investigations on the key mechanisms around cystogenesis.

To this end, we designed a perfusable multitubular kidney-on-chip where we can tune the hydrodynamic stresses that we present in the next chapter. Mimicking the kidney tubular geometry in a biomimetic scaffold will allow us to decipher the evolution of a kidney epithelium tubular geometry in respect to the expression of *Pkd1*. Then this, by controlling the hydrodynamic stresses, FSS, and intraluminal pressure applied on this tubule, will allow us to assess the impact of these constraints on the tubular geometry. Finally, we will study mosaicism and competition between cells expressing different levels of *Pkd1* in our chip.

	Complexity/ Fidelity to in vivo	Modularity	Scalability	Human cells?	Bottom-up approach?
Cell Culture in hydrogel	Simplest 3D model	-Very dependant on the type of hydrogel -Important variability across cell lines	highest throughput, easiest to analyse	Possible	Limited
Organoid	-Kidney elementary structure, with multiple cell types	-Dependant on the stem cell source -Possibility to culture in a MPS tomimic physiological stresses but no actual hydrodynamic control	-High throughput -Standardization	Possible	Not really
Embryonic kidney	-Closest in vitro model to an actual kidney	No example of culture under physiological stresses	Scalability?	Not possible	No
Kidney-on-chip	-Possibility to organize and structure multiple compartments with different cell-type	-Cell line variability -Geometric control and possibility to organize/compartimentalized the microenvironment -Control and mimicking of mechanical stresses	Standardization/Scalability VS complexity	Possible	Yes

Table 1 Summary of the different 3D *in vitro* models used for PKDs

2. A multitube and perfused kidney-on-chip

In the previous chapter, we delved into the importance of 3D geometry and hydrodynamic constraints, akin to another dimension. These are of capital importance to capture the physiology of the organ. If we bring the problem back to ADPKD, these features of the kidney epithelium are essential to decipher what happens when a cyst forms. The pertinent dimensions within the kidney put us in very low Reynolds number regime with flows in the order of nL/min and geometries in the order 10-100 microns. These dimensions are perfectly compatible with the use of microfluidics technologies. Hence these technologies offer relevant ways to mimic what happens in the kidney in terms of mechanics: a perfused tubular microfluidic channel offers a microenvironment similar to a nephron in a cell. Furthermore, in order to observe phenomena of tubular dilations, the materials used as a scaffold must be deformable or degradable simply by cells or by physiological pressures. The scaffold should possess mechanical properties closely resembling those of the kidney ECM. This is essential not only for enhancing cell differentiation but also for effectively capturing the equilibrium between the epithelium and the hydrodynamic constraints. Hydrogels stand out as materials that possess these mechanical attributes. Current techniques allow through multiple ways to emulate the kidney tubule microenvironment into hydrogels similar to the kidney ECM. We can find many kidney-on-chips in literature that capture potentially several or all these aspects. As such they represent untapped opportunities to study ADPKD with a reductionist approach. In the beginning of this chapter, we will review different approaches to address these features with different examples of a kidney-on-chip.

Nevertheless, to emulate the renal function, mimicking one tubule can be insufficient. The entanglement of parallel tubular structures, from the epithelial and endothelial compartment, is a central aspect of the kidney function. Furthermore, interactions between nephrons are seemingly critical for the ADPKD pathogenesis. Regrettably, this aspect has only been implemented in kidney-on-chip available in the literature with compromises concerning other essential features. Our group previously tackled the issue and designed its own multitube kidney-on-chip while preserving a tubular geometry as close as possible to the kidney tubules. We will briefly introduce this model.

However, this chip exhibited notable limitations in terms of capturing the hydrodynamic dimension of the kidney. In response, we will then see how we designed a new chip that encompassed both this aspect and multitube geometry. The culmination of our efforts is a three-dimensional construct that stands as one of the most faithful models of renal dynamics achieved thus far.

2.1. Overview of preexisting kidney-on-chip: why they are not enough for our question.

Kaysen et al in 1999 published the first *in vitro* cell culture mimicking shear stress on renal epithelial cells that provided evidence of shear stress modulated gene expression in renal

epithelial cells (Kaysen *et al.*, 1999). Their system consisted of a horizontally cylindrical culture vessel, turning on its long axis, with a coaxial oxygenator. Beads were used as substrates for the cells to be able to grow under shear, forming aggregates. Before them, Stathopoulos and Hellums published in 1984 a human embryonic kidney cell culture under shear stress in a flow chamber, which seems to be first work attempting at recapitulating the fluidic component of the kidney *in vitro* (Stathopoulos and Hellums, 1985). Cai *et al.*, followed by many, similarly cultured later renal confluent epithelium in parallel-plate flow chambers to study the phenotypic changes induced by physiological flow shear stress (Cai *et al.*, 2000a; Essig *et al.*, 2001; Duan *et al.*, 2008). All those cell cultures introduced flow, a modality essential to the organ function, they can thus qualify as proto-organ on chips. Ingber *et al.* lung-on-chip system published in 2010 is often pointed at as being a pioneering example of the organ-on-chip technology (Huh *et al.*, 2010). This chip adopted a transwell configuration, featuring two chambers in polydimethylsiloxane (PDMS) separated by a porous membrane. On each side of this membrane, two different cell types could be cultured and those chambers could be perfused independently. This chip introduced one more modality on top of flow and a functional interface: thanks to two side chambers pneumatically actuated, the chip could mimic contractions of breathing lung alveola. This system was adapted to many organs and the chip was later commercialized as a standard organ-on-chip system by the company Emulate. PDMS was subsequently often adopted by many for organ-on-chips because it is biocompatible, permeable to gas, easily deformable, transparent, and easily shaped with soft lithography technics.

The same group later published a similar system adapted to the kidney epithelium (**Figure 2.1.a**). Mimicking the proximal tubule, their PDMS chip consisted in two chambers separated by a porous membrane coated with collagen IV (Jang *et al.*, 2013). On the apical chamber laid a proximal tubule cells monolayer. The basolateral chamber on the bottom served as a reservoir collecting what was mimicking the kidney interstitial fluid readily available for sampling. Physiological flow was applied on the apical side (0.2 dyn.cm^{-2}).

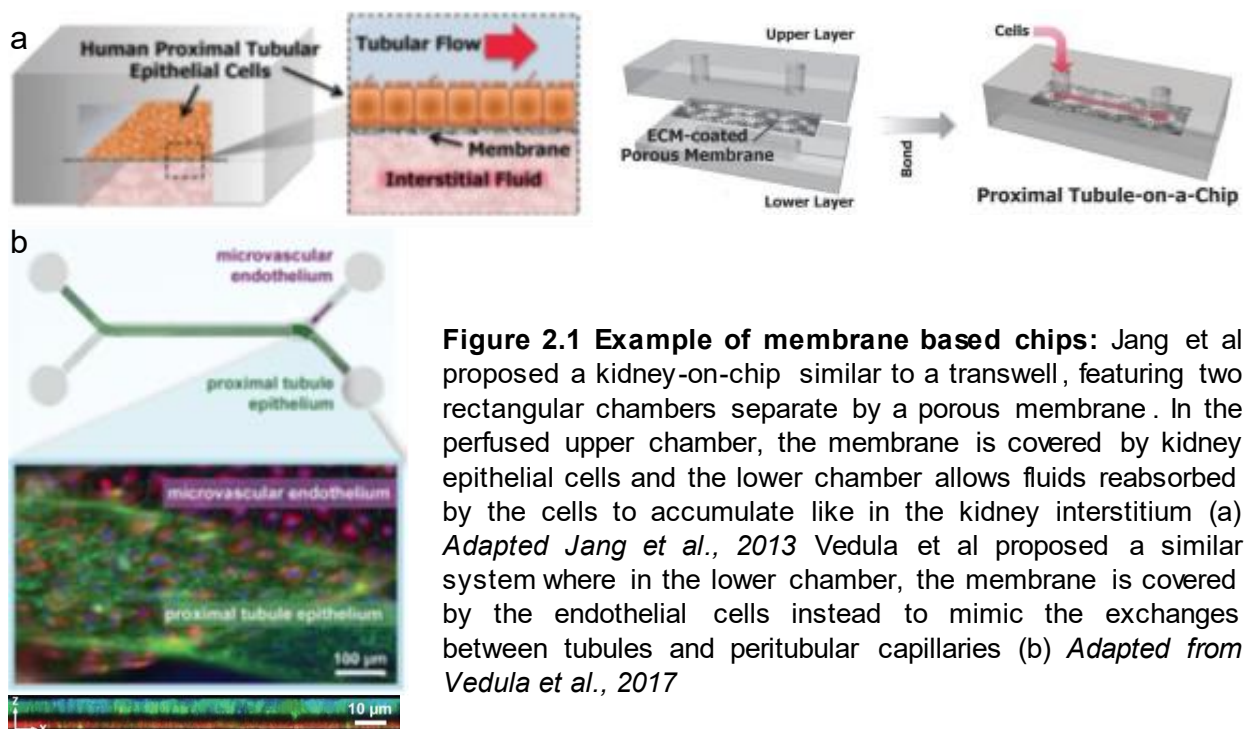


Figure 2.1 Example of membrane based chips: Jang *et al.* proposed a kidney-on-chip similar to a transwell, featuring two rectangular chambers separate by a porous membrane. In the perfused upper chamber, the membrane is covered by kidney epithelial cells and the lower chamber allows fluids reabsorbed by the cells to accumulate like in the kidney interstitium (a) Adapted Jang *et al.*, 2013 Vedula *et al.* proposed a similar system where in the lower chamber, the membrane is covered by the endothelial cells instead to mimic the exchanges between tubules and peritubular capillaries (b) Adapted from Vedula *et al.*, 2017

This chip was developed for nephrotoxicity assessment. Adjunction of FSS led to better barrier function from the kidney cells and overall better cell differentiation comparatively to chips in static conditions. Notably this chip displayed strikingly a more *in vivo* like response to kidney injuries, emphasizing on the limitation of classical *in vitro* model, notably for preclinical studies.

In a system very similar to Emulate's system, Vedula et al introduced a coculture bringing together an endothelial compartment and an epithelial compartment (Vedula *et al.*, 2017). The two chambers of the chip mimicked the interface between a proximal tubule and a peritubular vessel, separated by a porous membrane as the interstitium (**figure 2.1.b**). Although potentially capable of such integration, they did not include a flow shear stress in their study. Nonetheless this chip presented increased proliferation and metabolic activities compared to monocultures. If those two systems were a step forward to recapitulate the reabsorption functions of the kidney epithelium, they suffered however one major caveat as they did not reproduce the physiological tubular geometry of the kidney.

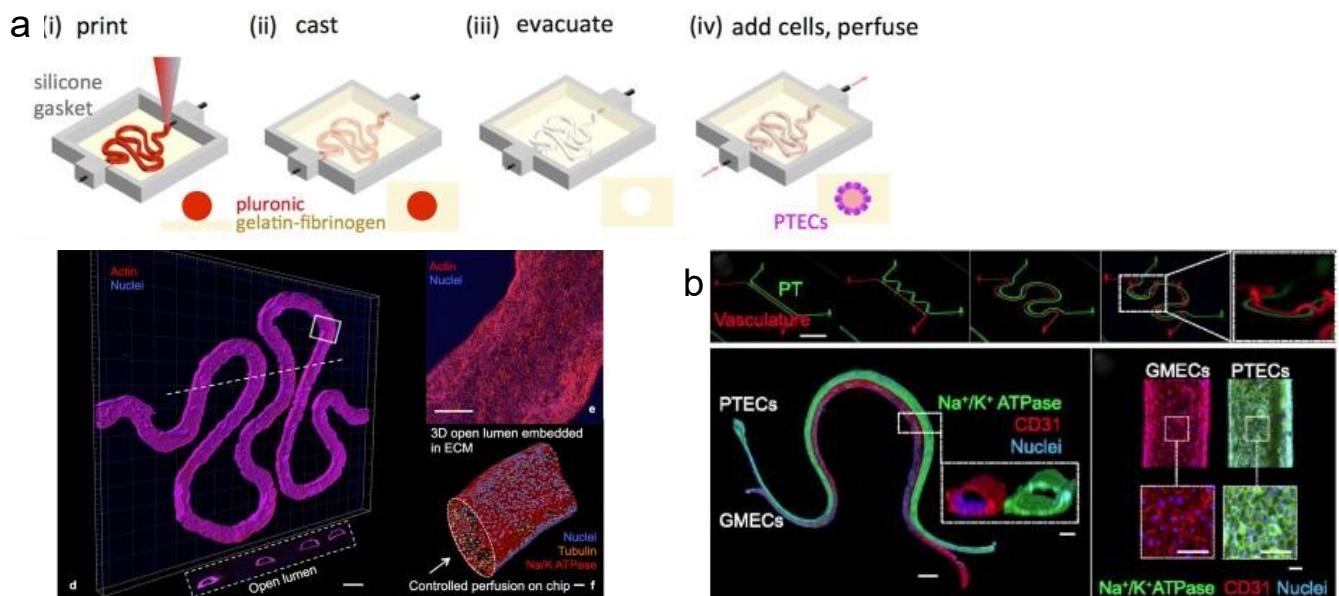


Figure 2.2: Example of chip using bioprinting Homan *et al* used 3D bioprinting to mimic tubular kidney epithelium. This technology allows them to print 3D convoluted tubules with a sacrificial hydrogel inside a gelatin-fibrinogen gel cast around. Once the sacrificial gel removed, a hollow channel can be seeded then perfused (a) *Adapted from Homan et al., 2016* Later the same group complexified their construct by printing side by side two convoluted channels, one of which is mimicking a peritubular capillary (b) *Adapted from Lin et al., 2019*

3D bioprinting offers a sophisticated approach to produce tubular structures made of hydrogel. Some kidney-on-chip models rely on this technology by printing negatively the tubular structures into a scaffold hydrogel with a sacrificial hydrogel (**figure 2.2.a**). In the Homan *et al.* system, a Pluronic convoluted tubule was deposited inside a gelatin-fibrinogen scaffold (Homan *et al.*, 2016). Pluronic was then liquified and washed away, leaving behind a hollow convoluted tubule. Interestingly, the Pluronic mixture contained thrombin which locally promoted fibrin polymerization surrounding the tubule, potentially mimicking a basement membrane conferring additional support to withstand perfusion. Subsequently, kidney cells were seeded into the tubule and let form a confluent monolayer. This tubule could be perfused because it was integrated into a perfusable PDMS chip wherein the channels were directly connected to the convoluted tubule. Although their system presented a much higher diameter

than a proximal tubule *in vivo* (450 μm the smallest that they showed vs 50 μm), the authors results suggest that such curvature on top of shear stress already had an interesting effect on kidney cells differentiation. This substantially increased their height and polarization. Indeed, we saw in the previous chapter that epithelial cells could already sense curvature as a tissue even if the curvature was too small to be perceived by a single cell. In a following study, they complexified this system by printing very closely (around 70 μm apart), an endothelial and an epithelial channel (Lin *et al.*, 2019). To the curvature and flow shear stress, this system added the kidney reabsorption dimension. In this system, epithelium and endothelium could be fluidically addressed independently (**figure 2.2.b**). The 3D tubular structure greatly increased the reabsorption of glucose from the epithelium to the endothelium compared to a transwell. Homan *et al.* group further demonstrated that 3D bioprinting offers a technique to closely approach the nephron in terms of geometry, hydrodynamic stresses, and interfaces. This technique is very powerful to template geometrically complex structures presenting several curvatures such as kidney convoluted tubules networks. However, probably due to the limitations of 3D printing, current models using 3D bioprinting can only generate tubular structures with a curvature at least an order of magnitude smaller than the actual nephrons.

Alternatively, to 3D bioprinting, it is possible to mold hydrogels with tubular objects with a predefined shape, notably using wires. Scaffolds made with soft lithography techniques, for instance, allow precise positioning of the wires and later integration of the resulting tubule upon wire removal into the fluidic chip. Using this technique, Weber *et al* adapted a commercial organ-on-chip scaffold developed by Nortis for formation of endothelial vessels (Tourovskiaia *et al.*, 2014; Weber *et al.*, 2016). The system was made of a PDMS chip guiding two 125 μm microfibers placed in parallel in a collagen I matrix. Upon removal, the microfibers left two

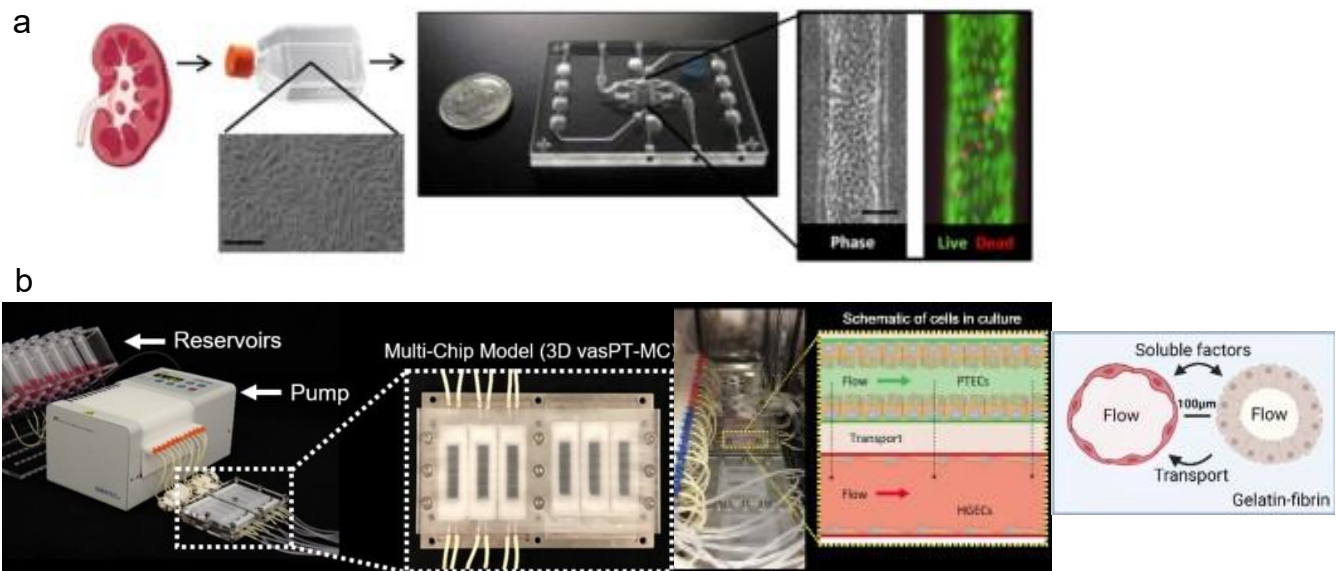


Figure 2.3: Example of chips based on wire molding. Weber *et al* used Nortis technology that consists of two parallel perfused channels molded by a wire into a hydrogel to mimic a kidney proximal tubule in one of them. The second channel has been used to mimic a peritubular capillary, however the important distant between the two channels limit the exchanges(a) Adapted from Weber *et al.*, 2016 Carracedo et al also used wire molding but this time bringing the two channels closer to facilitate exchanges. They also optimized their design to facilitate multiplexing (b) Adapted from Carracedo *et al.*, 2023

channels separated by 1 mm. The channels were then coated with collagen I to mimic the basement membrane. This chip allowed the development of an epithelial channel in parallel to

an endothelial channel to mimic the interactions between the two compartments. With their experiments, the authors could notably show that their proximal tubule-on-chip could recapitulate vitamin D metabolism as well as key reabsorption and secretion functionalities between the epithelial channel and the mock vascular channel. Chapron *et al.* then implemented an actual endothelial compartment (Chapron *et al.*, 2020). In their system, they focused on the secretive capacities of their proximal tubule epithelium from the intake from the endothelium. Their model demonstrated to be the first tubular system with good selective secretion capacities. Nevertheless, the important distance between channels certainly limited the performance of their system, as a 1000 μm interchannel distance is not comparable to the few microns separating channels in the kidney parenchyma. A chip recently developed by Astrazeneca managed to integrate perfused tubular structures as closed parallel channels. This multiplex kidney-on-chip consisted of 150 μm tubular channels duets separated by 100 μm (Carracedo *et al.*, 2023). In this model, the fibrin-gelatin matrix proved to be critical for enhanced differentiation. In their comparison with more classical models, the effect of shear stress and curvature were not decoupled compared to transwells, but increasing the complexity of the model shifted the transcriptional profile towards a profile of a healthy kidney in contrast to the simplest transwell-like models leaning toward a pathological transcriptional profile. Furthermore, their system allowed high throughput thanks to multiplexing, offering an interesting advantage for drug screening. Nevertheless, we must note that the use of gelatin-fibrin for their ECM does not offer a microenvironment with a component naturally present in the kidney ECM.

Finally, using stamping techniques on thin collagen layers, Rayner *et al* could achieve the closest proximity between channels in a kidney-on-chip, similar to kidney parenchyma. Their construct consisted of two stamped collagen layers separated by a collagen membrane. One layer was crossed by 150 μm wide parallel channels for the epithelium and the other layer was crossed by channels in a grid for the endothelium (**figure 2.4.a**). Interestingly, cells remodeled the ECM making the central membrane gradually shrink, and the two layers got closer after several days of culture until being separated by a few microns (**figure 2.4.b**) (Rayner *et al.*, 2018). However, fabrication of such a chip appeared to be particularly complex.

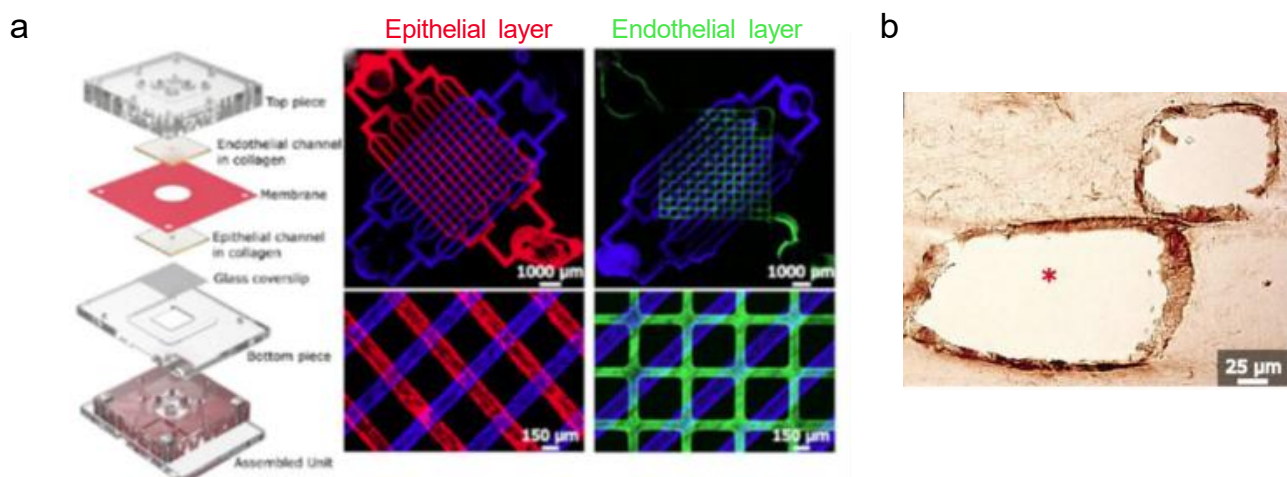


Figure 2.4: Rayner *et al* Engineered a human renal vascular-tubular unit by stacking collagen I layer. One features parallel epithelial tubules while another features a gride of endothelial vessels . They are separated by a thin collagen I membrane (a) As the tissue matures, the epithelium and endothelium almost come in contact in a manner resembling a lot what happens in the kidney parenchyma (b) Adapted from Rayner *et al.*, 2018

Of all the strategies that we just presented (**table 2.1**), we saw that globally increasing the system complexity to get closer to an *in vivo* configuration resulted in cells with more faithful phenotypes. Nevertheless, none of these systems had diameters under 100 μ m. In Xi *et al.* MDCK migration experiments under tubular confinement that we described in the previous chapter, going under this threshold on non-physiological scaffold in static conditions seemed critical for curvature alone to have a certain effect on the epithelium organization, migration capacities and cell polarity (Xi *et al.*, 2017). Moreover, as diameter decreases, confinement of the cells also increases. This likely facilitates epithelial paracrine signaling within the epithelium, particularly in a tubule configuration with perfusion, potentially leading to an elevation in the concentration of intraluminal molecules. This could serve to counterbalance the effects of flow clearance. Although unclear, paracrine signaling may serve to regulate the kidney reabsorption capacities, for example in reaction to stresses. In pathological contexts, paracrine signaling may become even more relevant. Notably, in the case of ADPKD, we established that chemical signaling may play an important role in propagating the cystic phenotype. Notably, when considering a snowball effect spreading the cystic phenotype between nephrons, proximity between said nephrons becomes a critical factor. This is all the truer if we consider the detrimental impact of the mechanical stress of expanding cysts on neighboring tubules. Aside from the three aforementioned models, it is difficult to find a kidney-on-chip allowing the generation of tubules reasonably close enough. Recognizing the limitations of preexisting models, there is an opportunity to create a kidney-on-chip platform that comprehensively addresses crucial facets of the kidney microenvironment for studying ADPKD.

Type of model	Published models	Geometry	Channel size	Spacing between different channels	perfusion
Transwell-like	Jang <i>et al.</i> , 2013 Vedula <i>et al.</i> , 2017	Rectangular	Several mm	A few microns	Yes
3D printed	Homan <i>et al.</i> , 2016 Lin <i>et al.</i> , 2019	Tubular convoluted	450 μ m the smallest	70 μ m	Yes
Wire molding	Weber <i>et al.</i> , 2016 Chapron <i>et al.</i> , 2020 Carracedo <i>et al.</i> , 2023	Tubular straight	120 μ m	1000 μ m	Yes
Stamped	Rayner <i>et al.</i> , 2018	Tubular straight	150 μ m	A few microns between layers and 300 μ m between parallel channels	Yes
Our chip	X	Tubular straight	80 μ m	100 μ m	Yes

Table 2.1: Comparison between different kidney-on-chip described in the literature and the final model described in this thesis

2.2. A previously developed solution in the lab

2.2.1 A multitubular chip design and fabrication

Previously we developed a chip that mimics the dense tubular structures in kidney parenchyma (**figure 2.5**)(Myram *et al.*, 2021). In this chip, hereafter designated as the COC chip, a scaffold made of hot-embossed COC (Cycloolefin Copolymer) features guides for up to 7 wires to be placed in parallel, spaced by either 100 μ m or 200 μ m. Five tungsten wires (80 μ m in diameter) are positioned precisely with the guides to cross a chamber regularly for the collagen pouring and molding, along with two identical main channels as well as PTFE tubing at the opposite of the chip which forms the input and the output. The chip is closed, except on the collagen chamber, by commercial PCR tape. The central chamber surface is treated for collagen adhesion and a drop of collagen I at 6mg/mL is placed on the chamber, surrounding the wires. After collagen polymerization, the wires are removed to generate the tubular channels inside the collagen. These channels are coated with laminin before being seeded with the kidney cells. Here we use tungsten wires because of their interesting mechanical properties. Tungsten being the sturdiest pure metal, much harder than stainless steel (around 400 GPa versus around 200 GPa) while still being biocompatible, is less exposed to deformations when manipulated which becomes critical with such thin wires. Furthermore, we use collagen at 6 mg/mL which is much more concentrated than what is typically found in the literature, where gels between 2-4 mg/mL are more frequent. There are two reasons for this, : first, a denser gel makes it easier to have much closer wires without risk of tearing the gel upon removal. Second, although 2-4 mg/mL collagen I gels have a similar Young modulus to the global kidney cortex (between 1-10 kPa), the basement membrane supporting the kidney cells has a modulus between 0.1-1MPa. By employing a 6mg/mL collagen I gel, the matrix gets to 10-100 kPa, at an intermediate range of stiffness. This can also present a good

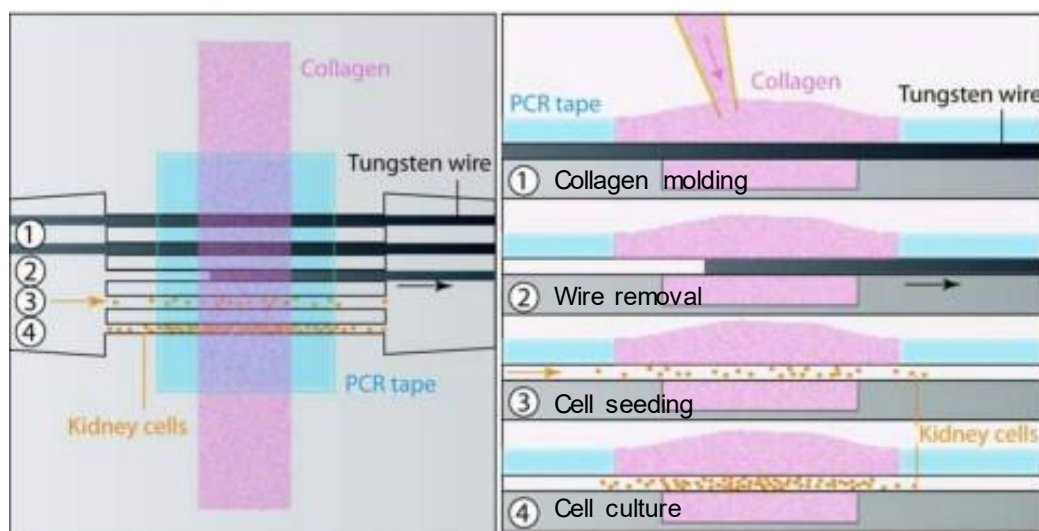


Figure 2.5: Multitubular COC chip. Our group developed a multitubular kidney-on-chip based on a COC scaffold. The scaffold allows to precisely position several tungsten wires to mold parallel channels in collagens. Here a sketch summarize the chip fabrication *Adapted from Myram et al., 2020*

compromise with the fact that the higher rigidity offered by the basement membrane is very localized. Without being able to reproduce this structure artificially,

2.2.2. Lowering the spacing of the channels in this chip may promote tubule deformation in an ADPKD model.

We used this chip to study for the first time the tubular deformation occurring in ADPKD. To do so, we seeded the chip with immortalized mouse Proximal Convoluted Tubule cells (PCT) obtained from Stefan Somlo's lab. A control cell line was heterozygous for *Pkd1* (*Pkd1*^{+/-}), while another, derived from this control cell line, had a deletion on both *Pkd1* alleles (*Pkd1*^{-/-}). After seeding 200µm-spaced channels with those cells, we saw an important difference in behavior regarding the tubule diameters as function of *Pkd1*. PCT *Pkd1*^{+/-} overall did not alter the original tubular shape while PCT *Pkd1*^{-/-} homogeneously dilated the channels (**Figure 2.6.a**). Interestingly, bringing the channels closer, at 100µm spacing, significantly increased dilation for PCT *Pkd1*^{-/-} cells but not for control cells (**Figure 2.6.b**). Remarkably in some instances, the channels could come in close contact, which would not have been possible with significantly higher channel interspace. This experiment validated the interest of having channels closer to each other to model ADPKD, as it could confirm the importance of interactions promoting cystogenesis between adjacent channels. We described previously how these interactions could be of chemical origin or mechanical origin. Unfortunately, this experiment does not allow decoupling of these two possible origins.

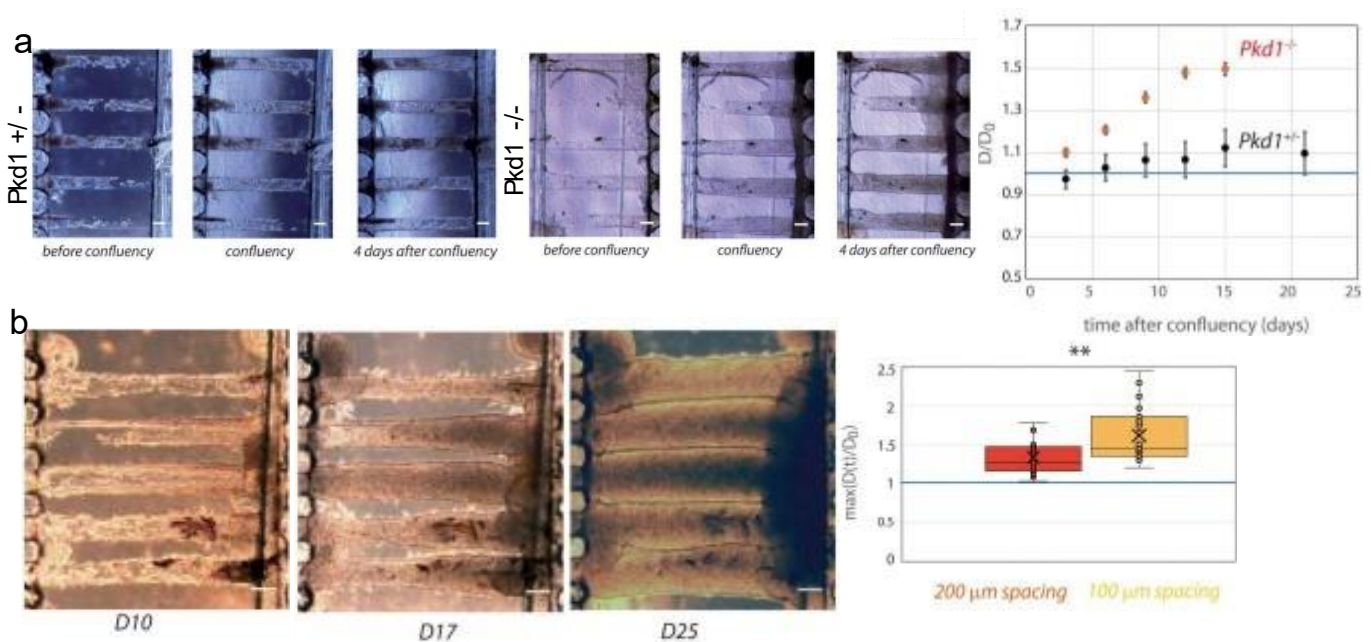


Figure 2.6: Important channel dilations possibly promoted by channel proximity in our COC chip modelling ADPKD We seeded the COC chip with PCT *Pkd1*^{+/-} and *Pkd1*^{-/-} cells and observed important dilations of the channels with *Pkd1*^{-/-} cells (a) Bringing the channels closer (100µm vs 200µm spacing) led to increase of channel deformation while in some instances channels almost ended up touching each other (b) scale bars, 50µm Adapted from Myram et al., 2020

2.2.3 A compromise between a design achieving faithful geometry and poor fluidic control?

The problem of multiplexing

With this COC chip, we could achieve one of the most physiologically relevant geometry for a multitubular kidney-on-chip. However, perfusion with this chip remains one of its weakest points. As a result of the way the wires are positioned in the chip, the resulting channels in the collagen are all fluidically connected. Furthermore, the narrowest sections in the chip are found in the collagen channels, which makes them the most fluidically resistive parts. Hydraulic resistance is inversely proportional to the radius at the power of 4, which means that small variation of radius between two channels rise to significant variation in term of resistivity. Such variations can be expected when molding a material like collagen I. Some channels may be noticeably smaller or wider. A channel 10% narrower, which is not uncommon, would result in a channel 50% more resistive in theory. Furthermore, there is probably an even higher uncertainty regarding the height of the epithelium. If we add to this the height of cells inside the lumen, differences between radius across channels get even higher.

If we want to perfuse this device with a fluid of viscosity μ , there are two available options. We want to set up a given shear stress τ_{target} on the channel walls with a radius r . To do so, we need to set up a given volumetric flow rate Q_{target} in the channel following:

$$\tau_{target} = \frac{4\mu Q_{target}}{\pi r^3} \quad (2.1)$$

It can be done with a control on pressure, wherein we initially set up a pressure gradient ΔP_{set} between the inlet and outlet of the system to reach the target volumetric flow rate in channels with an expected resistivity R_{H0} allowing a shear stress τ_{target} . If we neglect the resistivity of inlet and outlet channels:

$$\Delta P_{set} = Q_{target} R_{H0} \text{ and } \tau_{target} = \frac{4\mu \Delta P_{set}}{R_{H0} \pi r^3} \quad (2.2)$$

$$\text{For a channel with a length } L \text{ and a circular section: } R_H = \frac{8\mu L}{\pi r^4} \quad (2.3)$$

$$\text{Thus: } \Delta P_{set} = \tau_{target} \frac{2L}{r} \quad (2.4)$$

If we consider that one channel has an effective radius r_{eff} with a perturbation α compared to r_o because of slight dilations or obstruction:

$$r_{eff} = (1 + \alpha)r_o \text{ and } R_{Heff} = \frac{R_{H0}}{(1+\alpha)^4} \text{ then } Q_{eff} = (1 + \alpha)^4 Q_{target} \text{ and } \tau_{eff} = (1 + \alpha)\tau_{target} \quad (2.5)$$

In this case, the evolution of the resulting flow shear stress is proportional to the enlargement ratio of the channel, and a perturbation in one channel does not have a consequence on the other channels.

Alternatively, it can be done with a control on flow, with a syringe pump for instance. In this configuration we could impose an overall volumetric flow rate in the system (Q_{tot}). In the COC chip, the parallel channels join in an inlet channel and in an outlet channel. Any volumetric flow

from any of these two is therefore split between the channels. Ideally, because the channels would have the same radius, the flow would be split equally:

$$Q_{target} = \frac{Q_{tot}}{n} \quad (2.6)$$

If we take the case of two parallel channels with one channel that has a radius with a perturbation α compared to the other one:

$$r_2 = (1 + \alpha)r_1 = (1 + \alpha)r_0 \text{ and } R_{H2} = \frac{R_{H1}}{(1+\alpha)^4}$$

$$\text{then } Q_2 = (1 + \alpha)^4 Q_1 \text{ and as } Q_{tot} = Q_1 + Q_2 = 2Q_{target}$$

$$\text{then } Q_2 = \frac{2(1+\alpha)^4}{(1+\alpha)^4+1} Q_{target} \text{ and } Q_1 = \frac{2}{1+(1+\alpha)^4} Q_{target}$$

$$\text{and as a result } \tau_2 \propto \frac{2\alpha}{(1+\alpha)^4+1} \tau_{target} \text{ and } \tau_1 \propto \frac{(1+\alpha)}{1+(1+\alpha)^4} \tau_{target} \quad (2.7)$$

We can generalize this result with a chip with n channels:

$$r_n = (1 + \alpha)r_{1\dots n-1} \quad Q_n = \frac{n(1 + \alpha)^4}{(1 + \alpha)^4 + n - 1} Q_{target} \text{ so } \tau_n \propto \frac{n(1 + \alpha)}{(1 + \alpha)^4 + n - 1} \tau_{target}$$

$$\text{and } Q_{1\dots n-1} = \frac{n}{(1+\alpha)^4+n-1} Q_{target} \text{ so } \tau_{1\dots n-1} = \frac{n}{(1+\alpha)^4+n-1} \tau_{target} \quad (2.8)$$

We see here that a perturbation on the radius of one channel has repercussions on all the other channels. This perturbation is magnified when looking at the shear stress. For instance, with two channels, a radius increase of 10% in one channel translates into a decrease of shear stress of 20% in the other channels. Increasing the number of channels can limit the impact of a single channel perturbation. If we look at the perturbed channel, the situation is more complicated. The resultant alteration of shear stress due to a perturbation in radius is not monotonous and will also depend on the number of channels, and remarkably there is an optimal number of channels to limit the perturbation impact. An actual experimental situation will be the result of several perturbation across all channels, which will make the effective shear stress in these channels highly unpredictable. As a result, increasing the number of channels perfused in parallel to stabilize the system, on top of being technically challenging, does not guarantee a satisfactory result.

Taking this into account, we can say that controlling pressure may seem preferable. However, we only considered homogeneous deformations of the channels so far. The inner radius along the channel may vary significantly, especially in the presence of cells. Since resistivity evolves inversely proportional to radius⁴, the resulting volumetric flow rate will largely be set by the narrowest sections of the tubule. The consequence is that resulting shear stress on widest sections of the tubule will be largely perturbed. In conclusion, multiplexing with the COC chip, because of its design, does not allow for sufficient fluidic control on individual channels.

The problem of seeding.

Cell seeding in the COC chip is done by gently pipetting a cell suspension into the inlet of the chip. Consequently, there is little control over the number of cells that go into each channel in one pipetting. Indeed, here seeding is like a flow-controlled perfusion of the chip. Therefore, the volumetric flow rate of cell suspension going into each channel is very variable. Since cells are objects with an important diameter compared to the channels, for a given cell

concentration, different volumetric flow rates can translate into a bigger difference in term of number of cells entering one channel. Furthermore, after pipetting, channels tend to empty themselves from non-adherent cells. The reason for that is not entirely clear. Possibly deformations of the collagen due to the perfusion when releasing generate flows going out of the channels. It may also be that volume in collagen channels are several orders of magnitude inferior to the dead volumes in the chip. Manipulation of the chip resulting in even slight deformation of these dead volume may be enough to generate flows strong enough to completely renew the channels content. As a result, typically in a channel, upon seeding with a pipette, only a few cells remain. An additional difficulty is found in the fact that kidney cells are poorly adherent and need several minutes at least to adhere in one channel. Thus, we must count on the fact that only a few cells may adhere in one pipetting. We can consider that a cell has a given probability to adhere but also to detach from the surface for a certain period spent in the channel. Considering the important variability in flow rate across channels, the average number of cells that adhere after a seeding in a channel will vary a lot across channels

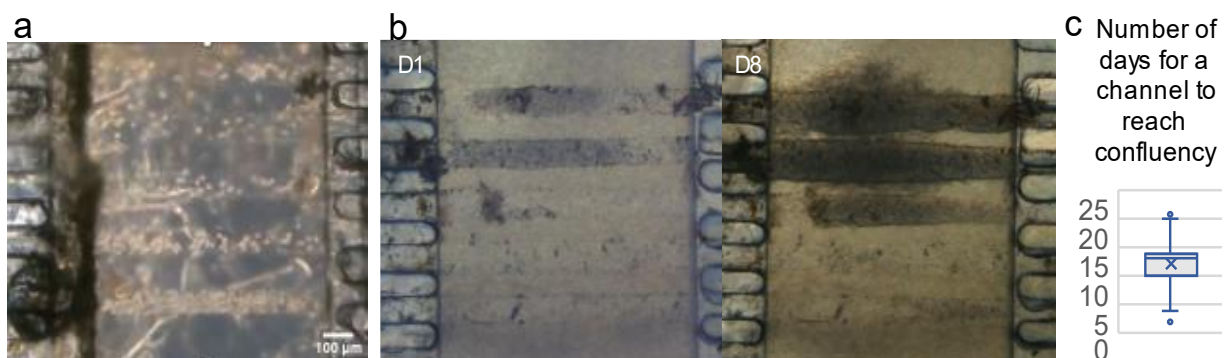


Figure 2.7: Important variability across channels for the time to reach confluency. Unfortunately, upon seeding the density of cells that can be maintained in one channel vary a lot in the same chip. Here we show a bright field image of representative seeding (a) Due to this variability, here for example, channels in the same chip are shown 1 day and 8 days after seeding to get to very different state of confluency (b) Overall, this leads to an unpredictable duration before confluency across channels as plotted in (c), lines: extrema, 1st and 3rd quartile and median, cross: mean

(figure 2.7.a). This will result in poor reproducibility regarding the seeding density across channels and chips. As a result, in one chip, channels may reach confluency with several days of interval **(figure 2.7.b-c)**, complicating experiments reproducibility, analysis and interpretation.

In summary, we have achieved one of the best approximations to the intricate tubular geometries observed within the kidney parenchyma. Thanks to this model, we could study the dynamics of tubular deformations in a kidney-on-chip due to the inactivation of the gene *Pkd1* for the first time to our knowledge. Furthermore, our experiment suggests that in this context channel proximity could promote tubular deformation, although the mechanisms behind such an observation remained unknown. Unfortunately, with the design of this chip we had to compromise regarding perfusion and were not able to stably maintain a flow in this model.

2.3. My solution: the next generation of kidney on chip

Given the limitations of the COC chip, there was a basis to develop a new model that would allow us to remain as faithful to the kidney geometry while allowing controlled tubules perfusion. Optimization of the cell seeding procedure was another important axis of development. In what follows, we will see how we gradually designed a chip optimized for perfusion and at the same time how we improved the seeding step to get a much more reproducible solution. The chip and its fabrication process are also described in detail in the Methods section with our paper “Construction of a Multitubular Perfusable Kidney-on-Chip for the Study of Renal diseases” inserted.

2.3.1. The concept and principles behind the first design to decouple fluidically parallel channels.

The initial objective regarding a new chip was to fluidically decouple the tubules. The chip would be centered around a collagen chamber crossed by parallel channels. To mold the channels, we would keep the tungsten wires that will be positioned and kept in place by a scaffold. The wires would be guided by channels in the scaffold that would be separated and in the continuity of the collagen channels (**figure 2.8**). For seeding and perfusion we would use a pressure-controlled perfusion operating separately on the different independent channels.

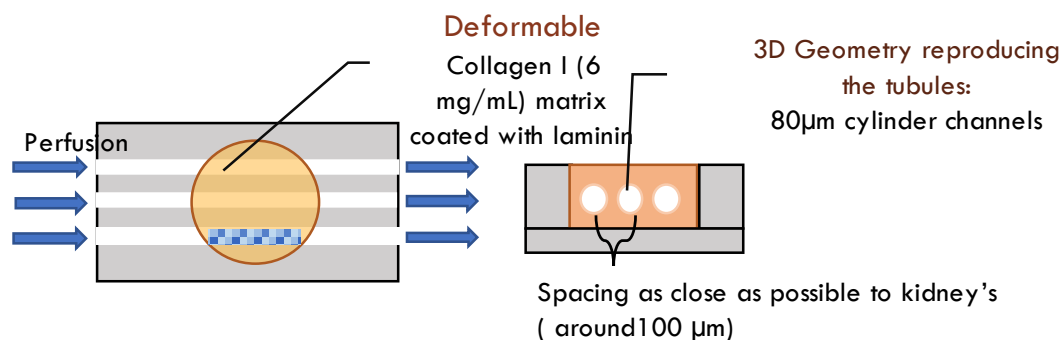


Figure 2.8: Concept for a chip with close parallel channels fluidically independent

Aside from the COC chip, another chip with similar specifications was developed in the lab for a muscle-on-chip. We decided to build on this chip and adapt it to our needs (**figure 2.9**). For this first prototype, we adopted a minimalistic interpretation of the concept stated above. In a PDMS scaffold, parallel 120µm channels connected to individual inlets and outlets allows positioning of the tungsten wires. To mold the scaffold for this prototype we use a 3D printed mold completed by stainless steel needles. This 3D printed mold consists of a frame with imprints of the inlets, outlets and collagen chamber pierced lengthwise to allow sliding of regularly spaced needles across the frame. By casting PDMS into the mold with the needle, we can negatively shape the chip. After un molding the scaffold, tungsten wires are inserted into PDMS channels. The chip fabrication is completed by injecting the collagen in the open chamber and removing the tungsten wires to generate the collagen channels.

For this chip, pressure control is used to perfuse the collagen channels individually. Notably for the seeding, we use a pressure controller from Fluigent to inject the cell suspension in the channels separately. Unfortunately, and despite individual control of each tube, similarly to the previous chip it was also difficult to maintain a minimal cell concentration inside the channels. Upon stopping the flow, cells would escape from the central collagen as before.

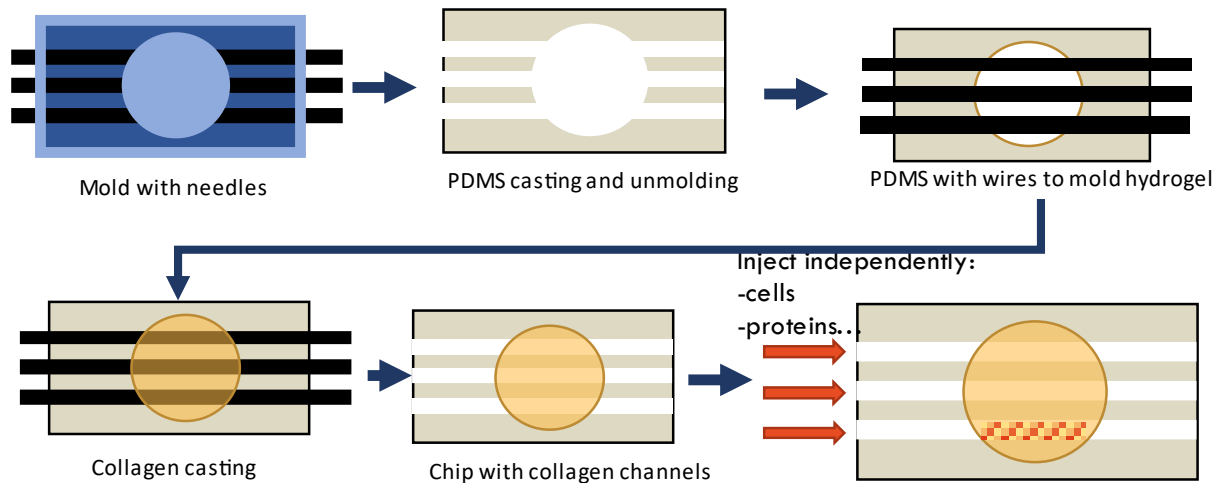


Figure 2.9: Fabrication of a chip with independent channels based on a 3D printed mold and wires For a first iteration of this concept, we used a 3D printed mold to make the chip PDMS scaffold. This mold allows to position needles that mold parallel independent PDMS channels. Wires are inserted into these channels/guide and are used to mold the hydrogel. After removing the wires, the parallel channels are perfused with a pressure controller that allows to injects cells and proteins independently in the channels

However, unlike previously, this seeding technique allows the experimenter to focus on one channel at a time. Nevertheless, with this prototype we were still far from our objectives regarding seeding reproducibility.

2.3.2. A resistive chip and a new seeding technique for a dense reproducible seeding and multiplexing.

Playing with wires to increase seeding density.

To increase seeding density, an interesting approach is to prevent the cells from escaping the channels and to force them to accumulate into the channels. To do so, we strategically employed the wires to create a dead-end at the extremity of the collagen channels. By partially removing the wires at the minimal position to generate the whole collagen channels, a flow is still possible inside because of the high porosity of collagen. Moreover, in that configuration, instead of a parallel laminar flow a radial flow towards the walls is amplified due to the conservation of flow. Upon seeding, the effect is double: cells are compelled to accumulate inside the collagen channels and the centrifugal flow drives the cells against the collagen walls, favoring adhesion. As a result, a channel can be totally filled with cells.

However, when stopping the flow and upon tubing removal, a backflow is still generated. If the backflow is too strong there is a risk of emptying the channels of cells partially or totally. In addition, seeding a channel adjacent to a channel already seeded can induce a flow within the pre-seeded channel that will also partially empty it. If this solution was an important leap forward regarding seeding reproducibility, there was still room for improvement.

A variation consists in reinserting the wires back inside the channels while it is filling with cells so that the wire is sandwiching a layer of cells against the collagen (**figure 2.10.a**). Then the wires can be removed once the cells have adhered to the collagen after a few hours. We assessed with a kidney epithelial cell line, mIMCD-3 cells, that this technique did not impose too important mechanical stresses on the cells. We performed a live/dead assay the

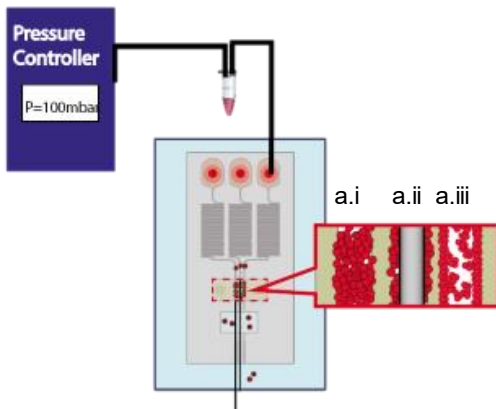
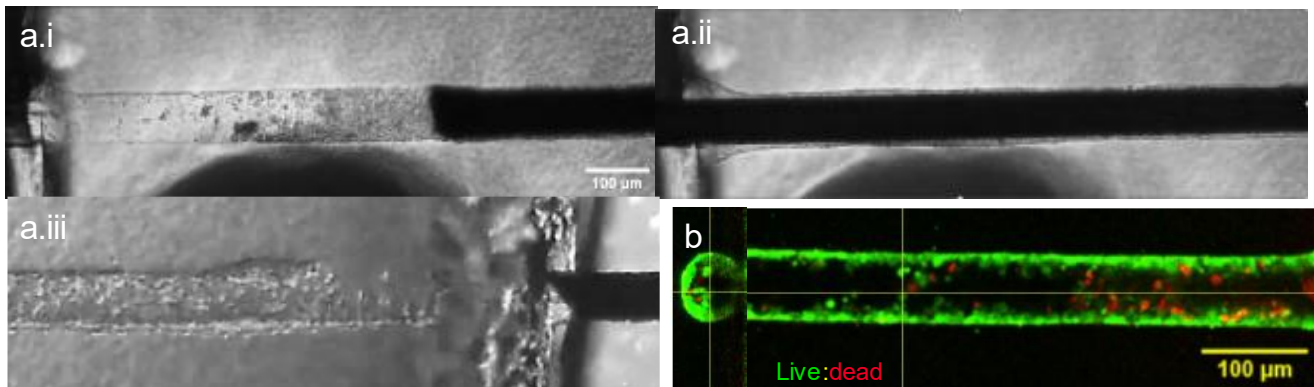


Figure 2.10: A seeding technic to reproducibly get confluent hollow channels from the start We developed a seeding procedure that allows to get dense hollow epithelium from the seeding day. Here we show an example of a channel seeding with mIMCD-3 cells. For this, the wire is partially removed only to reveal the collagen channel. This way, the wire blocks the cells injected into the channel that accumulate (a.i) In the meantime, the wire is reinserted into the channel (a.ii) and removed after the cells have adhered to force the generation of a hollow tubule. (a.iii) We checked with a live-dead assay on that this procedure only led to minimal cell death (b)

day following a seeding and demonstrated that it does not lead to significant cell death (**figure 2.10.b**). This technique presents a double advantage. First, regarding the backflow issue, complete reinsertion of the wires represents an obstacle preventing the cells from leaving the channels. Second, for certain cell lines, a seeding too dense results in a channel without a lumen. **This technique generates a confluent hollow epithelium from the start.**

Increasing the chip resistivity, solution to allow multiplexing.

Since we thought that the inability to maintain a sufficient cell concentration inside the collagen channels upon seeding was largely due to dead volumes, we decided to limit them to the minimum. Indeed, in the previous chip volume a collagen channel is in the order of 10nL while in the PDMS volumes are in the order of μL . Furthermore, in the designs presented before, the collagen channels represent the most resistive parts of the chips. As such they predominantly dictate the flow rate along a channel in the whole chip. We saw previously how slight variations in the collagen channel radius could make fluidic control difficult. PDMS molding, unlike collagen, yields more reliable geometries. Thus, having the PDMS part of the chip more resistive than the collagen makes the fluidic behavior more predictable, thus more controllable. Increasing the resistivity of the PDMS channels should in theory limit the backflow as well.

Therefore, in the next design, we decided to make the channels narrower in the PDMS section than in the collagen section (**figure 2.11.a**). Due to the resolution limitations of 3D printing, we used soft lithography to make the PDMS scaffolds for the chip. With silicon wafer, we could reasonably mold PDMS channels down to $40\mu\text{m}$ wide. Because PDMS is deformable and because tungsten has a very high elastic modulus, it is possible to insert $80\mu\text{m}$ wide tungsten wires into much smaller PDMS channel, however, it becomes challenging the narrower the channels. Furthermore, reducing the PDMS channels diameter too much can

lead to shear stress too important on the cells upon seeding as well as clogging of the PDMS channels. For these reasons we are limited, and 40 μ m wide channels were not enough to limit the backflow on their own. To further increase the channels' resistivity, we chose to increase their length as well. To do so, we implemented serpentine structures upstream a straight channel portion (**figure 2.11.b**). Implementing these features allowed us to render the collagen channel resistivity negligible as in this configuration, almost 1000 times lower than the PDMS channel resistivity according to **equation 2.3**. Not only could we limit backflows a lot when seeding but now we have a chip in theory compatible with multichannel perfusion. We published this design and its protocol; this publication is attached at the end of this manuscript. This design is the one mostly used in the following sections with a few minor adaptations when needed.

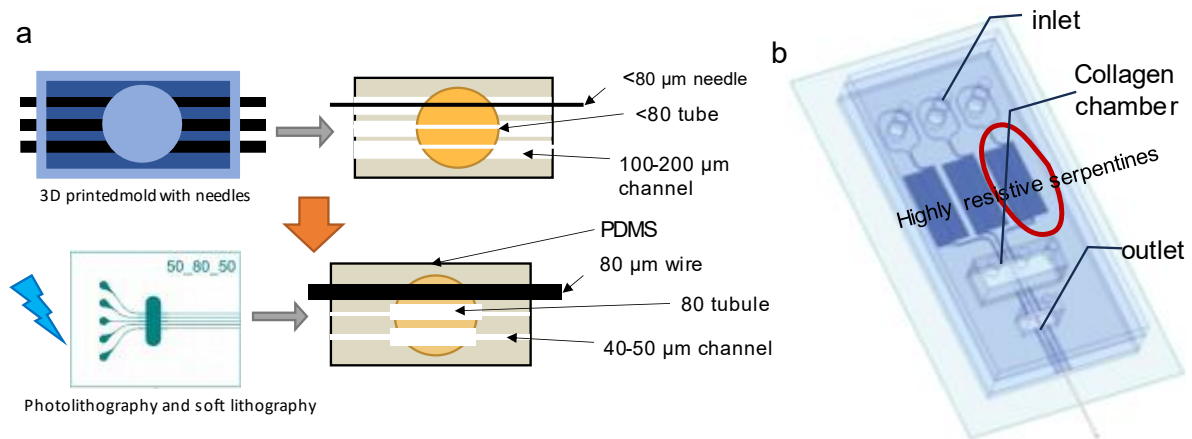


Figure 2.11: Increasing resistivity of PDMS channels allows more control of the channel perfusion. In a second iteration of the chip, we made the channels in the collagen (80 μ m) wider than the channels in the PDMS (40-50 μ m) to have the highest resistivity in the collagen. For this, the chip is now fabricated using soft-lithography technics. Thanks to PDMS deformability it is then possible to position precisely wider tungsten wires in parallel (a) To increase the channels resistivity even more and make the collagen channel resistivity negligible, we designed serpentine between the input and the collagen channels (b)

2.4. Chip perfusion to decouple flow from pressure.

2.4.1 Perfusion using hydrostatic pressure.

With a chip now compatible with perfusion of multiple channels, we had to decide between a control in flow and a control in pressure. Our objective was also to be able to run multiple flow experiments in parallel. Since we cannot easily multiply the number of chips at each experiment, the natural solution would be turning to control in pressure, where a clogged chip would not affect the other ones. This would require having either an individual dispositive per chip, which would represent a prohibitive cost, or to utilize multiplexing. Solutions for multiplexing may appear complex here and technically heavy. Furthermore, one of the main issues regarding perfusion in microfluidics is the generation of bubbles that will damage the tubular epithelium as well as clogging completely the channels. The multiplication of tubing and of different connections and interfaces here will provide as many opportunities as possible for bubble nucleation. Some groups like Barakat *et al.* presented an ingenious option for pressure-controlled flow in perfused organ-on-chips using hydrostatic pressure (Dessalles *et*

al., 2021). All that is needed to generate a flow with a given pressure gradient ΔP is a column of a certain height H :

$$\Delta P = \rho g H \quad (2.9)$$

with ρ being the fluid volume mass and g being the gravity acceleration

To generate a target shear stress inside the collagen tubules with a radius r in a system with a total hydraulic resistance R_{Htot} :

$$\Delta P = R_{Htot} \frac{\tau_{target} \pi r^3}{4\mu} \text{ then } H = R_{Htot} \frac{\tau_{target} \pi r^3}{4\mu \rho g} \quad (2.10)$$

If we consider that the resistivity of the collagen channels is negligible, given PDMS channels with a length L , a height h and a width w :

$$R_{Htot} = R_{HPDMS} = \frac{12\mu L}{1-0.63\frac{h}{w}} \frac{1}{h^3 w} \text{ then } H = \frac{1}{1-0.63\frac{h}{w}} \frac{3L\tau_{target}\pi r^3}{h^3 w \rho g} \text{ and } Q_{target} = \frac{\pi r^3 \tau_{target}}{4\mu} \quad (2.11)$$

In our chip: $L=6\text{cm}$, $h=w=60\mu\text{m}$ and typically in the nephron $\tau_{target} \sim 0.1 - 1 \text{ dyn.cm}^{-2}$, this results in a needed liquid height between 16 and 160 mm and a flow rate between 0.04 and 0.4 $\mu\text{L}/\text{min}$ or 57.6 and 576 $\mu\text{L}/\text{day}$. Such requirements can easily be achieved using standard lab syringes (**figure 2.12**). Thereafter, the volume of liquid wasted each day remains minimal when reported to liquid height and thus alteration of shear stress in the collagen channels within 24h also remains minimal. In addition, we can easily multiply the number of experiments run in parallel by having one syringe per chip. It is now possible to join the channels in a unique inlet or outlet without too much unpredictability. Thanks to the highly resistive serpentine, the flow rate is largely fixed by the PDMS channels, thus small fluctuations in the collagen channel radius become a marginal problem.



Figure 2.12: Using a gravity driven perfusion allow to run multiple experiments in parallel with a simple setup Using syringes as reservoirs, we can apply a gravity driven perfusion method to our chip. Making a unique input per chip allows to run multiple experiments in parallel. A picture of a typical setup is shown above

Finally, the use of gravity-driven perfusion offers new avenues regarding cell seeding. Classically we used a pressure controller to operate the perfusion of cell suspension in this critical step. A pressure controller, due to the number of connections and inputs necessary for its functioning, is in the end a bulky system that is hardly possible to operate under a sterile hood. For this reason, currently, this step is done in a non-sterile but clean atmosphere with the experimental risks that this entails. Furthermore, the current seeding procedure is hardly plug-and-play and requires a non-negligible learning curve. It also cannot be parallelized and can be time-consuming. This may represent one of the biggest limitations of our technology. We could also use our setup for long-term perfusion based on syringes to also seed the channels (**figure 2.13.a**). Advantages would be numerous. Unfortunately, this has not been the focus of this study. First attempts showed that it could be in theory possible when preventing cell sedimentation but would require numerous adjustments in terms of cell concentration, pressure or seeding time (**figure 2.13.b**). Interestingly, this technique did not require delicate wire manipulation to achieve high seeding density. Once optimized, such a procedure would no longer require important hands-on training and in the same way as long-term perfusion, could be parallelized for high throughput.

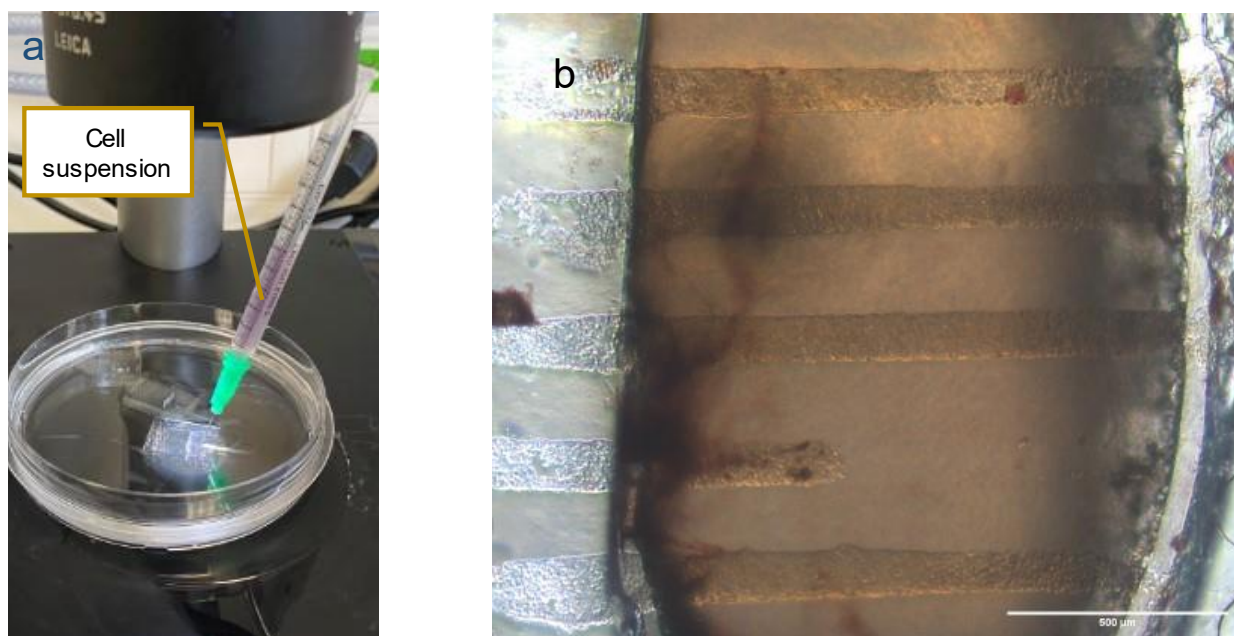


Figure 2.13: A gravity driven cell seeding would simplify the seeding step Using a syringe, it is possible to inject a cell suspension in a chip with a gravity driven flow (a) Preliminary tests show that this technic allows dense seeding even without using the wires. However, this procedure would necessitate some adjustments not to overcrowd the channels (b).

2.4.2. How to apply shear stress with limited intraluminal pressure?

Our design offers an additional opportunity, to decouple flow shear stress from intraluminal pressure in the channels. Depending on how the chip is perfused, we can have a configuration where the intraluminal pressure inside the collagen tube is essentially the hydrostatic pressure of the syringe or a configuration where the pressure inside the collagen tube channel is essentially the atmospheric pressure. Indeed, with collagen channels and PDMS channels forming a series circuit, knowing their respective hydraulic resistivities R_{H-PDMS} and $R_{H-collagen}$:

$$\Delta P_{collagen} = \frac{R_{H-collagen}}{R_{H-PDMS} + R_{H-collagen}} \Delta P_{tot} \quad (2.12)$$

where ΔP_{tot} is the pressure gradient across the whole chip and $\Delta P_{collagen}$ the pressure gradient across a collagen channel.

Hence since R_{H-PDMS} is approximately 1000 times higher than $R_{H-collagen}$, the charge loss in the collagen channel is 1000 times lower than the charge loss in the whole system. If the serpentine is upstream of the collagen channels, due to their high resistivity, most of the pressure loss will be concentrated in them, for a working 10 mbar above atmospheric pressure, this leaves in theory an intraluminal pressure of only 0,01 mbar above atmospheric pressure at the entrance of the collagen channels. This configuration will be called **the “flow only” or “FSS only” configuration**. On the other hand, if the serpentine is downstream of the

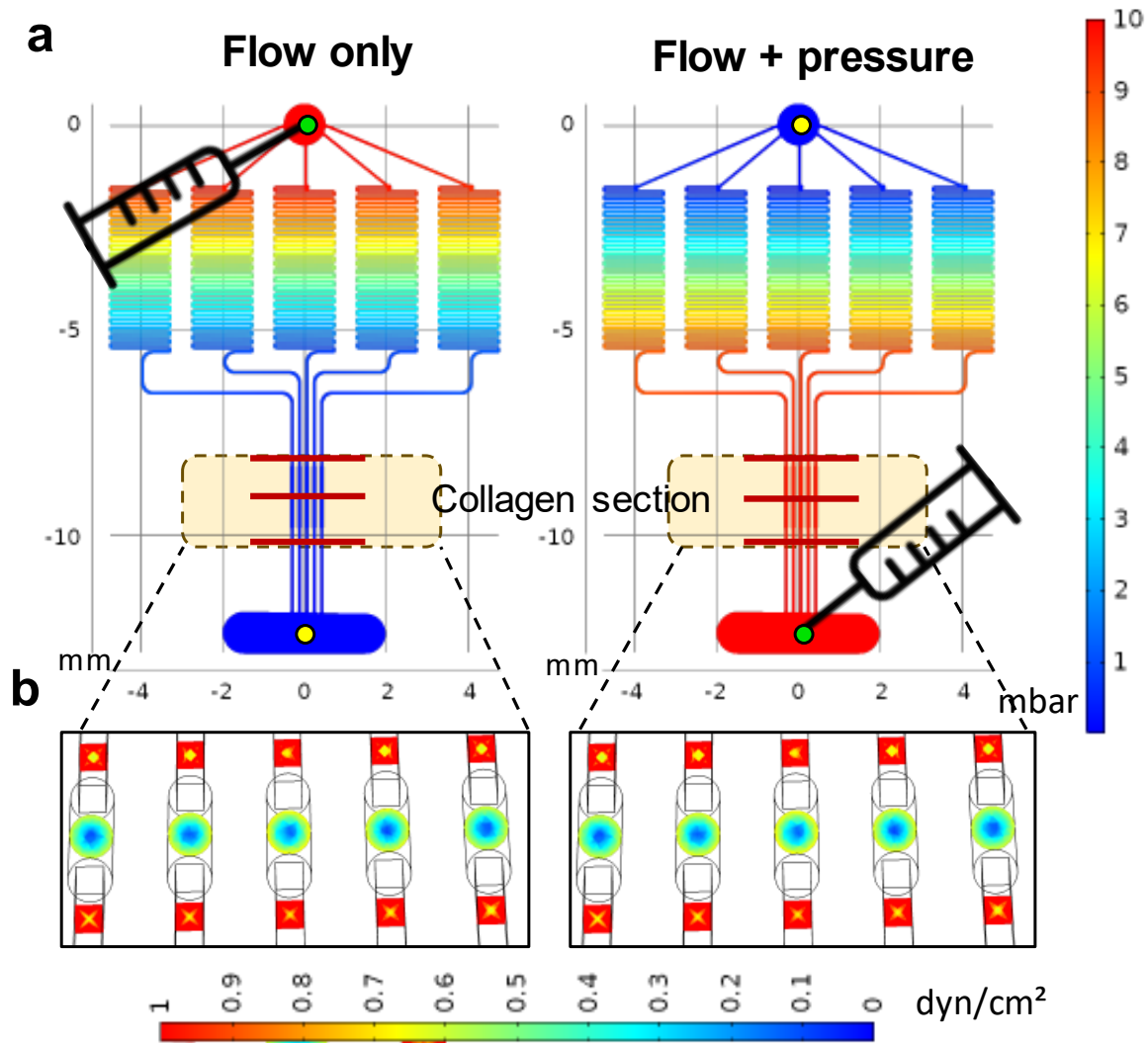


Figure 2.14: Two perfusion modes for the chip: “flow only” and “flow+pressure” and the resulting hydrodynamic stresses. Two modes of perfusion are possible for the collagen channels with our system depending on the input chosen for perfusion. If perfused the serpentine, the intraluminal pressure will be near zero in the channels but if perfused after the serpentine, the pressure will essentially be the same as the perfusion pressure. In (a), these two perfusion modes are illustrated and the results of a finite elements simulation (COMSOL) for these perfusion modes are shown for the pressure inside the system. Resulting shear stresses are shown in (b). Cross sections of the shear stresses in the collagen tubules are represented in the middle surrounded by cross section of shear stresses in the PDMS channels.

collagen channels, as most of the pressure loss would be downstream the collagen, the intraluminal pressure will be near the syringe pressure, this configuration will be called “**flow+pressure**” configuration (figure 2.14.a). We confirmed this by running a finite element simulation of the two perfusion configurations with the software COMSOL. As overall the system has the same geometry, in both cases the resulting flow rate, thus the resulting shear stresses would be the same (figure 2.14.b) and wall shear stress would fall close to 1 dyn/cm². To be able to modulate the pressure with the target flow rate, one would need to modulate the geometries in the chip accordingly. In table 2.2, we recapitulated the fluidic specifications we can achieve with the dimensions of the chip we set. We can mostly see that with the chip, in theory, we can apply forces in agreement with the physiological range we described in chapter 1.

	Nephron typical value	Chip target values
Outer diameter	50µm	80µm
Volumetric flow rate	~10nL/min	40-400nL/min (50 -500 µL/day)
Flow shear stress	~0.1-1dyn/cm ² (segment and diuresis dependent)	0,1-1dyn/cm ²
Intraluminal pressure	0-15mbar (segment and diuresis dependent)	0-10mbar (100 mmH ₂ O)

Table 2.2: Comparison between the nephron fluidic specifications and the specifications that we can reach with our chip

2.4.3. In practice, two main issues and how to solve them.

How to limit channel clogging to stabilize channel perfusion?

We evaluated the performance of our chip in practice. We measured the flow rate in each channel and estimated the resulting shear stress for an 80µm wide collagen channel in presence of confluent cells. To do so we perfused the chips with a 5µm fluorescent beads suspension with a syringe with a liquid height of approximately 10 cm, reproducing typical fluidic stresses that we would use in an experiment. This setup would correspond to a pressure of approximately 10 mbar and thus a shear stress for an 80µm wide channel of approximately 1 dyn/cm². We measured the speed of the beads, estimating from these flow rates and resulting flow shear stress (figure 2.15.a). We seeded the chips with m-IMCD3 cells WT or *Pkd1KO* confluent. We ran this experiment at 1 day after confluency and 7 days after confluency. Our results showed that flow and resulting shear inside the chips were lower from day 1 compared to the upper target (0.6 dyn/cm² on average instead of 1 dyn/cm²). Over time, there was an important decline in this performance, leading to flow rate measurements in certain chips being well below physiological values (figure 2.15.b).

Our investigations led us to suspect partial or total clogging of the PDMS channels due to dead cells as the main culprit. Indeed, after seeding some cells adhere in the PDMS channels and as they grow, they may form monolayers that will gradually die and detach from the PDMS (figure 2.15.c). To solve this issue, we evaluated different surface treatments to avoid cell adhesion on PDMS. PDMS on its own is already supposed to be cell repellent but to promote adhesion of collagen to the PDMS, we treat it with (3-aminopropyl)triethoxysilane

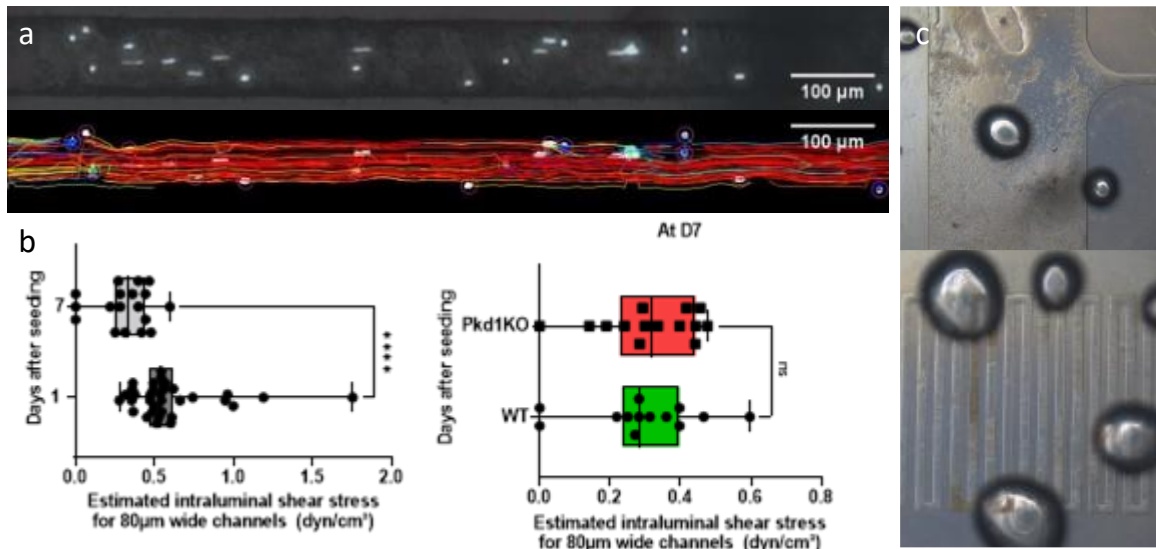


Figure 2.15: Cell clogging prevents the maintenance of a stable shear stress To evaluate the shear stresses in the channels, we visualized the flow thanks to fluorescent beads and the ImageJ plugin TrackMate as shown in (a) We tested our system using mIMCD-3 cells either WT or Pkd1KO. Unfortunately, after a week of perfusion, the flow rate decreased significantly in the channels between day 1 and day 7 after seeding as shown when plotting estimated shear stress for 80µm channels among our experiments (b-left). Plotting the same data at day 7 comparing WT and Pkd1KO showed no significant difference between the two cell types (b-right). (boxplots : lines are extrema, 1st and 3rd quartile and median, each point is an individual channel, ****: p-value<0,0001 with t-test, n=18-33) Probably, dead cells lead to partial or total clogging of the PDMS channels as showed by these pictures taken with a phase-contrast microscope. (c)

(APTES) and glutaraldehyde, which promotes protein adhesion. Furthermore, prior to cell seeding, we coat the collagen channels with laminin: this procedure could have a side-effect, as the PDMS channels are also coated with the adhesion protein. We then seeded mIMCD-3 cells on different PDMS flat surfaces treated or no with APTES and glutaraldehyde and treated or no with laminin. As it is impossible to coat the collagen channels without also making the PDMS incubate with laminin, using a protein repellent may prevent the proteins to adsorb on the surface. We also evaluated a PEG-PDMS surface where polyethylene glycol (PEG) molecules are concentrated at the surface of a PDMS substrate and act as protein repellents.

Laminin and surface treatment indeed promoted cell adhesion enough so that after 3 days the surfaces would be covered by a cell monolayer, even on the PDMS-PEG surface (**figure 2.16.a**). In the chip, after 7 days, performances of PDMS-PEG and PDMS treated chips were not significantly different (**figure 2.16.b**). Unexpectedly, PDMS without any treatment could also support cell adhesion. We suspect that protein adsorbed from the medium is sufficient to promote adhesion. Therefore, we decided to resuspend cells in PBS and quickly wash round cells in the PDMS channels with PBS after letting cells adhere to the collagen. To further prevent unwanted adhesion in PDMS, we treated the chips with a biocompatible anti-adhesion solution, the *Anti-adherens solution* from Stemcell Technologies, prior to laminin coating, assuming that the solution would not prevent adhesion on collagen. Tests on PDMS surfaces showed that even on treated surfaces, this solution could prevent cell adhesion almost entirely (**figure 2.17.a**).

In practice, combination of anti-adhesion treatment, seeding in PBS and washing with PBS greatly reduced cell adhesion. New measurements of flow rates after anti-adhesion treatment showed significant improvements after 1 day, and flow rates mostly matched the

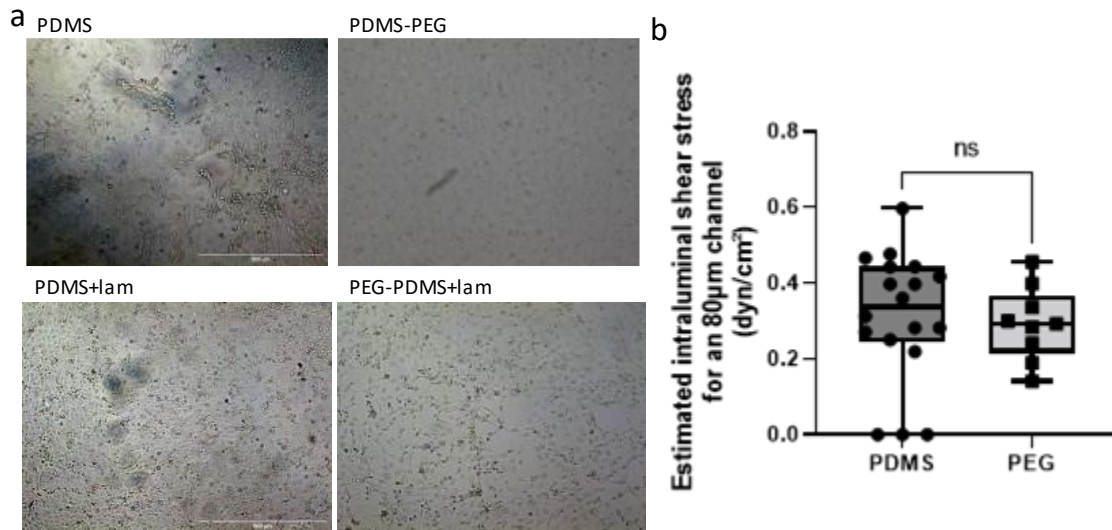


Figure 2.16: PDMS surfaces in the chip become cell-adhesive We evaluated the adhesion of mIMCD-3 cells on different surfaces with different treatments to find the least adhesive one. Unfortunately, cultures of these cells after 3 days leads to the formation of dense layers especially when adding laminin as shown by these phase contrast pictures (a) If PDMS-PEG looked promising, in practice when we plotted the estimated shear stress in PDMS-PEG chips, we found no significant difference with the PDMS chip after 8 days of culture (b) (boxplots : lines are extrema, 1st and 3rd quartile and median, each point is an individual channel. ns: not significant with t-test n=PDMS:18-PEG:9)

target flow rates (figure 2.17.b). However, after 8 days, we still could see a significant decrease in shear-stress around 50%. Nevertheless, the average shear was still around 0.6 dyn/cm², corresponding to the results of the finite elements simulation and this time it did not fall under 0.1 dyn/cm², **remaining in physiological range**. In fact, we noticed even after anti-adhesion treatment that some cells would still adhere on the PDMS channels and cellular debris would still clog the channels (figure 2.17.c). We observed filament-like structures that

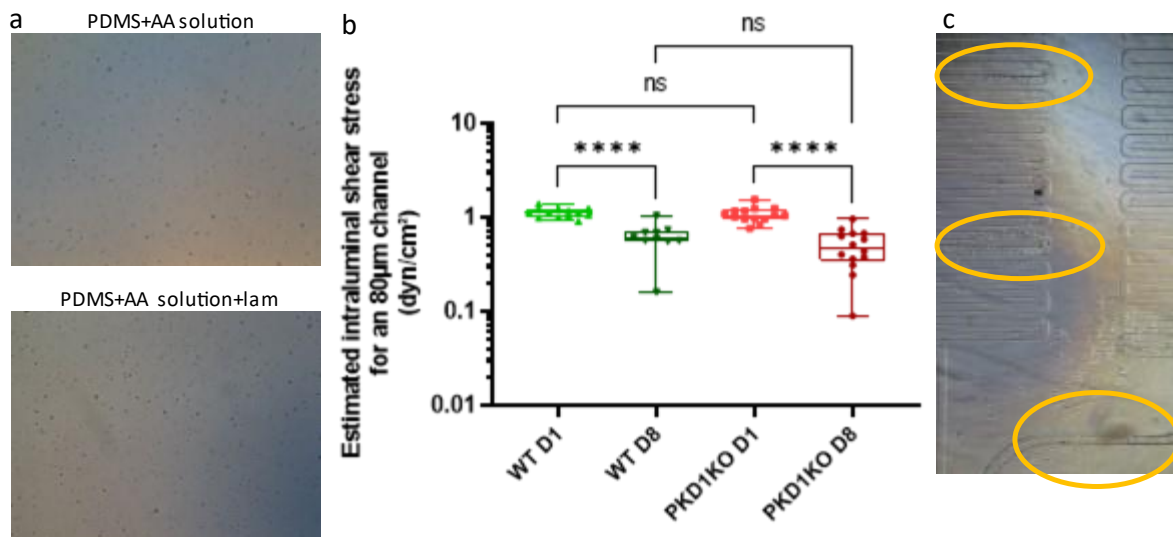


Figure 2.17: Anti-adhesion treatment limits channel clogging Adding an antiadhesion solution coating step prevent initial adhesion even when laminin is added after (a) Treating the chips with this solution leads to significant increase in shear stress in the channels from day 1 after seeding per our estimations. Unfortunately, there is still a significant decrease in shear after a week (boxplots with box lines being the 1st and 3rd quartile, middle line the median and outer lines the extremum, each point is a channel, ****: p-value<0,0001 with t-test n: WT=13-10 Pkd1KO=14-14) (b) This decrease may be due to the presence of persistent cell and debris accumulation in the PDMS channels (c)

we believe are from DNA released from cell debris. We think that these structures may promote cell debris aggregation at the origin of the flow rate drop. Adding DNase to the perfused medium would alleviate the formation of DNA filaments and thus may prevent cell clogging even further. Therefore, for our next attempt to stabilize the flow in the long, we added DNase at 1U/mL to the cell culture medium perfusing the chips. In our first experiments using DNase, this only marginally improved the flow after 8 days of culture (**figure 2.18**). Additional improvements may require compromise on the geometry of the PDMS channels increasing their width to allow better flushing of debris while not impacting too much the hydraulic resistivity of the whole system.

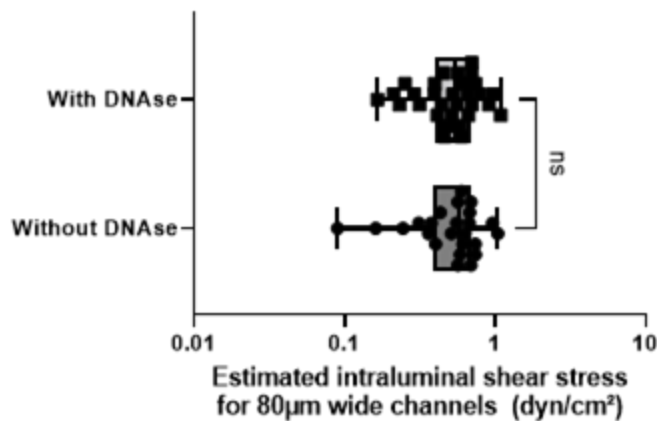


Figure 2.18: DNase seems to only marginally improve flow We added DNase at 1U/mL in the cell culture medium for the perfusion. These boxplots show the comparison between the estimated intraluminal FSS for an 80µm wide channel from the previous tubules and the preliminary tests of perfusion with DNase 8 days after seeding. (boxplots with box lines being the 1st and 3rd quartile, middle line the median and outer lines the extremum, each point is a channel, n= without DNase:24 with DNase:30)

How to strongly attach collagen to PDMS to prevent leakage?

Another critical assessment of the chip performances was to ensure that pressure in the channels could align with theory. We assumed until now that the tubules formed continuous tight channels with the PDMS channels. However, as demonstrated by the flow+pressure configuration, the stress induced by hydrostatic pressure can occasionally result in detachment of collagen from the PDMS substrate (**figure 2.19.a**). This, in turn, leads to the formation of leakage points at the interface between PDMS and collagen. In such instances, theoretical predictions will not be valid anymore for actual flows within the chip. Thus, we needed to strengthen the collagen adhesion on PDMS. Classically, to allow collagen adhesion as we mentioned earlier, we first silanized the PDMS surface with APTES and then added glutaraldehyde solution, wherein APTES molecules form a layer on an activated surface with amino groups and glutaraldehyde molecules form covalent bonds with these silane molecules. This surface modification allows protein to form peptide covalent bonds with the surface (Kuddannaya *et al.*, 2013). The efficiency of collagen grafting will then depend on the number of aldehyde groups available to form bonds with the protein. The critical step is the formation of the APTES layer, as the density of available APTES molecules on the surface will determine in the end how many bonds can ultimately form with collagen. For this step, through hydrolysis, the silane reacts with oxides at the activated PDMS surface forming siloxane bonds. Hydrolysis of APTES in presence of water also leads to polymerization of the molecules. This can lead to formation of APTES multilayers and aggregates that can destabilize the coating or modify the

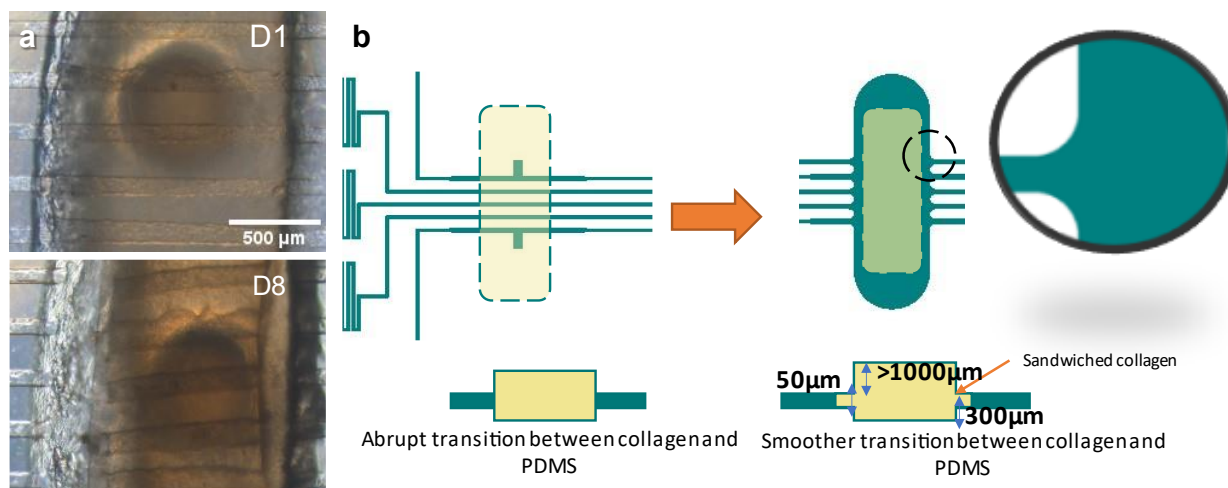


Figure 2.19: Constrictions between collagen chamber and channels helps the collagen to stay attach to the PDMS. Before a design optimization, due to important stresses from the cells and the flow, often after several days of culture, collagen channels detached from the PDMS, creating important leakage between the PDMS and the collagen and rendering the fluidic of the system unpredictable. Here is an example of a chip seeded with mIMCD-3 cells where after 8 days, collagen channels completely detached from the PDMS. (a) We modified the design of the chip slightly to sandwich the collagen at the junction with the PDMS, adding a step between the two. Furthermore, we smoothed the transition between collagen and PDMS channel to relieve some of the mechanical stress.

surface roughness and, in the end, alter the stability of the collagen grafting. Furthermore, we noticed that aggregates could affect the chip fluidics or optical properties through autofluorescence. Hydration, deposition time and APTES concentrations are critical parameters for the silanization process and require optimization to get a dense stable layer of silane. Many studies have proposed different solvents, anhydrous or with water traces, different concentrations, and time of reactions, but it seems unclear what the optimal protocol would be (Sypabekova *et al.*, 2023). Furthermore, the optimal conditions will greatly depend on variable experimental constraints. We tested several conditions for APTES+ glutaraldehyde

Type	APTES+glutaraldehyde				Polydopamine
Solvent	PBS	Ethanol 96%	Absolute ethanol	methanol	Tris-HCl pH 8,5
Concentration	APTES 2% Glutaraldehyde 0,5%	APTES 5% Glutaraldehyde 2,5%	APTES 5% Glutaraldehyde 2,5%	APTES 5% Glutaraldehyde 2,5%	25-50 mg/mL
Incubation time	30 min	45 min	45 min	1h	1h
rinsing	Overnight in ddH ₂ O	A few minutes in PBS			
residu	++++	+++	++	+	+
adhesion	++	+++	+++	++++	++

Table 2.3: Different surface treatment procedures for collagen adhesion on PDMS and qualitative assessments of their performances

coating and qualitative assessments of these variations are presented in **table 2.3**.

As an alternative to APTES-glutaraldehyde surface modification, it is possible to use polydopamine coated surfaces to facilitate collagen grafting (Chuah *et al.*, 2015). This coating requires fewer steps than APTES+glutaraldehyde treatment and is biocompatible. However, overall, even after increasing dopamine concentration, grafting was still weaker than what could be achieved with APTES+glutaraldehyde and may be too weak to reliably withstand stresses due to intraluminal pressures or cell contractility.

We also increased mechanically the stability of collagen grafting by playing on the geometry of the chip at the junction between PDMS and collagen. To do so, we added constriction of the same height as the PDMS channels between the collagen chamber and the PDMS channels. We also made the transition between the PDMS chamber and the PDMS channels more progressive. The constriction sandwiches a thin collagen layer in the PDMS, increasing the surface area of collagen-PDMS bonds, and progressive transitions release some of the stress at the junction.

As a last verification, we checked if the system presented any leakage by perfusing after a few days of culture tubules of mIMCD-3 cells with 10kDa FITC-dextran, a molecule with a molecular weight below the cutoff of the glomerular filtration and below most proteins. This experiment was carried out using pressures similar to pressures used for tubule perfusion. By showing that contrast due to fluorescent dextran between the channels and the matrix remains mostly constant after several hours, we can conclude that the system is tight (**figure 2.20**).

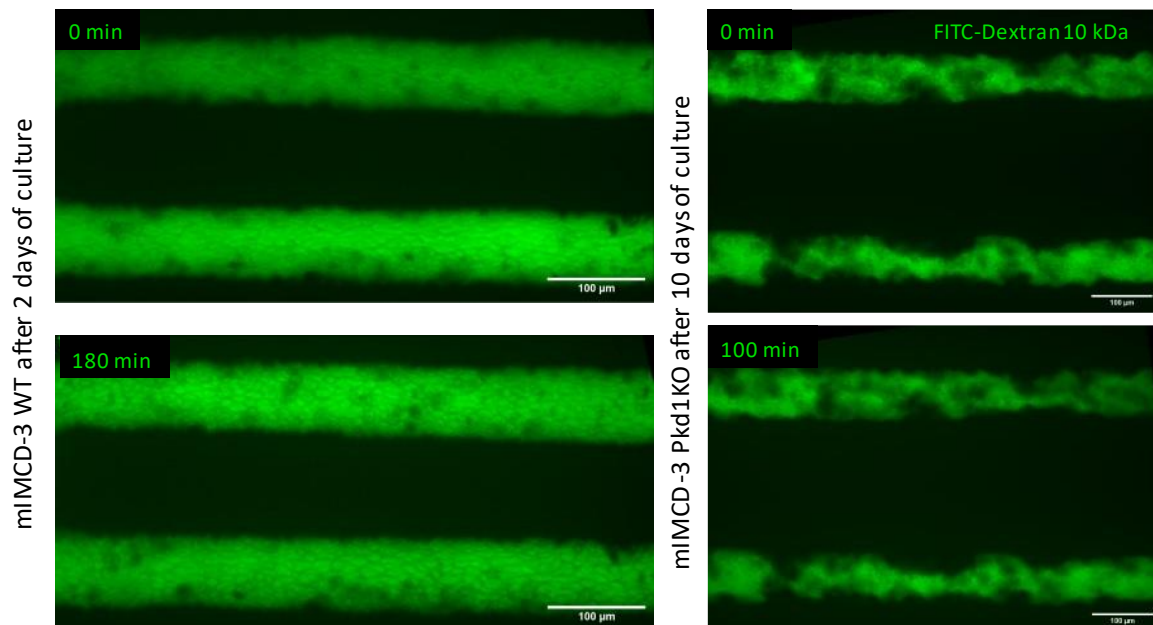


Figure 2.20: Kidney tubules in collagen together with PDMS channels form tight channels. To confirm that our system was tight, we injected 10 kDa FITC-Dextran in the channels in confluent mIMCD-3 tubules for a few minutes using similar pressures as we would use for a perfusion experiment and imaged the channels with a spinning-disk microscope right after and 2 to 3 hours after and did not notice any visible change in contrast (different tubule aspect between Pkd1KO and WT can be attributed to an accumulation of debris after 10 days of culture)

2.5 Conclusion

Over the last decade, the concept of kidney-on-chip has taken off. Pursuing the creation of high throughput faithful platforms for drug or toxicity testing, many groups are trying now to establish their platforms. Industrials have also pushed standardized platforms that can be adapted to the needs of a kidney model. Surprisingly however, kidney disease modelling and more precisely polycystic disease studies have largely been untapped by this field. Perhaps for this reason, there were significant improvements that could be made regarding the kidney-on-chip that we learned about in the literature. Especially when it comes to diseases affecting the structural integrity of the kidney, such as ADPKD, important compromises for geometry and mechanical stresses can become a deal breaker. Seizing this opportunity, we developed our own models to fill this gap. Going through different solutions (**table 2.4**), we settled on a chip where curvatures of the same order of magnitude as the nephron while featuring parallel channels close enough to allow interactions between them. The chip microfluidic channels also make it possible to decouple intraluminal pressure from flow shear stress, in order to study separately the influence of these two intricate but different mechanical stresses on the kidney epithelium. The versatility and facility inherent to the gravity driven perfusion we chose gave us a cost limited solution to our problem while allowing us to run numerous experiments in parallel. Moreover, we managed to optimize the cell seeding procedure to achieve reproducible and high cell density making it possible to get confluent monolayers the day after the seeding in a reproducible manner. Surprisingly, although representing a challenge for us across several projects and chip designs, the literature remains scarce on the issue. Possibly the small dimensions of our channels compared to what is common in kidney-on-chips exacerbate this potential issue, but here we proposed a solution. Although we use it to model parallel nephrons, with the possibility to separate fluidically these channels, our chip could also be used to mimic interactions between nephrons and peritubular capillaries. Most important areas of improvement can be found in the simplification of the fabrication and seeding procedures. For the latter we are confident that adapting gravity driven perfusion to this issue would be an elegant but simple answer.

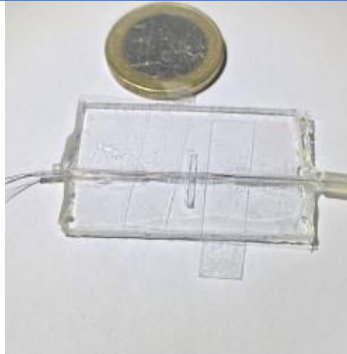
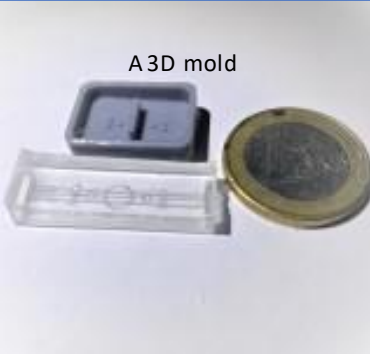
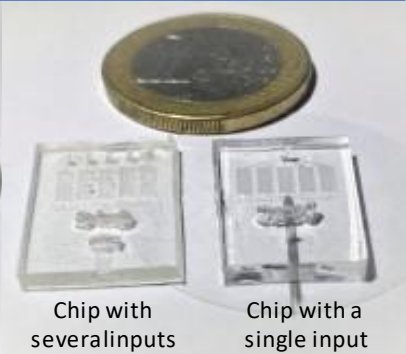
			
		A 3D mold	Chip with several inputs Chip with a single input
Material	COC	PDMS	PDMS
Fabrication technique	Hot embossing	3D printed molds	Soft lithography
Fabrication complexity	+++	+	++
Perfusability	Poor control due to fluidically connected channels	Independent channels but poor control due to channel geometries	-Independent channels possible -Higher control on channels fluidic with highly resistive channels -Designs with one input allow to run multiple perfused experiments in parallel using gravity driven perfusion
Cell seeding	Pipetting with poor reproducibility	Possible to seed at high density in a reproducible manner	Possible to seed at high density in a reproducible manner

Table 2.4: A summary of the three main type of kidney on chips that we developed

3. The importance of *Pkd1* for the maintenance of the tubular geometry

3.1. Introduction

3D constructs that mimic the kidney tubule geometry provide valuable insight on how a curved substrate could influence cell proliferation, migration, differentiation, and morphology. We discussed, in the previous chapter, several examples attesting the importance of curvature to approach a healthy kidney phenotype. The tight regulation of all these processes is important for the maintenance of the tubular structure. These processes are unbalanced in cells haploinsufficient for *PKD1*. It is unclear, however, what is the first cause of cyst formation in ADPKD. Despite significant advances, use of the murine model for ADPKD has not allowed researchers to exactly decipher the succession of events which leads to cyst formation. 3D *in vitro* models on the other hand have largely relied on the cells ability to self-organize. If organoids provide an elegant way to properly differentiate cells into packed tubular structures resembling nephrons, cultures of fully differentiated kidney cells in unstructured hydrogel often fail to recapitulate on their own a tubular microenvironment. As transformations leading to ADPKD happen in an already structured organ, a failure to use similar geometries in these models may not allow them to recapitulate the cascade of events leading to cyst formation in ADPKD. For instance, we previously examined how *PKD1* not only had a key developmental tubulogenic role but was also likely of great importance to actively maintain the kidney tubules. In the first chapter, we gave a brief overview of existing *in vitro* models for ADPKD and saw that, to date, none of them made use of a pre-structured tubular construct.

With their work, Subramanian *et al* (Subramanian *et al.*, 2018) modeled cystogenesis in their guided kidney tubules. However, in their model they artificially induced cystogenesis through cAMP overstimulation and subsequent overstimulated luminal secretion. In our group we previously studied the impact of the loss of *Pkd1* in our first generation of tubular construct. In the previous chapter, we summarized the extant previous work which showed that *Pkd1*^{-/-} proximal convoluted cells did not preserve the initial geometry and were homogeneously dilated the tubules (Myram *et al.*, 2021). We think that this behavior is probably due to increased levels of proliferation. The importance of proliferation, however, remains controversial regarding the initiation of localized tubular deformations in ADPKD (W N Leonhard *et al.*, 2015). Furthermore, in human ADPKD, cysts are more likely to form in more distal parts of the kidney at later stages. For these reasons, with our new generation of kidney-on-chip we decided to work with mIMCD-3, a kidney cell line derived from the collecting duct. The group of Michael Kötting selected wild-type mIMCD-3 clones that had a predisposition for tubulogenesis in collagen-matrigel gels (Westermann *et al.*, 2022), we had at our disposal these wild-type cells from which *Pkd1*KO cells generated were generated and *Pkd1* was constitutively reexpressed by the same group. This cell type has been used in several studies for *in vitro* cystogenesis experiments, notably by harnessing the cells capacity to either generate tubules or cysts as the main indicator. Working with these cells in our new kidney-on-chip allowed us to expand our investigation on the mechanisms potentially behind cyst formation in ADPKD. We first worked in static conditions, without flow or intraluminal pressure,

allowing us to compare this new work with our previous studies with the PCT. In what follows we will see how the loss of *Pkd1* in a different and potentially more relevant kidney cell type, differently affects the cell's ability to maintain a tubular structure.

3.2. Results

3.2.1. Loss of *Pkd1* leads to tubular dilation with cells derived from the collecting duct.

We first investigated the influence of *Pkd1* on the maintenance of the tubular shape imposed on the cells. From WT cells, several *Pkd1*KO clones were generated with CRISPR. We seeded at confluency our chips with a 6mg/mL collagen I matrix with WT cells alongside the clones and cultivated them for at least 11 days in static conditions. We imaged the chips at regular intervals with phase contrast microscopy to follow the evolution of the on-chip tubule diameter (**figure 3.1.a**). We evaluated the dilation of individual tubules by first computing their

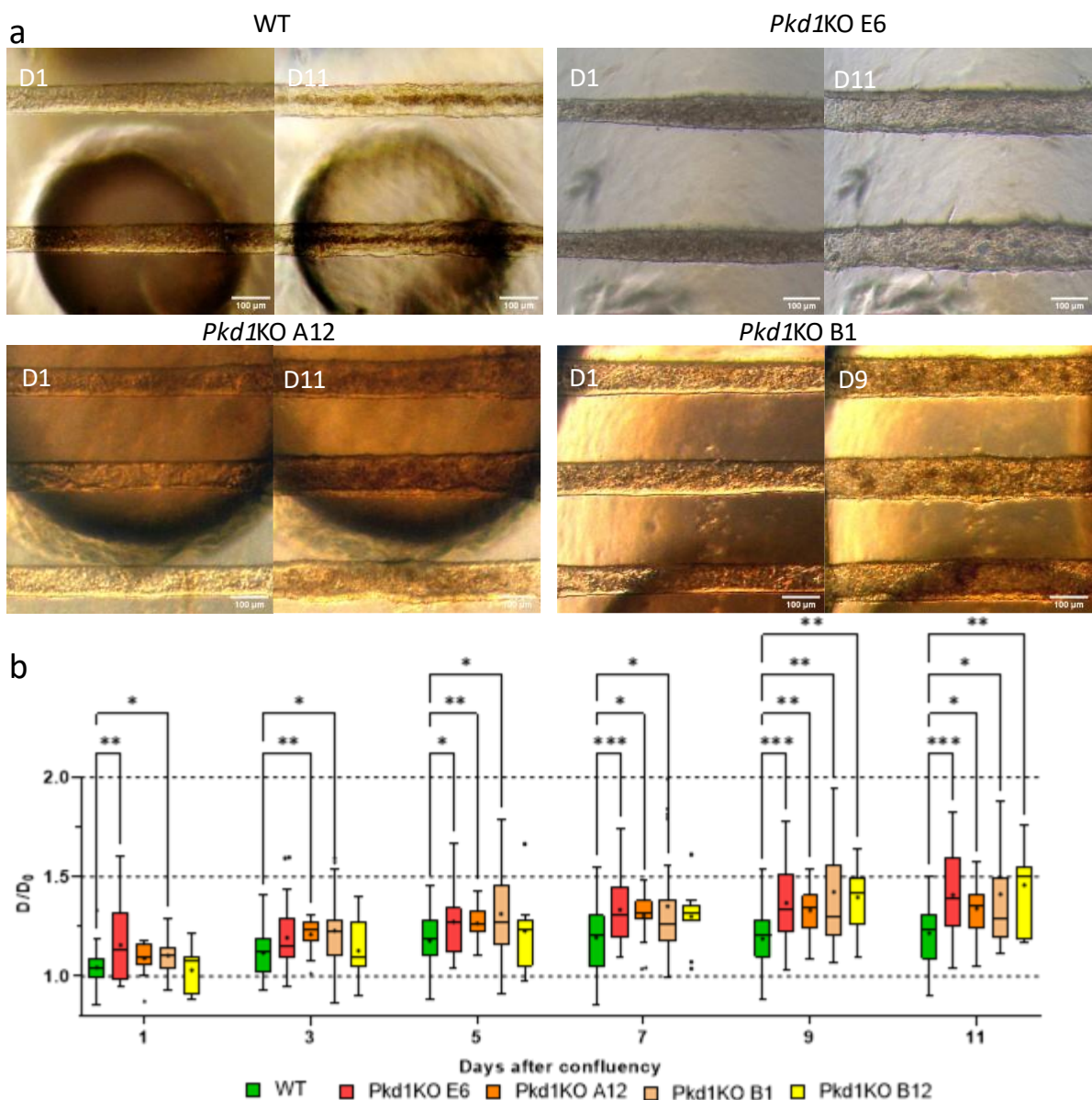


Figure 3.1. Loss of *Pkd1* favors homogeneous channel dilation in mlMCD-3. From WT mlMCD, several *Pkd1*KO clones were generated. These cells were seeded at confluency and cultivated in our multitubular chip. In (a) are contrast phase images showing the evolution of these tubules for different clones. We quantified a channel dilation by normalizing the average tubule diameter at given day (D) by the average tubule diameter at confluency (D₀). Boxplots in (b) are showing the evolution of the normalized channel diameters for all the clones tested (Box: 1st and 3rd quartile with median, whiskers: 25% IQR, +:mean, Statistical test: t-test p-value: *<0,05, **<0,01, ***<0,001, n: WT:62 E6:44 A12:18 B1: 31, B12:11)

average diameter (see Methods section for more details). We then normalized these diameters by the diameter of tubules at confluency. The results of this quantification are shown in **figure 3.1.b**.

Both WT and *Pkd1*KO dilated the channels after these 11 days. However, for each *Pkd1*KO clone, we clearly observed a greater degree of tubular dilation than with the WT, with on average a dilation of 21% for the WT and dilations of more than 40% for the *Pkd1*KO clones. Interestingly this difference was marked from the beginning of the experiment. There was also a notable difference in terms of tissue aspect between the WT and *Pkd1*KO tubules, with apparent thinner tubules for *Pkd1*KO clones. For the rest of the experiments, we selected the clone E6 because of its more striking difference with the WT.

Following up on these results, we verified whether loss of *Pkd1* was necessary for the dilations that we observed. We had at our disposal a cell line where *Pkd1* was constitutively reexpressed in the clone E6, hereafter denominated by *Pkd1**. We seeded these cells at confluency and cultivated them alongside *Pkd1*KO E6 and WT as controls. *Pkd1** tubules had an intermediate behavior compared to the WT and the *Pkd1*KO tubules (figure 3.2). After 11 days *Pkd1** tubules were dilated by 35%, while WT and *Pkd1*KO tubules were dilated by 25% and 50% respectively (**Figure 3.2**). Furthermore, the tubules had similar thickness as *Pkd1*KO and cells remained in monolayers taking a cuboidal shape (not shown). Interestingly, the *Pkd1** tubules showed important levels of tubulogenesis. We must note that this experiment has only been conducted once at this stage, but these preliminary results demonstrated that reexpressing *Pkd1* mitigated to a certain degree the dilation due to the loss of *Pkd1*.

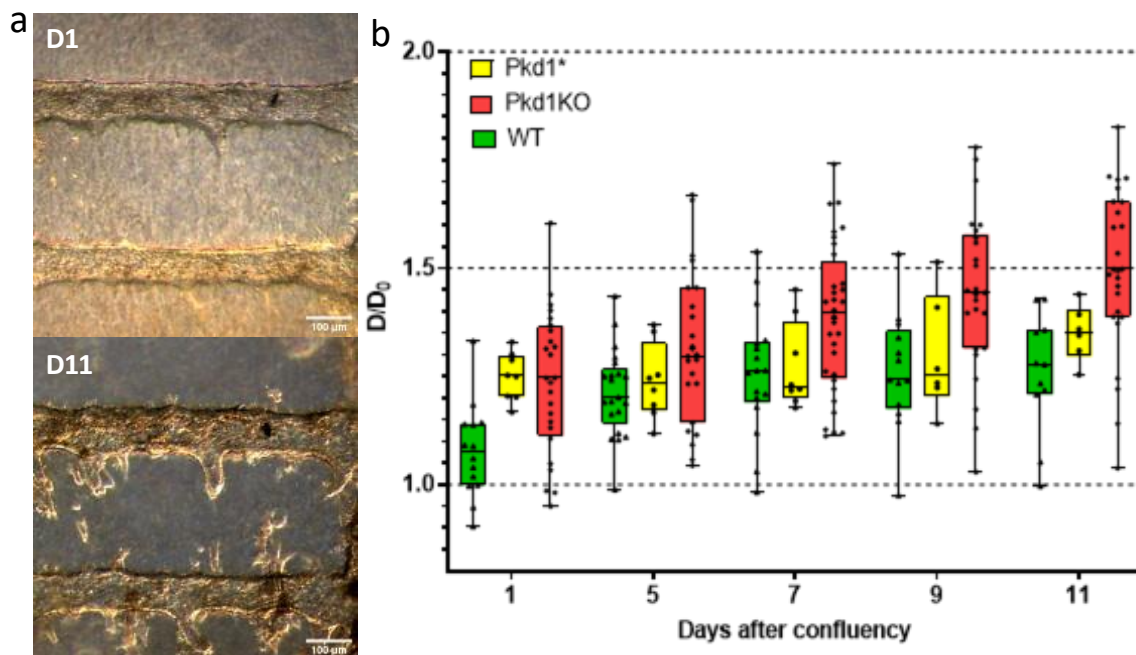


Figure 3.2. *Pkd1* may be necessary to prevent channel dilation in mIMCD-3. An mIMCD-3 *Pkd1*KO clone was modified to constitutively express *Pkd1*, noted *Pkd1**. These cells were cultivated in our multitubular chip alongside the parental *Pkd1*KO clone as a control and WT as a comparison point. In (a) are contrast phase images showing the evolution of *Pkd1** tubules. We quantified the channels dilations the same way as previously. Boxplots in (b) are showing the evolution of the normalized channel diameters. WT and *Pkd1*KO data here are from experiments ran in parallel with *Pkd1** experiment and are included in the previous figure (Box: 1st and 3rd quartile with median, whiskers: extrema, one dot is one tubule, *Pkd1**n=8, WT n=14, *Pkd1*KO n=24)

3.2.2. This increased dilation is not due to increased proliferation but is rather correlated to cell spreading.

We investigated the possible mechanisms behind the tubule dilations that we observed. Given the important differences that we could already observe in the aspect of tubules with contrast phase microscopy, we wanted to look more closely at the tissue organization and cell morphology. To do so, we fixed some of the chips 1 day and 11 days after confluency. A very common origin for tissue growth is cell proliferation which could be a possible explanation for channel dilation. We assessed the difference in proliferation levels depending on the *Pkd1* status of the tubules by performing at the same time a Ki-67 staining. Images of the tubules obtained with confocal microscopy confirmed that at late stages, while WT formed multilayers in an “onion-like” organization; in some cases, only a couple days after reaching confluency, *Pkd1*KO tubules remained robustly in monolayers (figure 3.3.a-b). In addition, we observed

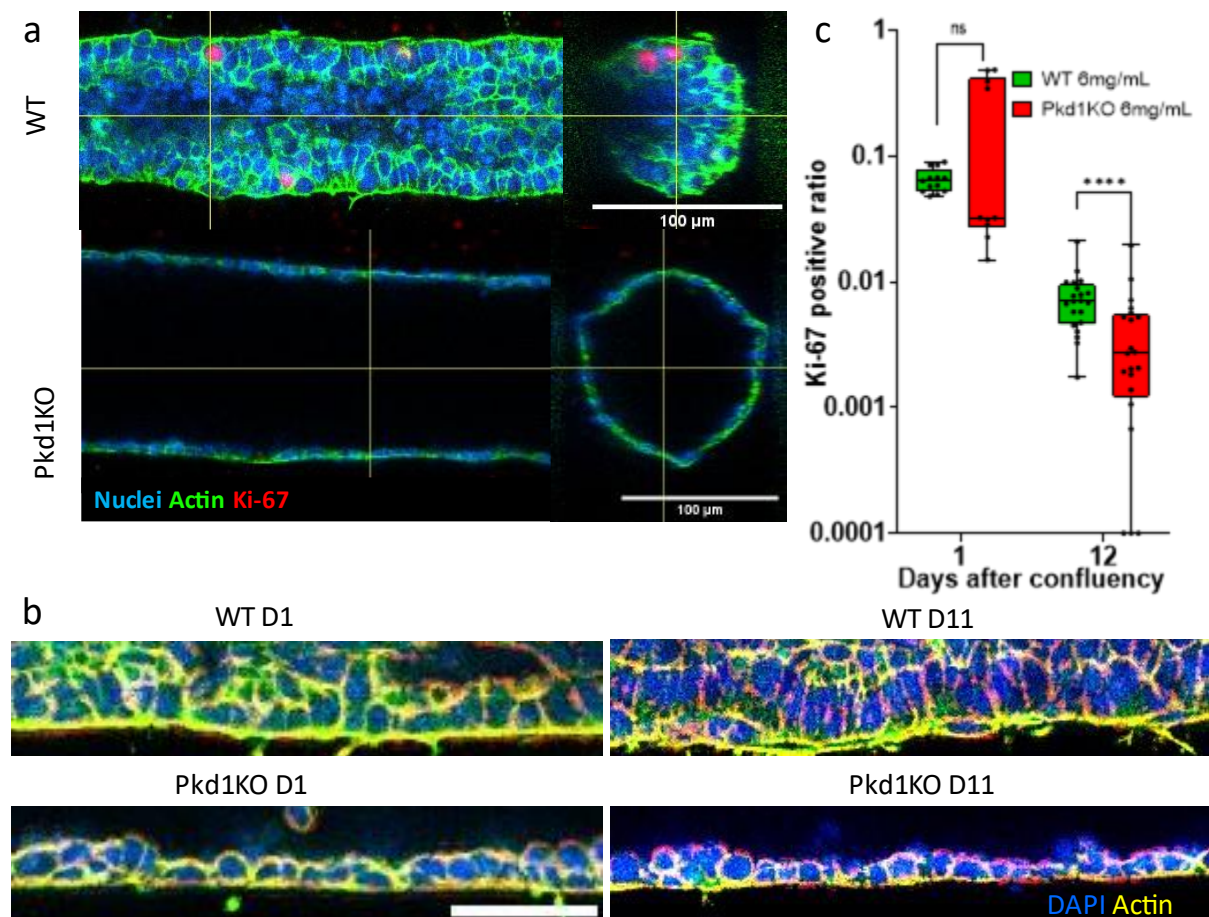


Figure 3.3. Loss of *Pkd1* is accompanied by increased proliferation but by important differences in cell morphology and tissue organization. We stained nuclei and Ki-67 in fixed mlMCD -3 tubules, WT and *Pkd1*KO, after 1 and 11 days after confluency to look at the tissue topology and proliferation. In (a) are cut of representative tubule images obtained with confocal microscopy after 12 days of culture. In (b) are zoom on representative tubules fixed at 1 day and 11 days after confluency focusing on cells morphology and tissue organization. WT tubules are characterized by multilayering and tall cuboidal cells whereas *Pkd1*KO remain robustly in monolayers with flatter cells (scale bar: 50μm). We quantified proliferation by computing the ratio of Ki-67 positive nuclei over the total number of nuclei in one tubule. Boxplots in (c) are comparing these ratios between *Pkd1*KO and WT tubules (Box: 1st and 3rd quartile with median, whiskers: extrema, one dot is one tubule. WT n=12-21, *Pkd1*KO n=8-21, ****: p-value<0,0001 obtained with t-test)

striking differences in terms of cell morphology. *Pkd1*KO cells remain flat with no perceptible changes in shape. WT cells took from day 1 after confluency a more cuboidal shape and the cells appeared to become taller, more densely packed, and stacked on each other 11 days after confluency (**figure 3.3.b**).

With these first observations, it appeared that a link between an increased proliferation and an increased dilation due to the loss of *Pkd1* was unlikely. To confirm this, we segmented automatically the nuclei in the tubules, identified the Ki67 positive ones and computed the ratio of Ki67 nuclei. These quantitative measurements of proliferation in our tubules are shown in **figure 3.3.c**. Indeed, there was no significant differences in proliferation 1 day after confluency between WT and *Pkd1*, and 11 days after confluency, proliferation levels were even significantly lower in *Pkd1*KO. Levels of proliferation between day 1 and day 11 were almost divided by 10 between day 1 and day 11, reaching near zero levels for *Pkd1*KO. Possibly the higher residual proliferation levels in WT cells explain why these tubules gradually lose their lumen and why they also ultimately dilate the tubules.

Given these observations, we could conclude that increased proliferation is not the reason behind increased tubular dilation. As we observed striking differences in cell morphology, notably in shape and apparent density, we looked more closely at a possible correlation between cell geometry and dilation. More specifically, we quantified the degree of cell spreading in the tubules. To do so, we used internuclei distances as a proxy since we could expect these two measures to be strongly correlated. We supposed these cells to be hexagonal and for a given cell we computed the average of the internuclei distance with the 6 closest neighbors and averaged over the outer layers of the tubules (**figure 3.4.a**, see Methods for more details on the automated technic). This quantification confirmed that *Pkd1*KO were more spread than WT, with an internuclei distance significantly more important of 15% at day 11. Internuclei distances were more important in tubules fixed the day after the tubules reached confluency as opposed to 11 days after. However, this difference was more important in the WT group than in the *Pkd1*KO group. This results confirmed that, as the tubule matures and cells proliferate, WT cells tend to be more densely packed whereas *Pkd1*KO cell morphology remains almost the same. We then wanted to assess whether tubule dilation was correlated to the degree of cell spreading. Plotting internuclei distances against tubules normalized diameters showed a weak positive correlation for the *Pkd1*KO and a weak negative to no correlation for the WT (**figure 3.4.b**). We must note that almost all of the *Pkd1*KO tubules analyzed for this experiments had a normalized diameter under the average we observed for this cell type in previous experiments. To get a proper conclusion we would need to perform this analyses on tubules with greater levels of dilation but these results show that differences in cell spatial organization rather than increased proliferation is more likely critical for tubular dilation.

3.2.3. ECM remodeling appears critical for this tube dilation.

Our tubules are embedded in a deformable and biodegradable collagen matrix. Depending on the mechanism behind dilations, the collagen matrix mechanical properties or fiber organization may greatly impact the tubule dilation. In the following experiments, we investigated the impact of the matrix fiber density and stiffness. To do so, instead of cultivating the cells in a 6mg/mL collagen I matrix, we increased the collagen density to 9-10 mg/mL. At this concentration, our group measured a traction elastic modulus of 86 kPa compared to 55

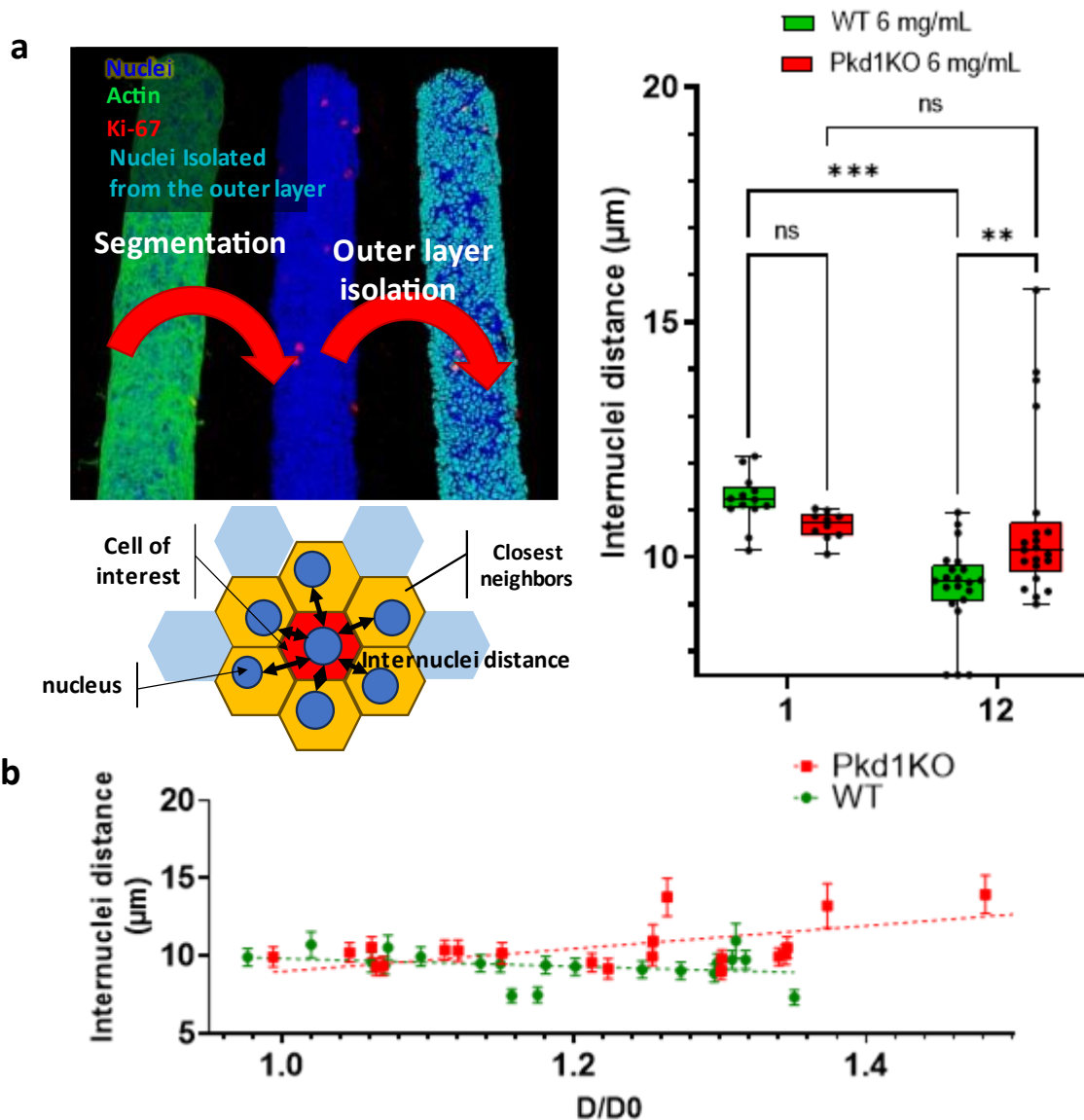


Figure 3.4. Increased dilation of *Pkd1KO* tubules is concomitant with a greater degree of cell spreading. From the previous staining we segmented the nuclei and isolated the nuclei from the outer layer. As a proxy for cell spreading, we computed the internuclei distance as such: the mean of the distance between one nuclei and its 6 closest nuclei was computed and this result was averaged over the one tubule. Boxplots compare internuclei distances between WT and *Pkd1KO* (a) (Box: 1st and 3rd quartile with median, whiskers: extrema, one dot is one tubule, WT n=12-21 *Pkd1KO* n=10-21, **: p-value <0.01***: p-value<0.001 obtained with ANOVA). We then plotted tubules average internuclei distance against normalized diameters to look at the correlation between cell spreading and tubular dilation (b) (error bars: SD)

kPa for the 6mg/mL gel. Interestingly, the increase in stiffness is almost proportional to the increase gel density.

We followed the tubules as we did previously. Increasing the matrix density did not visibly alter the tissue organization; WT cells after several days of culture formed multilayers whereas *Pkd1KO* cells remained in thin monolayers (**figure 3.5.a**). However, dilation for *Pkd1KO* were lowered to the same levels as WT cells for which there was no significant difference compared to the 6mg/mL. On day 11, the average tubule distension in the *Pkd1KO* group was reduced by almost 40%. The magnitude of this reduction was similar to the days before. It is remarkably comparable to the magnitude of the increase in stiffness and density of the collagen I matrix from 6 mg/mL to 9mg/mL. Hence, increasing the ECM density mitigated

the effects on tubular deformation due to loss of *Pkd1* (**figure 3.5.b**). Unfortunately, it is not possible to decouple the importance of the density of collagen fibers and the matrix stiffness as both are closely related. Nevertheless, the mechanism behind enhanced tubular dilation in the absence of *Pkd1* appears to be very sensitive to hydrogel's physical properties as they mirror the faculty of the cells to increase the tubule diameter.

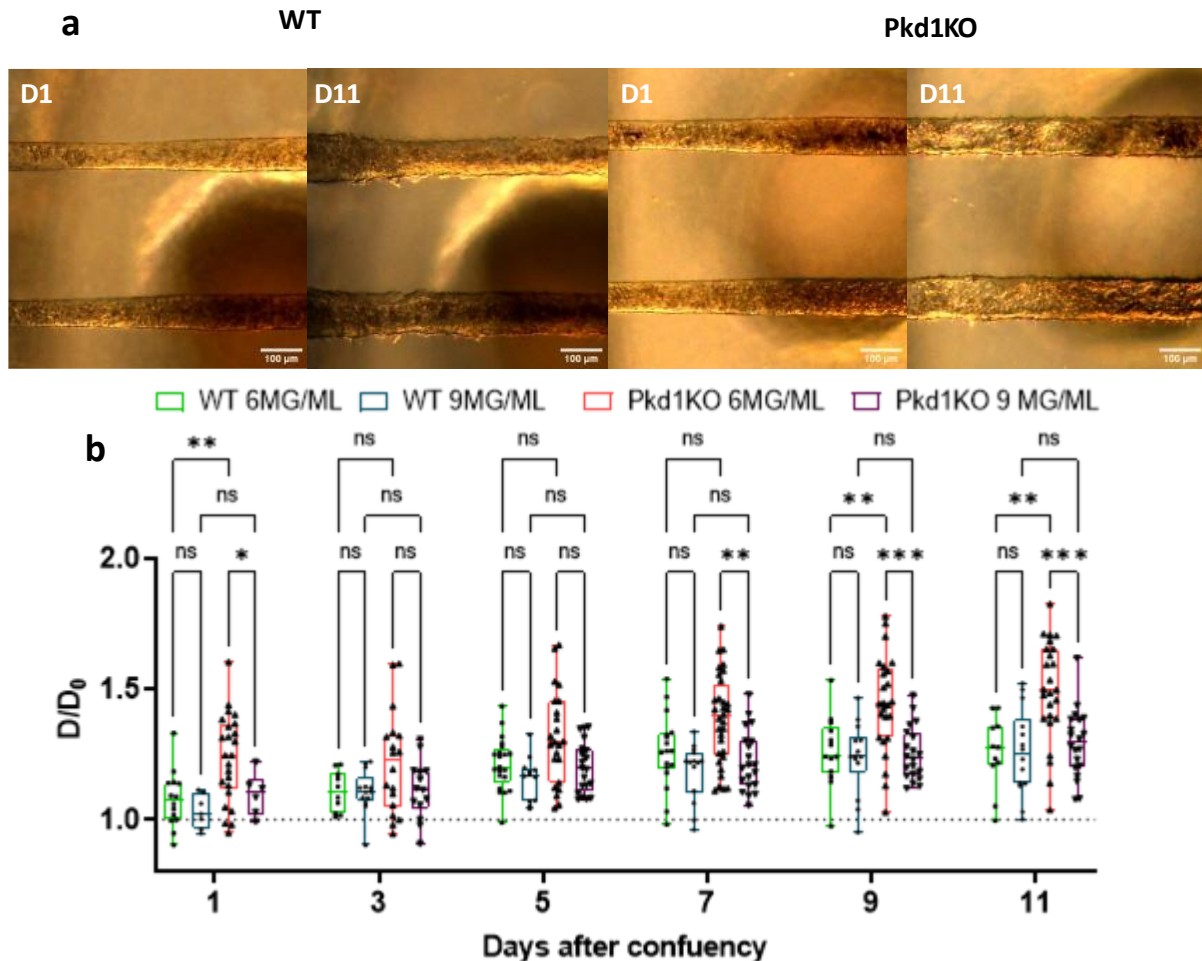


Figure 3.5. Tubular *Pkd1*KO dilation depends on ECM stiffness and density. We tested the influence of the matrix density by increasing the concentration of collagen I from 6mg/mL to 9 mg/mL. In (a) are contrast phase images showing the evolution of *Pkd1*KO and WT tubules in 9mg/mL gels. We quantified proliferation by computing the ratio of Ki-67 positive nuclei over the total number of nuclei in one tubule. Boxplots in (b) We quantified the channels dilations the same way as previously. Boxplots in (b) are comparing the evolution of the normalized channel diameters over time for WT and *Pkd1*KO in 6 or 9mg/mL collagen I (Box: 1st and 3rd quartile with median, whiskers: extrema, one dot is one tubule, WT 6mg/mL: n=23-11 WT 9mg/mL: n=14-7, *Pkd1*KO 6mg/mL: n=25-24 *Pkd1*KO 9mg/mL: n=20-6. Statistical test: 3-way ANOVA, p-values: *: < 0,05, **: < 0,01, ***: 0,001, ****: < 0,0001).

3.3 Discussion, perspectives, and conclusion

3.3.1. Loss of *Pkd1*, difference in cell morphology and curvature

To summarize, with these static experiments, we demonstrated that loss of *Pkd1* impaired the ability of cells from the collecting duct to maintain a near-physiological tubular geometry. Here we must note that both WT and *Pkd1*KO tubules are prone to tubular dilation in this context, but likely for two very different reasons. WT cells often differentiated into tall cuboidal cells much like cells normally found in the nephron collecting duct. However, possibly due to the absence of luminal flow shear stress, relatively high levels of proliferation that we saw even in tubules confluent for more than a day may have led to the multilayering that we observed. As they proliferated, the density of cells lining the tubule increased as cells became taller but less spread in order to adapt to the lack of space. When density within a layer gets past a critical threshold, cells are then forced to proliferate in an apico-basal axis or get pushed towards the lumen. This multilayering is the result of an incomplete extrusion. In our group, Deforet et al previously showed that epithelium going above a certain threshold of density as well, due to a growth constrained by confinement, could exhibit multilayering at the rim of a pattern of 50µm because of unbalanced mechanical forces at the border (Deforet *et al.*, 2014). In our case, important curvature also comes with an important level of confinement and a similar imbalance in mechanical forces which could be reinforced by an absence of flow shear stress. Cell morphology in *Pkd1*KO tubules on the other hand was very reminiscent of the morphology of cells lining cysts in late ADPKD, with relatively flatter cells resembling squamous cells. *Pkd1*KO tubules displayed similar levels of proliferation on the day following seeding, but although not significant in our result, they already displayed increased cell spreading on average. This level of cell spreading appeared to decrease much less than for WT cells. Possibly, instead of increased density within cell layers, continuous proliferation of these cells translates into an increase of tubule area and consequently in tubule diameter.

We looked at reported *in vitro* culture of mIMCD cells in gels and could not find any similar example of a culture exhibiting multilayering. 3D cultures with these cells were largely not accomplished using structured gels but instead relied on the cells tubulogenesis capacity. In the short review of preexisting tubules-on-chip from the previous chapter, we saw that most systems had tubules with diameters several times larger. The closest ones in terms of curvature used cells derived from the proximal convoluted tubule. Interestingly, on flat surfaces, we did not see differences as important in terms of cell morphology nor any multilayering. It may be that curvature in the WT tubules modulates the epithelium organization down to the cell shape. Luciano *et al* showed for instance with MDCK that epithelium thickness was modulated by local curvature with curvatures similar to those in our tubule leading to an increase in cell height (Luciano *et al.*, 2021). Homan et al, also reported a significant increase of cell height with proximal tubule cells, despite a system with diameters more than 5 times ours, due to curvature (Homan *et al.*, 2016). Overall, it seems also that on concave curved surfaces, cells experience an apico-basal elongation in a crowded context (Yu *et al.*, 2018; Di Meglio *et al.*, 2022), possibly due to purely geometrical effects. This faculty of proliferating kidney epithelial cells to adapt to their geometrical constraint may be limiting tubule dilation by moderating a so-called homeostatic pressure (Hannezo, Prost and Joanny, 2012). Somlo and colleagues showed that regression of tubule diameters after re-expressing *Pkd1* or *Pkd2* in their ADPKD mouse model was strongly correlated to a transition from flat shaped cells to cuboidal cells (Dong *et al.*, 2021). Similarly, preliminary results showed that re-expressing

Pkd1 in our cells limited tubule dilation and was accompanied by an intermediate cell morphology between WT and *Pkd1*KO. If the inverse was already an established fact, Somlo *et al* result draws a more evident role of polycystins in the regulation of cell spreading. It may be that *Pkd1* moves the homeostatic equilibrium towards physiological diameters of the tubules also *via* modulation of cell morphology. Such modulation may be in response to stresses induced by tissue curvature specifically, as we do not see important morphological differences between WT and *Pkd1*KO in 2D. To confirm this hypothesis, in the future, we could increase the initial tubule diameter and look for any modulation of tubule dilation and a correlation with a modulation of cell morphology.

3.3.2. The importance of the ECM properties

In our experiments, homeostatic pressure may be at the origin of tubule dilation. Such a mechanism would fit with our observation showing a sensitivity of tubular dilation to collagen deformability. Indeed, we observed that differences in dilation between 6 and 9mg/mL collagen seemed proportional to the increase in the gel stiffness. Albeit tempting, assimilating this behavior to a simple strain-stress response of the matrix to the stress due to cell proliferation may not fit with our results with WT cells. Strangely, increasing collagen concentration did not have the same effect for WT tubules and did not significantly decrease their dilation. Possibly, increasing gel stiffness may modulate proliferation levels, thus increasing resulting homeostatic pressure. However, we cannot exclude the importance of the interactions of the cells with their matrix, such as possible degradations of the matrix, especially given how the increase in matrix stiffness also correlates with fiber density.

In fact, we performed some preliminary experiments to decorrelate the fiber organization from stiffness. We incubated some chips with threose following a procedure previously used in our group for a gut-on-chip model. This chemical treatment crosslinks collagen fibers in a way that increases the gel stiffness only moderately, to levels comparable to the increase of gel density to 9mg/mL, while retaining the fibrillar structure of the collagen (Staneva *et al.*, 2018; Verhulsel *et al.*, 2021) but making the gel overall less susceptible to enzyme activity. This gel modification almost completely prevented any dilation from the *Pkd1*KO cells to a much more important degree than a 9mg/mL gel. Similarly, a study on the impact of artificial gel properties on tubulogenesis by mIMCD-3 cells showed that invasion and tubulogenesis in artificial ECM was correlated to their ability to both induce protease secretion by the cells and their sensitivity to proteolytic cleavage (Cruz-Acuña *et al.*, 2019). If confirmed, those results would rather point towards mechanisms linked to active gel remodeling by the cells, possibly linked to matrix metalloproteinases (MMPs) activity. In this case curvature may also modulate cell tendency to remodel their ECM. For instance, in their model of a fallopian tube, Fleszar *et al* showed that increasing the curvature of their construct enhanced fallopian tube cells matrix invasion (Fleszar *et al.*, 2019). Interestingly, curvature did not modulate MMPs activity. Rather, the initiation of invasion was dependent on cell-cell adhesion and contractility. The authors suggested that the process resulted from stresses due to curvature transmitted through the epithelium, which would be enhanced by cell-cell adhesion and contractility. In our case, if homeostatic pressure is not sufficient on its own to dilate the *Pkd1*KO tubules, we can speculate that it can initiate the process that would lead to ECM remodeling. Crosslinking of collagen hydrogels has been shown to greatly impair digesting enzyme activity. In our case, this would prevent any an enzymatic-activity-dependent dilation process. Nevertheless, some groups have also demonstrated that kidney cells remodel their ECM, notably their basement

membrane based on their expression of *Pkd1* (Subramanian *et al.*, 2012). Such results are in accordance with the widespread observation that basement membrane lining cysts present abnormal compositions (Grantham *et al.*, 1987; Mangos *et al.*, 2010; Zhang, Reif and Wallace, 2020b). Possibly the differences in dilation between WT and *Pkd1*KO may also be the results of subsequent different basement membrane mechanical properties in softer gels counterbalancing homeostatic pressure. However, it would not be intuitive for such differences to already be important enough to explain the early differences seen in tubular dilations. More immediate phenomena such as differences in cell morphology may be predominant in the beginning. In future experiments, it will be interesting to assess differences in basement membranes secreted by WT cells and *Pkd1*KO cells, either through immunochemistry or electron microscopy. Furthermore, direct observation of the collagen fibers through techniques such as Second Harmonic Generation would offer precious insight if we can assess whether fibers are compacted or digested along dilated tubules.

3.3.3. A generalized kidney tubular dilation due to loss of *Pkd1* but cell type dependent mechanisms

These results further demonstrated that *Pkd1* was fundamental for kidney cells to maintain their tubular shape in a 3D tubular construct. In a certain way they validate our observations made with our previous kidney-on-chip based on PCT cells. We think however that despite similar outcomes, mechanisms behind tubular dilations are not the same. Indeed, for PCT, there is a clear increase in proliferation due to the loss of *Pkd1*. In addition, similarly to WT mIMCD-3, overproliferation for *Pkd1*^{-/-} cells leads to multilayering in the long term. Unlike WT mIMCD-3, *Pkd1*^{-/-} cells remained in monolayers. There are also not such striking differences in cell morphology in a tubular configuration. On the contrary, *Pkd1*^{-/-} cells appeared less spread than their *Pkd1*^{+/-} counterpart. The differences in behavior of *Pkd1*^{+/-} PCTs and WT mIMCD-3 cells may reflect into the differences between their *Pkd1*KO counterparts. These divergences may also translate phenotypic differences arising from their nephron segment origin.

At the level of ADPKD, cysts appear not to form uniformly in all segments. Attempts to locate exactly the origin of cysts in human have produced mixed results, but naive isolation of cells from cysts indicates a predominance of cells presenting markers for the distal parts of the nephron (Loghman-Adham *et al.*, 2003). Recent works using cutting edge RNAseq techniques tend to confirm the predominance of cysts from the distal tubule or collecting duct (Li *et al.*, 2021). These works confirmed that tubule distensions were observed mainly in these segments rather than in the proximal tubules (Grantham, Mulamalla and Swenson-Fields, 2011). The reasons behind this discrepancy remain unclear. Possibly, kidney cells are exposed to a more compliant environment in the distal parts of the nephron and collecting duct (Marsh and Martin, 1975; Sakai *et al.*, 1986; Grantham *et al.*, 1987). Inducible mouse models provide a wide range of different timing and preferred locations for cyst formation. Cyst distribution seems very sensitive to the timing and number of *Pkd1* mutations. Leonhard *et al* suggested that cysts arise preferentially from segments still prone to increased levels of proliferation due to persistent tubular elongation in these segments. Likewise, during development, *Pkd1* expression follows a different pattern depending on the segment. *Pkd1* has an early strong expression in the proximal tubules but faint expression at late stages and undetectable after birth, whereas *Pkd1* expression is the highest in the collecting ducts at late developmental stages and remains faint after birth. Possibly these timing differences are due to different roles fulfilled by *Pkd1* along the nephrons and cyst formation in different segments

may arise from different mechanisms. This may be reflected in differences in behavior of tubules lacking *Pkd1* leading to increased dilations.

3.3.4 Conclusion

In conclusion, we showed here with another cell line than PCT, derived from another segment of the nephrons, that the absence of *Pkd1* in the tubule leads to homogeneous tubular dilation. We have identified here a mechanism independent of an increase in proliferation compared to wild-type cells, contrary to our previous study with cells derived from the proximal tubule. Rather, tubular distention is here the consequence of profound changes in cell morphology and tissue organization that build an increased homeostatic pressure along the cells lining the tubules. These differences may only arise from a possible *Pkd1*-mediated response to a tubular substrate. Studying the interplay between *Pkd1*, curvature, and tissue and cell morphologies may be an exciting path to follow. This process is also very sensitive to the matrix density. Although we cannot tell for the moment with certainty if it is due to involvement of matrix remodeling or matrix compression, some preliminary data suggests that it may be the former. Nevertheless, we must note here that in the absence of flow shear stress, wild-type mIMCD-3 exhibits an over-proliferative phenotype that translates into a multilayer tubule diverging from the physiological conditions. In addition, if mIMCD-3 *Pkd1*KO cells remain strongly in monolayers, in our previous study we saw that PCT *Pkd1*^{-/-} were also prone to multilayering probably for similar reasons. Therefore, studying tubular dilation in the most relevant context possible appears to require hydrodynamic stresses in addition to a geometry mimicry.

4. The importance of flow shear stress and intraluminal pressure for the tubule homeostasis with or without *Pkd1*

4.1. Introduction

In the first chapter, we discussed how renal epithelial cells are submitted to hydrodynamic stresses. These stresses are the source and consequence of kidney excretory activity. They influence and guide the kidney epithelial cells morphology, polarization and activity. Many implemented flows shear stress to an *in vitro* cell culture platform to study its effect on kidney epithelial cells (see chapter 1 part 1.1.3, “*The importance of hydrodynamic cues*” and chapter 2 part 2.1). Intraluminal pressure in the kidney is inevitably associated with FSS but the effects of these pressures have not been the focus of much study. As intraluminal pressure on a tubular epithelium is expected to generate tension through the cell membranes, leading to possible circumferential strains, the presence of stretch-activated channels could be a modality for pressure mechanotransduction. Much like FSS, pressure may also lead to cytoskeleton reorganizations in kidney cells (Li *et al.*, 2009). Additionally, some researchers have demonstrated that kidney cells respond to transepithelial pressure by modulating their ion pump location, organization and gene expression associated to these pumps (Choudhury *et al.*, 2022).

We previously discussed how a recent study on a kidney organoid which modelled polycystic kidney disease showed that exposition to flow shear stress was necessary in this context for cystogenesis. This further exemplified that the ensuing stresses are of utmost importance to build relevant *in vitro* models. We also discussed how PC1 and PC2 were shown to be tightly involved in regulation of FSS mechanotransduction, possibly with a moderating role. Similarly, PC2 has been shown to regulate stretch-activated channels opening probability in tandem with PC1 (Sharif-Naeini, Joost H A Folgering, *et al.*, 2009). Due to PC1 or PC2 imbalance, these processes are altered in ADPKD. Notably loss of PC1 or PC2 has been shown to hinder the cellular response to pressures, altering mechanical transduction from SACs and gene transcription.

In addition, FSS is also perturbed by the cysts due to obstructions of the healthy tubules (Grantham, Mulamalla and Swenson-Fields, 2011); as flow is pressure driven in kidney tubules, these perturbations also lead to increased luminal pressure (Tanner *et al.*, 1996). The exact involvement of these two mechanical stresses and their alteration in ADPKD remains to be elucidated. We can draw some parallels here with Unilateral Ureteral Obstruction models (UUO) that have been used to study the pathological impact of nephron obstruction. UUO in murine models have led to kidney tubule atrophy, kidney cell dedifferentiation as well as fibrosis (Evan *et al.*, 1986; Chevalier, Forbes and Thornhill, 2009; Galarreta *et al.*, 2014). These catastrophic transformations of the kidney parenchyma may be aggravated by increased luminal pressure that contributes to profound alterations of the kidney cells phenotype (Li *et al.*, 2009).

Many studies using kidney-on-chip do not focus on intraluminal pressure, instead focusing on physiological flow shear stress in the tubules. We could not identify a tubular system in the literature which specifically intended to reproduce in a controlled manner the stress due to intraluminal pressure, nor which addressed separately the role of intraluminal pressure or flow shear stress in kidney homeostasis. A similar effort was conducted in a recent microvessel-on-chip study to build a tubular endothelium focusing at the same time on the role of physiological FSS and on the control of the resulting intraluminal pressure strain (Dessalles *et al.*, 2021). In this chapter, we describe and discuss experiments in another system where we can control intraluminal pressure and flow shear stress separately. This allows us to go further by decoupling those two mechanical stresses to characterize specifically the impact of added intraluminal pressure on the kidney epithelium. We first focused on a model for the collecting duct, cultivating our mIMCD-3 cells in our perfused kidney-on-chip. We also decided to expand our investigation to cell lines from the PCT that we used for our previous study.

4.2. Results

4.2.1. Flow shear stress helps to maintain the homeostasis of tubules.

We investigated the necessity of intraluminal FSS for kidney tubules to maintain the homeostasis of the epithelial layer, that we define here by cells with a cuboidal shape and forming a monolayer independently of intraluminal pressure. In our kidney-on-chip with a 6mg/mL collagen I extracellular matrix and laminin coating in tubes, we first seeded WT and *Pkd1KO* mIMCD-3 cells and perfused the chips with the gravity driven system we described in chapter 2 (see Methods for more details). For these first experiments, we perfused the system in the “flow only” configuration, maintaining a physiological FSS around 1 dyn.cm⁻² in the tubules for at least 7 days with minimal intraluminal pressure below the mbar (see chapter 2 part 2.4.1). The chips were seeded at high cell density and perfused a few hours after seeding, allowing enough time for the cells to adhere. Tubules were generally confluent the following day. We took images of the tubules at regular intervals with phase contrast microscopy to follow the evolution of the tubule shape (**figure 4.1.a**). Qualitatively, we could already observe an important divergence from the tubule’s behavior compared to static conditions. In static conditions, normally 5 days after confluency, we could already observe perceptible dilation for the *Pkd1KO* tubules as well as a loss of lumen in many cases involving the WT cells. In the presence of FSS, although the tubules aspect still suggests differences in terms of cell morphology between WT and *Pkd1KO*, we did not observe any perceptible dilation from the *Pkd1KO* and strikingly the WT tubules likewise retained a clear lumen. We quantified the evolution of the tubular shapes by computing the tubules’ average diameter at a given day and normalizing by their diameter at confluency (**figure 4.1.b**). After 5 days, both WT and *Pkd1KO* dilated the channel by 10% on average but without a significant difference between the two. As a comparison, the average dilation was already above 25% by day 5 after confluency without applied FSS in the *Pkd1KO* tubules.

We looked more closely at the tubule’s organization, proliferation and cell morphology by staining nuclei, actin and Ki-67 of cells in tubules and imaging the tubules 1 day and 5 days after confluency with confocal microscopy. We first confirmed that, under FSS, WT cells largely maintained a monolayer. However, we could distinguish local masses of multilayered WT cells in the tubules. Differences in morphology were also less perceptible between the WT and *Pkd1KO* cells compared to the static conditions, with the *Pkd1KO* cells seemingly gaining a more cuboidal shape under FSS (**figure 4.1.c**). We quantified the level of cell spreading by measuring the internuclear distance similarly to the analysis contained in the previous chapter (**figure 4.1.d**); our quantifications confirmed that there was no longer a significant difference between *Pkd1KO* and WT in terms of cell spreading 1 day after confluency. However, completely dissimilar to our observations without FSS, cells were denser for the *Pkd1KO* after 5 days while cell density did not significantly increase in WT tubules. In addition, there was no significant difference between proportion of mitotic cells between at early stage (Day1) for both cell types whereas after 5 days *Pkd1KO* cells were significantly more proliferative than WT cells. Within these 5 days, the average level of proliferation significantly increased in *Pkd1KO* tubules while it significantly decreased in WT cells. Unfortunately, we lacked a static control on day 5 that could corroborate an enhanced contact inhibition for WT tubules under FSS. Alternatively, levels of proliferation may remain similar between static culture and culture under FSS, but the extrusion of excess cells may be facilitated by FSS. This potentially explains the

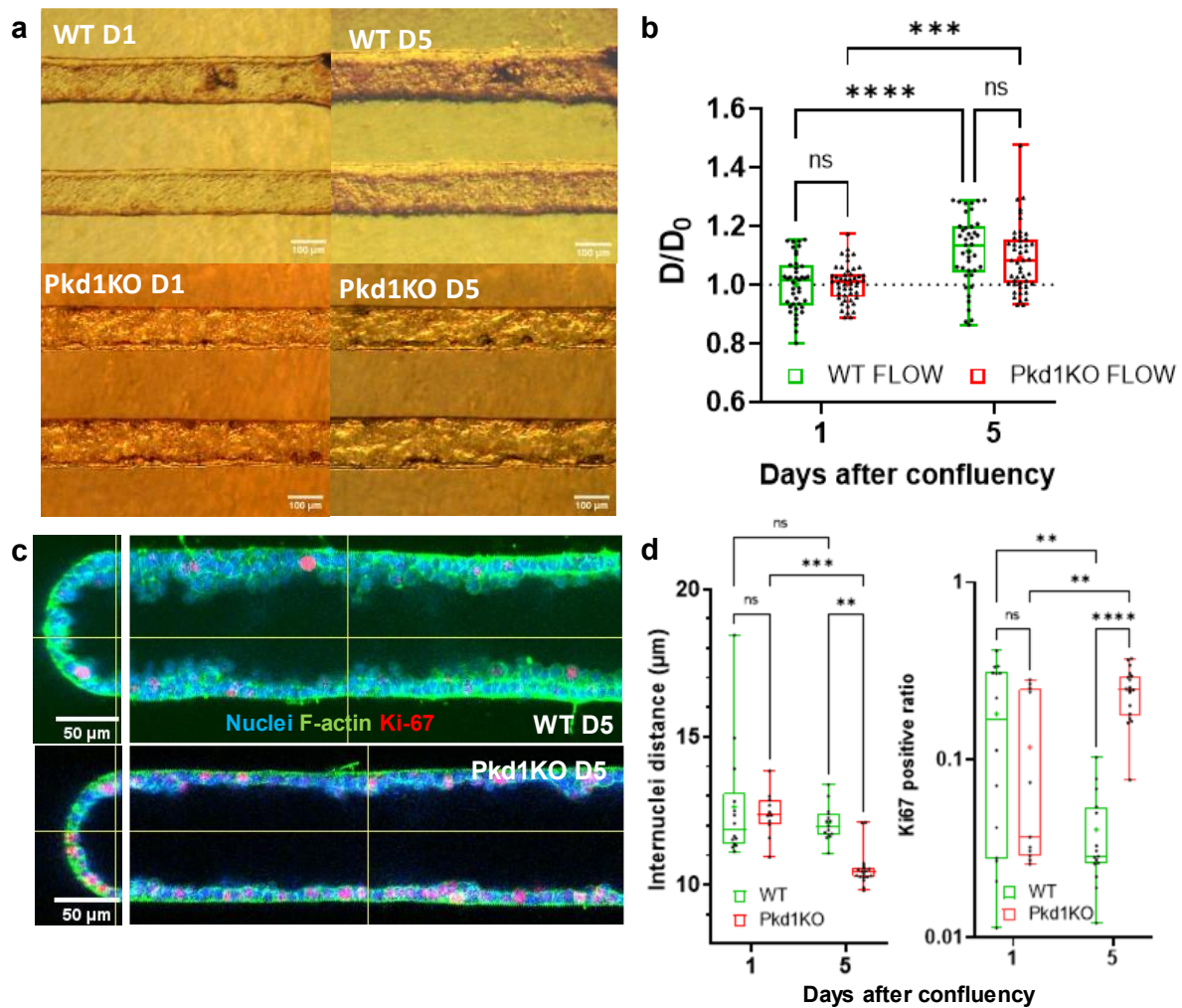


Figure 4.1. FSS favors the maintenance of the initial tubular geometry in mIMCD-3 cells. We seeded at confluency *Pkd1KO* and WT mIMCD-3 cells and cultivated them in our multitubular chip under FSS without intraluminal pressure. In (a) are contrast phase images showing the evolution of these tubules between day 1 and 5. We quantified channel dilation by normalizing the average tubule diameter at a given day (D) by the average tubule diameter at confluency (D₀). Boxplots in (b) are showing the evolution of the normalized channel diameters (Box: 1st and 3rd quartile with median, whiskers: extrema, +: mean, Statistical test: ANOVA p-value: *<0,05, **<0,01, ***<0,001, n: WT:41 *Pkd1KO*:47). We then stained those tubules at day 1 and day 5 for F-actin, nuclei and Ki-67 and image them with confocal microscopy (c) and quantified cell spreading by computing the internuclear distances and proliferation with the ratio of Ki-67 positive nuclei within all nuclei (d) thanks to automatic segmentation of the nuclei. (Box: 1st and 3rd quartile with median, whiskers: extrema, one dot is one tubule. WT n=11-15, *Pkd1KO* n=14-18, p-value: ns>0,05, **<0,01, ***<0,001 obtained with ANOVA)

persistence of local multilayer masses. Increased proliferation levels under FSS for *Pkd1KO* tubules may translate into an increased cell density rather than channel dilation, which is consistent with observed cuboidal shape, akin to the behavior of WT cells in static conditions without multilayering.

We must also note that perfusion does not only introduce an intraluminal FSS but also constantly renews the cell medium inside the lumen, providing an environment enriched in nutrients and growth factors compared to static conditions. This may explain the increased levels of proliferation that we observed for both cell types at day 1 compared to static condition (well above 10% of mitotic cells on average for culture under FSS and well under 10% for culture in static condition). An impaired contact inhibition due to the loss of *Pkd1* may explain why in *Pkd1KO* tubules, proliferation levels did not decrease but rather increased through time after an initial recovery time. Longer experiments would determine if these higher proliferation

levels in *Pkd1*KO tubules would eventually lead to more tubular dilation than WT cells. Taken together, these results suggest that FSS helps mIMCD-3 in our tubular system to maintain a stable hollow tubular geometry. First, FSS aids preserving a lumen in WT tubules. FSS also appears to mitigate the effects of the loss of *Pkd1* on the tubular geometry while paradoxically promoting overproliferation of these cells.

4.2.2. Addition of intraluminal pressure leads to important tubular dilations favored by loss of *Pkd1*.

Flow shear stress is normally accompanied by intraluminal pressure in physiological conditions. To mimic this scenario, we added a controlled intraluminal pressure in addition to the physiological-like FSS. To achieve this, we perfused WT and *Pkd1*KO tubules following the same procedure as previously described until confluency, generally reached the day after seeding. Subsequently, we put the chips in the “flow+pressure” configuration. The idea here is to allow the tubes to become tight enough, allowing them to maintain the desired intraluminal pressure. Indeed, we determined previously that the tubes should become tight shortly after confluency (see chapter 2 figure 2.20). We set in our syringe a level of 10 cm of cell culture medium, leading to an intraluminal pressure of approximately 10 mbar, and maintained this perfusion for up to 5 days. Luminal pressure is quite variable along the nephron unlike FSS. Moreover, intraluminal pressure is subject to fluctuations dependent on the diuresis state of the organism, resulting in significant variations throughout the day. Nonetheless, most of the loss of charge is located in two segments: the loop of Henle and the collecting duct (see chapter 1 figure 1.5). Thus, we expect intraluminal pressure to be moderate inside the intramedullary collecting duct lumen with values no greater than 10 mbar.

Surprisingly these moderate pressures were enough to induce levels of tubular dilation within 5 days in a greater magnitude than what we had observed before with our system (**figure 4.2.a-b**) that cannot be only explained by the compliance of the tubules, as we expect such moderate pressure not to be enough to induce such important deformations of the collagen tubules. After 5 days, WT tubules dilated by more than 50% on average, up to almost 3-fold in extreme cases. Meanwhile, *Pkd1*KO tubules dilated by 150% on average, up to almost 4 folds in extreme cases. Interestingly, most of the dilation happened within the first day for the WT, as levels of dilation were not significantly higher the following days. However, there was a significant increase of diameter for the *Pkd1*KO tubules between day 1 and day 5 after we set the intraluminal pressure. These findings imply a mechanism behind dilation under intraluminal pressure unique to *Pkd1*KO cells that would only make a difference after several days of culture.

We likewise examined the tissue organization, cell morphology and proliferation of kidney cells in these experiments, mirroring the approach taken for the previous ones. In this new context, WT cells strongly remained in monolayers, and we did not observe any significant localized multilayering (**figure 4.2.c**). This suggests that intraluminal pressure is an important physiological cue for WT cells to maintain the tubule lumen. Qualitatively, we also already observed here that adding an intraluminal pressure restored the difference in morphology between WT and *Pkd1*KO cells. WT cells remained largely cuboidal, while *Pkd1*KO cells were initially hard to distinguish from WT cells, and then transitioned to a more squamous morphology after 5 days under luminal pressure (**figure 4.2.d**). These differences were confirmed when looking at internuclear distances to assess cell spreading (**figure 4.2.e**). We observed no significant differences between WT tubules and *Pkd1*KO tubules on day 1 and

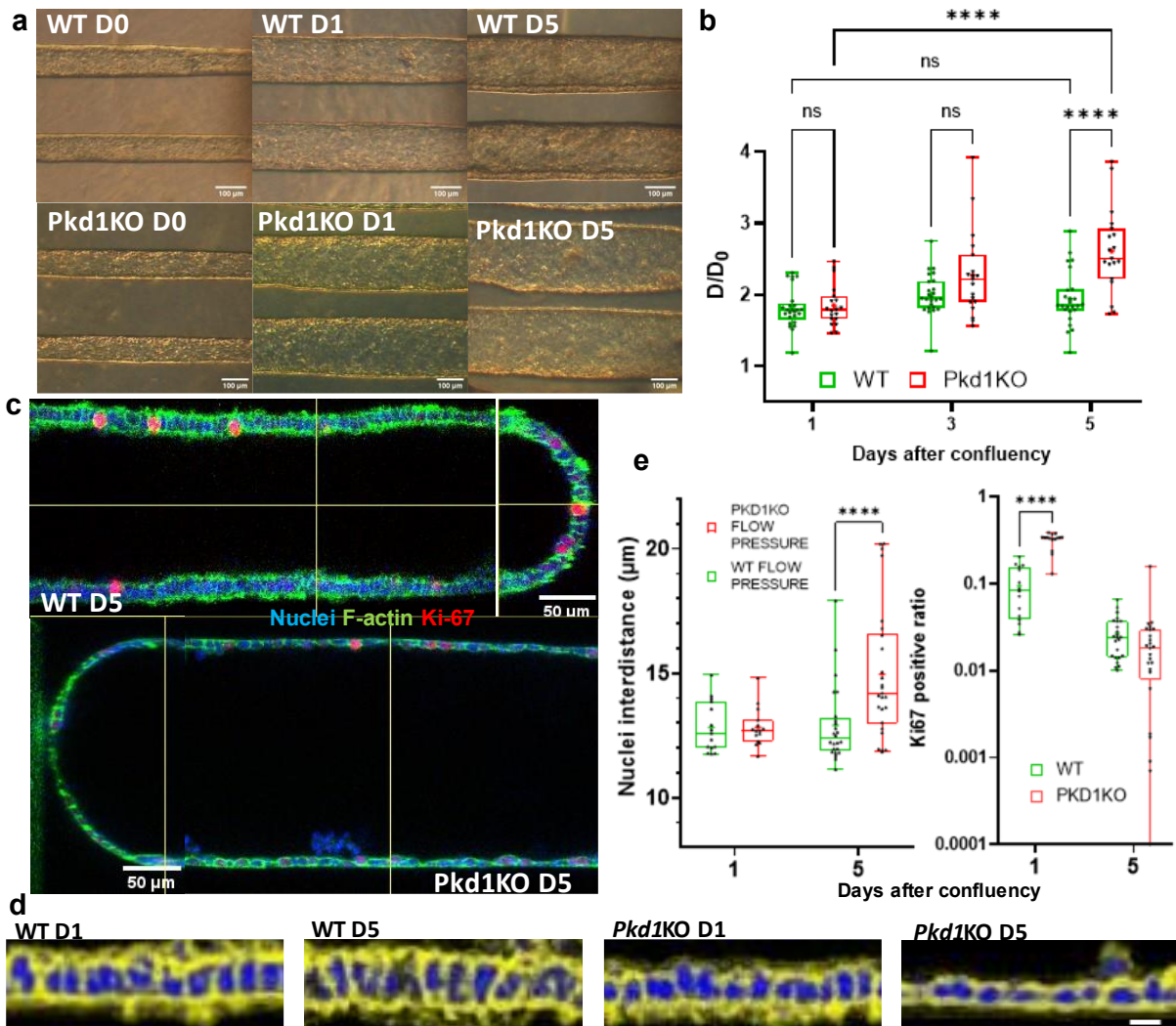


Figure 4.2. Intraluminal pressure leads to an important dilation in mIMCD-3 tubules favored by loss of *Pkd1*. We cultivated WT and *Pkd1*KO mIMCD-3 cells under FSS with 10 mbar intraluminal pressure. In (a) are contrast phase images showing the evolution of these tubules between day 1 and 5. We quantified channel dilation by normalizing the average tubule diameter at a given day (D) by the average tubule diameter at confluency (D₀). Boxplots in (b) are showing the evolution of the normalized channel diameters (Box: 1st and 3rd quartile with median, whiskers: extrema, +:mean, Statistical test: ANOVA, p-value: ns>0,05 ****<0,0001, n: WT:19 *Pkd1*KO:25). We then stained those tubules at day 1 and day 5 for F-actin, nuclei and Ki-67 and image them with confocal microscopy (c). In (d) are close-up of cells in those tubule automatically delimited with deep-learning (scale bar: 10μm). We quantified cell spreading by computing the internuclear distances and proliferation with the ratio of Ki-67 positive nuclei within all nuclei (e) thanks to automatic segmentation of the nuclei. (Box: 1st and 3rd quartile with median, whiskers: extrema, one dot is one tubule. WT n=15-26, *Pkd1*KO n=15-24, p-value: ****<0,0001 obtained with ANOVA)

measured similar cell spreading between day 1 and 5 for WT tubules. In contrast, internuclear distances increased significantly in *Pkd1*KO tubules after 5 days under luminal pressure. These results mirrored what we observed with the dilations. Proliferation levels were initially higher in *Pkd1*KO tubules under these conditions but similar to those without intraluminal pressure. There was no longer any significant difference in proliferation after 5 days of culture between WT and *Pkd1*KO tubules that would explain an increased dilation for the *Pkd1*KO cells. In addition, proliferation levels fell to values similar to this condition without intraluminal pressure in WT tubules. A notable difference with the static condition is that *Pkd1*KO cells exhibited increased spreading after several days of culture under luminal pressure compared to their initial state. This could be attributed to the culture under FSS prior to pressure induction which seems to promote in tissues of *Pkd1*KO tubules a cell morphology comparable to that of WT tubules. However, under FSS, we did not observe denser tubules compared to the static

condition at early stages. Consequently, it is not likely that the high dilation that we observe would be the result of initially denser tissues prior to pressure induction.

Taken together, these observations suggest that, similar to static conditions, enhanced tubular dilation due to loss of *Pkd1* is not the result of enhanced proliferation levels when cells are subjected to FSS combined with intraluminal pressures. Rather, once again increased dilation correlates with higher cell spreading in *Pkd1*KO tubules that seems to increase with time.

The difference in behavior between WT tubules and *Pkd1*KO in response to intraluminal pressure appears to stem from a difference in mechanical response from the tubules. We then ran preliminary experiments to assess any difference in these mechanical responses. We cultivated as before the tubules under FSS only until they reached confluency (day 0). We then imaged the tubules right before a perfusion in the “flow+pressure” configuration with a hydrostatic pressure around 10mbar. We imaged the tubules again a few minutes after. The day after (day 1), we released the pressure, imaged the tubules, put the tubules back under a 10 mbar hydrostatic pressure and imaged them again. We compared the short-term response of the tubules by quantifying dilations at day 0 and day 1 after inducing the intraluminal pressure. This gave us a measure of the influence of *Pkd1* on the evolution of tubule compliance under luminal pressure (**figure 4.3**). We observed no significant difference in dilation at day 0 between WT and *Pkd1*KO tubules (around 9% in both cases), however at day 1, *Pkd1*KO tubules were significantly more compliant than WT tubules. Their level of compliance did not evolve significantly while WT tubules hardly show any significant dilation due to pressure. If confirmed, this result would further demonstrate that the mechanism behind enhanced dilation in the absence of *Pkd1* is not initially significant but becomes more important as the phenotypes of the two cell types diverge. Furthermore, WT tubules may have an adaptation mechanism making them less sensitive to pressure-induced deformation in the long run. Indeed, as the *Pkd1*KO cells adopt a more squamous phenotype, WT cells on the other hand become more cuboidal and taller, which would suggest a lessened ability to deform under constraint.

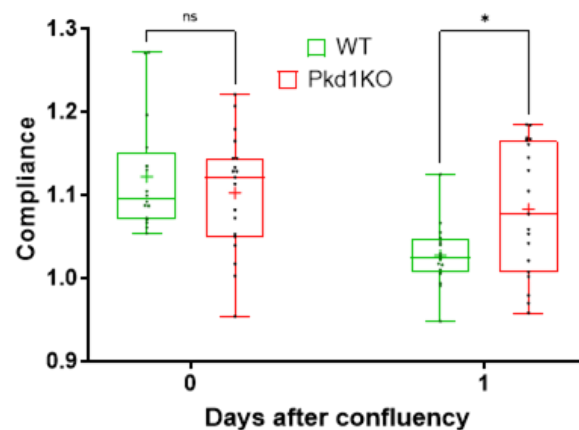


Figure 4.3. Preliminary results: Compliance of mIMCD-3 tubules decreases with time with WT cells but not with *Pkd1*KO cells. To assess the short-term mechanical response of the tubules to intraluminal pressure, we normalized the average tubule diameter right after induction of pressure by the average tubular diameter right before at day 0 and day 1 after culture under luminal pressure. (Box: 1st and 3rd quartile with median, whiskers: extrema, one dot is one tubule. WT n=16, *Pkd1*KO n=19, p-value: ns>0.05,*<0.05 obtained with ANOVA)

4.2.3. Dilation under luminal pressure is very sensitive to extracellular matrix density.

The different mechanical responses we measured from the tubules could stem from different mechanical properties of the cells or from the ECM (collagen type I at 6 mg/mL). Although the two cell types grew on the same ECM, it was shown that loss of *Pkd1* in kidney epithelial cells leads to the development of different basement membranes when cultured in hydrogels (Subramanian *et al.*, 2012). To evaluate the importance of the ECM in the pressure-induced dilation, we seeded WT and *Pkd1*KO cells in a 9mg/mL collagen I matrix and cultivated them perfused in the “flow+pressure” configuration for up to 5 days.

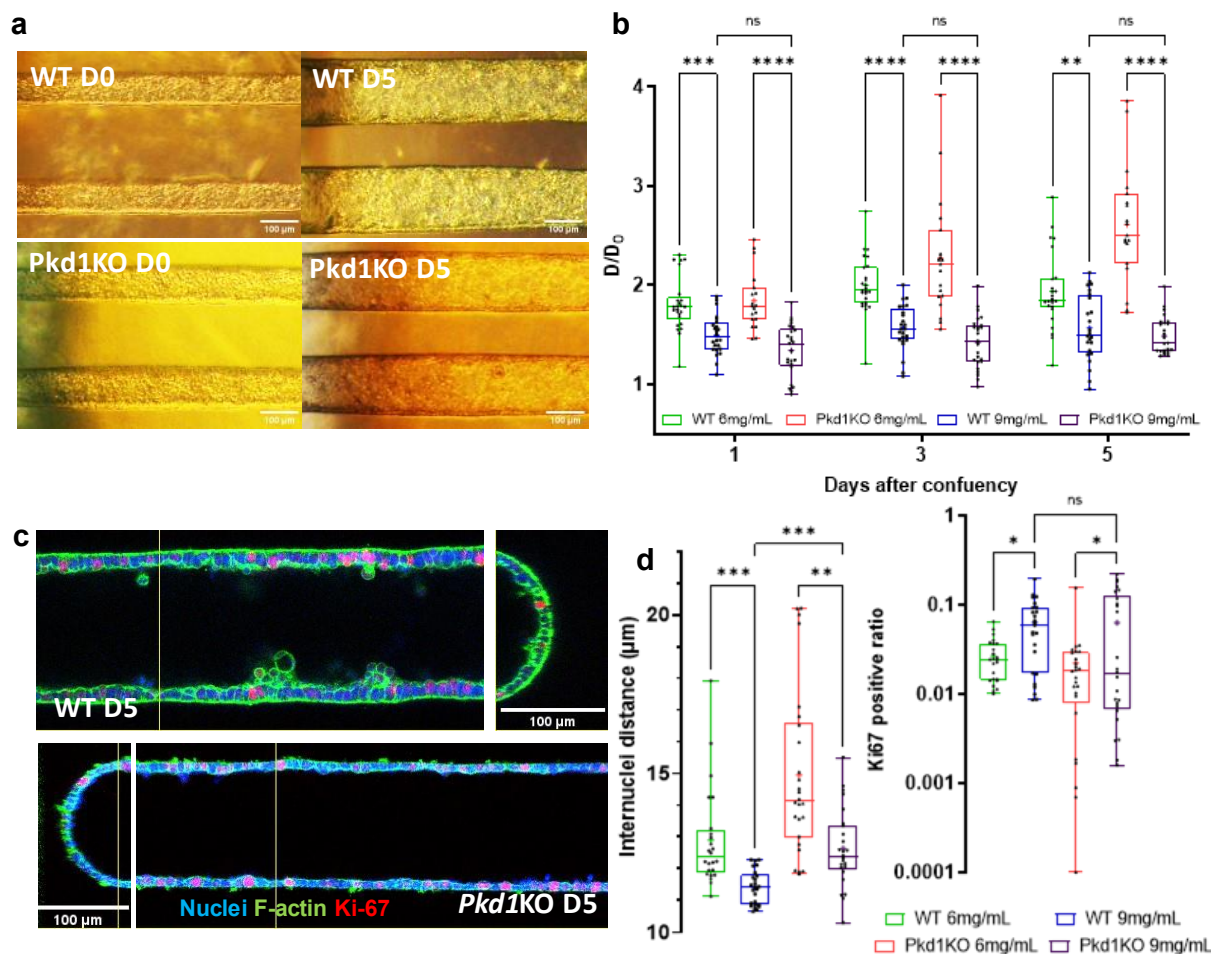


Figure 4.4. Pressure driven tubular dilation in mIMCD-3 cells is mitigated by denser extracellular matrix. To study the effects of matrix density on pressure driven dilation, we cultivated WT and *Pkd1*KO mIMCD-3 cells under FSS with 10 mbar intraluminal pressure in 9mg/mL collagen matrix. In (a) are contrast phase images showing the evolution of these tubules between day 0 and 5. Boxplots in (b) are showing the evolution of the normalized channel diameters (Box: 1st and 3rd quartile with median, whiskers: extrema, +:mean, Statistical test: ANOVA, p-value: ns>0,05 **<0,01, ***<0,001, ****<0,0001, n: WT 6-9mg/mL: 24-25 *Pkd1*KO 6-9 mg/mL:25-19). We then stained those tubules at day 5 for F-actin, nuclei and Ki-67 and image them with confocal microscopy (c). We quantified cell spreading by computing the internuclear distances and proliferation with the ratio of Ki-67 positive nuclei within all nuclei (d) thanks to automatic segmentation of the nuclei. (Box: 1st and 3rd quartile with median, whiskers: extrema, one dot is one tubule. n: WT 6-9mg/mL: 24-25 *Pkd1*KO 6-9 mg/mL:26-25, p-value: ns>0,05, *<0,05, **<0,01, ***<0,001 obtained with ANOVA)

Intraluminal pressure still led to important tubular dilation, around 50% on average with some tubules doubling in size, but these levels of dilation were significantly lower than in a 6mg/mL collagen matrix (**figure 4.4.a-b**). Increasing the ECM density also abrogated any significant difference in dilation between WT and *Pkd1*KO tubules. Similar to WT tubules in 6mg/mL collagen, WT and *Pkd1*KO tubules no longer significantly dilated the tubules after day 1. While still being distinguishable from WT cells, *Pkd1*KO cells after 5 days of culture did not display the squamous morphology, we observed on the 6mg/mL but rather an intermediate morphology (**figure 4.4.c**). Quantification of internuclear distances 5 days after induction of intraluminal pressure confirmed that *Pkd1*KO cells were significantly less spread on the 9mg/mL gel than in the 6 mg/mL gel yet remained significantly more spread than WT cells (**figure 4.4.d**). WT cells also appeared denser in the 9mg/mL gel, possibly due to heightened levels of proliferation on the more rigid substrate. Similarly, a significantly enhanced proliferation in *Pkd1*KO tubules may have contributed to their increased tissue density. These results put in evidence how the ECM density has an important role to play in the tubule response to intraluminal pressure, most notably how a denser ECM can protect the tissue against dilation. One possibility is that being stiffer, a denser ECM offers a higher mechanical resistance to dilation. Alternatively, ECM remodeling becomes less relevant as the gel gets denser because remodeling of the ECM becomes less effective with denser gel; or difference in mechanical properties due to remodeling are less significant next to the gel initial properties.

4.2.4 Loss of *Pkd1* in cells from the proximal convoluted tubules may also favor dilation under pressure as flow shear stress only partially thwarted its effects.

We previously showed in chapter 2 part 2.2 and chapter 3 that loss of *Pkd1* led to tubular dilation in static conditions for two unrelated cell lines. In this work, with mIMCD-3 cells, we saw that tubular dilation was not due to increased level of proliferation while results from a previous study with PCT cells showed that it appeared to be the case for those cells. Building on this previous study, in preliminary experiments we also investigated the impact of FSS and intraluminal pressure on tubular geometry within these PCT cells. To decipher the effects of FSS from intraluminal pressure, we ran similar perfusion experiments as with the mIMCD-3 cells in 6mg/mL collagen matrix.

Under FSS only, *Pkd1*^{-/-} cells dilated the tubules significantly while no dilation was observed for *Pkd1*^{+/-} cells, marking the first important divergence from the mIMCD-3 cells where there is no significant increased dilation due to the absence of *Pkd1* (**figure 4.5.a-c**).

Being the first segment of the nephron, proximal convoluted cells are normally submitted to level of intraluminal pressure superior to the 10mbar that we applied in parallel experiments. Nevertheless, a 10 mbar intraluminal pressure was sufficient to induce important dilations for both *Pkd1*^{+/-} and *Pkd1*^{-/-} with loss of *Pkd1* significantly enhancing dilation similarly to mIMCD-3 cells. With or without intraluminal pressure, *Pkd1*^{+/-} cells largely remained in monolayer, whereas without intraluminal pressure, *Pkd1*^{-/-} cells had a strong tendency to multilayering forming intraluminal cell masses, but a clear lumen was still present 5 days after confluency (**figure 4.5.d**).

Compared to the *Pkd1*^{+/-} cells, the *Pkd1*^{-/-} tissue was significantly denser, which coincided with significantly higher proliferation levels at least without pressure (**figure 4.5.e**). Thus, in this case, increased proliferation levels due to the loss of *Pkd1* remains a convincing

explanation for the tubular dilation. This tendency to form multilayers was still present when adding intraluminal pressure, although in this case the tissue was more homogeneous. Internuclear distance was significantly higher under intraluminal pressure for both cell types, with no statistically significant difference between the two while proliferation levels decreased. Oddly from our current data, the higher average level proliferation in the *Pkd1*^{-/-} compared to the other cell type, that would then explain why *Pkd1*^{-/-} cells dilated more, was not significant. This could be explained by the relative small size of our sample or alternatively, as we only assessed proliferation levels on day 5, it is highly likely that proliferation levels were higher before day 5 for the *Pkd1*^{-/-} cells but then decreased. With this similar cell spreading we can expect larger tubule purely due to geometrical effect. Taken together, these results suggest that FSS alone is not enough to limit PCT *Pkd1*^{-/-} overproliferation and preserve the initial tubular geometry. In addition, subphysiological intraluminal pressure can lead to cell spreading in this system that correlates for both *Pkd1*^{+/-} and *Pkd1*^{-/-} cells, with important tubular dilation potentially enhanced in *Pkd1*^{-/-} cells by higher levels of proliferation.

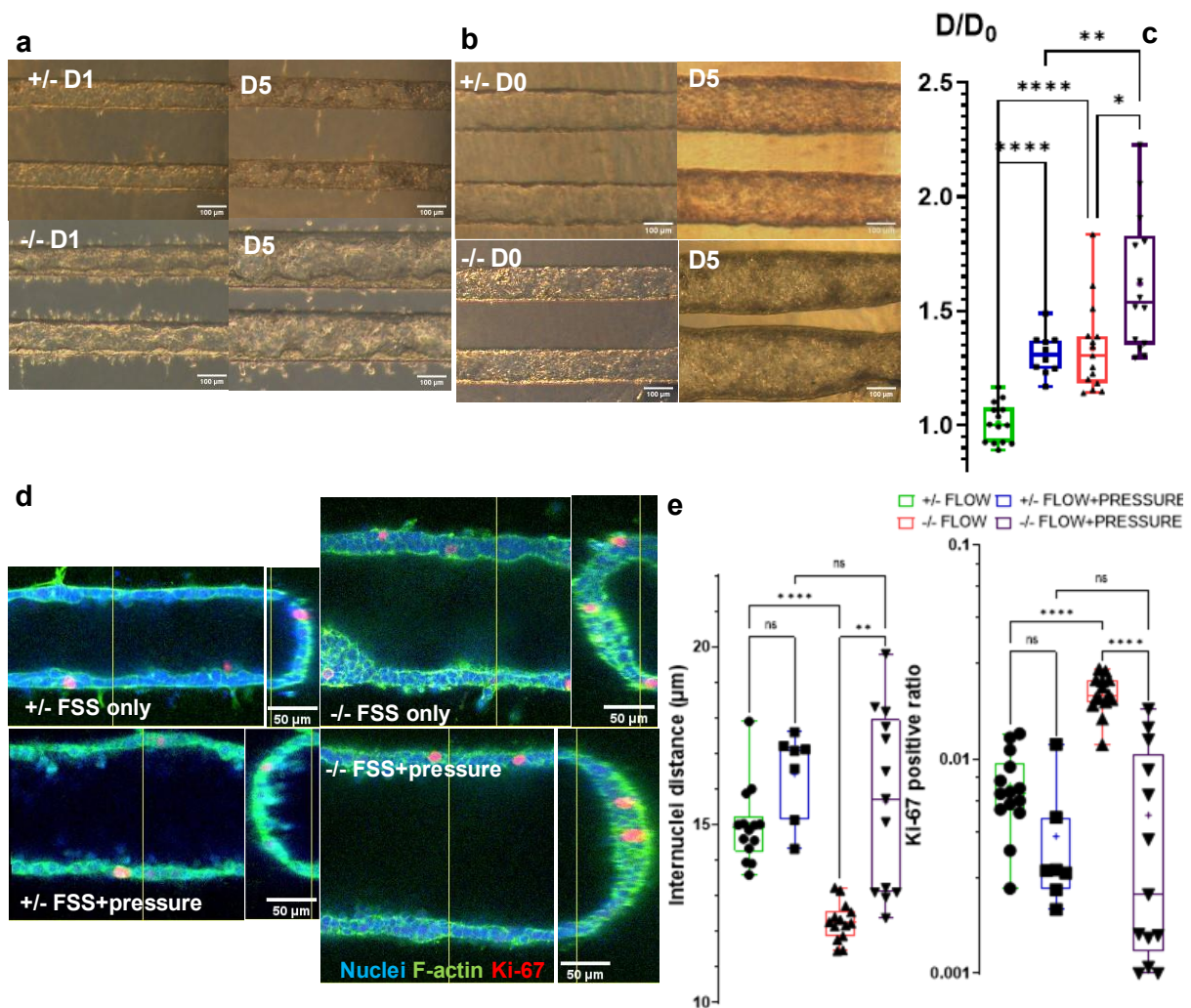


Figure 4.5. Preliminary results suggest that a tubular dilation in PCT tubules submitted to hydrodynamic stress is driven by sustained increased proliferation due to loss of *Pkd1*. In preliminary experiments we cultivated *Pkd1*^{+/-} and *Pkd1*^{-/-} PCT cells under FSS with and without 10 mbar intraluminal pressure in 6mg/mL collagen matrix. In (a) and (b) are contrast phase images showing the evolution of these tubules with and without pressure respectively. Boxplots in (c) are showing the normalized channel diameters at day 5 (Box: 1st and 3rd quartile with median, whiskers: extrema, +:mean, Statistical test: ANOVA, p-value: *<0,05 **<0,01, ****<0,0001, n: +/- with pressure-without pressure: 10-14, -/- with pressure-without pressure: 14-15). We then stained those tubules at day 5 for F-actin, nuclei and Ki-67 and imaged them with confocal microscopy (d). We quantified cell spreading by computing the internuclear distances and proliferation with the ratio of Ki-67 positive nuclei within all nuclei (e) (Box: 1st and 3rd quartile with median, whiskers: extrema, one dot is one tubule. n: +/- with pressure-without pressure: 7-14, -/- with pressure-without pressure: 13-14, p-value: ns>0,05, **<0,01, ****<0,0001 obtained with ANOVA)

4.3 Discussion

4.3.1. On the importance of flow shear stress to maintain the tubule homeostasis

Our first aim with this study was to decipher the specific importance of FSS for the maintenance of tubule homeostasis; decoupling it from luminal pressure. Many models have accounted for the importance of FSS for the kidney tubules by mimicking this stress, however FSS in these models is typically generated with a flow rate-driven perfusion characterized by poor control and characterization of the resulting intraluminal pressure. We managed with our kidney-on-chip and our perfusion system to induce a physiological FSS in our tubules while minimizing intraluminal pressure.

First, with WT m-IMCD3 cells, we showed that FSS alone could greatly limit the multilayering that we observed under static condition probably due to overproliferation. We could also largely maintain tubules mostly in monolayers and preserve the presence of a clear lumen. However, we could still see the presence of local ingrowth in the tubules. Thus, given these observations and as the cells retained a strong proliferative phenotype comparatively to the static condition, we do not think that FSS alone enhanced contact inhibition and prevented crowding. Alternatively, FSS potentially facilitated elimination of excess cells due to such crowding. In crowded epithelium, cells are eliminated through extrusion. Multiple perfused *in vitro* models of kidney epithelium showed that FSS leads to actin rearrangement with stronger actin bundles at the junction of cells, specifically at the apical region (Duan *et al.*, 2008; Jang *et al.*, 2011). For those extrusions to happen, surrounding cells need to form actin rings which apply the necessary tension to displace the cell in the apical direction out the tissue (Schwayer *et al.*, 2016; Gagliardi and Primo, 2019). Thus, FSS favoring the presence of actin bundles at the apical junction of cells could also favor the extrusion of excess cells. While from a different origin, shear stress has similarly been shown to facilitate extrusion of aberrant cells in breast cancer epithelium (Friedland *et al.*, 2022). To draw conclusions in our case, we would need more specifically to look at the actin organization in our tissues. Moreover, FSS can create a drag force in the direction of the flow on cells being extruded that mechanically favors their elimination. Further investigation, looking specifically at the F-actin location and looking at the effect of inhibition of actomyosin contractility could confirm this hypothesis. Presence of ingrowth and loss of lumen in static condition could then be the result of partial extrusions. We must also note that as lumen diameter eventually decreases due to multilayering, the local FSS would increase magnifying its effect, thus preventing cell accumulation in the lumen up to a certain degree only.

Paradoxically, FSS also preserved the tubular geometry with the *Pkd1*KO m-IMCD3 cells by limiting their dilation, despite our results suggesting that a loss in contact inhibition due to the loss of *Pkd1* in m-IMCD3 cells leads to enhanced proliferation under flow. The paradox is lifted when considering the cellular rearrangement favoring cell packing under FFS. Indeed, we attributed the increased cell density in *Pkd1*KO tubules to increased proliferation. However, as there was no significant difference in cell spreading between WT and *Pkd1*KO tubules, we should consider a positive impact of FSS on cell polarization and differentiation that would mitigate the deleterious effects of the loss of *Pkd1*, as many prior studies have demonstrated in a more general context. This would provide an explanation as to why proliferation of *Pkd1*KO

cells in static condition geometrically results in channel dilation while under FSS it results in increased cell density. More specifically, a cytoskeleton reorganization due to FSS could favor at the cell level, a plasticity similar to WT cells that they lacked otherwise: an ability to modulate their shape to cope with cell crowding. Enhanced proliferation may then be balanced enough by enhanced extrusion, mitigating early tubular dilation. Longer experiments would show if the potential loss of contact inhibition and the resulting increased homeostatic pressure would still eventually lead to increased tubular dilation compared to WT, through a different mechanism than what happened in static dilation, but like what happened with the loss of *Pkd1* with PCT cells.

The disappearance of significantly increased dilation for *Pkd1*KO cells under FSS could also be explained by decreased secretion from the cells to the lumen and more balanced osmotic pressures across the tissue. It was shown that under FSS, ADPKD cells no longer had an important secretion activity towards their apical side. On the contrary, these cells resumed a reabsorption activity towards their basal side like WT cells (Choudhury *et al.*, 2022). This reabsorption activity would virtually create a negative pressure inside the lumen, thus favoring the maintenance of the initial tubular shape with a crowded epithelium. More generally, in perfused *in vitro* cultures of collecting duct cells, it was shown that FSS was an important cue for the homeostasis of apical fluid. This can be accomplished by increased water permeability through aquaporin-2 translocation (Jang *et al.*, 2011) and through nitric oxide-mediated inhibition of reabsorption of ions (Cai *et al.*, 2000b), potentially balancing in our case the intraluminal osmolarity.

4.3.2. On the importance of intraluminal pressure to maintain the tubule homeostasis

When we added a controlled intraluminal pressure in the system, it prevented almost entirely the presence of luminal ingrowths in WT m-IMCD-3 tubules, suggesting that this additional cue may be necessary for the maintenance of the monolayer. Subsequent dilation along with the addition of intraluminal pressure may geometrically result in less crowding, as suggested by the slightly increased internuclear distances (around 13 μ m on average with intraluminal pressure vs 12 μ m on average without), thus limiting multilayering. However, levels of proliferation did not decrease with the addition of intraluminal pressure, while internuclear distance remained approximately the same for the duration of the experiment without significant dilation past day 1. This suggests that there could be more behind than a simple geometric effect. Intraluminal pressure has been shown to impact actin organization, disorganizing F-actin filaments in the cytoplasm similarly to FSS (Martin, Brown and Haberstroh, 2005; Li *et al.*, 2009; Jang *et al.*, 2011). We can speculate that the combined action of a moderate intraluminal pressure and a physiological FSS could result in potentially stronger junctional actin, favoring the stability of the monolayer. Moreover, intraluminal pressure represents an additional stress increasing the tension in the tissue which could stabilize it and would not energetically favor tissue outgrowth.

We observed under the same moderate luminal pressure, high tubular dilations with the PCT *Pkd1*^{+/-}, that are not associated in other context with overproliferation, spontaneous multilayering or dilation. Furthermore, knowing that the proximal convoluted tubule is normally subjected to higher pressures, this suggests that a the 6mg/mL collagen matrix on its own may

constitute a matrix too compliant. Thus, it appears that a basal high tubular dilations that we observe with all the cell types would be from mechanical origin. *In vivo*, the relatively rigid basement membrane constitutes an additional barrier against tubular distension that is lacking in our model. Indeed, in our experiments, increasing the matrix density greatly reduced the pressure-driven tubular dilation, while still allowing for the maintenance of monolayers. However, reproducing a basement membrane *in vitro* appears as a challenging ordeal. In preliminary experiments, we rigidified the extracellular matrix with low concentrations of glutaraldehyde, but culture of m-IMCD-3 cells with FSS and intraluminal pressure on this substrate led to rapid loss lumen (not shown). This was possibly due to a combination of a stiffness-enhanced proliferation and confinement. Nevertheless, finding the right extracellular matrix mechanical properties may allow us to ally a physiological intraluminal pressure with a physiological FSS that maintains the tubular homeostasis of our mIMCD-3 tubules in the long term. Alternatively, we could investigate the effects of higher residual luminal pressure or intraluminal pressures between 0 and 10 mbar allied to a physiological FSS. Doing so would simply require decreasing the hydraulic resistivity of the system.

4.3.3 On the different response of tubules to intraluminal pressure due to *Pkd1*

The role of *Pkd1* for tubule homeostasis appeared significant again under luminal pressure, possibly demonstrating further the importance of this protein for the mechanical response of kidney tubules to this stress. Indeed, we showed that loss of *Pkd1* enhanced tubular dilation. Like what happened under static conditions, this enhanced dilation was mitigated by increasing the density of the collagen. Furthermore, our preliminary results suggest that short-term response to intraluminal pressure is attenuated for WT tubules with time, but is not for *Pkd1*KO tubules. In addition, longer term exposition to intraluminal pressure does not yield significantly more response from WT tubules, while *Pkd1*KO tubules kept dilating to reach a diameter 2.5 times longer than the initial diameter. Taken together, these observations would mean that the additional dilation we observed with *Pkd1*KO tubules, besides the difference in cell organization, would also be the result of differential remodeling of the extracellular matrix by WT cells and *Pkd1*KO cells. Such mechanism behind *Pkd1*-dependant tubular dilation could be the same as behind the dilations that we described in the previous chapter, where dilations from *Pkd1*KO cells under static conditions were also very sensitive to the ECM density. In WT tubules, intraluminal pressure would eventually be balanced by the matrix rigidity through a *Pkd1*-dependent matrix remodeling. Absence of *Pkd1* would lead to a matrix with altered properties that would favor tubular dilation.

In addition, *Pkd1*KO cells have a propensity to adopt squamous morphology counterbalanced by FSS. The additional stress that intraluminal pressure represents may jeopardize any cytoskeletal reorganization promoted by FSS by perturbing the cytoskeleton through formation of actin filaments. Pathologically high hydrostatic pressures have been shown in renal cells and other tubular cells to perturb the actin networks (Martin, Brown and Haberstroh, 2005; Li *et al.*, 2009; Yang *et al.*, 2011). More moderate levels of hydrostatic pressures were shown to produce similar effects, especially in junctional actin, but only when applied from basal side of the tissue (Tokuda *et al.*, 2009). Loss of *Pkd1* has been widely associated with impaired polarization of kidney cells, that we have yet to confirm in our cells. Nonetheless, the squamous morphology that could be observed under static conditions with

our *Pkd1*KO cells would go in that direction. Partial loss of apicobasal polarization could then potentially lead to similar effects irrespective of the side from which hydrostatic pressure is applied. It would also be interesting to investigate if these differences in morphology would indeed lead to a more compliant tissue aside from the surrounding ECM. Nevertheless, lower cell spreading on stiffer collagen coinciding with decreased dilation, but higher proliferation suggests that the predominant effect would come from the ECM and the squamous morphology may be here at least partially a consequence of dilation.

Additionally, an alternative or complementary mechanism through which loss of *Pkd1* can favor tubular dilation may be found in transepithelial transport. As we mentioned earlier, ADPKD cells tend to have an aberrant secretion activity instead of reabsorbing fluids. The reabsorption activity appears to compensate for the moderate pressure we applied creating an opposing pressure. Such reabsorption in WT cells would be sufficient to partially nullify the intraluminal pressure in our experiments, while *Pkd1*KO tubules would fail in this compensatory mechanism as well. Playing on the osmolarity of the intraluminal or extraluminal fluid could be a way to alter these reabsorption mechanisms and assess their importance for the maintenance of the tubular shape under intraluminal pressure.

Finally, in the literature, stretching is usually accompanied by increased levels of proliferation. Here for mICMD-3 *Pkd1*KO cells, even if initial pressure resulted in increased proliferation levels, proliferation rates remained significantly lower than with FSS only while many tubules fell to very low levels. Our preliminary results with PCT *Pkd1*^{-/-} cells aligned with this result. Previous studies on the resistance of kidney cells to mechanical stress pointed out that the loss of *Pkd1* favored apoptosis of the cells may be due to mechanical stresses (Peyronnet, Sharif-Naeini, Joost H A Folgering, et al., 2012). Our observations may go in this direction and further investigations could comparatively assess levels of apoptosis in the tubules relative to *Pkd1* and intraluminal pressure.

4.4. Conclusion and significance for ADPKD

In summary, we showed that FSS on its own partially preserves the homeostasis of artificial kidney tubules on chips. But it is not sufficient and should probably be completed with intraluminal pressure to strongly maintain monolayers. An intraluminal pressure at physiological levels on the other hand is sufficient to alter the tubular geometry through dilation in a too compliant extracellular matrix but can be counterbalanced by local stiffening of the matrix. Therefore, FSS associated with intraluminal pressure and the right extracellular matrix could constitute the right combination for a long-term maintenance of the tubular homeostasis. Loss of *Pkd1* jeopardizes the tubular response to intraluminal pressure, favoring pressure driven distension. However, FSS can partially rescue the tubular homeostasis in the absence of *Pkd1* in a cell type dependent manner, possibly in relation to the different mechanisms behind tubular dilation with those cells.

In a normal context, kidney tubules are subject to physiological intraluminal pressures resulting from the organ function. The tubular mechanical properties, with their intraluminal and extraluminal fluid homeostasis, allows them to withstand such pressures. Our results suggest that haploinsufficiency for *PKD1* found in ADPKD impairs the tubular adaptation to this stress, possibly through aberrant extracellular matrix remodeling. Similarly, an altered basement membrane is a hallmark of cyst microenvironments in ADPKD. Further investigation on the precise role of ECM remodeling in our system could then provide additional evidence for pressure driven cyst growth due to altered basement membrane. Moreover, in ADPKD, both FSS and intraluminal pressure can be altered in tubules in the vicinity of growing cysts. Such perturbations were proposed as a third-hit triggering event for cyst formation. Our findings suggest that certain *Pkd1* haploinsufficient cells may not alter the tubular geometry due to a protective effect from FSS. Perturbation of the FSS may then allow the development of cystic phenotypes. The addition of an increased intraluminal pressure also characteristic of tubules surrounding cysts would further promote tubular distensions.

Until now, we only addressed the behavior of homogeneous tubules expressing or not *Pkd1* to decipher the mechanisms behind cystogenesis. However, *in vivo*, ADPKD cells form a mosaic tissue of potentially cystic cells and tubular cells that shape together the kidney microenvironment, adding another layer of complexity if we want a relevant model of cystogenesis in ADPKD. In the next chapter, we will address how modelling mosaicism in ADPKD in our tubular system impacts the epithelium homeostasis.

5. Modelling mosaicism in ADPKD

5.1. Cell mosaicism and competition

Mosaicism occurs when normally homogeneous cells within the same tissue cohabit while having distinct gene expression associated to divergent cell fates. Mosaicism can be the result of somatic mutations. Thanks to recent advances in sequencing, we are now aware that somatic mutations are ubiquitous even in healthy individuals, therefore mosaicism is a normally occurring phenomenon (Ogawa *et al.*, 2022). However, in some instances of differently fated cells within an epithelium, the homeostatic equilibrium of the tissue can be broken, and mosaicism can lead to life threatening disorders. Cancer and ADPKD are examples of such acquired genetic mosaicism. Notably in ADPKD, typically somatic mutations result in subpopulation of cells deprived of *PKD1* or *PKD2* gene expression that may form cysts.

In these setups normal cells are progressively eliminated as cells compete for space and limited resources. Normally, cell competition is a vital process for the maintenance of functional tissues. From the embryonic stage unfit cells are eliminated to ensure proper organ development (Clavería *et al.*, 2013; Sancho *et al.*, 2013). These unfit cells are generally eliminated either through programmed death or extrusion. Moreover, epithelium notably has built-in surveillance mechanisms preventing the development of cells with potentially detrimental behavior, for instance in the case of precancerous cells. However, this “survival of the fittest” does not always result in healthy cells being selected. In pathological cases malignant or aberrant cells emerge as “winners” (Eichenlaub, Cohen and Herranz, 2016; Suijkerbuijk *et al.*, 2016). As a result, tissue homeostasis can be compromised.

The precise formula behind transformations of unfit cells into “super-competitors”, where cells clonally expand uncontrollably completely replacing different cells, is still the object of many investigations, however specific proteins such as Myc have been identified as being determinant for cells to acquire a super competitor phenotype (Moreno and Basler, 2004; Clavería *et al.*, 2013). Nevertheless, the outcome of cell competition integrates more variables than a single protein expression. Indeed, becoming a super competitor does not seem to be an absolute trait but rather context dependent. For instance, YAP nuclear localization, associated with higher Myc expression, has been shown in certain contexts to promote clonal dominance in a crowded epithelium (Price *et al.*, 2021), eventually promoting tumorigenesis (Liu *et al.*, 2019), while in other constitutive YAP overexpression can lead to cell elimination from the epithelium (Chiba *et al.*, 2016). Similarly, in ADPKD, somatic loss of *PKD1* is not systematically accompanied by cystogenesis, rather the right microenvironment may be needed for these cells to become locally dominant and drive cyst formation.

Lately, to generate somatic mosaicism of ADPKD *in vivo*, inducing mutations post-birth in mouse model seems to have become the gold standard as already discussed at the end of the first chapter. Alternatively, Nishio *et al.* proposed a chimeric mouse model, mimicking ADPKD mosaicism generating embryonic chimeras of wild-type morulae and of morulae from *Pkd1*^{-/-} embryos (Nishio *et al.*, 2005). With this model, they could follow the evolution cell population depending on their *Pkd1* genotype and showed evidence of cell competition mechanisms in growing cysts.

To study mosaicism in ADPKD, similarly we decided to mix *Pkd1*⁺ cells with *Pkd1*^{-/-} cells in a controlled ratio. Our control on the seeding density allow to get from the start a

confluent monolayer with a desired ratio between cell types, notably when they display different levels of proliferation.

5.2. Results

5.2.1 Modelling cell mosaicism in the proximal tubule

Experiment design and cell validation

We first chose to model ADPKD mosaicism with a mix of *Pkd1*^{+/-} and *Pkd1*^{-/-} PCT cells. We had already characterized and studied these two cell lines separately in 2D and in our previous kidney-on-chip and saw that *Pkd1*^{-/-} PCT cells dilated their tubules uniformly while *Pkd1*^{+/-} did not. Thus, we hoped that mixing both cell type would lead to localized dilations where *Pkd1*^{-/-} cells were located. Beforehand, to be able to monitor live cells depending on their *Pkd1* expression, we modified them to have their actin fluorescent at different wavelengths. For that, we used stable transfections or CRISPR: Cas9 mediated gene insertion with the help of UMR168 BMBC platform. Both these procedures require clonal selection, and specific clones may display particular properties of cytoskeleton and adhesion protein organization that may have an impact on competition properties (e.g., E-cadherin levels playing on cell sorting, proliferation levels). Therefore, we had first to check that these modifications would not alter the cell behavior in a mosaic tissue: they should have similar adhesive and proliferative properties as the parental cells. To simply test this, we seeded laminin-coated 500µM thick 6mg/ml collagen I flat substrates with different fluorescent *Pkd1*^{+/-} and *Pkd1*^{-/-} clones mixed with their parental cells at confluency at a 1:1 ratio. Following these mixes 8 days after seeding allowed us to identify clones that neither segregated from their parental cells, nor exhibited a behavior that could be assimilated to cell competition towards

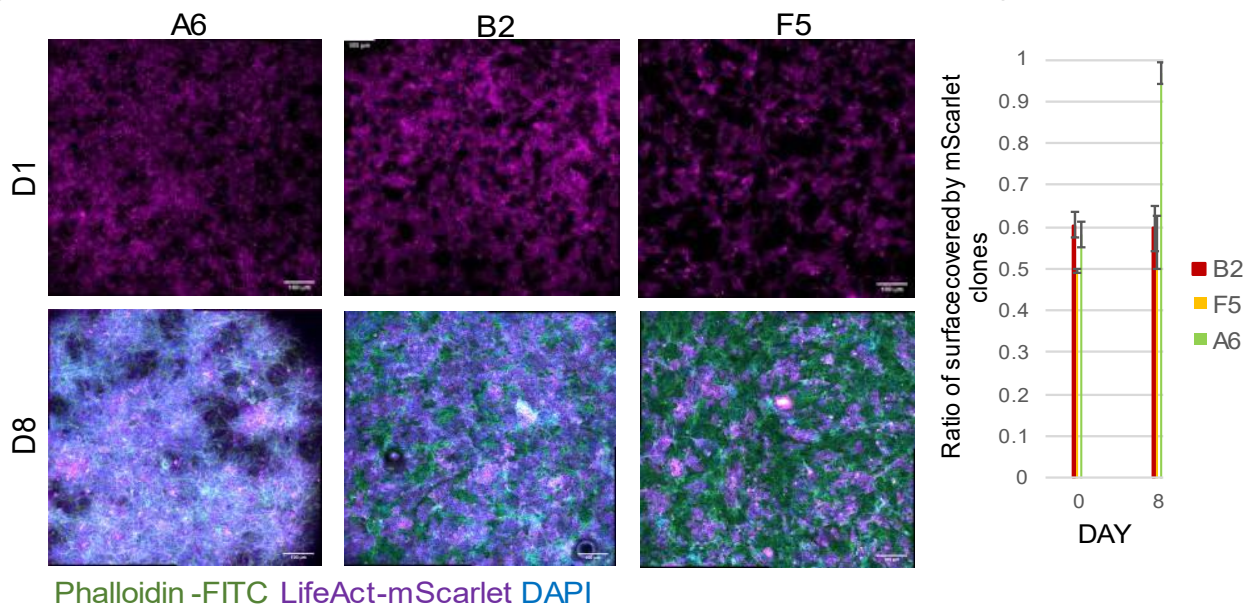


Figure 5.1: Example of preliminary tests conducted for the validation of PCT fluorescent clones. Seeding on 2D collagen surfaces at a 1:1 *Pkd1*^{+/-} LifeAct mScarlett:*Pkd1*^{+/-} allowed the identification of 2 fluorescent clones that could be considered equivalent to the parental clones (B2 and F5). One clone (A6) exhibited an aberrant behavior, totally replacing the parental cells. Here are Z projections of confocal images taken of for these preliminary tests and corresponding quantification (error bars: SD, n=3).

them (figure 5.1). With RT-qPCR comparing a subset of key genes with the parental gene

expression (not shown), we validated two combinations of *Pkd1*^{+/-}/*Pkd1*^{-/-} differently fluorescent clones. For instance from the example shown in **Figure 5.1**, we chose the clone F5 because it was the closest from the parental *Pkd1*^{+/-}.

The importance of the substrate: how the geometry and stiffness of the surface can impact the outcome of cell competition

In ADPKD, *Pkd1*^{-/-} cells are initially present in an overwhelming minority. On the other hand, we wanted to make sure we had a substantial number of cells over the whole collagen-based tubules. For that, we initially chose cell mix ratio of 1:9 *Pkd1*^{-/-} mCherry-beta-actin :*Pkd1*^{+/-} Lifeact GFP. We first investigated the effect on cell competition of the cell substrate stiffness in 2D by seeding this mix either on glass slide coated with collagen I at 0.1 mg/mL and laminin or on 500µm-thick flat 6mg/mL collagen I surfaces coated with laminin, hereafter denominated “2D stiff” and “2D soft”. In these preliminary experiments, we observed competition between the two cell types and interestingly two very different outcomes. On the 2D stiff collagen, *Pkd1*^{-/-} cells gathered in clusters and ended up being extruded by the *Pkd1*^{+/-}

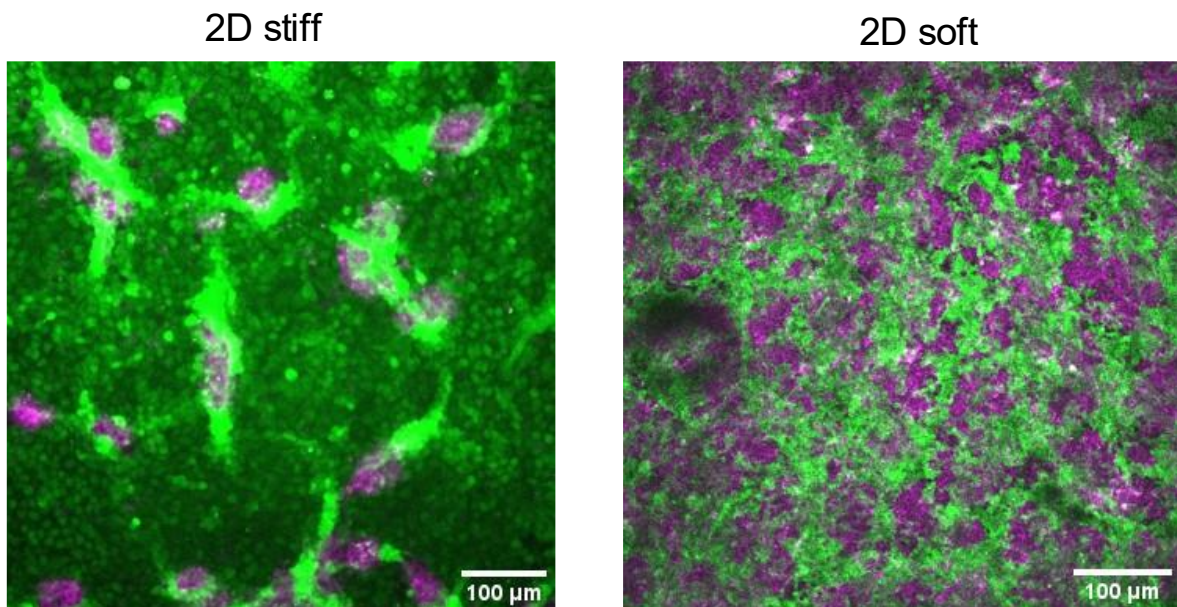


Figure 5.2: Cell competition outcome resulting from mosaicism of PCT *Pkd1*^{+/-} and *Pkd1*^{-/-} cells depends on substrate stiffness Preliminary experiments of mosaic seeding of PCT on a 2D soft surface and on 2D stiff surfaces at a 1:9 *Pkd1*^{-/-}:*Pkd1*^{+/-} ratio showed cell competition between the cells with *Pkd1*^{-/-} occupy most of the surface after a few days on a soft surface whereas *Pkd1*^{+/-} cells extrude most of the *Pkd1*^{-/-} cells on a stiff surface. Here are Z projections of confocal images taken of a 2D soft surface and of a 2D stiff surface seeded with this ratio after 14 days. Green: *Pkd1*^{+/-} cells, magenta *Pkd1*^{-/-} cells

cells, whereas on the soft collagen surfaces *Pkd1*^{-/-} ended up being in majority. Spontaneous cell-sorting here are likely the result of very different levels of E-cadherins and N-cadherins expressed by *Pkd1*^{+/-} and *Pkd1*^{-/-} cells that we characterized in our previous study (Myram *et al.*, 2021). Differences in competition outcomes could denote an influence of substrate stiffness in competition between these two cell types (**figure 5.2**). This result validates the pertinence of our choice to work on substrates with mechanical properties close to the kidney. We could next expect to observe *Pkd1*^{-/-} to become gradually predominant in our chips

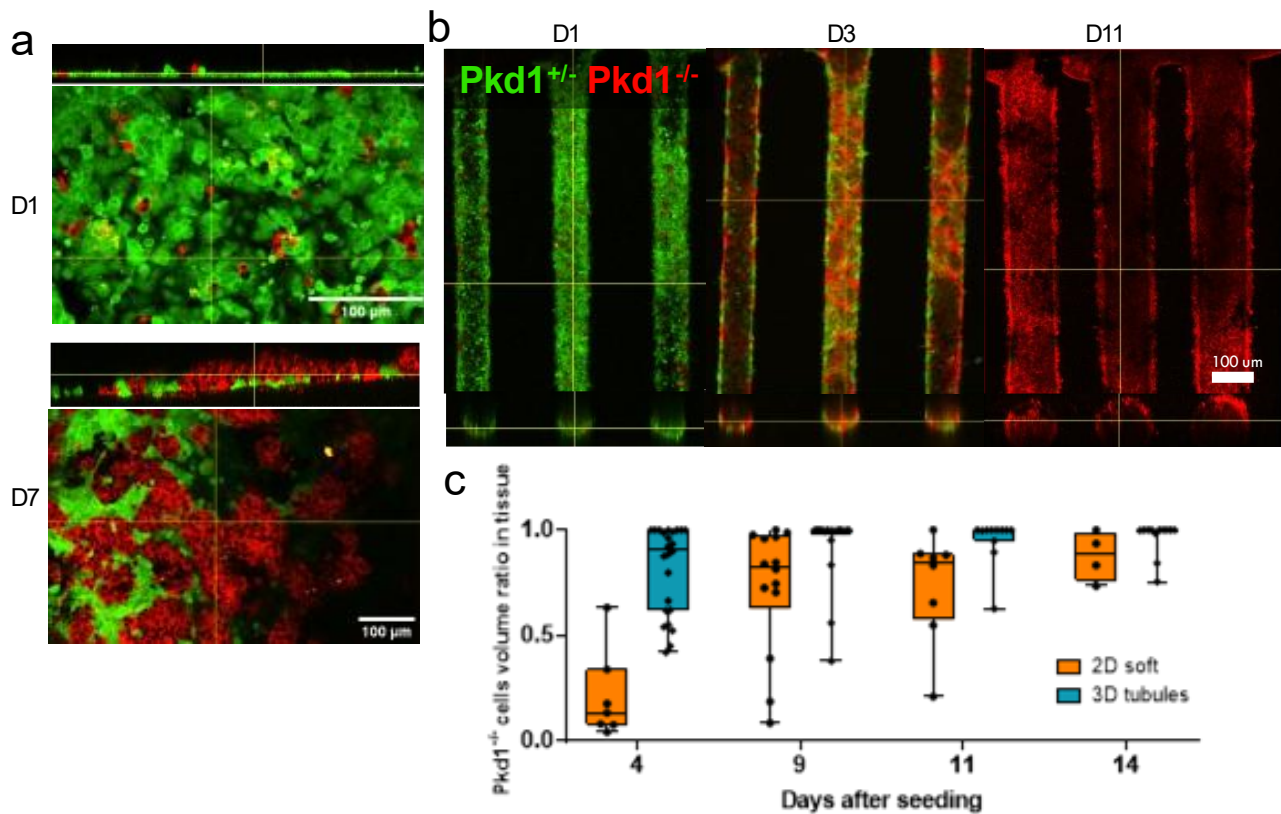


Figure 5.3: Cell competition resulting from mosaicism of PCT *Pkd1*^{+/−} and *Pkd1*^{−/−} cells is favored in a tubular geometry Mosaic seeding of PCT on a 2D soft surface and in 3D tubules at a 1:9 *Pkd1*^{−/−}:*Pkd1*^{+/−} ratio showed *Pkd1*^{−/−} occupy most of the surface after a few days *Pkd1*^{+/−} cells followed by loss of lumen and homogeneous dilation after 11 days. Here are showed cuts of confocal images taken of a 2D soft surface (a) and in a 3D multitubular chip (b) seeded with this ratio. In (c) are the results for the quantifications of these experiments comparing cell competition in 2D and 3D tubular configurations. (lines: extrema, 1st and 3rd quartile and median, each point represents a tubule (3D, n=24-12) or a collagen covered coverslip (2D, n=14-4))

We then proceeded to seed our chips with a 6mg/mL collagen I matrix confluent with the same ratio and on 2D soft collagen as a control for curvature and confinement effects. We first cultured them in static conditions and followed the evolution of the live mosaic epithelia, imaging chips and 2D soft collagen at regular intervals with confocal microscopy. Like on the 2D surfaces we could also observe competition in tubules (**figure 5.3.a-b**), with *Pkd1*^{−/−} cells overwhelmingly occupying the tissue from day 4. We quantified this competition by computing the percentage of total tissue volume occupied by one cell type or the other (see Methods for more information on the quantification) (**figure 5.3.c**). Interestingly, the tubular geometry increased the effects of competition between the two cell types and accelerated the predominance of *Pkd1*^{−/−}. In 3D, only 4 days after seeding, 90% of the tissue was already occupied by *Pkd1*^{−/−} while in 2D, they were still in minority. At the end of the experiments, *Pkd1*^{−/−} seemed to reach a plateau on 2D soft surfaces with around 80% of the tissue volume colonized but with substantial clusters of *Pkd1*^{+/−} that persisted. In contrast, in most tubules *Pkd1*^{−/−} ended up monopolizing all the tissue space and within 9 days after seeding all the *Pkd1*^{+/−} cells almost disappeared.

The predominance of *Pkd1*^{-/-} cells is followed by luminal growth and homogeneous channel dilation.

We repeated the previous 1:9 seeding in tubules with different clones, *Pkd1*^{-/-} LifeAct GFP and *Pkd1*^{+/-} LifeAct mScarlett cells and observed similar behaviors (**figure 5.4.a**). On 2D surfaces settings, *Pkd1*^{-/-} cells exhibited a tendency to grow atop *Pkd1*^{+/-} cells before gradually replacing them (**figure 5.3.a**). We investigated if the same behavior could be seen in tubules. We automatically segmented apical and basal surfaces within the tubules (see Methods) and computed the area of surfaces occupied by the *Pkd1*^{-/-} cells in the apical and basal side of the tubular epithelium normalized by the total tubule apical and basal areas respectively. We then calculated the ratio between the two to compare them (**figure 5.4.b**). Our analysis showed that the *Pkd1*^{-/-} cells tended to localize apically. They were more and more secluded to this region of the tissue within the first 3 days of culture, until they eventually occupied a majority of the tubule. Furthermore, within tubular settings *Pkd1*^{-/-} cells showed a propensity to form digit-like structures across the lumen, establishing bridges between the two sides of a tubules (**figure 5.4.c**). This generally led to *Pkd1*^{-/-} cells eventually filling the channels and as a consequence, the lumen was in most cases completely or partially lost. Although we did not quantify it, in tandem with the progressive predominance of *Pkd1*^{-/-} cells, there was a homogeneous dilation of the channels (**figure 3.b and figure 4.a**). These dilations never manifested through localized distension coinciding with *Pkd1*^{-/-} clusters. In fact, when we also computed the tubule basal area contiguously occupied by these clusters, we observed a sudden increase in area once most of the tissue was constituted of *Pkd1*^{-/-} cells. This indicates that once the *Pkd1*^{-/-} become predominant, the tissue becomes more homogeneous at its basal side, which we expect not favor localized distensions (**figure 5.4.d**).

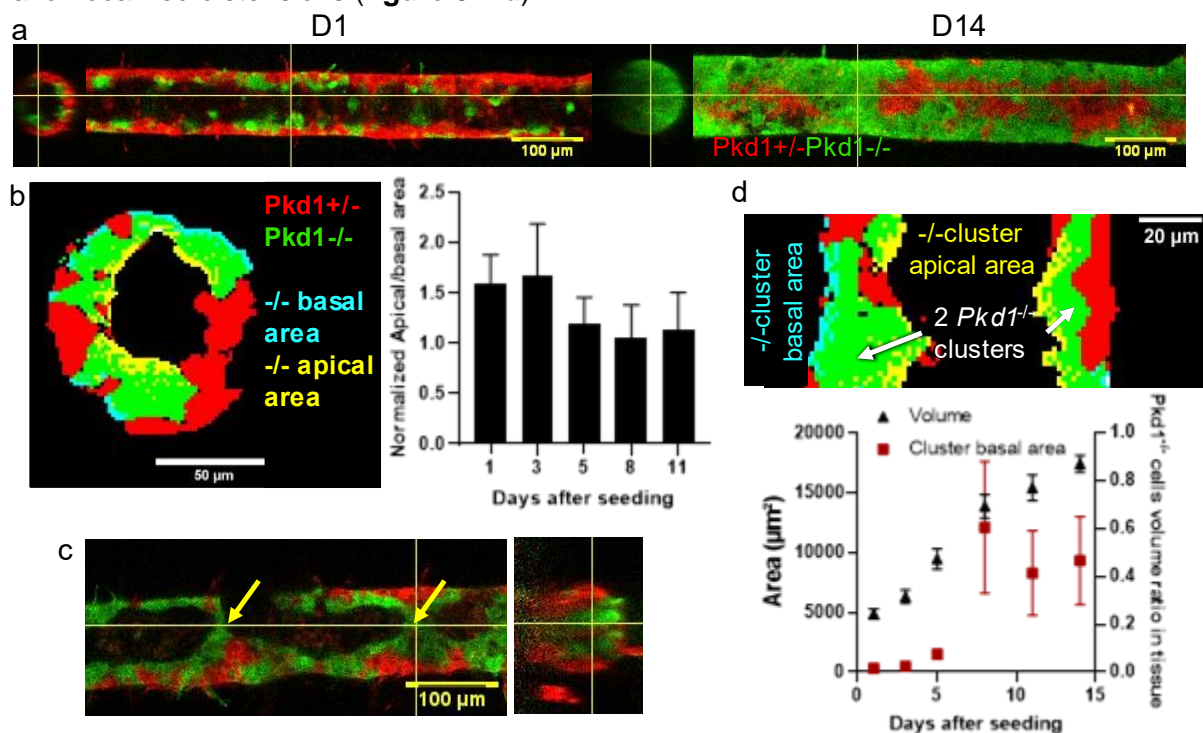


Figure 5.4: PCT *Pkd1*^{-/-} progressively grow inside luminal space leading to homogenous dilation of the tubules. Confocal imaging of live tubules seeded with *Pkd1*^{-/-} LifeAct GFP : *Pkd1*^{+/-} LifeAct mScarlett at 1:9 ratio confirmed that loss of *Pkd1* transformed them in super competitors (a). We segmented apical and basal region area of the tubules (b-left) and computed ratios of normalized apical:basal area occupied by *Pkd1*^{-/-} cells to confirm that they tended to grow on the apical side of the tissue first (b-right), error bars: 95%CI. Cross sections of confocal images showed that apical growth of *Pkd1*^{-/-} cells is accompanied by formations of digit-like bridges across the lumen (c) We also computed the basal area belonging to *Pkd1*^{-/-} cells clusters and compared it to their ratio in total tissue volume (d), error bars: 95% CI, n=15.

A proliferation driven competition

After observing that aggressive behavior exhibited by *Pkd1*^{-/-} cells within the tubules, we wondered if there was a critical ratio threshold under which *Pkd1*^{-/-} cells could not take over the tissue as fast or if even there was a critical threshold under which they could not become predominant at all. Furthermore, we hoped that preventing *Pkd1*^{-/-} overgrowth we could prevent disappearance of the lumen in static condition or observe localized dilations. To address these questions, we seeded *Pkd1*^{-/-} LifeAct GFP and *Pkd1*^{+/-} LifeAct mScarlett cells in 1:69 ratio, still guaranteeing a few *Pkd1*^{-/-} cells per tubule while minimizing their number.

With this initial ratio, *Pkd1*^{-/-} cells were still eventually outgrowing *Pkd1*^{+/-} cells (**figure 5.5.a**). At this stage, it seemed that *Pkd1*^{-/-} cells were undergoing uncontrollable proliferation at the expense of *Pkd1*^{+/-} cells. Indeed, in a conventional cell culture, when cultivated separately, in 2D, *Pkd1*^{-/-} cells proliferate 1.8 times faster than *Pkd1*^{+/-} cells in their exponential phase. For this experiment, we made similar quantifications as previously (**figure 5.5.b**). This time, to assess the role of proliferation, we computed a proliferation model to fit with our data.

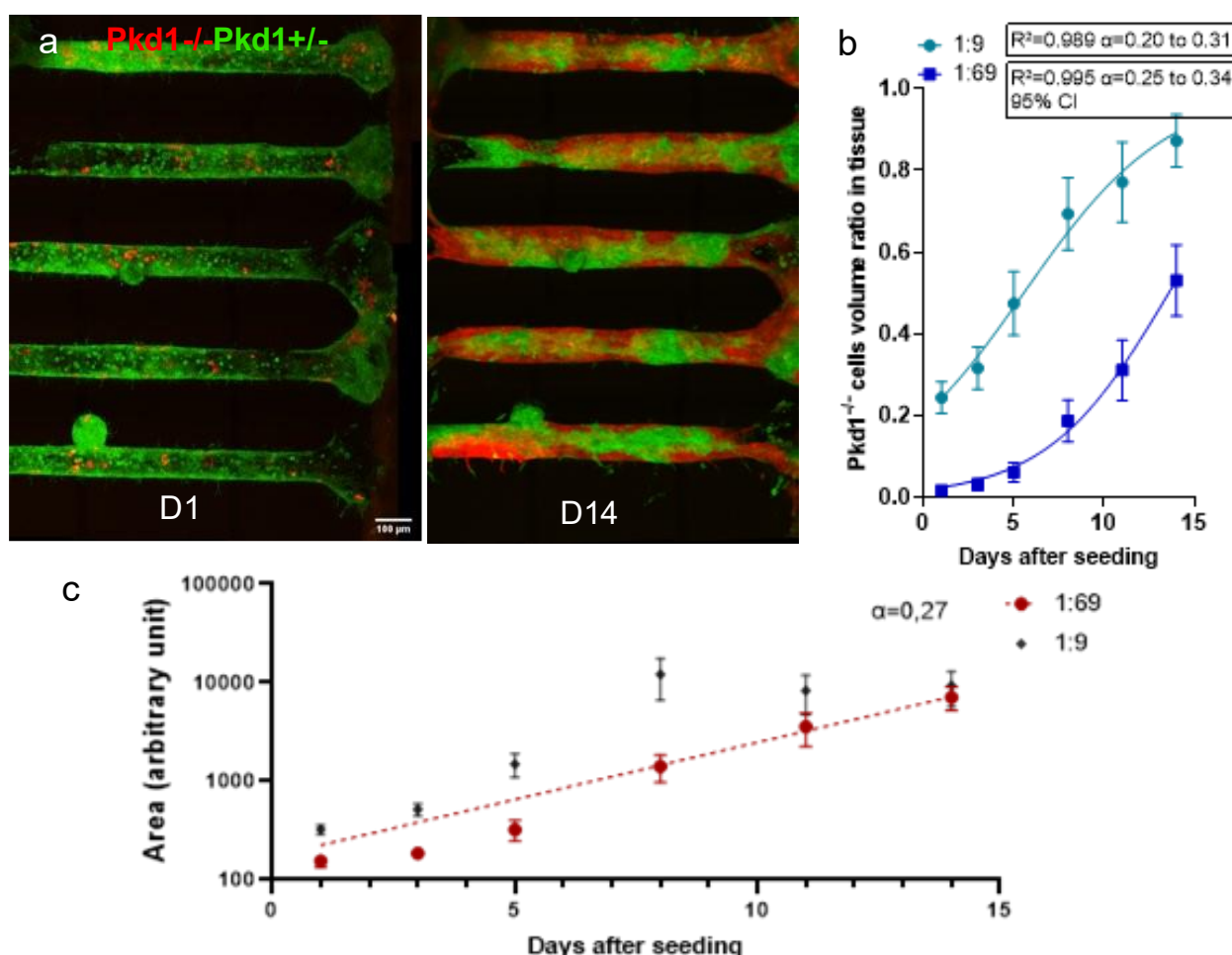


Figure 5.5: Cell competition in tubules between PCT *Pkd1*^{+/-} and *Pkd1*^{-/-} cells is a proliferation driven process Mosaic seeding of PCT in tubules at a 1:69 *Pkd1*^{-/-}:*Pkd1*^{+/-} ratio showed that even when initially present at a very low ratio *Pkd1*^{-/-} will end up completely replacing the *Pkd1*^{+/-} cells followed by loss of lumen and homogeneous dilation. In (a) are showed z-projections of confocal images taken of a chip seeded with this ratio. In (b) are the results for the quantifications of 1:9 and 1:69 ratio in these experiments. Fitting the data to a logistic growth shows that here cell competition may be proliferation driven process.(error bars: 95% CI, α : exponential growth rate). Computing tubule basal area of *Pkd1*^{-/-} domains with an exponential growth fit showed that the domain expansion parallels proliferation and eventually catch up with sizes seen with higher 1:9 ratio (c), error bars: 95% CI, 1:9 n=15, 1:69 n=13

Based on our previous observations, we hypothesized that *Pkd1^{-/-}* cells divided unhindered by a confluent state while *Pkd1^{+/-}* cells stop multiplying upon confluency. Thus, the *Pkd1^{-/-}* cell number should follow an exponential growth and, in the end, *Pkd1^{-/-}* tissue ratio should follow a logistic growth wherein:

$$\frac{N^{-/-}}{N^{+/-}}(t) = \frac{1}{1 + \frac{N_{t0}^{+/-}}{N_{t0}^{-/-}} e^{-\alpha t}} \quad (\text{Equation 5.1})$$

with $N^{-/-}$ and $N^{+/-}$ being the number of *Pkd1^{-/-}* or *Pkd1^{+/-}* cells respectively, t the time after seeding, $N_{t0}^{-/-}$ and $N_{t0}^{+/-}$, being the number at $t=0$ of *Pkd1^{-/-}* or *Pkd1^{+/-}* cells respectively, computed with the fit α being the *Pkd1^{-/-}* growth rate computed with the fit.

For both tested ratios, this model offers a good fit, indicating the preponderant role of proliferation in the competition we observed. Moreover, we can speculate given very similar growth rates, within the same margin of error, that decreasing the initial ratio of *Pkd1^{-/-}* cells would not change the outcome of the competition. Indeed *Pkd1^{-/-}* growth was not slowed as we got very similar doubling time in both cases between two and three days (equivalent to growth rates between 0.20/day and 0.31/day for the 1:9 ratio and 0.25/day and 0.34/day for 1:69 ratio). Additionally, with the smaller 1:69 initial seeding ratio, we observed similar digitations and loss of lumen as before. We fitted the tubule basal area occupied by *Pkd1^{-/-}* to a classical exponential growth (**figure 5.5.c**). This fit gave a growth rate of 0.27/day, virtually the same as the growth rate in the tissue, was higher than the early data points and was closest to the data at later time points. This denotes a clear segregation between cell types clusters at the basal side of the tubules over time and a switch between a privileged apical growth to a more homogeneous growth. Still, we could not observe any localized distension possibly due to a too rapid homogenization of the basal side of the tubules.

The impact of flow shear stress and pressure

After demonstrating the impact of geometry and substrate on competition between *Pkd1^{+/-}* and *Pkd1^{-/-}* cells, we also wanted to assess the impact of FSS and intraluminal pressure on cell competition in tubules. To do so, we seeded confluent PCT in a 1:9 *Pkd1^{-/-}* mCherry-beta-actin: *Pkd1^{+/-}* to minimize the experiment time window to durations for which we could guarantee a FSS near physiological conditions. Subsequently we subjected the cells to flow or flow with intraluminal pressure, with static experiments as a control. We kept the flow for the entire course of the experiment, only stopping it for live confocal imaging at regularly spaced time points. We maintained the experiment for a total of 8 days, the maximum duration for which we could certify that flow shear stress was still in physiological range.

We anticipated that flow would prevent the loss of lumen and interestingly it partially did. In most cases we could observe that flow shear stress helped limit luminal overgrowth of the *Pkd1^{-/-}* cells (**figure 5.6a**). However, we could still observe the same transluminal digitations between *Pkd1^{-/-}* clusters in some cases. We could not observe localized dilations either. Similar quantifications as before showed that flow shear stress had a protective effect for *Pkd1^{+/-}* against *Pkd1^{-/-}*. Compared to static tubule controls where almost 90% of tissue was constituted of *Pkd1^{-/-}* cells, in tubules under FSS after 8 days almost 50% of the tissue was still constituted of *Pkd1^{-/-}* cells (**figure 5.6b**). Preliminary data in flow+pressure conditions showed that intraluminal pressure could add to this protective effect from the FSS by limiting the growth of *Pkd1^{-/-}* cells even more. Unfortunately, a similar analysis as before to assess the role of

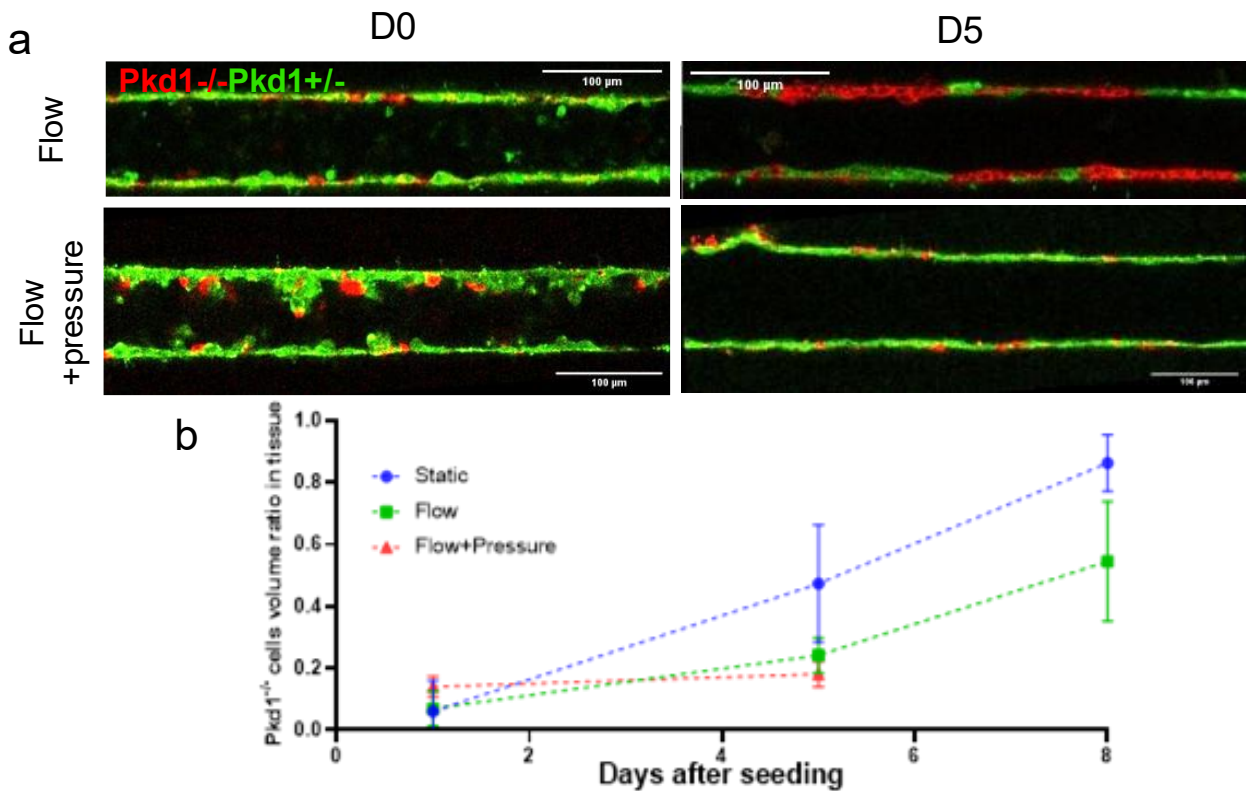


Figure 5.6: FSS and intraluminal pressure may protect *Pkd1*^{+/-} cells, Preliminary results of mosaic seeding of PCT in tubules at a 1:9 *Pkd1*^{-/-}:*Pkd1*^{+/-} ratio showed that in a tubular geometry FSS preserved the lumen and protects *Pkd1*^{+/-} cells, the addition of intraluminal pressure further protects the *Pkd1*^{+/-} cells. In (a) are showed cuts of confocal images taken of tubules seeded with this ratio under flow or flow+ pressure. In (b) are the results for the quantifications of these acquisitions, error bars: 95% CI, static n=6, flow n=14, flow pressure n=7

proliferation in this context was not possible due to the limited number of timepoints. Nevertheless, seeing that the lumen was largely conserved, we can speculate that overproliferation from *Pkd1*^{-/-} cells had a reduced role here.

5.2.2 Modelling cell mosaicism in the collecting duct

Experiment design and cell validation

In parallel to our experiments with PCTs, we also conducted mosaic cultures with mICMD-3. Aside from their different origin in the nephron, mICMD-3 cells were available with a wild-type genotype (*Pkd1*^{+/+}), instead of a heterozygote genotype or a with *Pkd1* knock-out (*Pkd1*^{-/-}). Unlike previously, we worked with transfected pools of cells without clonal selection to render the cells fluorescent. Nevertheless, we verified that fluorescent mICMD-3 cells mixed well with the parental cells without competition and validated that the fluorescent pools were similar enough. Similarly to PCT we wanted initially to work with a ratio of 1:9 *Pkd1*KO:WT cells but preliminary tests on 2D soft collagen showed an absence of apparent competition at this ratio (**figure 5.7**), marking a first important difference with PCTs. Furthermore, we did not notice any particular difference in proliferation between the two cell types when grown separately as we saw in the chapter 3. Over this absence of competition in 2D on a soft substrate contrary to PCTs, we concluded that we might have to work with a higher ratio of *Pkd1*KO cells.

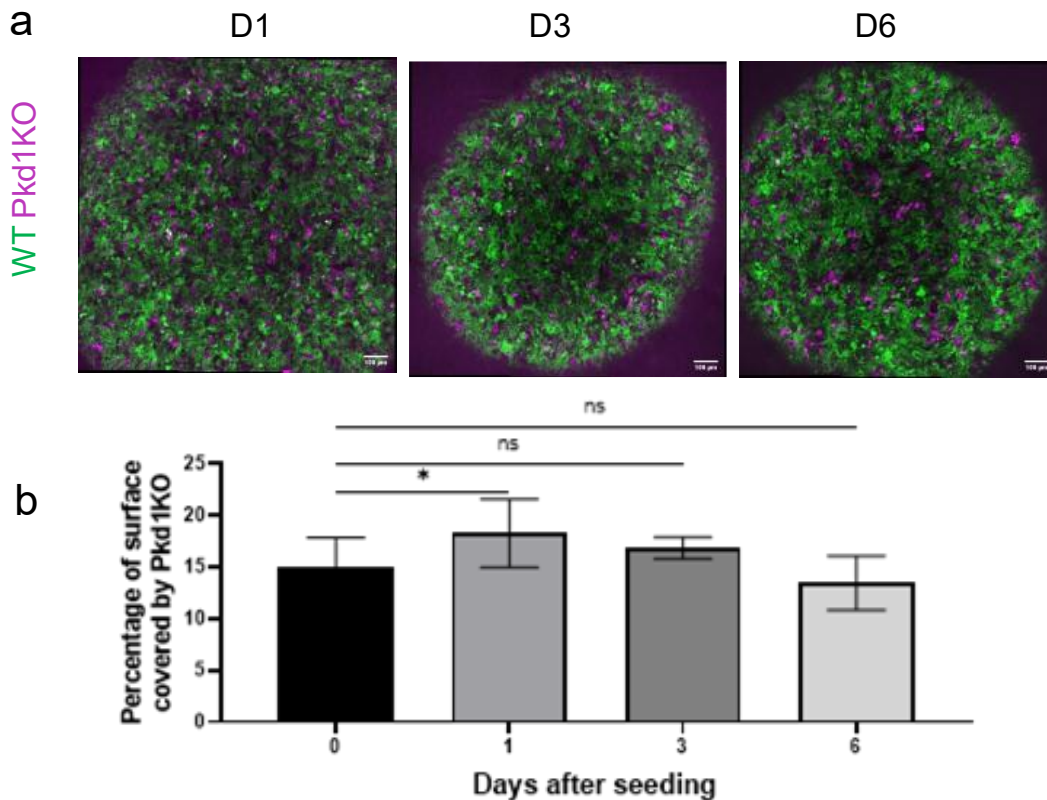


Figure 5.7 No competition on a flat surface between WT and *Pkd1KO* mIMCD-3 cells
 Seeding mIMCD-3 on 2D soft collagen at a 1:9 *Pkd1KO*:WT ratio showed that there was not any significant cell competition in this configuration. On the top are showed z-projections of confocal images taken of a 2D soft collagen sample (a). At the bottom are the results for the quantifications of these acquisitions (b) error bars: standard deviations, n=8

Strong tissue surveillance mechanisms from wild-type cells?

Following these first observations, we chose to mix the IMCD cells at 1:1 *Pkd1KO* LifeAct GFP:WT LifeAct mScarlett ratio in our tubules. We started with cultures in static conditions. We followed the evolution of the mosaic epithelia live, like we did with the PCTs (**figure 5.8a**). This time we observed competition in the tubules, but unexpectedly *Pkd1KO* cells lost. This was confirmed by quantification of ratios of *Pkd1KO* cells in the tissue. Indeed, over time they gradually disappeared from the tissue, almost totally in some tubules after 14 days (**figure 5.8b**). Overall, we observed that in the long run the tissue was adopting the same morphology as homogeneous WT tubules in static conditions, with a slight dilation and multilayering. We did not observe any localized tissue dilation coincident with *Pkd1KO* clusters. In fact, decrease of tubule basal surface contiguously covered by *Pkd1KO* strongly paralleled removal of the cells from the tissue (**figure 5.8c**). Seeing this, we also wanted to assess the importance of proliferation here and check if what we were seeing was inherent to WT overgrowth in static condition. As this time WT were the overwhelmingly predominant cells in the tissue at the end of the experiments, we performed a fitting analysis of the evolution of *Pkd1KO* using a complementary logistic function (1-logistic growth function described in equation 5.1) but the results were less convincing than with PCTs with a much poorer fit. Looking more closely at what happened in the tissue, we noticed that the *Pkd1KO* cells were pushed towards the lumen in a way reminiscent of apical extrusion (**figure 5.8d**), possibly hinting at mechanisms of tissue surveillance against aberrant cells from the wild type. Computing ratio of apical:basal tubule area covered by *Pkd1KO* tended to confirm this

hypothesis, as these cells seemed to localize more and more but in a moderate degree in the apical area of the tissue within the first 5 days of culture (**figure 5.8e**).

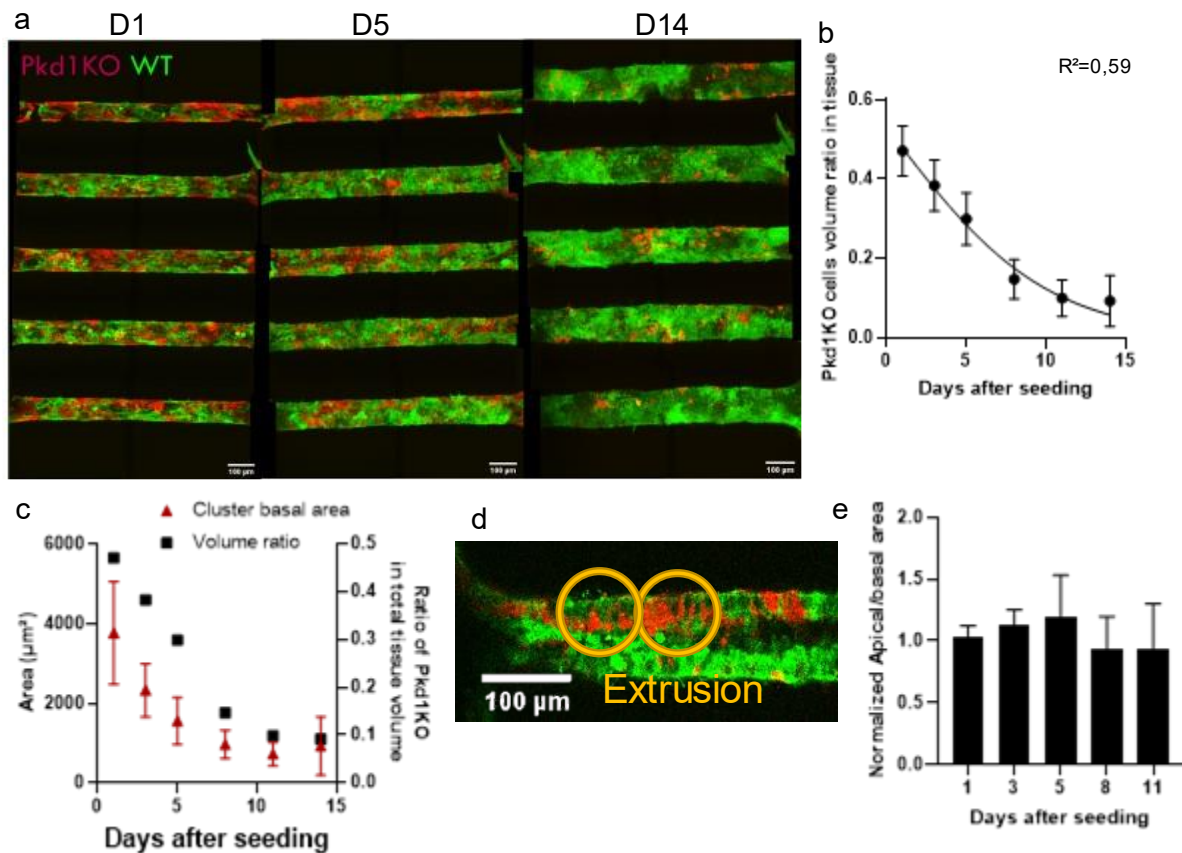


Figure 5.8: Cell-competition in tubules between miCMD-3 *Pkd1KO* and WT cells lead to extrusion of *Pkd1KO* from the tissue. Mosaic seeding of miCMD-3 in tubules at a 1:1 *Pkd1KO*:WT ratio showed that there was cell competition in a tubular geometry where WT gradually extrude cells. In (a) are shown z-projections of confocal images taken of a chip seeded with this ratio. In (b) are the results for the quantifications of these acquisitions with a fit with a logistic growth showing a progressive removal of *Pkd1KO* from the tissue, error bars: 95% CI. (c) Decrease of tubule basal surface covered by *Pkd1KO* clusters paralleled removal of *Pkd1KO* from the tissue. In (d) a closeup on one these tubules shows probable extrusions of *Pkd1KO* cells. (e) Computing normalized apical:basal tubule area occupied by *Pkd1KO* tend to confirm extrusion as the removal mechanism in this setting, error bars: 95% CI, n=24-14

The impact of flow shear stress and pressure

As we previously observed that FSS mitigated overproliferation of WT cells within the tubules lumens, we were intrigued to determine whether paradoxically FSS would not have a protective effect for the *Pkd1KO* cells this time. Furthermore, because dilation under flow+pressure happens quite fast, we wanted to see if intraluminal pressure would not allow differential dilations between the two cell types before *Pkd1KO* could be eliminated from the tissue. Anticipating these possibilities, we conducted preliminary experiments under flow and flow+pressure using a lower initial ratio of *Pkd1KO* cells of 1:2 *Pkd1KO*:WT cells with a static control to be closer to an *in vivo* case where *Pkd1KO* cells are in minority (**figure 5.9**).

As we could expect, in static conditions at this ratio, *Pkd1KO* cells were almost entirely removed from the tissue even faster than before. Interestingly, removal of the *Pkd1KO* cells seemed to accelerate right before the end of the experiment. FSS while preserving the lumen also had a protective effect for *Pkd1KO* cells, but we observed the same acceleration of

removal of *Pkd1KO* cells in this context. Adding intraluminal pressure had the greatest protective effect for *Pkd1KO* cells. In the flow+pressure condition, after 8 days the ratio of *Pkd1KO* did not change significantly. However, despite the preservation of most *Pkd1KO* clusters, we did not observe any localized dilation here either.

So far for the mICMD-3 we could not identify a condition that could allow *Pkd1KO* cells cluster to spread at the expense of WT cells. As a last experiment we seeded the cells in a

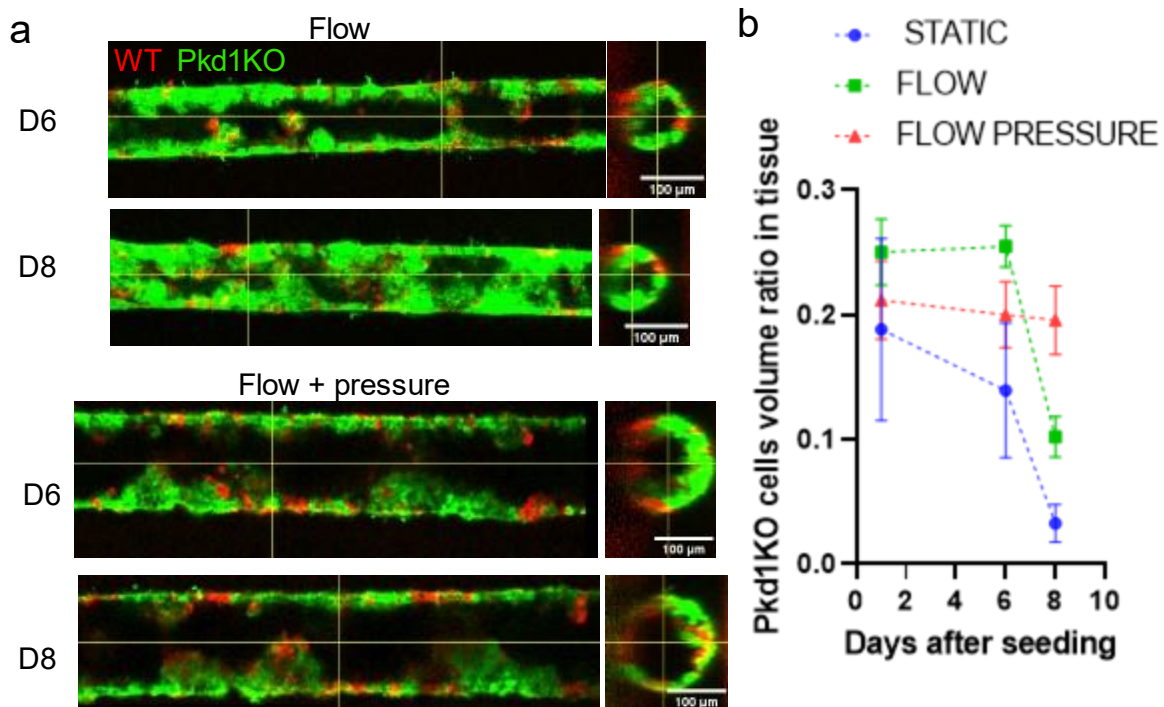


Figure 5.9: FSS and intraluminal pressure may prevent *Pkd1KO* extrusion

Preliminary results of mosaic seeding of mIMCD-3 in tubules at a 1:2 *Pkd1KO*:WT ratio showed that in a tubular geometry FSS reduced extrusion of *Pkd1KO* by WT cells, the addition of intraluminal pressure further protects the *Pkd1KO* cells. In (a) are showed cuts of confocal images taken of tubules seeded with this ratio under flow or flow+pressure. In (b) are the results for the quantifications of these acquisitions, error bars: 95% CI, static n=8, flow and flow-pressure n=10

ratio 3:2 *Pkd1KO*:WT in static condition and with flow and followed them for 6 days (figure 5.10). With *Pkd1KO* cells initially in majority, we wanted to see if we had an inverted outcome to the cell competition. Surprisingly, even in this condition, *Pkd1KO* cells were gradually removed from the tissue with or without FSS, with a slight protective effect from the FSS for the *Pkd1KO* cells. By the 6th day after seeding, we could not observe important clusters of *Pkd1KO* cells and less so localized dilations. The fact that even with an initial majority of *Pkd1KO* the outcome of cell competition remained largely the same, shows that in this context WT are supercompetitors compared to *Pkd1KO*. We can conclude that our previous observations were inherent to the interactions between *Pkd1KO* and WT cells in a tubular geometry, wherein WT cells display a robust surveillance mechanism against loss of *Pkd1*.

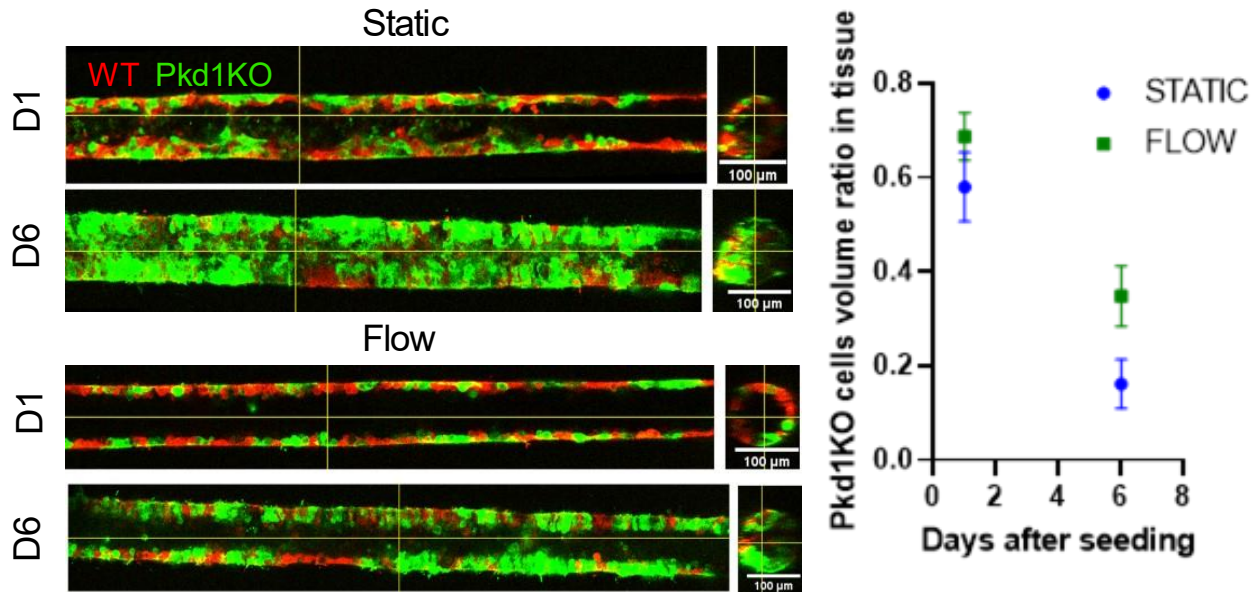


Figure 5.10: *Pkd1*KO initially in majority still results in their removal from the tissue Preliminary results of mosaic seeding of mIMCD-3 in tubules under FSS and FSS+pressure at a 3:2 *Pkd1*KO:WT ratio showed that even when initially in majority *Pkd1*KO cells still get removed from the tissue. In (a) are showed cuts of confocal images taken of tubules seeded with this ratio under flow or flow+ pressure. In (b) are the results for the quantifications of these acquisitions, error bars: 95% CI, static and flow n=10

5.3 Discussion and conclusion

On the fundamental differences of behavior of PCTs and mIMCD-3

Loss of *Pkd1* leads to cell competition in our system. The outcome depends on the substrate, the geometry and on the hydrodynamic constraints. Tubular geometry accelerated competition for both PCT and mIMCD-3 and favored the predominant cells in the outcome, while switching from a stiff to a soft surface for the PCTs reversed the outcome of the competition. However, we did not decouple here confinement and curvature resulting from this geometry. We already discussed how YAP and Myc upregulation could be strong vectors of cell competition, the former when differently active across an epithelium and the latter creating super-competitors. YAP and Myc are also critical for cystogenesis in ADPKD, and thus can be considered of important relevance in cell competition in the context of *Pkd1* expression mosaicism. In a normal context, concave surfaces modulate YAP nuclear localization, possibly through an influence on cell density. It has also been established in epithelial cells, notably with MDCK, that response to pressures due to tissue growth under confinement contributes to limit cell proliferation (Di Meglio *et al.*, 2022). This response is modulated by β -catenin. In the context of *Pkd1* loss, those regulation mechanism may be less effective (Lee *et al.*, 2020). Similarly, extracellular stiffness sensing affects cell proliferation and YAP nuclear activity, and these mechanisms are also disturbed without *Pkd1* (Nigro *et al.*, 2019).

Interestingly we also observed that cell competition was cell line sensitive, with PCT derived from the proximal tubule and mIMCD-3 from the collecting ducts giving opposite results.

For PCTs, loss of *Pkd1* created super competitors that will end up almost completely replacing cells still expressing *Pkd1*. We showed that their super competitor phenotype was mostly the result of uncontrolled overproliferation. Of note, *Pkd1*^{-/-} growing apically to *Pkd1*^{+/-} cells before replacing them seems unusual in cell competition in epithelium (Bielmeier *et al.*, 2016). Generally, in similar contexts, “loser” cells seem to be extruded. PCT *Pkd1*^{-/-} are less adherent than their *Pkd1*^{+/-} counterpart, notably due to abnormal levels of E-cadherin and N-cadherins. These differences in adhesion properties lead to segregations from the *Pkd1*^{+/-} cells. Furthermore, it is not excluded that in fact *Pkd1*^{+/-} cells could actively drive them out of the tissue to the apical side of the tissue, which would be helped by their reduced affinity for the ECM. Digitation structures that we observed would be due to the cell resulting lower affinity for the stromal side of the tubule relatively to *Pkd1*^{+/-} cells, leading to the *Pkd1*^{-/-} cluster minimizing their interface with it. Gradually this tissue would grow from the lumen. Possibly then, increased homeostatic pressure from this uncontrolled growth, specifically on the apical side of tubule, in a confined environment could drive PCT *Pkd1*^{+/-} cells to apoptosis or profoundly alter their proliferation (Di Meglio *et al.*, 2022). Nevertheless, this type of process would be more reminiscent of a carcinoma than of cyst growth in ADPKD, where cells remain polarized and in monolayers. This behavior was however strongly limited by flow shear stress. With our current data the origin of this protective effect remains unknown. We previously observed that FSS limits proliferation of PCT *Pkd1*^{-/-} cells towards the lumen, thus limiting the homeostatic pressure from overproliferating *Pkd1*^{-/-} cells. Here as well it mostly seemed to be the case. FSS may also change the phenotype of both *Pkd1*^{+/-} and *Pkd1*^{-/-} cells, possibly reducing the gap between the two. Duan *et al* also showed that FSS applied to a proximal tubule epithelium leads to a reinforced *adherens* junction and concentrates E-cadherin at the apical junctions. Alternatively, a similar shift may help *Pkd1*^{+/-} cells to exclude *Pkd1*^{-/-} cells from the tissue.

For mIMCD-3 cells in all the tested conditions, *Pkd1*KO cells were successfully excluded from the tissue by WT cells, even when initially in majority. It seems that WT are inherently super competitors compared to *Pkd1*KO. Given the tissue organization, we think that this was mostly the result of apical extrusion of *Pkd1*KO cells by WT. We must note however a similarity with the PCT here. Like PCT *Pkd1*^{-/-}, WT cells are prone to multilayering and may also induce a homeostatic pressure on *Pkd1*KO cells incompatible with their survival. For this reason, possibly this time, instead of favoring WT cells FSS favored *Pkd1*KO cells. Paradoxically, the more physiological tissue organization promoted by FSS may release some pressure on the *Pkd1*KO due to WT growth. Furthermore, as we noticed previously, under FSS morphological differences between WT and *Pkd1*KO are reduced, which could further explain why they are less easily excluded from the tissue in these conditions. Nevertheless, in this condition *Pkd1*KO cells are eventually eliminated from the tissue although at a slower pace. Contrary to *Pkd1*^{-/-} PCT, *Pkd1*KO mIMCD-3 cells may display in the end decreased levels of proliferation compared to their WT counterpart and this may be another evidence for an active elimination of these cells by WT cells reminiscent of tissue surveillance. Adding luminal pressure seemed to further protect *Pkd1*KO despite the fact that morphological differences between the two cell types are more apparent in this context when taken separately. The additional luminal pressure could mechanically oppose apical extrusion.

Overall, what we observed with mIMCD-3 appears to be the result of a successful tissue surveillance from WT cells against loss of *Pkd1* that could be analogous to physiological mechanisms preventing development of aberrant cells within the kidney tubules. PCT cells demonstrate an inability to perform analogous surveillance. First, we must note one fundamental difference between the two. PCT *Pkd1*^{+/-} cells may exhibit haploinsufficiency

when WT mIMCD-3 cells should possess a more normal level of *Pkd1* expression. This resonates with some ADPKD *in vivo* models where haploinsufficiency in a *Pkd1*^{+/-} cells background favored cyst growth compared to a *Pkd1*^{+/+} cells background. In humans, milder ADPKD cases have also been identified as the result of mosaicism of *de novo* *PKD1* mutations among cells with a normal *PKD1* genome (Hopp *et al.*, 2020). Second, these cell lines are derived from different segments of the nephron. As we noted in the previous chapter, in ADPKD, cysts originate mainly from the medulla where most of the collecting ducts are located, as opposed to the cortex where proximal tubules are located. Coincidentally, increased proliferation in ADPKD may not be a cause of initial cystogenesis but rather a secondary effect coming at later stages of the disease or can be an aggravating factor. Privileged segment location for cysts may be due to kidney micro-environmental factors that vary along the nephrons but may also be due to intrinsic differences in phenotypes. In the context of our study, the fundamental differences observed between a proliferation driven cell competition for the PCTs and the efficient tissue surveillance from mIMCD-3 cells may translates once again different effects of *Pkd1* loss with respect to different phenotypes.

On the absence of cyst-like differential tubular dilation

With our mosaic seedings, we could not observe localized dilation resembling cysts, despite observing significant tubule dilations in tubules where *Pkd1* is homogeneously absent. In their study on differently fated epithelium, Bielmeier et al showed that to generate cysts, mutated cells needed to cover a critical cluster size in the epithelium due to an interplay between elasticity and interface contractility possibly generated by different adhesion properties, if the cluster covered is too small then the cells will tend to be extruded. On the contrary if the cluster is too large, then the local curvature will remain unchanged. In our experiments with mIMCD-3, we observed that the *Pkd1*KO tended to be extruded apically, perhaps before being able to induce local deformations. Possibly the size of the clusters they formed before being extruded from the tissue were never important enough to generate cyst-like structures. It is hard to know from previous studies what the initial size of a cyst would be since to be detected cysts need to be over a certain size that already diverged from their initial size. However, if we refer to Bielmeier et al hypothesis on an optimal size cluster for cystogenesis, they established in *Drosophila* that it would be between 60 and 80 cells in a cluster. Given the *Pkd1*KO cluster basal area that we measured, the surface occupied on the basal side of the tubules by *Pkd1*KO is initially well above that optimal point but falls rapidly below an estimated number of less than 30 cells. Starting with *Pkd1*KO overwhelmingly in majority might pass a threshold allowing differential dilations, but it may also hinder this phenomenon due to excessively large clusters. Furthermore, it is important to recognize that this scenario would be less relevant to what happens in ADPKD.

Despite PCTs *Pkd1*^{-/-} aggressive behavior, we could not observe localized dilations either. Reducing the relative number of *Pkd1*^{-/-} cells several times in our tubules was not sufficient to produce localized deformations. *Pkd1*^{-/-} had a propensity to locate toward the lumen. This growth initially concentrated mostly apically would be incompatible with monolayer outgrowth like cysts. Furthermore, once most of it was constituted by *Pkd1*^{-/-} cells, the tissue, more particularly its basal side, was overall too homogeneous to allow localized distention.

In both cases, the ECM forms a barrier opposing dilation. *In vivo*, this barrier is essentially a thick basement membrane that predominantly contributes to the tissue elastic properties. In our model, the tubules are surrounded by an ECM that is softer and essentially homogeneous when starting the experiments. We expect the cells to locally remodel the ECM

to form a more physiological basement membrane. Loss of *Pkd1* has been shown to influence matrix deposition (Mangos *et al.*, 2010). In their *in vitro* ADPKD model with mIMCD cells, Subramanian *et al.* showed that loss of *Pkd1* led to abnormal excessive collagen IV deposition that was necessary for *in vitro* cyst growth (Subramanian *et al.*, 2012). Substantial divergences in localized remodeling of the ECM due to mosaicism would need time to be established. This process may be incompatible with the typical timescales of the competition that we observed. Furthermore, we saw that *Pkd1*^{-/-} cells tended to localize away from the ECM at initial stages. This would render any significant local differences in basement membrane compliance unlikely, not allowing the creation of a microenvironment favorable for localized dilations.

In general, mosaic seeding may not suitably recapitulate what happens after scattered loss of *Pkd1* *in vivo*. Indeed, by the time of somatic mutations, the tissue is already well differentiated with a mature microenvironment. Murine models have demonstrated that the timing of the deletion was correlated to the gravity of the disease, with more immature kidney epithelium leading to more pronounced cyst growth. In our experimental setup, we reproduced a scenario of mosaicism concurrent to the tissue maturation. Therefore, phenotypic alterations due to loss of *Pkd1* may be paradoxically too exacerbated to allow localized deformations: in mIMCD-3 cells, *Pkd1*KO may not be able to escape tissue surveillance and in PCTs, an overproliferative behavior combined with significant alterations in adhesion culminate in abnormal growth more reminiscent of a carcinoma than of a cyst in ADPKD. Although FSS seemed to mitigate the effects of cell competition to a certain extent, we were still unable to observe any localized dilation. This suggests that distinct mechanisms necessary for cystogenesis possibly subsequent to timely mutations of *Pkd1* may be diverted or erased due to concurrent tissue differentiation or that our system lacks a key component of the kidney microenvironment.

Nevertheless, we established to our knowledge the first 3D *in vitro* model specifically addressing mosaicism in the context of ADPKD. With our model we could test the influence of several factors essential for kidney tubules homeostasis, the geometry, the mechanical properties of the microenvironment and finally the luminal hydrodynamic constraints. Loss of *Pkd1* is a source of cell competition *in vitro* and each of those previous parameters is of crucial importance for the outcome. This highlights further the importance of perfused 3D construct to model key processes in ADPKD, here with somatic mutation. Improving this model with *in situ* mutations might be the crucial last piece to be able to replicate cyst formation in a kidney-on-chip and to understand more comprehensively the dynamics involved in ADPKD.

6. Conclusion and perspectives

6.1. Overall conclusion

During this PhD, we aimed at developing a new kidney-on-chip that would provide the simplest solution yet faithful to mimic the complex dense multitube assembly that are the kidney tubules while integrating and controlling the essential hydrodynamic cues going along with the kidney function. The device we developed recapitulates the geometries of the nephron segments in one the most faithful ways among what the literature describes. Thanks to the design of its microfluidic channels and with a simple and cost-efficient gravity driven perfusion system, we are able to run in parallel dozens of experiments with physiological hydraulic stresses and validated the stability of the perfusion system for up to a week. We have also demonstrated that our design is able to decouple the two stresses inherent to perfusion, flow shear stress and intraluminal pressure. We showed that both stresses were necessary to maintain a physiological-like monolayer epithelium. However, our results also suggest that integrating an extracellular matrix with mechanical properties closer to the kidney basement membrane is necessary to withstand a physiological intraluminal pressure without tubular distension. In the experiments we have described, we only integrated the epithelial compartment in the kidney; however, we think that the close independently perfusable channels could be adapted to integrate the endothelium and offer a relevant model to mimic the exchanges between the endothelium and the epithelium. Preliminary studies have shown the possibility to seed and grow endothelial cells in similar hollow tubules. Differential perfusion would allow to cultivate both cell types with their respective optimized medium.

The motivation behind this effort was to decipher the mechanisms of cyst formation in ADPKD; a fairly common life-threatening condition yet still not entirely understood disease. When using normal and ADPKD murine kidney cell models, we showed that *Pkd1* was essential for the maintenance of the near-physiological tubular geometry. The absence of *Pkd1* in our artificial tubules led to tubular dilations through mechanisms independent of an increased cell proliferation but which is very sensitive to ECM density with cells derived from the collecting duct. On contrary, with cells derived from the proximal tubules, the tube dilation observed seems to originate from increased proliferation. Flow shear stress appears to counterbalance the absence of the gene at least partially, through cytoskeletal remodeling and modulation of the cell morphology and tissue organization. However, this fails to do so when increased proliferation is the main reason behind dilation, probably because this stress seems not to promote cell contact inhibition. These results provide arguments in the debate over the role of proliferation in cystogenesis, suggesting that it is not necessary in the early steps of cyst formation. Intraluminal pressure appears sufficient to nullify the beneficial effects of FSS in tubules lacking *Pkd1*. Indeed, moderate levels of pressure are enough to sustain important and uninterrupted tubular dilation in the absence of *Pkd1* while promoting a pathological squamous phenotype. However, intraluminal pressure seems to be necessary for proper maintenance of a monolayer tubule otherwise. Taken together, our results illustrate how cyst growth due to tubular obstructions could be driven by perturbations in physiological hydraulic stresses but also potentially by physiological stresses due to an altered mechanical response of the tubules. It is unclear why, but our results suggest that the ECM properties and the ability of the cells to modulate them are at the core of mechanical stress-driven tubular distensions in ADPKD.

Finally, we aimed at recapitulating cyst formation in ADPKD by modelling in our kidney-on-chip the mosaicism subsequent to somatic mutations. Mosaic seeding and hydrodynamic stresses were not enough to allow formation of cyst-like localized distension. We could however put in evidence phenomena of cell competition between *Pkd1*⁻ and *Pkd1*⁺ cells, wherein we could observe a strong surveillance mechanism from WT mIMCD-3 cells against *Pkd1*KO cells, whereas overproliferation in PCT *Pkd1*^{-/-} cells transformed them into supercompetitors. If we take the bottom-up approach, we are convinced that finding the missing variable to favor the appearance of localized cyst-like distensions will in itself answer essential questions on the mechanisms behind cystogenesis.

Overall, we are convinced that 3D engineered microenvironments like kidney-on-chips are of the utmost relevance when it comes to deciphering the mechanisms behind polycystic kidney disease. They offer over a wide range of controllable parameters that appear at the core of cystogenesis: extracellular matrix properties, geometry and fluidics. Thanks to our ability with our kidney-on-chip to easily modulate those parameters, we were able to specifically address them *in vitro*, which appears a much complex ordeal *in vivo* and is impossible with most of currently reported *in vitro* models.

We also briefly explore other parameters that may be essential for the comprehension of cystogenesis and that may represent exciting paths to take to mature our understanding of ADPKD. To finish this manuscript, we will briefly present some of these proof-of-concept experiments.

6.2. Towards mimicking cyst-tubule interactions

During our experiments with perfused tubule under flow shear stress with intraluminal pressure, we noticed interesting occurrences of balloon-shaped inhomogeneous dilations reminiscent of a cyst or more accurately of an aneurysm (**figure 6.1**). Those balloon-like dilations took proportions surpassing all the other tubular distensions that we saw so far. We did not analyze those tubules with the rest of the samples because there was manifestly a different parameter or mechanism at play that we have not identified yet. Thus, we are currently not able to reproduce these results in a controlled manner.

We have several hypotheses for this phenomenon. Possibly these inhomogeneous deformations are the result of heterogeneities in the collagen gel. However, such gel inhomogeneities typically result in invasion from the cells instead. It may also be due to inhomogeneous tensions in the tissue. If we follow Laplace's law, at equilibrium, the inner pressure results in a wall tension proportional to the product of the radius and the pressure gradient across the tubules. When we modified the chip design to sandwich the collagen at the edges of the chamber; a side-effect is that the tubule extremities are more or less sandwiched as well, possibly counterbalancing tensions at the extremities. Due to greater tension, distension is more favored at the center of the tubule. It is possible that when the tension disparity is too important, distensions localized only at the center grow like aneurysms. According to Laplace's law, once the distension is formed, tension in the epithelium increases as the local radius increases which may then escalate into a vicious cycle fueling the aneurysm growth. The dilation is so important that even with 200 μm separating adjacent tubules, the growing cyst ends up in contact with its neighbors, even fusing with some of them. We could also observe deformations of the adjacent tubules due to this growth that seemed to favor the dilation of these tubules suggesting the existence of mechanical couplings. Continuous growth

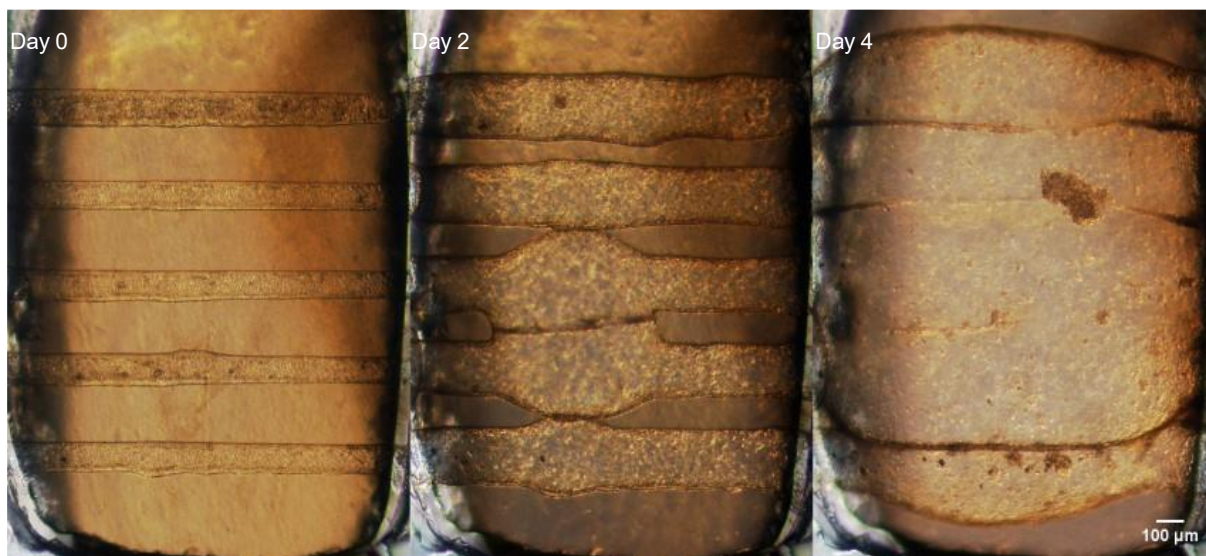


Figure 6.1. Example of an aneurysm-like tubular dilation under intraluminal shear stress. Phase contrast images showing the evolution of mICMD-3 *Pkd1*KO cells perfused in the “flow+pressure” mode that display an inhomogeneous tubular dilation reminiscent of aneurysm that ended up occupying almost all of the volume of the collagen chamber

of the aneurysm ends up occupying most of the volume in the chamber.

In ADPKD, growing cysts can similarly have an impact on the neighboring tubules through obstruction and deformations as well as potentially through chemical signaling. To favor these interactions in dedicated experiments we could, as in our previous study with the PCT cells, bring the channels closer separated by only a 100 μm . With our chip, we can also

play individually on the perfusion of the different tubules (**figure 6.2.a**). This allows us to apply pressure and FSS in some tubules but not in other ones. This also allows us to seed the tubules differently (**figure 6.2.b**). Having a *Pkd1*⁻ tubule surrounded by *Pkd1*⁺ tubules in close proximity, we can approach *in vitro* what happens when healthy tubules have a tubule that becomes cystic in their vicinity. Using the wires to plug one or several tubules and inducing higher intraluminal pressure in those tubules, we could then mimic growing cysts adjacent to normal tubules.

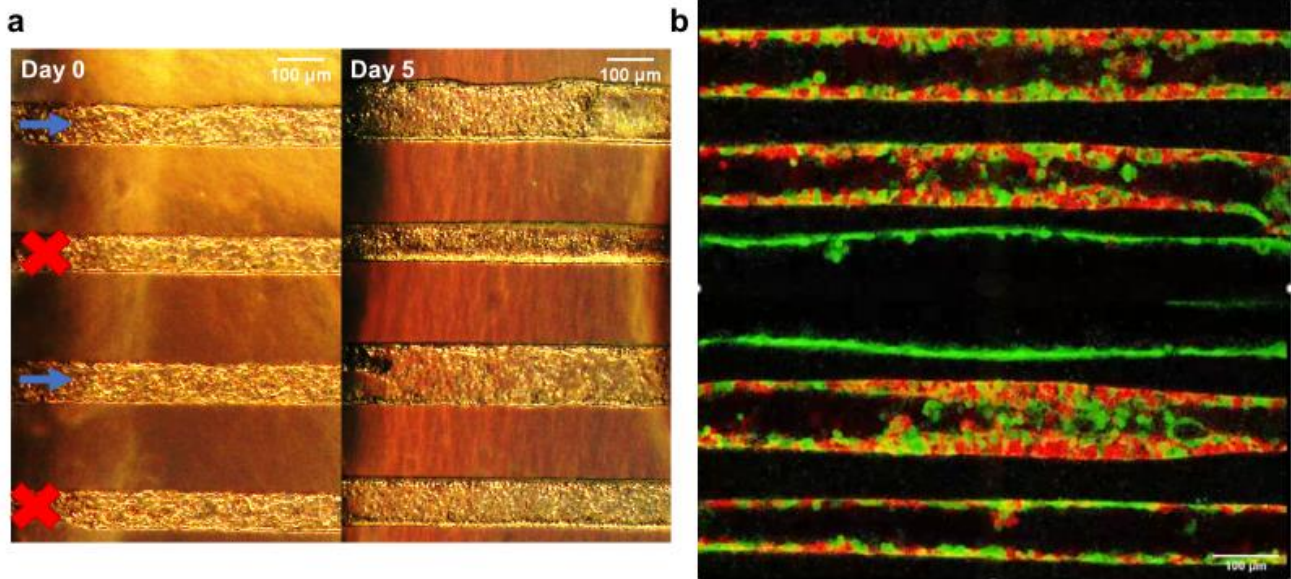


Figure 6.2. Towards modelling of cyst-tubule interaction in our kidney-on-chip. Our chip allows us to perfuse differently adjacent tubule. In (a) we show an example of mIMCD-3 tubules under “flow+pressure” perfusion (arrows) undergoing tubular dilation next to obstructed tubules (crosses). This also enable different perfusion of the tubules. In (b) we show an example of mosaic mIMCD-3 tubules with *Pkd1*KO (green) and WT (red) cells surrounding a *Pkd1*KO tubule

6.3. Extending the model to the stromal compartment

So far, we have only really discussed the epithelial compartment in ADPKD but cystogenesis is accompanied by inflammatory response and an ensuing fibrosis which plays an important role in the loss of function of the kidney parenchyma. Given the late occurrence of significant fibrosis, it appears that it does not intervene as an early motor of the exponential cystogenesis seen in ADPKD. Furthermore, the kidney stroma is not known to be particularly rich in other cell types like fibroblasts prior to late-stage polycystic disease. However, recent results have pointed to a potential role from the pro-inflammatory response of the immune system or from myofibroblast in cyst growth. Notably, specific deletion of *Pkd1* in the stromal compartment resulted in important defects in the kidney ECM as well as cyst growth in a murine model (Nie and Arend, 2017). Similarly, the presence of myofibroblasts in mouse ADPKD kidney was shown to promote cyst growth in another model likely through chemical signaling (Dwivedi *et al.*, 2023).

With our kidney-on-chip, we are able to coculture epithelial cells in the tubules and fibroblasts in the collagen I matrix. To do so, at the ECM molding stage, we prepare the collagen I mixture including a suspension of fibroblasts. As a proof of concept, we used murine NIH-3T3

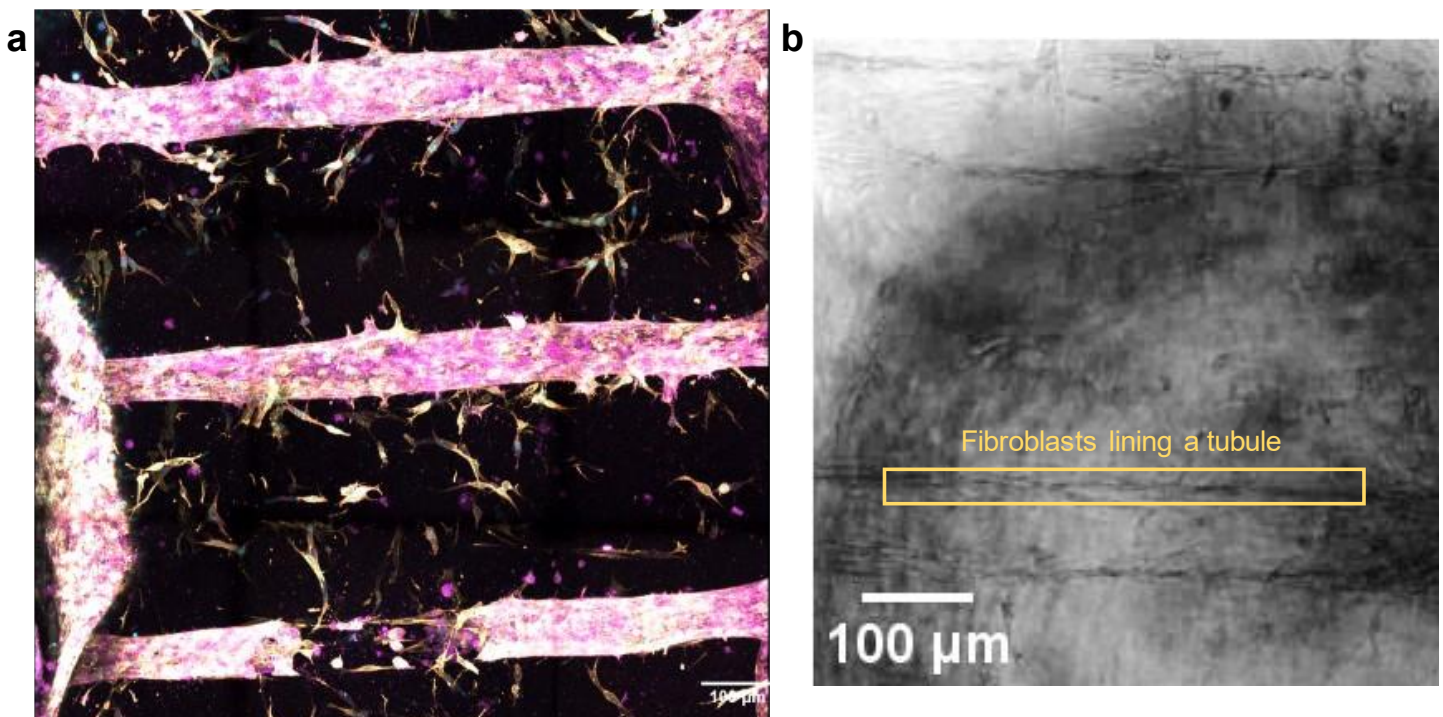


Figure 6.3. Proof of concept of a coculture of kidney epithelial cells in tubules with fibroblasts in the ECM. (a) In this image obtained with confocal microscopy, embedded fibroblasts (yellow), here NIH-3T3, and subsequently seeded the tubules with kidney epithelial cells, here mIMCD-3 *Pkd1*KO (magenta), are in a coculture (nuclei are in blue). (b) A phase contrast image of NIH-3T3 cultivated alone in the chip show that they tend to localize at the interface with the tubules

fibroblasts, and let the collagen polymerize with the cells at 37°C. We kept the chips in the incubator submerged in the fibroblast medium until we did the seeding in the tubules exactly like we normally have done. For this proof-of-concept, we seeded mIMCD-3 cells *Pkd1*KO (**figure 6.3.a**) in the tubules. We also kept in the culture chips with fibroblasts from which we had removed the molding wires but not seeded in order to compare the fibroblasts organization in absence or presence of mIMCD-3 cells. Interestingly, we observed that the fibroblasts tended to localize at the interface with the tubules and apparently to align with them from our

preliminary observations (**figure 6.3.b**). This demonstrates that in such a model, there will be strong opportunities for interactions between those cells and the epithelial cells. An interesting direction to take will be to reproduce the experiments we described in this manuscript including fibroblasts, possibly with *Pkd1* deficiency or no. Cultures under flow and intraluminal pressure will particularly be interesting because, due to their tendency to locate around the tubules, we expect myofibroblast to greatly change the ECM nature and properties around the kidney epithelial cells. Finally, we could also imagine a coculture adding immune cells that would gather in a kidney-on-chip all the actors involved in APDKD from the initial tubular dilation to the ensuing inflammation.

Methods

Chip fabrication

Hereafter is joined a detailed protocol of the fabrication of kidney-on-chip that was used throughout this thesis. Minor adaptation after the publication of this article were made to optimize the chip for flow. Notably this paper describes a chip with five independent outputs, the design was modified for a single-output chip, that could be perfused with only one syringe or tubing. The adaptations are detailed after this paper

Construction of a Multitubular Perfusable Kidney-on-Chip for the Study of Renal diseases

See paper on the next page



Construction of a Multitubular Perfusable Kidney-on-Chip for the Study of Renal Diseases

Brice Lapin, Sarah Myram, Manh-Louis Nguyen, Giacomo Groppero, Sylvie Coscoy, and Stéphanie Descroix

Abstract

The organ-on-chip model offers versatility and modularity of in vitro models while approaching the biological fidelity of in vivo models. We propose a method to build a perfusable kidney-on-chip aiming at reproducing key features of the densely packed segments of nephrons in vitro; such as their geometry, their extracellular matrix, and their mechanical properties. The core of the chip is made of parallel tubular channels molded into collagen I that are as small as 80 μm in diameter and as close as 100 μm apart. These channels can further be coated with basement membrane components and seeded by perfusion of a suspension of cells originating from a given segment of the nephron. We optimized the design of our microfluidic device to achieve high reproducibility regarding the seeding density of the channels and high fluidic control of the channels. This chip was designed as a versatile tool to study nephropathies in general, contributing to building ever better in vitro models. It could be particularly interesting for pathologies such as polycystic kidney diseases where mechanotransduction of the cells and their interaction with adjacent extracellular matrix and nephrons may play a key role.

Key words Organ-on-chips, Kidney-on-chip, Polycystic kidney disease, Microfluidics, Collagen, Wire molding, Nephron, Tubular scaffold, 3D epithelium, Luminal pressure

1 Introduction

Reproducing the densely packed structures of the nephrons in vitro is a challenge that can be addressed thanks to the developing field of organ-on-chip. Organ-on-chip technologies reduce the gap between in vitro and in vivo models by exploiting the strength of both types of models. Organ-on-chip models use 3D constructs which can be built to reproduce the microenvironment of an organ and be actuated to reproduce key functionalities of an organ or aspects of a disease. They are often associated with microfluidics due to the possibilities that such a construct offers. In particular, it offers an ideal framework in the kidney where organ functionality is through the exchange of fluids.

Most advanced kidney-on-chip models recapitulate several key features of the structure on a single chip. By using models built to reproduce kidney reabsorption functionalities, they allow us to integrate geometrical and mechanical aspects of nephron segments and to develop perfused cylindrical structure made of cell monolayers embedded in hydrogel. In particular, Homan et al. used bioprinting to develop single kidney tubule [1], while Weber et al. molded hydrogel around wires to develop a cylindrical scaffold for cell culture [2]. Both devices could be perfused to reproduce the *in vivo* kidney flow. These models showed strongly improved cell morphology, biological activity, reabsorptions, and secretions compared to 2D epithelium or 2D perfused equivalent. This demonstrated a real advantage which arose from the geometrical and mechanical features of these 3D biomimetic models. Nevertheless, these devices did not address the multitube aspect of the kidney, with the underlying proximity between nephrons, and had a significantly lower curvature than what is observed *in vivo*.

In a previous study [3], we conceived a first generation of collagen-based kidney-on-chip closer to *in vivo* conditions which recapitulated the geometry of the densely packed nephrons which, to the best of our knowledge, has never been reported in the literature. This design allows us to generate, in a 6 mg/mL collagen I gel, five parallel 80 μm -wide kidney cells tubules separated by only 100 μm . We used cell line models of autosomal polycystic kidney disease (ADPKD) in this platform to study the dilation of nephrons in polycystic kidney disease; our results suggest a possible coupling between dilating channels due to their close proximity. However, at this stage, the device did not allow for individually controllable tube perfusion, and the microfabrication was based on a complex plastic chip embossing. Furthermore, this kidney-on-chip design was limited regarding the reproducibility of the cell seeding because the density of cells in the tubes could not be properly controlled. In this model, as kidney cells are only moderately adherent, they do not adhere to the collagen tube sufficiently to reach initially the required density with most of the cells flowing outside of the tubular scaffold.

Here, we designed a new platform allowing for a better fluidic control while retaining the geometrical features of the previous model. Conceptually, the new chip still revolves around a series of parallel channels molded in collagen I with wires. As in the previous generation, we could generate channels as close as 100 μm and as narrow as 75 μm in diameter (*see Note 1*). A polydimethylsiloxane (PDMS) scaffold, which features fluidically independent channels to guide the wires allows for collagen channel perfusion. To promote cell accumulation in the collagen during cell seeding, and to better control the cell seeding density, we designed the PDMS channels with a particular geometry to make them several orders

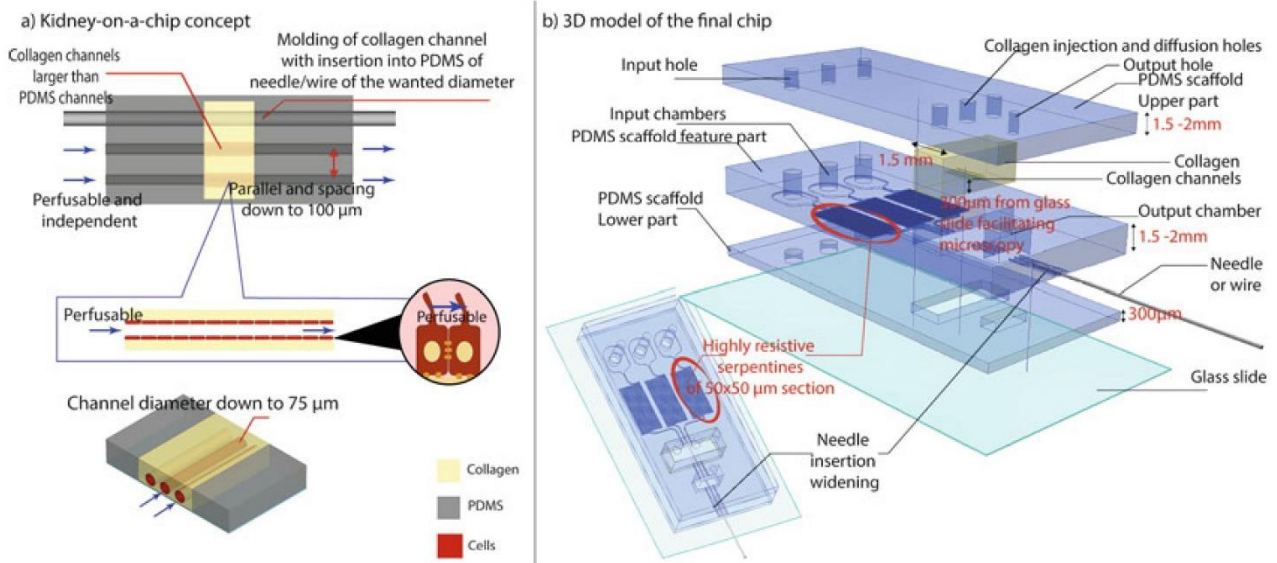


Fig. 1 Chip concept. (a) The chip consists of parallel tubular channels molded in collagen with needles or wires. Those are guided by channels in a PDMS scaffold. Resulting channels can be as small as $75\ \mu\text{m}$ wide and as close as $100\ \mu\text{m}$ -spaced. In this design, they are perfusable and fluidically independent. Channels in collagen are wider (less fluidically resistive) than in PDMS to promote accumulation of cells in the collagen upon seeding. (b) In the chip, a collagen chamber is embedded in 3 PDMS layers. A sandwiched PDMS layer features the wire guides and microfluidic channels, including highly resistive serpentine preventing cells from escaping the collagen part. A lower PDMS layer elevates the features so that the collagen tubes are at a distance optimized for microscopy, and finally an upper part caps the collagen chamber

of magnitude more resistive than the collagen ones (Fig. 1). They also now have independent inputs and an optionally common output, allowing either independent or parallel perfusion of the channels. Perfusion of this new chip is achieved with controlled input positive pressure. Overall, this chip offers greater fluidic control of individual channels. Finally, it allows reproducibility in seeding; the experimenter can now choose to use either scarce or confluent tubes on the first day of the experiment.

First, the kidney-on-chip fabrication consists of making the mold used for the chip PDMS scaffold (Fig. 2). Next, we build the PDMS scaffold that will feature the microfluidic channels. This serves as a chamber to cast the collagen as well as being a guide for the wires that will mold the collagen (Fig. 1b). Second, once the PDMS scaffold is built, PDMS and glass surfaces need to be treated to covalently graft collagen [4, 5]. The collagen molding can thus be performed after inserting wires or needles of controlled diameter through the guides. Here, we use $75\ \mu\text{m}$ wide wires to mold channels of the same diameter in the collagen, but it is possible to use larger wires or needles to produce larger channels (*see Note 1*). After wire insertion, collagen I at the desired concentration (from $6\ \text{mg/mL}$ to $10\ \text{mg/mL}$) is injected into the chip central chamber and polymerized to produce a ready-to-use chip (Fig. 3). Third, prior to cell injection, collagen channels can be coated with

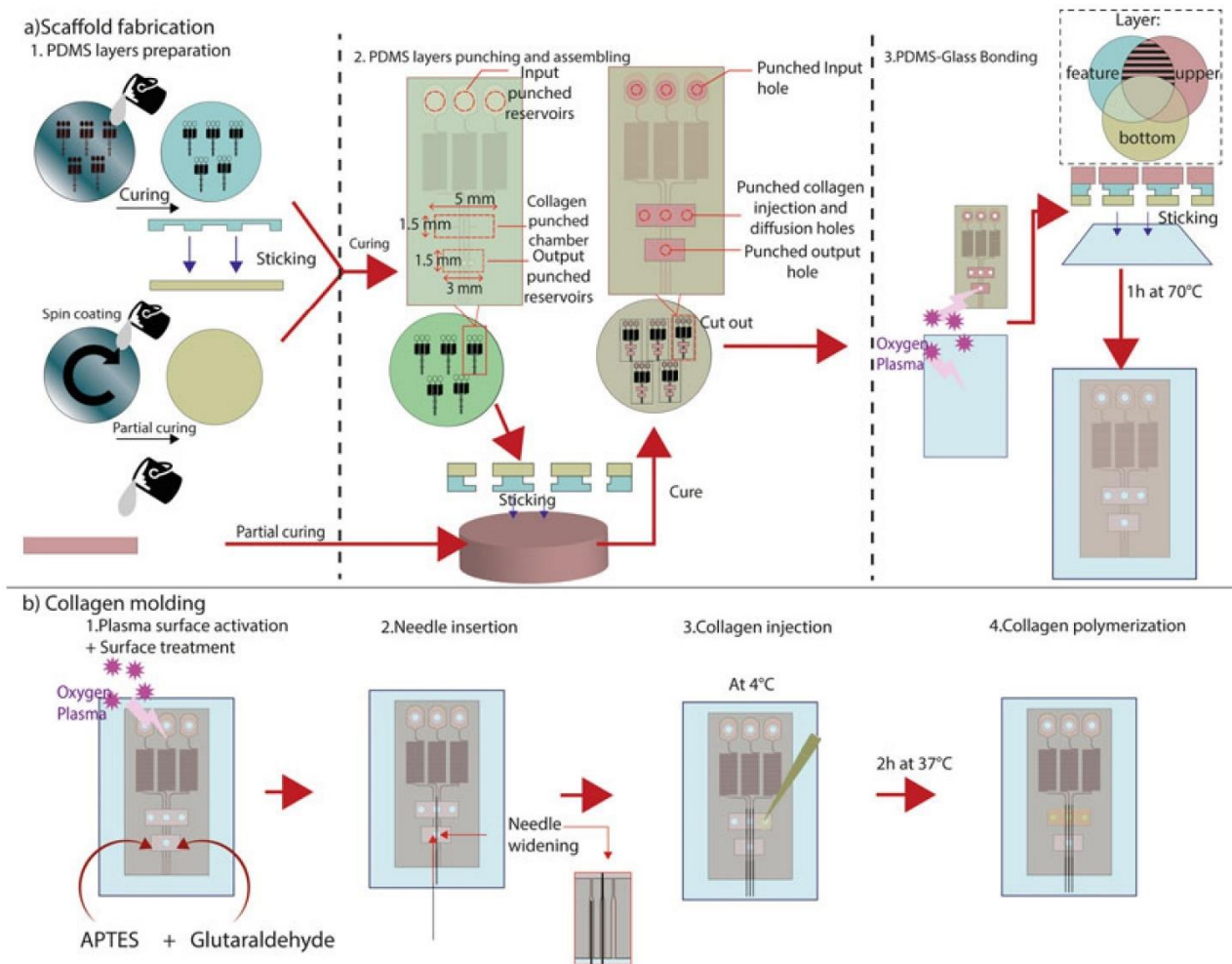
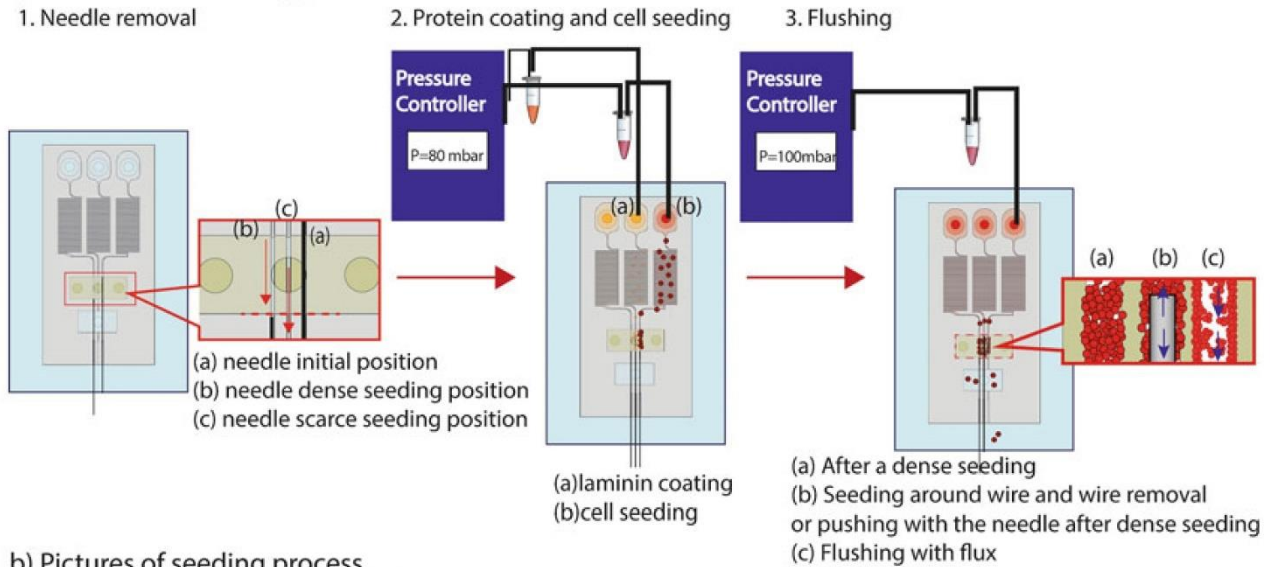


Fig. 3 Making the PDMS scaffold and molding collagen. **(a)** The first step to make the PDMS scaffold is the PDMS layers preparation. PDMS prepared at 1:10 ratio is poured on a wafer with the features, and then let to cure. We also spin-coat PDMS on a flat surface for the lower part and partially cure it until solid but sticky. The feature part is stuck on the lower part and let to cure completely. In parallel, we pour a thin layer on another flat surface for the upper part and cure it until soft and sticky. In the second step, reservoir holes are punched on the assembled two lower parts, and then they are stuck to the upper part and are completely cured. Finally, we punch the injection holes and stick the PDMS to a thin glass layer with plasma bonding. **(b)** The complete scaffold is activated with plasma and surface is treated with APTES and then Glutaraldehyde. Then needle or wires are inserted into the scaffold, which is facilitated by needle flaring. Unpolymerized collagen is injected into the collagen chamber. After polymerization 2 h at 37 °C, the chip is ready to use

2.2 PDMS Scaffolding

1. SYLGARD™ 184 Silicone Elastomer Kit (PDMS) (Dow corning, Midland, Michigan, USA).
2. 0.17 mm thick and 30 mm large round cover slips.
3. Oxygen plasma generator (Diener electronic GmbH & Co. KG, Ebhausen, Germany).
4. Vacuum chamber.
5. 70 °C oven.
6. 10.5 cm diameter Petri dishes.

a) Schematic of seeding process



b) Pictures of seeding process

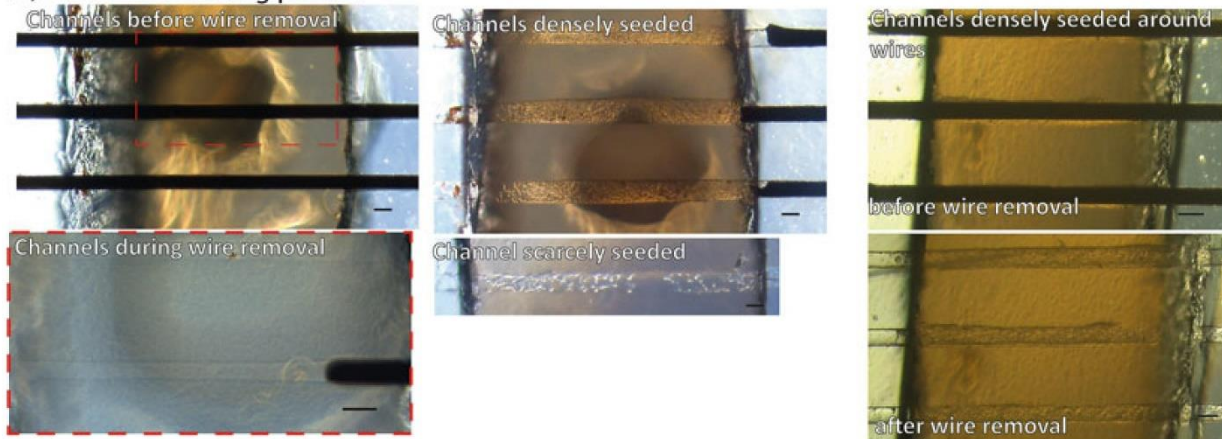


Fig. 4 Seeding. (a) For coating and seeding, needles can be removed into two positions. Either they are partially removed to obtain a dense seeding, or they are completely removed for a scarce seeding. Thanks to a pressure controller, a laminin solution is injected into the collagen channel. After the laminin coating, a cell suspension is injected with the same system to either fill the collagen channels or around the wire inserted back into the channel to force a lumen. In case of a seeding around the wires, the wires are then removed or an optional flushing step can be done right after the cell adhesion in case of a dense seeding: either using the wire in a back-and-forth motion in the channel or using the same system as before injecting media. Pictures of an actual seeding process are shown in (b) (scale bars 100 μm)

7. Spin-coater.
8. PDMS hole puncher kit with 0.75 mm, 1 mm, 1.5 mm, 2 mm punchers (Integra LifeSciences Services, France).
9. (Optional) 1.5 \times 3 mm² leather punch.
10. Solvents: Acetone, ethanol, isopropanol.

2.3 Collagen Molding

1. 0.75 mm straight tungsten wires (Goodfellow SARL, Lille, France) (*see Note 2*).
2. Phosphate-buffered saline (PBS), pH 7.4.

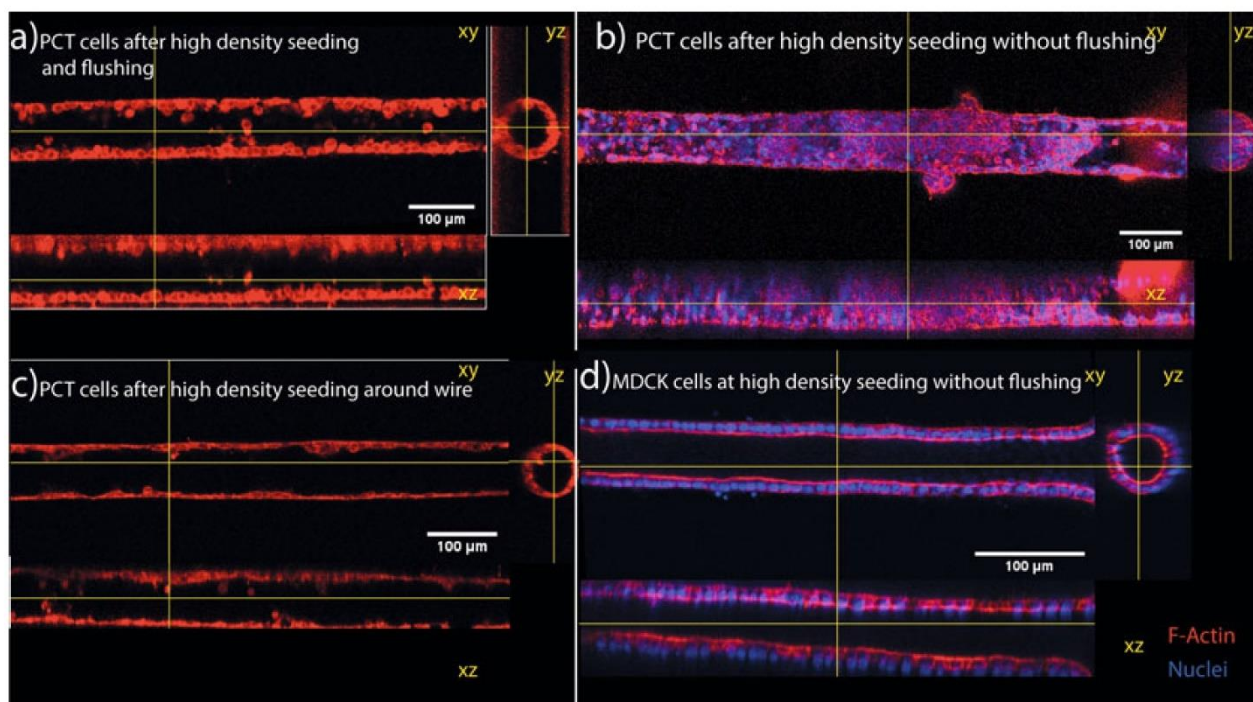


Fig. 5 Representative images of confluent tubes seeded with kidney cell lines. **(a)** With PCT *Pkd1*^{+/-} after a high seeding density followed by a flushing step. **(b)** With PCT *Pkd1*^{+/-} [8, 9] after a high seeding density without flushing. **(c)** With PCT *Pkd1*^{+/-} after a high density seeding around a wire. **(d)** With MDCK (here *Pkd1*-KO) [10, 11], similar organization with native MDCK cells after a high seeding density without flushing. Images were obtained with confocal microscopy and are showing different cross-sections of the tubes. Red, F-actin, blue, nuclei, scale bar 100 µm

3. Bovine serum albumin.
4. 0.2 µm filter with syringe.
5. Double-deionized water (ddH₂O) (e.g., milliQ™ water).
6. (3-Aminopropyl)triethoxysilane, 99% (APTES) (Sigma-Aldrich, St).
7. Methanol.
8. Glutaraldehyde, 50% (Sigma-Aldrich).
9. Ultrasonic bath.
10. High concentration collagen from rat tail (Corning Inc., Corning, NY, USA): at least 8 mg/mL stock concentration to produce at least 6 mg/mL collagen working solution.
11. 1 N NaOH .
12. Phosphate-buffered saline (PBS) 10×.
13. (Optional) UV-Ozone oven.
14. 37 °C incubator.
15. Ice.

2.4 Coating and Cell Seeding

1. PTFE tubing with 0.3 mm inner diameter and 0.76 mm outer diameter (*see* **Note 3**).
2. Pressure controller: Flow EZ (Fluigent, Le Kremlin-Bicêtre, France) with pressurized air.
3. Laminin.
4. Mammalian epithelial cell line of choice with suitable complete medium. In this paper PCT *Pkd1*^{+/-} cells (PH2 cell line) [6, 7] and Madin-Darby canine kidney (MDCK) *Pkd1*-KO [8, 9]. (These cells modified for *Pkd1* expression are kind gifts from S. Somlo and F. Bienaimé, respectively.)
5. Sterile hood.
6. Binocular microscope with a screen.
7. 6-well plates.
8. Percoll™, pH 8.5–9.5 (25 °C), suitable for cell culture (Sigma-Aldrich).

2.5 Staining

1. Hoechst, phalloidin.
2. Triton™ X100.
3. Tween20™.
4. (Optional) Goat serum.
5. (Optional) Primary and secondary antibodies.

3 Methods

3.1 Making of the PDMS Feature Mold

The PDMS feature mold will allow the experimenter to reproduce the microfluidic features for perfusion and guides for the wires in the PDMS scaffold thanks to soft lithography. This mold can be obtained using photolithography techniques on a 50–75 μm-thick dry film photoresist, with the procedure we describe here, or using any other classical negative photoresist such as SU-8 (Fig. 2 for plans of the mask) [10, 11].

3.1.1 Prepare the Wafer and Laminator

1. Set one hot plate at 200 °C for dehydration and another one at 100 °C for soft baking (or soft baking temperature indicated on the dry film datasheet). Set the laminator temperature at 100 °C.
2. Clean the silicon wafer first with acetone and then with isopropanol and finally with ddH₂O water, drying well between each rinsing.
3. Put the wafer on the 200 °C hot plate for at least 10 min for complete dehydration.

3.1.2 Apply and Bond the Dry Film to the Wafer

1. Use a wafer of the same size as a guide to cut into the 50 μm thick dry film a slightly bigger piece that would have the same shape.
2. Put the wafer at the entrance of laminator.
3. Set the laminator on speed 0.2 mm/s.
4. Peel off one protective layer of the dry film, put the exposed face toward the spatula on the spatula and carefully stick one end of the dry film to the wafer while maintaining the rest on the spatula at a 45° angle.
5. Set the laminator on forward motion while maintaining the spatula between the rest of the dry film and the wafer until it reaches the laminator roll. The goal is to guide the dry film gently, while it progressively gets stuck on the wafer. Some tension must be maintained on the film to prevent formation of bubbles. To do so, hold the film ends with your hands while maintaining tension as the wafer goes under the roll.
6. Once the whole film is stuck on the wafer, make it go back and forth under the laminator at least 4 times to completely bond the dry film.
7. If too many bubbles have formed under the dry film, you can start over by removing the other adhesive protection of the dry film, remove the dry film with the photoresist developer, and start over from **step 1** with the same wafer.

3.1.3 Expose Dry Film to UV

1. Peel off the other side of the dry film protective film and load the mask and the wafer in the UV exposure device.
2. Set the device for hard contact between the mask and wafer (no spacing between the mask and the wafer).
3. Expose the dry film per the manufacturer recommendations, and calculate the exposure time depending on the UV power and the recommended amount of energy needed according to the dry film datasheet. As an example, for a DF1050 dry film, the energy required is 95 mJ/cm^2 , which gives a 3 s exposure time for a 35 mW/cm^2 UV light at 365 nm.

3.1.4 Develop the Wafer

1. Unload the wafer and set it on the soft baking hot plate. This soft baking step should take about 10 min but may vary depending on the dry film used.
2. After the soft baking, put the wafer into a developer bath for the recommended amount time while gently swirling (10 min for the DF1050). Do not hesitate to change the developer bath mid-course.
3. Gently spray the wafer with developer to remove any left-over undeveloped dry film. You should not see any irisation on the surface. If this is the case, you can develop the wafer for a few more mins.

4. Rinse with isopropanol.
5. Optional: Hard bake the wafer for 2 min at 200 °C on a hot plate.
6. Optional: Check the features on the wafer by profilometry.

3.1.5 Silanize the Wafer

1. Clean the wafer with isopropanol.
2. Activate the surface with oxygen plasma for 45 s.
3. Immediately afterwards, in a vacuum chamber placed into a 15 mL falcon cap, put 50 µL of 1H,1H,2H,2H-perfluorooctyltriethoxysilane. Place the wafer in the vacuum chamber.
4. Switch the vacuum on for 30 min, and then switch the vacuum off while keeping the wafer under vacuum for another 30 min.
5. Check the wafer for hydrophobicity by gently pouring water on it. The water should slide on it in droplets. If it is the case, the wafer is now ready to use.

3.2 Fabrication of the PDMS Scaffold

The scaffold consists of an assembly of 3 PDMS layers bonded to a glass slide. One part of the scaffold features the microfluidic channels. This part lies on a flat PDMS membrane which elevates the channels from the glass slide while maintaining them at a distance compatible with imaging (approximately 500 µm between the bottom of the chip and the bottom of the channels). On top, another flat PDMS membrane closes the chip (Fig. 1b).

3.2.1 Prepare PDMS at a 1:10 Ratio Curing Agent/ Base

1. Mix curing agent and base thoroughly (around 40 g of PDMS is needed for a complete wafer).
2. Put the PDMS under vacuum to rid of bubbles formed during mixing.

3.2.2 Prepare Substrate for PDMS

1. Clean the wafer as well as the top of the lid, and the bottom of a Petri dish bigger than the wafer, with isopropanol.
2. Put the wafer in a dish of approximately the same size or surround it with aluminum to recreate such a dish.

3.2.3 Pour and Cure PDMS

1. Pour approximately 12 g of PDMS on the wafer for the feature part, the same amount into the clean dish for the top (to get a 1.5–2 mm thick layer) part and spread the PDMS evenly.
2. Put under vacuum the feature and the top part until no bubble is left.
3. In parallel, pour approximately 5 g on the top of the lid of the Petri dish for the bottom part. To spread PDMS for the top part, spin-coat at 350 rpm for one minute to get a 300 µm-thick membrane.

4. Let the feature part cure at 70 °C until almost completely cured (approximately 40 min), the upper part until soft and sticky (approximately 20 min) and the bottom part until solid and sticky (18–20 min) (*see* **Notes 4** and **5**).

3.2.4 Assemble the PDMS Layers

1. Unmold the feature part and delicately stick it to the lower part still attached to the Petri dish lid with the features facing it (Fig. 3a), avoiding bubble formation between the two layers.
2. Let the assembled two parts completely cure for another 30 min at least (Fig. 3a part 1).
3. Detach the two lower parts carefully from the lid.
4. Punch the chambers for the input (2 mm diameter), the chamber for the output ($3 \times 1.5 \text{ mm}^2$), and for the collagen chamber ($5 \times 1.5 \text{ mm}^2$), centering the punch around the marks (Fig. 3a part 2, *see* **Note 6**).
5. Stick the punched layers on the top layer with features facing upward.
6. Let the assembled layers completely cure at least 45 min at 70 °C.
7. Cut out individual chips, making sure the chips are cut open at the level of the wire entry.
8. Punch 0.75 mm diameter holes for inputs and outputs, as well as 1–1.2 mm diameter holes for collagen injection and diffusion holes (Fig. 3a part 2).

3.2.5 Bond the PDMS to the Glass Slide

1. Clean the glass slide with acetone, then isopropanol, and clean the PDMS with ethanol only. Dry well.
2. Put PDMS chips with bottom layer facing up and glass slides under oxygen plasma during 45 s, and then stick the PDMS bottoms to the glass slides right away.
3. Immediately put at 70 °C for approximately 1 h to finish bonding.

3.3 Collagen Molding

3.3.1 Treat the Surface of the Chip with APTES (Fig. 3b Part 1)

1. Prepare an APTES solution at 4% volume ratio in methanol (*see* **Note 7**). You should prepare enough solution for an APTES bath that completely immerses the chips (around 100 mL).
2. Activate the surface of the chips with oxygen plasma for 45 s, and immediately put them in the APTES bath (*see* **Note 8**).
3. Let chips sit into the covered bath for 2 h.
4. Afterwards, briefly immerse the chips in a methanol bath for a first rinsing.
5. Put them back into methanol in an ultrasonic bath and sonicate for 30 min (*see* **Note 9**).
6. Rinse one more time briefly in fresh methanol and dry well.

3.3.2 Treat the Surface of the Chip with Glutaraldehyde

1. Prepare the glutaraldehyde solution at 2.5% volume ratio in ddH₂O water.
2. Inject 30 μ L into each chip through the collagen chamber injection holes to fill the chamber.
3. Let react for 30 min.
4. After, blow air into the chambers to expel the solution and rinse the chips in ddH₂O water briefly.
5. Put chips into a fresh ddH₂O water bath and put under vacuum to force water inside the chip.
6. Renew the water in the bath and place under ultrasound sonication for 30 min at least.
7. Renew the water solution and let rinse overnight (*see Note 10*).
8. Store treated chips in the most sterile possible environment.

3.3.3 Prepare Wires

1. Prepare a 0.2 μ m-filtered BSA 4% (w/v) solution in PBS.
2. Cut the tungsten wires into 1–2 cm pieces.
3. Wash wires with acetone, and then rinse with ddH₂O water.
4. Put wires into the BSA solution for 30 min at least, and then rinse with ddH₂O water.
5. Keep treated wires in ddH₂O in the most sterile possible conditions.

3.3.4 Insert Wires

1. Insert wires delicately into the wet chips with clamps under a bright light: Target the wire insertion widening first and make sure the wires are not penetrating the PDMS next to the insertion instead.
2. Keep pushing wires delicately through the guides until they go past the collagen chamber (*see Note 11*).
3. This operation should be performed in the most sterile possible environment.

3.3.5 Prepare the Collagen

1. Sterilize the chips with UV for at least 15 min (*see Note 12*) and chill them at 4 °C.
2. On ice, prepare the collagen solution by diluting it at right concentration (from 6 mg/mL to 10 mg/mL) and neutralizing. You will need 40 μ L of final solution per chip on average (*see Notes 13 and 14*).
3. Check that the pH of the collagen solution is around 7. If pH is not around 7, it probably means that the solution has not been mixed well enough.
4. Centrifuge for a few secs to remove bubbles.
5. Dry the collagen chambers of each chip by blowing air into it.

6. Still on ice, after making sure that the collagen chamber is dry, slowly and gently inject 30 μ L of collagen into the chamber through one injection hole.
7. Make sure the wires are surrounded with collagen and that no bubble is injected around the wires (*see Note 15*).

3.3.6 Allow Collagen to Polymerize

1. Keep the chips at 37 °C under humid atmosphere for 2 h minimum to polymerize the collagen.
2. After polymerization, collagen should be clear and yellowish under microscope (Fig. 4b).
3. Store the chips immersed in PBS with 2% P/S at 4 °C at least overnight (*see Note 16*).

3.4 Coating and Cell Seeding

Before cell seeding, to mimic the basement membrane, the experimenter can coat the collagen channels with proteins such as laminin. This step also allows the experimenter to check for good perfusion of the channels prior to cell seeding. Solutions and cell suspensions are injected into the chip with a pressure controller, allowing control of the perfusion flow rate. Adjusting wire positioning allows the user to increase the channel resistivity even further and allows tuning of the cell density. Three modes of seeding are possible, either a scarce seeding, a dense seeding with channels completely filled, or a seeding forcing a lumen from the start. Finally, the channels can be flushed to remove cells that did not adhere to the collagen or to force a lumen from day 1 in case of dense seeding.

3.4.1 Prepare the Working Environment

1. The seeding and coating are performed under a microscope outside of a sterile hood; it is therefore necessary to keep the environment as sterile as possible. Set up the pressure controller by connecting all the necessary tubing (*see Note 3*). Clean the PTFE tubing that will be used for coating by passing 1 mL of ethanol through it. Let also air flow through it to remove all the excess ethanol inside the tubing. Clean all surfaces that may be touched during the procedure with ethanol. Clean all instruments as well with ethanol, clamps, and scissors.
2. Prepare a Petri dish filled with enough PBS so that chips can be submerged and heat it to 37 °C. Prepare a sterile bath with PBS plus antibiotics (2% Penicillin/Streptomycin) for the coated chips (*see Note 17*).

3.4.2 Prepare the Coating Solution

1. On ice, prepare a 50 μ g/mL solution of laminin in the complete medium suitable for the cells.
2. Connect it to the tubing system and put it under pressure until the PTFE tubing is totally filled with solution, waiting for a droplet to form at the end (*see Note 18*).
3. Keep the solution on ice.

3.4.3 Check for the Absence of Bubbles in the Chip Channels

1. Put the PBS Petri dish under the microscope. Immerse the chip into the solution with a clamp.
2. Inspect the serpentine channels in PDMS for bubbles. If bubbles are still present in a channel, the chip may require to be immersed longer in PBS. In any case, do not inject flow through this channel, as a bubble ending into the collagen will damage it (*see Note 19*).

3.4.4 Coat with Laminin

1. If aiming at a dense seeding, remove the wires carefully until they just reach the end of the collagen chamber. For a scarce seeding, remove the wires completely (Fig. 4a part 1 and Fig. 4b).
2. Set the pressure around 50 mbar, making sure that a droplet forms at the end of the tubing.
3. Connect the tubing to an input and increase the pressure to around 80 mbar (Fig. 4a part 2, *see Note 20*).
4. Make sure there is flow by checking any debris moving from the inlet throughout the PDMS channels. You can also make sure there is flow by looking for slight deformations in the connected collagen channel.
5. Flow laminin solution for approximately 1 min and remove tubing from inlet.
6. Repeat for each channel, and then put the chip into the fresh PBS (*see Note 19*).
7. After all chips have been coated with laminin, put them at 37 °C for 1 h.
8. Let overnight at 4 °C to remove any bubble that may have nucleated.

3.4.5 Prepare the Working Environment for Cell Seeding

1. Prepare the working environment the same way as for the coating.
2. Additionally, in well plates or Petri dishes large enough to contain the chips, prepare as many PBS wells as there are chips to seed and warm the wells at 37 °C.

3.4.6 Prepare Cells

1. Detach your cells as you regularly would (e.g., trypsinization).
2. Resuspend them at the right seeding concentration in complete media (with fetal bovine serum). For the dense seeding procedure, a concentration of 5–10 million cells/mL and for the scarce seeding procedure, 10 million cells/mL to 15 million cells/mL.
3. Put the cell suspension in the container for the pressure controller. You will need at least 100 μ L of cell suspension to which you may add 50 μ L per chip (*see Note 21*).

3.4.7 Check the Chip Configuration

1. Put the PBS Petri dish under the microscope. Immerse the chip in PBS and check for bubbles. If bubbles formed in a channel, it means that the chip may need to be immersed at 4 °C longer (*see Note 19*).
2. Check also that the wires are in the right position for the seeding (Fig. 4a part 1).

3.4.8 Seed Cells

1. Connect the tubing to the chip with a droplet of cell suspension pearling by setting at 50 mbar.
2. When the tubing is connected, increase the pressure to around 80 mbar (*see Note 19*). You should normally see cells coming out the tubing and flowing through the serpentine after a short time. If the flow seems too slow, do not hesitate to increase the pressure gradually.
3. During seeding, the serpentine may get partially clogged if some cells are in aggregates. If this happens, do not hesitate to increase the pressure progressively and temporarily within hundreds of mbar, just to unclog the serpentine before decreasing it back to the previous setting. Do not keep the pressure too high, as it will damage both the cells and the collagen.
4. When cells are flowing, keep the microscope focused on the collagen channels to assess its filling.
5. There are three possible ways to seed the channel:
 - (a) Either keep the wire removed in position right past the collagen channel and let the cells fill the channels completely. This will give you channels completely filled with cells initially.
 - (b) Or as the cells are filling the channels, progressively and carefully reinsert the wire so that cells only fill the channel around the needle. This second possibility will force a dense seeding with a lumen as the cells will fill the channels around the wires only.
 - (c) Alternatively, remove the wires completely and seed the cells trying to reduce progressively the flow by decreasing the pressure trying to keep the cells into the channel. This will result in a chip scarcely seeded.
6. When the channel is as filled as required (Fig. 4b), stop the pressure and rapidly cut the PTFE tubing just above the input (*see Note 22*).
7. While working in a sterile hood, immediately put the chip in a warm well of PBS.
8. Repeat the process until all chips are seeded.
9. During the seeding, make sure to resuspend the cell suspension at a regular interval as they will sediment (*see Note 23*).

3.4.9 *Let Cells Adhere*

1. Aspirate PBS from all wells and put a drop of 100 μ L complete media on the top of each chip, making sure it does not fall on the side (*see Note 24*).
2. Put the chips in an incubator and wait for the cells to just adhere (generally between 2 and 3 h).

3.4.10 *Remove Wires and Tubing*

1. Under a microscope, remove wires from the chips with a clamp, as well as any leftover tubing in the inputs.
2. If the cells have adhered, upon wire and tubing removal, cells coating the channels should not move. If the cells are still moving, a longer incubation is necessary before removal.
3. Store any undeformed wire piece into ethanol for later utilization.

3.4.11 *Flushing (Optional)*

1. In case of dense seeding with channels filled with cells, it is possible to flush the channels to remove cells which are along the center of the channel. To do so, there are two possibilities: flushing with media or pushing cells with the wire (Fig. 4b).
2. For flushing with media, completely remove the wires, inject warm media through inputs into the chip, and increase pressure until cells at the core of the channels are removed.
3. To push cells with the wires, insert the wire in the seeding position back into the collagen channel delicately, so as not to damage collagen. Push the wires through collagen channels in a back-and-forth motion before removing the wire completely (*see Note 25*).

3.4.12 *Seal the Wire Insertion with PDMS (Optional for Later Perfusion)*

1. Put 1:10 PDMS under UV or UV-ozone for sterilization for 15 min.
2. Apply a generous drop of PDMS in sterile conditions on the wire insertions to clog them.
3. Put the chip back in incubators at 37 °C with a drop of media on top for at least 2 h to let the PDMS cure enough not to be liquid-like anymore.
4. Put the chips back into the wells and rinse them with PBS. Finally, put enough warm media in the wells for the chips to be completely immersed and put back into incubators.

3.5 Cell Culture, Fixation, and Staining

3.5.1 *Changing Medium*

1. Change medium the day following the seeding and then every other day by removing completely the old medium and replacing with fresh one, keeping the chip submerged.

3.5.2 *Fixing the Cells*

1. Remove media from the wells and rinse the chip with PBS.
2. Submerge the chip in PBS with paraformaldehyde at 4% volume ratio.

3.5.3 Staining

3. Incubate at room temperature for 30 min.
 4. Rinse twice with PBS and store in PBS at 4 °C.
1. Permeabilize the cells by submerging the chip into PBS + 0.3% TritonX100 for 30 min.
 2. Rinse 3 times for 30 min with PBS-BSA 2%.
 3. (Optional for immunostaining, *see Note 26*) Saturation: Submerge the chip in PBS-BSA 2% with 0.1% Tween20™ and 2% Goat Serum.
 4. (Optional for immunostaining, *see Note 26*) Primary antibodies: Delicately add a 100–150 µL drop of primary antibody at the appropriate dilution (typically 1/200), 2% BSA, 1% Tween20™ in PBS. Let incubate for 24 h in a humid environment at room temperature. Check at mid-stage to make sure that the drop has not dried out. You can add a fresh drop PBS-BSA 2% solution if the volume has significantly decreased.
 5. (Optional for immunostaining, *see Note 26*) Rinse 3 times for 30 min in PBS-BSA 2%.
 6. In case of immunostaining for secondary antibodies: Delicately add, so that it does not fall, a 100 µL drop of a solution of 1 µg/mL Hoechst, 0.25 µg/mL fluorescent phalloidin, secondary antibody at the appropriate dilution, 2% BSA, 1% Tween20 in PBS. You can coat the edges of the chip with mineral oil to help the drop not spilling. Let incubate for 24 h in a humid environment at room temperature. Check at mid-stage if the drop has not dried. You can add a fresh drop of PBS-BSA 2% solution if the volume has significantly decreased.
 7. Rinse 3 times in PBS for at least 30 min at room temperature.

4 Notes

1. The presented design should work for wires or needles up to 100 µm diameter. For larger wires or needles, we advise widening and spacing the guides to be able to insert them properly and keep the desired distance between channels. Note also that in the presented design, channels are 300 µm apart.
2. Here, we used 75 µm tungsten wires, but stainless-steel needles can be used for diameters over 100 µm. Under 100 µm, stainless steel may be too ductile for handling with this chip. We also preferably work with straighten wires, which can facilitate insertion into the chip. If only rolled wire is available, try to keep only the straightest cuts.
3. The PTFE tubing dimensions in the Materials section are indicative. The key is to have a tubing which has a small enough

inner diameter for a high enough resistivity and a large enough outer diameter to fit the input holes tightly. PTFE is preferred as material, as it is highly hydrophobic.

4. To ensure PDMS is spread out evenly, alternatively, it is possible to let the top and feature parts cure overnight on a leveled surface such as an optical table. Overnight curing should be enough to get the right consistency for the top layer. The feature part would require additional curing at 70 °C for approximately 20 min, while lower part is curing.
5. Feature part should not be too undercured to avoid getting PDMS stuck into the wafer features on demolding. This leads to damage to the wafer as well as features reproduced unfaithfully by PDMS. The bottom part should be sticky enough to allow bonding with feature part, but not too sticky to prevent channels clogging. As for the upper part, it should be just cured enough so that the PDMS can no longer spread.
6. To make the output and collagen chamber punch, several holes of 1.5 mm diameter can be aligned.
7. APTES is highly reactive with water and will be deactivated in a wet atmosphere, leading to the formation of APTES aggregates. Avoid contact with any aqueous element. Furthermore, prolonged exposure of PDMS with ethanol can lead to swelling, hence why we prefer methanol here.
8. While chips are in the APTES bath, you can put them under vacuum to force APTES solution inside the chips channels. This will increase the hydrophilicity of the overall system and will help prevent bubble formation later.
9. Rinsing of APTES should be very thorough as an under-rinsed chip will lead to formation of clogging APTES aggregates when reacting with ambient humidity. This is helped with sonication. Before the second rinsing of the chips, it is also possible to blow nitrogen into the channels through the central collagen chamber to evacuate stagnant APTES solution.
10. Although necessary for collagen adhesion to PDMS, glutaraldehyde is highly toxic to cells even at low concentrations. Rinsing of excess glutaraldehyde should be very thorough, as under-rinsing may lead to cell death after the seeding step. Finally, glutaraldehyde reacts with APTES aggregates inside the chip, leading to autofluorescent aggregates that may impair the quality of fluorescent microscopy.
11. Water is used here as a lubricant that facilitates wire insertion: as wires are wider than some of the PDMS sections, doing it in a dry condition will complicate insertion. Furthermore, wires should be inserted delicately without requiring too much force: as PDMS is much softer than tungsten, forcing the

wires may result in piercing the PDMS next to the channels and deviate the wires from the right course. Although normally visible with the naked eye, do not hesitate to check right insertion under binocular microscope. In case of missed insertion, start over with a new piece of wire.

12. This operation is preferably performed with a UV-ozone oven.
13. Preparing the collagen solution requires diluting the concentrated stock solution to the desired concentration, while neutralizing the pH. To do so, we use the following ratios of reagents:

Volume of collagen I stock solution = Target concentration / stock concentration \times final volume of collagen solution.

Volume of NaOH (to neutralize the stock solution) = Volume of collagen I stock solution \times 0.023.

Volume of PBS 10 \times (to buffer the final solution and maintain osmolarity) = final volume of collagen solution / 10.

Completed with PBS or media until reaching the target final volume of collagen solution.

14. When diluting and neutralizing the solution, be very gentle to avoid inserting bubbles into the solution and leading to incorrect polymerization of collagen. To that end, you can do one gentle back and forth motion with a micropipette to mix the solution and continue mixing it with a spatula and rotation motions. Furthermore, if preparing more than 500 μ L of collagen, preferably do it in several batches. Finally, when neutralized, collagen must be handled on ice to avoid polymerization.
15. In case a bubble has been injected into the chamber: If it is not close to the wires, there should be no problem. If a bubble is located next to the channels, inject PBS in excess in the chamber, dry it, and try again.
16. Leaving the chips in PBS at 4 $^{\circ}$ C should get rid of the bubbles that formed into the PDMS channels in previous steps. Before use, make sure that no bubble is present in the channels. Chips can be stored up to a month before use.
17. As the seeding procedure occurs outside of sterile conditions, it is necessary to keep the environment as clean as possible to avoid antibiotic-resistant contamination. Adding antibiotics to PBS used for incubation at higher concentration than usual is a way to prevent bacterial development during these phases.
18. Connecting the tubing to the chip may introduce air into the chip, leading to the formation of bubbles. To prevent this, it is preferable to work in immersed condition. The droplet coming out of the tubing will prevent a water/air interface to appear that would lead to bubble formation.

19. For faster coating or seeding, or in case a serpentine is clogged or has bubbles, it is possible to inject flow from the output. To do so, remove the wire right past the output chamber and inject flow using lower pressures (around 20 mbar for the described configuration) taking care not to damage collagen channels because of the lower resistivity of the wire guides. It is possible to inject flow in multiple channels at the same time by simply simultaneously removing the wires. In case of coating, this will result in faster injection of laminin. This will also result in denser seeding due to the high resistivity of serpentes. When enough cell suspension has been injected, close the channels by reinserting the wire to the dense seeding position. For seeding or coating, do not set pressure to zero right away, but cut the PTFE tubing right above the chip first as a suction effect could lead channels to collapse. Beware that a seeding from the output chamber may result in a lot of cells accumulating then dying in the chamber, which may possibly become toxic for cells in the channels.
20. Pressures here are indicative; the right pressure may vary with the fluidic setup with larger or more narrow tubing or channels. The key is to have a pressure not too high that could damage the collagen channels or detach the collagen from PDMS. Pressure should not be too low either, as cells would sediment before being able to reach the collagen.
21. For dense seeding configuration, cell concentration can go as low as wanted in theory. It may result in an intermediate density of seeding, but the process will take much longer (from approximately 1 min to seed one channel to more than 10 min if using concentrations under 1 million cell/mL), which may be counterbalanced by increasing the pressure. This can however be another viable configuration for low density seeding.
22. Stopping the flow results in a backflow that may empty the collagen slightly; the serpentes are there to mitigate the phenomenon. Furthermore, removing the tubing will result in an even stronger backflow because of a suction effect. This is why it is preferable to cut it. Alternatively, you can remove the tubing slowly while keeping the pressure on.
23. To prevent sedimentation, it is possible to add Percoll™ to the cell suspension at a 10–20% volume ratio.
24. Rinsing the chip in PBS will remove as many cells as possible that may have attached to the outside of the chip. This will prevent as much as possible a cell monolayer to form outside of the chip. Depriving any leftover cell outside of the chip of media during adhesion time will also help prevent this.

25. Flushing may be unnecessary for certain cell lines (Fig. 5c) while recommended for others to promote lumen formation (Fig. 5b). Indeed, some cell lines will tend to strongly form monolayers, while others, if constrained in the channels, may partially form multilayers if they are too densely packed. If it is not necessary that channels are confluent as quick as possible, scarce seeding can be preferred to obtain reproducible monolayers (Fig. 5a).
26. Here, we describe an immunostaining protocol optimized for a typical Ki-67 labeling. However, parameters for immunofluorescence staining (durations, concentrations, etc.) may vary for detection of other proteins. Due to the presence of a millimeter-thick collagen matrix surrounding the cells not slowing diffusion, we recommend increasing the concentration compared to that used for exposed cells.

Acknowledgments

The authors acknowledge all the members of the MMBM and PBME groups for their precious support in the process development and in microfabrication. We are grateful to Bastien Venzac, Sophie Demolombe, Frank Bienaimé, Stefan Somlo and Eric Honoré for the insightful discussions, and to Irène Le Moine Caubarère for her participation in the experiments. We thank Frank Bienaimé (Institut Necker Enfants Malades, Paris) for kindly giving us MDCK *Pkd1*-KO cell lines, George M. O'Brien Kidney Center at Yale (NIH P30 DK079310) and Stefan Somlo for the kind gift of PCT *Pkd1*^{+/-} cell lines. This work benefited from the technical contribution of the joint service unit CNRS UAR 3750. The authors would like to thank the engineers of this unit (and in particular Bertrand Cinquin) for their advice during the development of the experiments. We are grateful to Fanny Tabarin and Aude Battistella (BMBC) for technical support with cells. The authors greatly acknowledge the Cell and Tissue Imaging core facility (PICT-IBiSA), Institut Curie, member of the French National Research Infrastructure France-BioImaging (ANR10-INBS-04).

Conflicts of Interest The authors declare no conflict of interest. The funders had no role in the design of the study; in the collection, analyses, or interpretation of data; in the writing of the manuscript, or in the decision to publish the results.

Funding

This work was supported by a doctoral grant from AMX (“*Ministère de la Recherche et de l’Enseignement supérieur*”, France) (recipient B. Lapin), and the “Fondation pour la Recherche Médicale” (FRM, recipient B. Lapin, program FDT). It was supported by the European Commission grant FET Open program (FETOPEN-01-2016-2017). This work has received the support of “Association Polykystose France,” provided by the “Société Francophone de Néphrologie, Dialyse et Transplantation” (SFNDT). This work has received the support of “Institut Pierre-Gilles de Gennes” laboratoire d’excellence, “Investissements d’avenir” program ANR-10-IDEX-0001-02. This work received support from the grants ANR-11-LABX-0038, ANR-10-IDEX-0001-02 (LabEx CelTisPhyBio - Cell(n)Scale). This work was supported by the Centre National de la Recherche Scientifique (CNRS), Sorbonne Université, and Institut Curie.

References

1. Homan KA, Kolesky DB, Skylar-Scott MA et al (2016) Bioprinting of 3D convoluted renal proximal tubules on perfusable chips. *Sci Rep* 6:1–13. <https://doi.org/10.1038/srep34845>
2. Weber EJ, Chapron A, Chapron BD et al (2016) Development of a microphysiological model of human kidney proximal tubule function. *Kidney Int* 90:627–637. <https://doi.org/10.1016/j.kint.2016.06.011>
3. Myram S, Venzac B, Lapin B et al (2021) A multitubular kidney-on-chip to Decipher pathophysiological mechanisms in renal cystic diseases. *Front Bioeng Biotechnol* 9:624553. <https://doi.org/10.3389/fbioe.2021.624553>
4. Kuddannaya S, Chuah YJ, Lee MHA et al (2013) Surface chemical modification of poly (dimethylsiloxane) for the enhanced adhesion and proliferation of mesenchymal stem cells. *ACS Appl Mater Interfaces* 5:9777–9784. https://doi.org/10.1021/AM402903E/SUPPL_FILE/AM402903E_SI_001.PDF
5. Mohammed D, Pardon G, Versaevl M et al (2020) Producing collagen micro-strips with aligned fibers for cell migration assays. *Cell Mol Bioeng* 13:87–98. <https://doi.org/10.1007/S12195-019-00600-4>
6. Shibasaki S, Yu Z, Nishio S et al (2008) Cyst formation and activation of the extracellular regulated kinase pathway after kidney specific inactivation of Pkd1. *Hum Mol Genet* 17: 1505–1516. ddn039 [pii]. <https://doi.org/10.1093/hmg/ddn039>
7. Joly D, Ishibe S, Nickel C et al (2006) The polycystin 1-C-terminal fragment stimulates ERK-dependent spreading of renal epithelial cells. *J Biol Chem* 281:26329–26339. M601373200 [pii]. <https://doi.org/10.1074/jbc.M601373200>
8. Viau A, Bienaimé F, Lukas K et al (2018) Cilia-localized LKB1 regulates chemokine signaling, macrophage recruitment, and tissue homeostasis in the kidney. *EMBO J* 37(15):e98615. <https://doi.org/10.15252/EMBJ.201798615>
9. Hofherr A, Busch T, Huber N et al (2017) Efficient genome editing of differentiated renal epithelial cells. *Pflugers Arch Eur J Physiol* 469:303–311. <https://doi.org/10.1007/S00424-016-1924-4>
10. Mukherjee P, Nebuloni F, Gao H et al (2019) Rapid prototyping of soft lithography masters for microfluidic devices using dry film photore-sist in a non-cleanroom setting. *Micromachines* 10(3):192. <https://doi.org/10.3390/MI10030192>
11. Pinto VC, Sousa PJ, Cardoso VF, Minas G (2014) Optimized SU-8 processing for low-cost microstructures fabrication without cleanroom facilities. *Micromachines* 5:738–755. <https://doi.org/10.3390/MI5030738>

Chip optimized for syringe perfusion

In **Figure M.1**, we show the design adapted for a perfusion by a single syringe. In this version, all the channels converge to a single input. The fabrication process remains the same. Before the laminin coating step, the anti-adhesion solution is perfused in the tubules for a few seconds followed by a 1h incubation at room temperature. After, laminin coating was done accordingly to the protocol described previously.

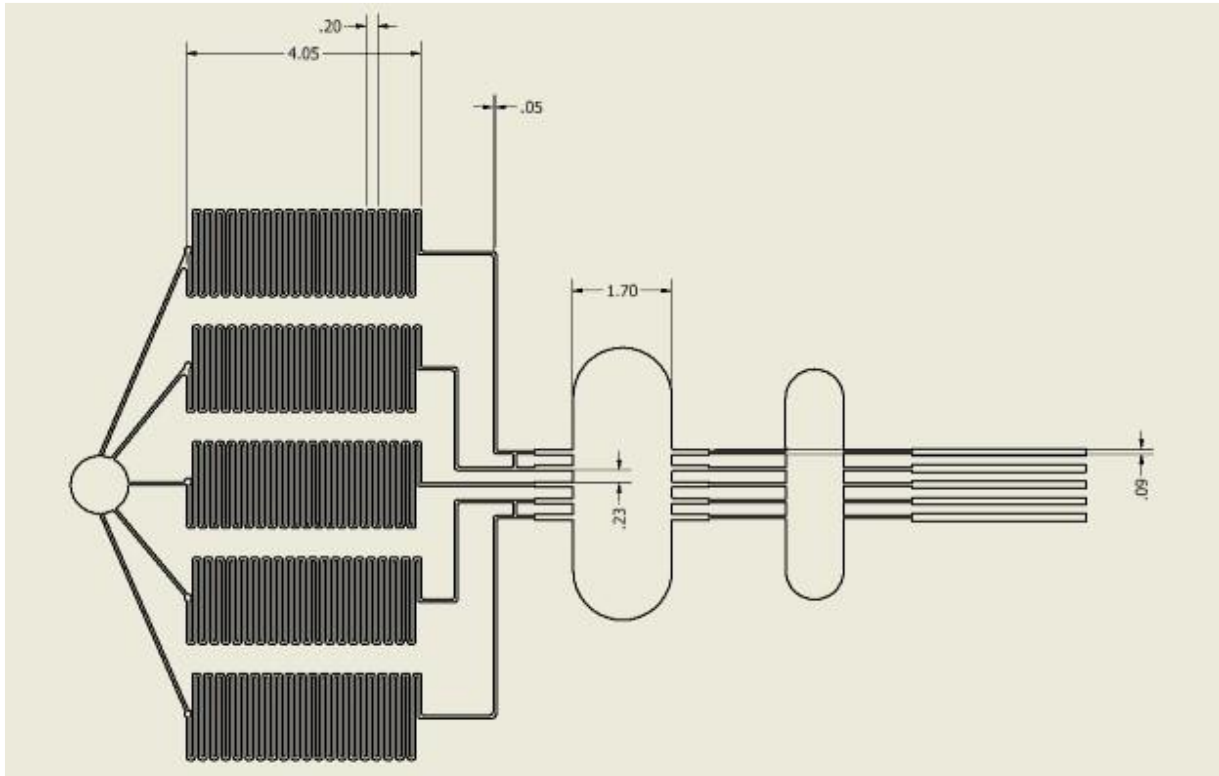


Figure M1: Design of the mask for the microfluidic channels of the chip with a single inlet (dimensions are in mm)

Chip made with PDMS-PEG

In Chapter 2, we described an experiment in which we tested a PDMS functionalized with polyethylene glycol (PEG), denominated as PDMS-PEG. This substrate was obtained by mixing PDMS 10:1 with curing agent up to 1% in mass/mass of a polyethylene glycol. The uncured PDMS-PEG was used as the uncured PDMS previously. Adding too much PEG into the mix results in an opaque material with significantly different mechanical properties. In addition, a 24h rinsing step in isopropanol of the cured PDMS-PEG is necessary to ensure the migration and concentration of PEG molecules towards the surface.

2D flat collagen surfaces

To obtain 500µm collagen flat substrates, rings of 14mm outer and 10mm inner diameters were cut into a 500µm thick PDMS 10:1. Ring were plasma bonded to glass coverslips and the assembly was treated with APTES and glutaraldehyde similarly to chips.

To obtain a 500µm thick collagen surface, collagen I at 6mg/mL was added inside to fill the inside of a ring and polymerized at 37°C in humid atmosphere for 1h and stored at 4°C in PBS until use.

To obtain a stiff collagen-coated surface, instead, the ring was filled with a solution of 0.1mg/mL of collagen I dissolved in a 0.02N acetic acid solution. Then the collagen solution was incubated at 37°C for 1 hour, then the ring was rinsed with PBS and stored at 4°C until use.

Cell culture

Medium for mIMCD-3 consisted in DMEM:F-12 1:1 Glutamax (Thermofisher) with 10% FBS (Dutscher), 1% penicillin-streptomycin 100x (Thermofisher) for culture in chips and without antibiotics for culture in flasks. Cultures in flask were discarded after passage 20.

For the PCT there were two media, a proliferation medium for cell culture in flasks and a differentiation medium for cell culture in chips. Proliferation medium consisted in DMEM:F-12 1:1 Glutamax (Thermofisher) with 3% FBS (Dutscher), 1% penicillin-streptomycin 100x (Thermofisher), 7.5 nM of sodium-selenite, 1.9 nM of T3, 5 mg/mL of insulin (from bovine pancreas), 5mg/mL of transferrin and 10 u/mL of interferon gamma. In flasks cells were maintained at 33°C with 5% CO₂ and discarded upon reaching passage 20. In chips, cells were maintained in the proliferation medium for the first 24 hours then the medium was changed for a differentiation medium. This medium consisted in DMEM:F-12 1:1 Glutamax (Thermofisher) with 1% FBS (Dutscher), 1% penicillin-streptomycin 100x (Thermofisher), 7.5 nM of sodium-selenite, 1.9 nM of T3, 5 mg/mL of insulin (from bovine pancreas), 5mg/mL of transferrin.

The cell culture in chips under static condition is described in the previous paper.

Cell culture in chips with perfusion

The chips were perfused a few hours, generally 3 hours, after seeding, letting the cells adhere to the collagen. Before perfusion, with a pressure controller (Fluigent Flow E/Z), the chip channels are flushed with an input of 50 mbar with a 37°C PBS solution to remove any unadhered cells and chips are place back in cell culture medium. Chips were perfused with sterile single-use syringes commonly found in a lab (e.g.: 3mL) TERUMO syringe without needle. Syringes were connected to needles previously sterilized with ethanol with a large diameter in comparison to the microfluidic channels (e.g.: TE needle 18 gauge x ½”). To hold, the syringe, a custom sterilized biocompatible 3D-printed stand is positioned on the chip. Cell-culture medium is then collected with the syringe until it is completely filled and the syringe piston was removed. After ensuring that medium was slowly dripping from the syringe, the syringe was connected either from the input to apply flow without intraluminal pressure or from the output to apply intraluminal pressure with flow. Medium is removed or added to the syringe to reach the liquid level necessary for a given hydrostatic pressure and the chip is submerged

in appropriate cell-culture medium completed with 0.5% of nystatin as anti-fungal with a level of 1mm over the chip top. This setup is placed in a sterile box with openings to limit contaminations while allowing exchanges of gas, then placed in an incubator at 37°C with 5% CO₂. Medium in the syringes was completed every day to the initial level and medium was completely renewed every other day.

Immunostaining

Immunostaining in chips is described in the previous paper. For the Ki-67 staining we used a monoclonal recombinant anti-Ki67 antibody obtained in rabbit (Abcam). For the secondary antibody we used an 641nm anti-Rabbit highly cross-absorbed antibody (Sigma).

Image analysis

Tubule diameter

Description of the method used is available in the paper above.

Nuclei segmentation for internuclear distance and Ki-67 ratio computation

The nuclei segmentation was done in two main step. The first step was a presegmentation step done with the software Ilastik. A representative set of confocal images of tubules with the different cell types at different time points were selected as a training pool. In this training pool nuclei were then labeled by hand at the same time as actin and background. The Ilastik classifier was trained labelling more and more pixels by hand, until the automatic detection was stable and gave satisfactory results with the training dataset. Then images of tubules were processed in batch and as output we obtained 3D stacks of images for each tubule with the probability of a pixel to belong either to the nuclei or actin label.

The second step consisted in the actual segmentation with Matlab with an homemade algorithm (code found in the Appendix). Briefly, 3D stacks of nuclei-actin probabilities and of stained ki-67 confocal channel were loaded. A threshold was applied to binarize each of the stacks selecting where pixels in nuclei probability stack that were more probable to be nuclei were set to 1 and otherwise were set to 0 to obtain the nuclei mask. The same rule was applied for the actin probability stack to obtain the actin mask.

The actin probability stack was used for two purposes: delimit the cell tissue in the tubule and help segment the nuclei. Small artefacts were removed from the actin stack based on a size criteria. The actin mask was then morphologically closed then subtracted from the nuclei stack. To delimit the tissue, holes in the actin stack were morphologically filled. The tissue stack was then used on the nuclei stack to filter out elements not belonging to the tissue. The tissue lumen was then filled to delimit the tubule.

Nuclei were then morphologically open to help separate clusters of nuclei and remove small artefacts. Remaining small artefacts in the nuclei were filtered out based on a size criteria. An H-minima transform was applied to the nuclei to prevent oversegmentation with a subsequent watershed operation. Post segmentation artefacts were filtered out with a size criteria. Nuclei belonging to the outer-layer of the tubule were determined by computing the

average distance between closest elements as outer layer thickness. Using the tubule mask, only nuclei with a center of mass localized within a distance from the outside of the tubule less than twice the outer layer thickness were considered belonging to the periphery of the tubule. The final segmented nuclei were used as a mask on the Ki-67 3D stacks.

To compute the internuclear distance, for each nucleus, the 6 closest nuclei were determined. To filter out outliers due to nuclei localized next to a border of the image or isolated nuclei, we considered that the distances between nuclei and their 6 closest neighbors should follow a gaussian distribution. Only elements falling between the 1st quartile and 3rd quartile of such distribution were kept. Then distances between nuclei and their 6 closest neighbors were average over each nuclei and finally averaged over all the nuclei.

To compute the Ki-67 ratio, nuclei were counted and independent elements from the Ki-67 3D stack were counted as Ki-67 positive nuclei. Then the ratio between Ki-67 positive nuclei and nuclei was computed.

Segmentation of GFP and mCherry/mScarlet fluorescent cells in the mosaic tubules

The first step was a presegmentation step done with the software Ilastik. A representative set of confocal images of tubules with the different cell types at different time points were selected as a training pool. In this training pool GFP fluorescent cells and mCherry/mScarlet fluorescent cells were labeled by hand at the same time as the background. The Ilastik classifier was trained labelling more and more pixels by hand, until the automatic detection was stable and gave satisfactory results with the training dataset. Then images of tubules were processed in batch and as output we obtained 3D stacks of images for each tubule with the probability of a pixel to belong either to the a GFP or a mCherry/mScarlet cell.

The second step consisted in the actual segmentation with Matlab with an homemade algorithm (code found in the Appendix). Briefly, 3D stacks of GFP-mCherry/mScarlet probabilities were loaded. A threshold was applied to binarize each of the stacks selecting where pixels in GFP probability stack that were more probable to be GFP were set to 1 and otherwise were set to 0 to obtain the GFP mask. The same rule was applied for the mScarlet/mCherry probability stack to obtain the mScarlet/mCherry mask. Small artefacts were removed from the GFP-mCherry/mScarlet stack based on a size criteria. The GFP-mCherry/mScarlet mask was then morphologically closed then topological holes were filled.

To obtain the mask for the whole tissue, GFP and mCherry/mScarlet were simply added. Then to determine basal and apical surfaces in the tissue, we used a polar coordinate system. For each transversal cut of the tubules, the center of mass of the tissue was chosen as the center of the polar coordinate system. The non-0 pixels from the whole tissue given a certain angle were considered as the basal surfaces and the farthest as the apical surfaces.

Measure of flow rate in channels

To assess the flow rate in the collagen tubules we used 5 μ m latex fluorescent beads (Polyscience, Inc) resuspended in PBS. We loaded the beads suspension into the syringes used for perfusion of the chips. We imaged the flow of beads with a fluorescence microscope. We binarized the videos of the bead flow and analyzed them with Image J and the extension Trackmate. Each bead leads in theory to one track. We collected the maximum velocity of each track as the velocity of that track. We then averaged all the track velocities in one tubule to obtain the average flow velocity in a tubule and then the flow rate in that tubule.

Glossary

ADPKD	Autosomal Dominant Polycystic Kidney Disease
ARPKD	Autosomal Recessive Polycystic Kidney Disease
BM	Basement Membrane
COC	Cyclic Olefin Copolymer
ECM	Extracellular Matrix
FSS	Flow Shear Stress
IMCD	Inner Medullary Collecting Duct
mIMCD-3	murine Inner Medullary Collecting Duct cells 3
PC1/2	Polycystin protein 1/2
PCT	Proximal Convoluted tubule
PDMS	Polydimethylsiloxane
PKD	Polycystic Kidney Disease
PKD1/2	Polycystic Kidney Disease gene 1/2

References

- Aragona, M. *et al.* (2013) 'A mechanical checkpoint controls multicellular growth through YAP/TAZ regulation by actin-processing factors', *Cell*, 154(5), pp. 1047–1059. Available at: <https://doi.org/10.1016/J.CELL.2013.07.042>.
- Avner, E.D. *et al.* (1986) 'Regression of genetically determined polycystic kidney disease in murine organ culture', *Experientia*, 42(1), pp. 77–80. Available at: <https://doi.org/10.1007/BF01975904>.
- Bastos, A.P. *et al.* (2009) 'Pkd1 Haploinsufficiency Increases Renal Damage and Induces Microcyst Formation following Ischemia/Reperfusion', *Journal of the American Society of Nephrology*, 20(11), pp. 2389–2402. Available at: <https://doi.org/10.1681/asn.2008040435>.
- Bhave, G., Colon, S. and Ferrell, N. (2017) 'The sulfilimine cross-link of collagen IV contributes to kidney tubular basement membrane stiffness', *American Journal of Physiology - Renal Physiology*, 313(3), pp. F596–F602. Available at: <https://doi.org/10.1152/ajprenal.00096.2017>.
- Bhunia, A.K. *et al.* (2002) 'PKD1 Induces p21^{waf1} and Regulation of the Cell Cycle via Direct Activation of the JAK-STAT Signaling Pathway in a Process Requiring PKD2', *Cell*, 109(2), pp. 157–168. Available at: [https://doi.org/10.1016/S0092-8674\(02\)00716-X](https://doi.org/10.1016/S0092-8674(02)00716-X).
- Bielmeier, C. *et al.* (2016) 'Interface Contractility between Differently Fated Cells Drives Cell Elimination and Cyst Formation', *Current Biology*, 26(5), pp. 563–574. Available at: <https://doi.org/10.1016/j.cub.2015.12.063>.
- Boca, M. *et al.* (2006) 'Polycystin-1 Induces Resistance to Apoptosis through the Phosphatidylinositol 3-Kinase/Akt Signaling Pathway', *Journal of the American Society of Nephrology: JASN*, 17(3), p. 637. Available at: <https://doi.org/10.1681/ASN.2005050534>.
- Boehlke, C. *et al.* (2010) 'Primary cilia regulate mTORC1 activity and cell size through Lkb1', *Nature Cell Biology*, 12(11), pp. 1115–1122. Available at: <https://doi.org/10.1038/ncb2117>.
- Boletta, Alessandra *et al.* (2000) 'Polycystin-1, the gene product of PKD1, induces resistance to apoptosis and spontaneous tubulogenesis in MDCK cells', *Molecular Cell*, 6(5), pp. 1267–1273. Available at: [https://doi.org/10.1016/S1097-2765\(00\)00123-4](https://doi.org/10.1016/S1097-2765(00)00123-4).
- Booij, T.H. *et al.* (2017) 'High-Throughput Phenotypic Screening of Kinase Inhibitors to Identify Drug Targets for Polycystic Kidney Disease', *Slas Discovery*, 22(8), p. 974. Available at: <https://doi.org/10.1177/2472555217716056>.
- Broaders, K.E., Cerchiari, A.E. and Gartner, Z.J. (2015) 'Coupling between apical tension and basal adhesion allow epithelia to collectively sense and respond to substrate topography over long distances', *Integrative Biology*, 7(12), pp. 1611–1621. Available at: <https://doi.org/10.1039/C5IB00240K>.
- Cai, J. *et al.* (2018) 'A RhoA-YAP-c-Myc signaling axis promotes the development of polycystic kidney disease.', *Genes & development*, 32(11–12), pp. 781–793. Available at: <https://doi.org/10.1101/gad.315127.118>.
- Cai, Y. *et al.* (2004) 'Calcium Dependence of Polycystin-2 Channel Activity Is Modulated by Phosphorylation at Ser812', *Journal of Biological Chemistry*, 279(19), pp. 19987–19995. Available at: <https://doi.org/10.1074/jbc.M312031200>.
- Cai, Z. *et al.* (2000a) 'Shear stress-mediated NO production in inner medullary collecting duct cells', *American Journal of Physiology - Renal Physiology*, 279(2 48-2), pp. 270–274. Available at: <https://doi.org/10.1152/AJPRENAL.2000.279.2.F270/ASSET/IMAGES/LARGE/H20800044004.JPEG>.
- Carracedo, M. *et al.* (2023) '3D vascularised proximal tubules-on-a-multiplexed chip model for enhanced cell phenotypes', *Lab on a Chip*, 23(14), p. 3226. Available at: <https://doi.org/10.1039/D2LC00723A>.

- Castelli, M. *et al.* (2015) 'Regulation of the microtubular cytoskeleton by Polycystin-1 favors focal adhesions turnover to modulate cell adhesion and migration', *BMC Cell Biology*, 16(1). Available at: <https://doi.org/10.1186/S12860-015-0059-3>.
- Chapron, A. *et al.* (2020) 'An Improved Vascularized, Dual-Channel Microphysiological System Facilitates Modeling of Proximal Tubular Solute Secretion', *Cite This: ACS Pharmacol. Transl. Sci.*, 2020, pp. 496–508. Available at: <https://doi.org/10.1021/acspsci.9b00078>.
- Chauvet, V. *et al.* (2004a) 'Mechanical stimuli induce cleavage and nuclear translocation of the polycystin-1 C terminus', *Journal of Clinical Investigation*, 114(10), pp. 1433–1443. Available at: <https://doi.org/10.1172/JCI21753>.
- Chen, D. *et al.* (2004) 'Differential expression of collagen- and laminin-binding integrins mediates ureteric bud and inner medullary collecting duct cell tubulogenesis', *American Journal of Physiology - Renal Physiology*, 287(4 56-4), pp. 602–611. Available at: <https://doi.org/10.1152/AJPRENAL.00015.2004>.
- Chevalier, R.L., Forbes, M.S. and Thornhill, B.A. (2009) 'Ureteral obstruction as a model of renal interstitial fibrosis and obstructive nephropathy', *Kidney International*, 75(11), pp. 1145–1152. Available at: <https://doi.org/10.1038/KI.2009.86>.
- Chiba, T. *et al.* (2016) 'MDCK cells expressing constitutively active Yes-associated protein (YAP) undergo apical extrusion depending on neighboring cell status', *Scientific reports*, 6. Available at: <https://doi.org/10.1038/SREP28383>.
- Choudhury, M.I. *et al.* (2022) 'Kidney epithelial cells are active mechano-biological fluid pumps', *Nature Communications*, 13(1). Available at: <https://doi.org/10.1038/S41467-022-29988-W>.
- Chuah, Y.J. *et al.* (2015) 'Simple surface engineering of polydimethylsiloxane with polydopamine for stabilized mesenchymal stem cell adhesion and multipotency', *Scientific Reports 2015 5:1*, 5(1), pp. 1–12. Available at: <https://doi.org/10.1038/srep18162>.
- Clavería, C. *et al.* (2013) 'Myc-driven endogenous cell competition in the early mammalian embryo', *Nature 2013 500:7460*, 500(7460), pp. 39–44. Available at: <https://doi.org/10.1038/nature12389>.
- Cowley, B.D. *et al.* (2006) 'Elevated c-myc protooncogene expression in autosomal recessive polycystic kidney disease.', *Proceedings of the National Academy of Sciences*, 84(23), pp. 8394–8398. Available at: <https://doi.org/10.1073/pnas.84.23.8394>.
- Cruz, N.M. *et al.* (2017) 'Organoid cystogenesis reveals a critical role of microenvironment in human polycystic kidney disease', *Nature Materials* [Preprint], (October). Available at: <https://doi.org/10.1038/nmat4994>.
- Cruz-Acuña, R. *et al.* (2019) 'Identification of matrix physicochemical properties required for renal epithelial cell tubulogenesis by using synthetic hydrogels', *Journal of Cell Science*, 132(20). Available at: <https://doi.org/10.1242/JCS.226639>.
- Dasgupta, I. and McCollum, D. (2019) 'Control of cellular responses to mechanical cues through YAP/TAZ regulation', *The Journal of biological chemistry*, 294(46), pp. 17693–17706. Available at: <https://doi.org/10.1074/JBC.REV119.007963>.
- Deforet, M. *et al.* (2014) 'Emergence of collective modes and tri-dimensional structures from epithelial confinement', *Nature Communications 2014 5:1*, 5(1), pp. 1–9. Available at: <https://doi.org/10.1038/ncomms4747>.
- Delling, M. *et al.* (2016) 'Primary cilia are not calcium-responsive mechanosensors', *Nature*, 531(7596), pp. 656–660. Available at: <https://doi.org/10.1038/NATURE17426>.
- Delmas, P. *et al.* (2004) 'Gating of the polycystin ion channel signaling complex in neurons and kidney cells.', *The FASEB journal: official publication of the Federation of American Societies for Experimental Biology*, 18(6), pp. 740–742. Available at: <https://doi.org/10.1096/fj.03-0319fje>.

- Dessalles, C.A. *et al.* (2021) 'Luminal flow actuation generates coupled shear and strain in a microvessel-on-chip', *Biofabrication*, 14(1). Available at: <https://doi.org/10.1088/1758-5090/AC2BAA>.
- Ding, H. *et al.* (2021) 'Extracellular vesicles and exosomes generated from cystic renal epithelial cells promote cyst growth in autosomal dominant polycystic kidney disease', *Nature Communications* 2021 12:1, 12(1), pp. 1–18. Available at: <https://doi.org/10.1038/s41467-021-24799-x>.
- Dong, K. *et al.* (2021) 'Renal plasticity revealed through reversal of polycystic kidney disease in mice', *Nature genetics*, 53(12), p. 1649. Available at: <https://doi.org/10.1038/S41588-021-00946-4>.
- Duan, Y. *et al.* (2008) 'Shear-induced reorganization of renal proximal tubule cell actin cytoskeleton and apical junctional complexes', *Proceedings of the National Academy of Sciences*, 105(32), pp. 11418–11423. Available at: <https://doi.org/10.1073/PNAS.0804954105>.
- Dwivedi, N. *et al.* (2023) 'Myofibroblast depletion reduces kidney cyst growth and fibrosis in autosomal dominant polycystic kidney disease', *Kidney international*, 103(1), pp. 144–155. Available at: <https://doi.org/10.1016/J.KINT.2022.08.036>.
- Eichenlaub, T., Cohen, S.M. and Herranz, H. (2016) 'Cell Competition Drives the Formation of Metastatic Tumors in a Drosophila Model of Epithelial Tumor Formation', *Current Biology*, 26(4), pp. 419–427. Available at: <https://doi.org/10.1016/J.CUB.2015.12.042>.
- Essig, M. *et al.* (2001) 'Mechanical strains induced by tubular flow affect the phenotype of proximal tubular cells', *American Journal of Physiology - Renal Physiology*, 281(4 50-4). Available at: <https://doi.org/10.1152/AJPRENAL.2001.281.4.F751/ASSET/IMAGES/LARGE/H21010469007.JPEG>.
- Evan, A.P. *et al.* (1986) 'Proximal tubule morphology after single nephron obstruction in the rat kidney', *Kidney International*, 30(6), pp. 818–827. Available at: <https://doi.org/10.1038/KI.1986.261>.
- Facioli, R. *et al.* (2021) 'Kidney organoids generated from erythroid progenitors cells of patients with autosomal dominant polycystic kidney disease', *PLoS ONE*, 16(8). Available at: <https://doi.org/10.1371/JOURNAL.PONE.0252156>.
- Fleszar, A.J. *et al.* (2019) 'Substrate curvature induces fallopian tube epithelial cell invasion via cell–cell tension in a model of ovarian cortical inclusion cysts', *Integrative Biology*, 11(8), pp. 342–352. Available at: <https://doi.org/10.1093/INTBIO/ZYZ028>.
- Flores, D. and Gusella, G.L. (2011) 'Fluid Shear Stress Induces Renal Epithelial Gene Expression through Polycystin-2-Dependent Trafficking of Extracellular Regulated Kinase', pp. 27–36. Available at: <https://doi.org/10.1159/000321640>.
- Freedman, B.S. *et al.* (2013) 'Reduced Ciliary Polycystin-2 in Induced Pluripotent Stem Cells from Polycystic Kidney Disease Patients with PKD1 Mutations', *Journal of the American Society of Nephrology: JASN*, 24(10), p. 1571. Available at: <https://doi.org/10.1681/ASN.2012111089>.
- Friedland, F. *et al.* (2022) 'ECM-transmitted shear stress induces apoptotic cell extrusion in early breast gland development', *Frontiers in Cell and Developmental Biology*, 10, p. 947430. Available at: <https://doi.org/10.3389/FCELL.2022.947430/BIBTEX>.
- Fu, X. *et al.* (2008) 'The subcellular localization of TRPP2 modulates its function', *Journal of the American Society of Nephrology: JASN*, 19(7), pp. 1342–1351. Available at: <https://doi.org/10.1681/ASN.2007070730>.
- Gagliardi, P.A. and Primo, L. (2019) 'Death for life: a path from apoptotic signaling to tissue-scale effects of apoptotic epithelial extrusion', *Cellular and molecular life sciences: CMLS*, 76(18), pp. 3571–3581. Available at: <https://doi.org/10.1007/S00018-019-03153-X>.
- Galarreta, C.I. *et al.* (2014) 'Tubular obstruction leads to progressive proximal tubular injury and atubular glomeruli in polycystic kidney disease', *American Journal of Pathology*, 184(7), pp. 1957–1966. Available at: <https://doi.org/10.1016/j.ajpath.2014.03.007>.

- Gąsiorowski, L. *et al.* (2021) 'Molecular evidence for a single origin of ultrafiltration-based excretory organs', *Current Biology*, 31(16), pp. 3629–3638.e2. Available at: <https://doi.org/10.1016/j.cub.2021.05.057>.
- Giebisch, G. and Windhager, E.E. (1964) 'Renal tubular transfer of sodium, chloride and potassium', *The American Journal of Medicine*, 36(5), pp. 643–669. Available at: [https://doi.org/10.1016/0002-9343\(64\)90178-0](https://doi.org/10.1016/0002-9343(64)90178-0).
- Gilmer, G.G. *et al.* (2018) 'Flow resistance along the rat renal tubule', *American Journal of Physiology - Renal Physiology*, 315(5), pp. F1398–F1405. Available at: https://doi.org/10.1152/AJPRENAL.00219.2018/SUPPL_FILE/SUPPLEMENTAL.
- Grantham, J.J. *et al.* (1987) 'Viscoelastic properties of tubule basement membranes in experimental renal cystic disease', *Kidney international*, 32(2), pp. 187–197. Available at: <https://doi.org/10.1038/KI.1987.191>.
- Grantham, J.J., Mulamalla, S. and Swenson-Fields, K.I. (2011) 'Why kidneys fail in autosomal dominant polycystic kidney disease', *Nature Reviews Nephrology*, 7(10), pp. 556–566. Available at: <https://doi.org/10.1038/nrneph.2011.109>.
- Ha, K. *et al.* (2020) 'The heteromeric PC-1/PC-2 polycystin complex is activated by the PC-1 N-terminus', *eLife*, 9, pp. 1–23. Available at: <https://doi.org/10.7554/ELIFE.60684>.
- Hannezo, E., Prost, J. and Joanny, J.F. (2012) 'Mechanical instabilities of biological tubes', *Physical Review Letters*, 109(1), p. 018101. Available at: <https://doi.org/10.1103/PhysRevLett.109.018101>.
- Happé, H. *et al.* (2009) 'Toxic tubular injury in kidneys from Pkd1-deletion mice accelerates cystogenesis accompanied by dysregulated planar cell polarity and canonical Wnt signaling pathways'. Available at: <https://doi.org/10.1093/hmg/ddp190>.
- Hiratsuka, K. *et al.* (2022) 'Organoid-on-a-chip model of human ARPKD reveals mechanosensing pathomechanisms for drug discovery', *Science Advances*, 8(38), p. 866. Available at: https://doi.org/10.1126/SCIADV.ABQ0866/SUPPL_FILE/SCIADV.ABQ0866_DATA_S1_TO_S7.ZIP.
- Homan, K.A. *et al.* (2016) 'Bioprinting of 3D Convulated Renal Proximal Tubules on Perfusable Chips', *Scientific Reports*, 6, pp. 1–13. Available at: <https://doi.org/10.1038/srep34845>.
- Hopp, K. *et al.* (2020) 'Detection and characterization of mosaicism in autosomal dominant polycystic kidney disease.', *Kidney international*, 97(2), p. 370. Available at: <https://doi.org/10.1016/J.KINT.2019.08.038>.
- Hu, P. and Luo, B.H. (2013) 'Integrin bi-directional signaling across the plasma membrane', *Journal of cellular physiology*, 228(2), pp. 306–312. Available at: <https://doi.org/10.1002/JCP.24154>.
- Huan, Y. and Van Adelsberg, J. (1999) 'Polycystin-1, the PKD1 gene product, is in a complex containing E-cadherin and the catenins', *Journal of Clinical Investigation*, 104(10), pp. 1459–1468. Available at: <https://doi.org/10.1172/JCI5111>.
- Huh, D. *et al.* (2010) 'Reconstituting Organ-Level Lung Functions on a Chip', *Science (New York, N.Y.)*, 328(5986), p. 1662. Available at: <https://doi.org/10.1126/SCIENCE.1188302>.
- Islamoglu, M.S., Gulcicek, S. and Seyahi, N. (2022) 'Kidney tissue elastography and interstitial fibrosis observed in kidney biopsy', *Renal Failure*, 44(1), p. 314. Available at: <https://doi.org/10.1080/0886022X.2022.2035763>.
- Issigonis, M. and Newmark, P.A. (2015) 'Planarian "kidneys" go with the flow', *eLife*, 4(JULY 2015). Available at: <https://doi.org/10.7554/eLife.09353>.
- Jang, K.J. *et al.* (2011) 'Fluid-shear-stress-induced translocation of aquaporin-2 and reorganization of actin cytoskeleton in renal tubular epithelial cells', *Integrative Biology*, 3(2), pp. 134–141. Available at: <https://doi.org/10.1039/C0IB00018C>.

- Jang, K.J. *et al.* (2013) 'Human kidney proximal tubule-on-a-chip for drug transport and nephrotoxicity assessment.', *Integrative biology : quantitative biosciences from nano to macro*, 5(9), pp. 1119–1129. Available at: <https://doi.org/10.1039/C3IB40049B>.
- Kaysen, J.H. *et al.* (1999) 'Select de novo gene and protein expression during renal epithelial cell culture in rotating wall vessels is shear stress dependent', *The Journal of membrane biology*, 168(1), pp. 77–89. Available at: <https://doi.org/10.1007/S002329900499>.
- Kim, J.W. *et al.* (2022) 'Kidney Decellularized Extracellular Matrix Enhanced the Vascularization and Maturation of Human Kidney Organoids', *Advanced science (Weinheim, Baden-Wurttemberg, Germany)*, 9(15). Available at: <https://doi.org/10.1002/ADVS.202103526>.
- Koulen, P. *et al.* (2002) 'Polycystin-2 is an intracellular calcium release channel', *Nature Cell Biology*, 4(3), pp. 191–197. Available at: <https://doi.org/10.1038/ncb754>.
- Kriz, W. (1981) 'Structural organization of the renal medulla: comparative and functional aspects', *The American journal of physiology*, 241(1). Available at: <https://doi.org/10.1152/AJPREGU.1981.241.1.R3>.
- Kuddannaya, S. *et al.* (2013) 'Surface chemical modification of poly(dimethylsiloxane) for the enhanced adhesion and proliferation of mesenchymal stem cells', *ACS Applied Materials and Interfaces*, 5(19), pp. 9777–9784. Available at: <https://doi.org/10.1021/AM402903E>.
- Kunnen, S.J. *et al.* (2018) 'Comprehensive transcriptome analysis of fluid shear stress altered gene expression in renal epithelial cells', *Journal of Cellular Physiology*, 233(4), pp. 3615–3628. Available at: <https://doi.org/10.1002/jcp.26222>.
- Kurbegovic, A. and Trudel, M. (2016) 'Acute kidney injury induces hallmarks of polycystic kidney disease', *American journal of physiology. Renal physiology*, 311(4), pp. F740–F751. Available at: <https://doi.org/10.1152/AJPRENAL.00167.2016>.
- Lantinga-van Leeuwen, I.S. *et al.* (2004) 'Lowering of Pkd1 expression is sufficient to cause polycystic kidney disease', *Human Molecular Genetics*, 13(24), pp. 3069–3077. Available at: <https://doi.org/10.1093/hmg/ddh336>.
- Lantinga-van leeuwen, I.S. *et al.* (2007) 'Kidney-specific inactivation of the Pkd1 gene induces rapid cyst formation in developing kidneys and a slow onset of disease in adult mice', *Human molecular genetics*, 16(24), pp. 3188–3196. Available at: <https://doi.org/10.1093/HMG/DDM299>.
- Lee, E.J. *et al.* (2020) 'TAZ/Wnt- β -catenin/c-MYC axis regulates cystogenesis in polycystic kidney disease', *Proceedings of the National Academy of Sciences of the United States of America*, 117(46), pp. 29001–29012. Available at: https://doi.org/10.1073/PNAS.2009334117/SUPPL_FILE/PNAS.2009334117.SAPP.PDF.
- Leonhard, Wouter N *et al.* (2015) 'Scattered Deletion of PKD1 in Kidneys Causes a Cystic Snowball Effect and Recapitulates Polycystic Kidney Disease.', *Journal of the American Society of Nephrology : JASN*, 26(6), pp. 1322–33. Available at: <https://doi.org/10.1681/ASN.2013080864>.
- Li, F.Y. *et al.* (2009) 'Hydraulic pressure inducing renal tubular epithelial-myofibroblast transdifferentiation in vitro', *Journal of Zhejiang University. Science. B*, 10(9), p. 659. Available at: <https://doi.org/10.1631/JZUS.B0920110>.
- Li, Q. *et al.* (2021) 'Heterogeneity of cell composition and origin identified by single-cell transcriptomics in renal cysts of patients with autosomal dominant polycystic kidney disease', *Theranostics*, 11(20), p. 10064. Available at: <https://doi.org/10.7150/THNO.57220>.
- Li, X. *et al.* (2008) 'A tumor necrosis factor- α -mediated pathway promoting autosomal dominant polycystic kidney disease', *Nature Medicine* 2008 14:8, 14(8), pp. 863–868. Available at: <https://doi.org/10.1038/nm1783>.
- Lin, N.Y.C. *et al.* (2019) 'Renal reabsorption in 3D vascularized proximal tubule models', *Proceedings of the National Academy of Sciences of the United States of America*, 116(12), pp. 5399–5404. Available at: https://doi.org/10.1073/PNAS.1815208116/SUPPL_FILE/PNAS.1815208116.SM02.MOV.

- Little, M.H. and Kairath, P. (2017) 'Does Renal Repair Recapitulate Kidney Development?', *Journal of the American Society of Nephrology : JASN*, 28(1), p. 34. Available at: <https://doi.org/10.1681/ASN.2016070748>.
- Liu, W. *et al.* (2003) 'Effect of flow and stretch on the [Ca²⁺]_i response of principal and intercalated cells in cortical collecting duct', *American Journal of Physiology - Renal Physiology*, 285(5 54-5), pp. 998–1012. Available at: <https://doi.org/10.1152/AJPRENAL.00067.2003/ASSET/IMAGES/LARGE/H21131332012.JPEG>.
- Liu, Zhijun *et al.* (2019) 'Differential YAP expression in glioma cells induces cell competition and promotes tumorigenesis', *Journal of Cell Science*, 132(5). Available at: <https://doi.org/10.1242/JCS.225714>.
- Loghman-Adham, M. *et al.* (2003) 'Immortalized epithelial cells from human autosomal dominant polycystic kidney cysts', *American Journal of Physiology-Renal Physiology*, 285(3), pp. F397–F412. Available at: <https://doi.org/10.1152/ajprenal.00310.2002>.
- Low, S.H., Vasanth, S., Larson, Claire H, *et al.* (2006) 'Polycystin-1, STAT6, and P100 function in a pathway that transduces ciliary mechanosensation and is activated in polycystic kidney disease.', *Developmental cell*, 10(1), pp. 57–69. Available at: <https://doi.org/10.1016/j.devcel.2005.12.005>.
- Lu, W. *et al.* (1999) 'Late onset of renal and hepatic cysts in Pkd1-targeted heterozygotes', *Nature genetics*, 21(2), pp. 160–161. Available at: <https://doi.org/10.1038/5944>.
- Luciano, M. *et al.* (2021) 'Cell monolayers sense curvature by exploiting active mechanics and nuclear mechanoadaptation', *Nature Physics* 2021 17:12, 17(12), pp. 1382–1390. Available at: <https://doi.org/10.1038/s41567-021-01374-1>.
- Ma, M. *et al.* (2013) 'Loss of cilia suppresses cyst growth in genetic models of autosomal dominant polycystic kidney disease', *Nature Genetics*, 45(9), pp. 1004–1012. Available at: <https://doi.org/10.1038/ng.2715>.
- Ma, M. (2020) 'Cilia and polycystic kidney disease', *Seminars in Cell and Developmental Biology* [Preprint]. Elsevier Ltd. Available at: <https://doi.org/10.1016/j.semcd.2020.05.003>.
- Mak, K.M. and Mei, R. (2017) 'Basement Membrane Type IV Collagen and Laminin: An Overview of Their Biology and Value as Fibrosis Biomarkers of Liver Disease', *The Anatomical Record*, 300(8), pp. 1371–1390. Available at: <https://doi.org/10.1002/AR.23567>.
- Malas, T.B. *et al.* (2017) 'Meta-analysis of polycystic kidney disease expression profiles defines strong involvement of injury repair processes', *American journal of physiology. Renal physiology*, 312(4), pp. F806–F817. Available at: <https://doi.org/10.1152/AJPRENAL.00653.2016>.
- Mangos, S. *et al.* (2010) 'The ADPKD genes pkd1a/b and pkd2 regulate extracellular matrix formation', *DMM Disease Models and Mechanisms*, 3(5–6), pp. 354–365. Available at: <https://doi.org/10.1242/DMM.003194/-/DC1>.
- Marsh, D.J. and Martin, C.M. (1975) 'Effects of diuretic states on collecting duct fluid flow resistance in the hamster kidney', *The American journal of physiology*, 229(1), pp. 13–17. Available at: <https://doi.org/10.1152/AJPLEGACY.1975.229.1.13>.
- Martin, J.S., Brown, L.S. and Haberstroh, K.M. (2005) 'Microfilaments are involved in renal cell responses to sustained hydrostatic pressure', *Journal of Urology*, 173(4), pp. 1410–1417. Available at: <https://doi.org/10.1097/01.JU.0000149031.93643.A5>.
- McAteer, J.A., Evan, A.P. and Gardner, K.D. (1987) 'Morphogenetic clonal growth of kidney epithelial cell line MDCK', *The Anatomical Record*, 217(3), pp. 229–239. Available at: <https://doi.org/10.1002/AR.1092170303>.
- Di Meglio, I. *et al.* (2022) 'Pressure and curvature control of the cell cycle in epithelia growing under spherical confinement', *Cell Reports*, 40(8), p. 111227. Available at: <https://doi.org/10.1016/J.CELREP.2022.111227>.

- Moreno, E. and Basler, K. (2004) 'dMyc transforms cells into super-competitors.', *Cell*, 117(1), pp. 117–129. Available at: [https://doi.org/10.1016/s0092-8674\(04\)00262-4](https://doi.org/10.1016/s0092-8674(04)00262-4).
- Moreno-Celis, U., García-Gasca, T. and Mejía, C. (2022) 'Apoptosis-Induced Compensatory Proliferation in Cancer', *Metastasis*, pp. 149–162. Available at: <https://doi.org/10.36255/EXON-PUBLICATIONS.METASTASIS.APOPTOSIS-PROLIFERATION>.
- Myram, S. *et al.* (2021) 'A Multitubular Kidney-on-Chip to Decipher Pathophysiological Mechanisms in Renal Cystic Diseases', *Frontiers in Bioengineering and Biotechnology*, 9. Available at: <https://doi.org/10.3389/FBIOE.2021.624553>.
- Nag, S. and Resnick, A. (2017) 'Biophysics and biofluid dynamics of primary cilia: Evidence for and against the flow-sensing function', *American Journal of Physiology - Renal Physiology*, 313(3), pp. F706–F720. Available at: <https://doi.org/10.1152/AJPRENAL.00172.2017/ASSET/IMAGES/LARGE/ZH20081782980002.JPEG>.
- Nagao, R.J. *et al.* (2016) 'Decellularized Human Kidney Cortex Hydrogels Enhance Kidney Microvascular Endothelial Cell Maturation and Quiescence', *Tissue Engineering - Part A*, 22(19–20), pp. 1140–1150. Available at: <https://doi.org/10.1089/ten.tea.2016.0213>.
- Nagata, R. and Igaki, T. (2018) 'Cell competition: Emerging mechanisms to eliminate neighbors', *Development, Growth & Differentiation*, 60(9), pp. 522–530. Available at: <https://doi.org/10.1111/DGD.12575>.
- Natoli, T.A. *et al.* (2008) 'Pkd1 and Nek8 mutations affect cell-cell adhesion and cilia in cysts formed in kidney organ cultures', *American journal of physiology. Renal physiology*, 294(1). Available at: <https://doi.org/10.1152/AJPRENAL.00362.2007>.
- Nauli, S.M. *et al.* (2003) 'Polycystins 1 and 2 mediate mechanosensation in the primary cilium of kidney cells', *Nature Genetics*, 33(2), pp. 129–137. Available at: <https://doi.org/10.1038/ng1076>.
- Nauli, S.M. *et al.* (2008) 'Endothelial cilia are fluid shear sensors that regulate calcium signaling and nitric oxide production through polycystin-1.', *Circulation*, 117(9), pp. 1161–71. Available at: <https://doi.org/10.1161/CIRCULATIONAHA.107.710111>.
- Nickel, C. *et al.* (2002) 'The polycystin-1 C-terminal fragment triggers branching morphogenesis and migration of tubular kidney epithelial cells', *The Journal of clinical investigation*, 109(4), pp. 481–489. Available at: <https://doi.org/10.1172/JCI12867>.
- Nie, X. and Arend, L.J. (2017) 'Deletion of Pkd1 in renal stromal cells causes defects in the renal stromal compartment and progressive cystogenesis in the kidney', *Laboratory Investigation*, 97(12), pp. 1427–1438. Available at: <https://doi.org/10.1038/LABINVEST.2017.97>.
- Nigro, E.A. *et al.* (2019) 'Polycystin-1 Regulates Actomyosin Contraction and the Cellular Response to Extracellular Stiffness', *Scientific Reports*, 9(1), pp. 1–15. Available at: <https://doi.org/10.1038/s41598-019-53061-0>.
- Nishio, S. *et al.* (2005) 'Pkd1 regulates immortalized proliferation of renal tubular epithelial cells through p53 induction and JNK activation', *Journal of Clinical Investigation*, 115(4), pp. 910–918. Available at: <https://doi.org/10.1172/JCI22850>.
- Ogawa, H. *et al.* (2022) 'Somatic Mosaicism in Biology and Disease', <https://doi.org/10.1146/annurev-physiol-061121-040048>, 84, pp. 113–133. Available at: <https://doi.org/10.1146/ANNUREV-PHYSIOL-061121-040048>.
- Ong, A.C.M. *et al.* (1999) 'Polycystin-1 expression in PKD1, early-onset PKD1, and TSC2/PKD1 cystic tissue', *Kidney international*, 56(4), pp. 1324–1333. Available at: <https://doi.org/10.1046/J.1523-1755.1999.00659.X>.
- Parnell, S.C. *et al.* (2018) 'A mutation affecting polycystin-1 mediated heterotrimeric G-protein signaling causes PKD.', *Human Molecular Genetics*, 27(19), pp. 3313–3324. Available at: <https://doi.org/10.1093/HMG/DDY223>.

- Parrot, C. *et al.* (2019) 'c-Myc is a regulator of the PKD1 gene and PC1-induced pathogenesis', *Human Molecular Genetics*, 28(5), pp. 751–763. Available at: <https://doi.org/10.1093/hmg/ddy379>.
- Patel, A.J., Lazdunski, M. and Honoré, E. (2001) 'Lipid and mechano-gated 2P domain K(+) channels', *Current opinion in cell biology*, 13(4), pp. 422–428. Available at: [https://doi.org/10.1016/S0955-0674\(00\)00231-3](https://doi.org/10.1016/S0955-0674(00)00231-3).
- Peyronnet, R., Sharif-Naeini, R., Folgering, Joost H.A., *et al.* (2012) 'Mechanoprotection by polycystins against apoptosis is mediated through the opening of stretch-activated K2P channels', *Cell reports*, 1(3), p. 241. Available at: <https://doi.org/10.1016/J.CELREP.2012.01.006>.
- Peyronnet, R., Sharif-Naeini, R., Folgering, Joost H A, *et al.* (2012) 'Mechanoprotection by polycystins against apoptosis is mediated through the opening of stretch-activated K(2P) channels.', *Cell reports*, 1(3), pp. 241–50. Available at: <https://doi.org/10.1016/j.celrep.2012.01.006>.
- Piontek, K., Menezes, Luis F., *et al.* (2007) 'A critical developmental switch defines the kinetics of kidney cyst formation after loss of Pkd1', *Nature medicine*, 13(12), p. 1490. Available at: <https://doi.org/10.1038/NM1675>.
- Piontek, K., Menezes, Luis F, *et al.* (2007) 'A critical developmental switch defines the kinetics of kidney cyst formation after loss of Pkd1', *Nature Medicine*, 13(12), pp. 1490–1495. Available at: <https://doi.org/10.1038/nm1675>.
- Pöschl, E. *et al.* (2004) 'Collagen IV is essential for basement membrane stability but dispensable for initiation of its assembly during early development', *Development*, 131(7), pp. 1619–1628. Available at: <https://doi.org/10.1242/DEV.01037>.
- Price, C.J. *et al.* (2021) 'Genetically variant human pluripotent stem cells selectively eliminate wild-type counterparts through YAP-mediated cell competition', *Developmental Cell*, 56(17), pp. 2455-2470.e10. Available at: <https://doi.org/10.1016/J.DEVCEL.2021.07.019>.
- Qian, F. *et al.* (1996) 'The molecular basis of focal cyst formation in human autosomal dominant polycystic kidney disease type I', *Cell* [Preprint]. Available at: [https://doi.org/10.1016/S0092-8674\(00\)81793-6](https://doi.org/10.1016/S0092-8674(00)81793-6).
- Qian, F. *et al.* (2005) 'The Nanomechanics of Polycystin-1 Extracellular Region', *The Journal of biological chemistry*, 280(49), p. 40723. Available at: <https://doi.org/10.1074/JBC.M509650200>.
- Rayner, S.G. *et al.* (2018) 'Reconstructing the Human Renal Vascular–Tubular Unit In Vitro', *Advanced Healthcare Materials*, 7(23). Available at: <https://doi.org/10.1002/ADHM.201801120>.
- Roitbak, T. *et al.* (2004) 'A Polycystin-1 Multiprotein Complex Is Disrupted in Polycystic Kidney Disease Cells', *Molecular Biology of the Cell*, 15(3), p. 1334. Available at: <https://doi.org/10.1091/MBC.E03-05-0296>.
- Sakai, T. *et al.* (1986) 'Fluid waves in renal tubules.', *Biophysical Journal*, 50(5), p. 805. Available at: [https://doi.org/10.1016/S0006-3495\(86\)83521-4](https://doi.org/10.1016/S0006-3495(86)83521-4).
- Sancho, M. *et al.* (2013) 'Competitive Interactions Eliminate Unfit Embryonic Stem Cells at the Onset of Differentiation', *Developmental Cell*, 26(1), pp. 19–30. Available at: <https://doi.org/10.1016/J.DEVCEL.2013.06.012>.
- Schwayer, C. *et al.* (2016) 'Actin Rings of Power', *Developmental Cell*, 37(6), pp. 493–506. Available at: <https://doi.org/10.1016/J.DEVCEL.2016.05.024>.
- Sharif-Naeini, R., Folgering, Joost H.A., *et al.* (2009) 'Polycystin-1 and -2 Dosage Regulates Pressure Sensing', *Cell*, 139(3), pp. 587–596. Available at: <https://doi.org/10.1016/j.cell.2009.08.045>.
- Shillingford, J.M. *et al.* (2006) 'The mTOR pathway is regulated by polycystin-1, and its inhibition reverses renal cystogenesis in polycystic kidney disease', *Proceedings of the National Academy of Sciences*, 103(14), pp. 5466–5471. Available at: <https://doi.org/10.1073/pnas.0509694103>.

- Staneva, R. *et al.* (2018) 'A new biomimetic assay reveals the temporal role of matrix stiffening in cancer cell invasion', *Molecular Biology of the Cell*, 29(25), pp. 2979–2988. Available at: <https://doi.org/10.1091/MBC.E18-01-0068/ASSET/IMAGES/LARGE/MBC-29-2979-G004.JPEG>.
- Stathopoulos, N.A. and Hellums, J.D. (1985) 'Shear stress effects on human embryonic kidney cells in Vitro', *Biotechnology and bioengineering*, 27(7), pp. 1021–1026. Available at: <https://doi.org/10.1002/BIT.260270713>.
- Streets, A.J. *et al.* (2009) 'Homophilic and heterophilic polycystin 1 interactions regulate E-cadherin recruitment and junction assembly in MDCK cells', *Journal of Cell Science*, 122(10), p. 1702. Available at: <https://doi.org/10.1242/jcs.053603>.
- Su, Q. *et al.* (2018) 'Structure of the human PKD1/PKD2 complex', *Science*, 9819, p. eaat9819. Available at: <https://doi.org/10.1126/science.aat9819>.
- Subramanian, B. *et al.* (2012) 'The Regulation of Cystogenesis in a Tissue Engineered Kidney Disease System by Abnormal Matrix Interactions', *Biomaterials*, 33(33), p. 8383. Available at: <https://doi.org/10.1016/J.BIOMATERIALS.2012.08.020>.
- Subramanian, B. *et al.* (2018) 'Guided tissue organization and disease modeling in a kidney tubule array', *Biomaterials*, 183, pp. 295–305. Available at: <https://doi.org/10.1016/j.biomaterials.2018.07.059>.
- Suijkerbuijk, S.J.E. *et al.* (2016) 'Cell Competition Drives the Growth of Intestinal Adenomas in Drosophila', *Current Biology*, 26(4), pp. 428–438. Available at: <https://doi.org/10.1016/J.CUB.2015.12.043>.
- Sypabekova, M. *et al.* (2023) 'Review: 3-Aminopropyltriethoxysilane (APTES) Deposition Methods on Oxide Surfaces in Solution and Vapor Phases for Biosensing Applications', *Biosensors*, 13(1). Available at: <https://doi.org/10.3390/BIOS13010036>.
- Takakura, A. *et al.* (2008) 'Pkd1 inactivation induced in adulthood produces focal cystic disease.', *Journal of the American Society of Nephrology : JASN*, 19(12), pp. 2351–63. Available at: <https://doi.org/10.1681/ASN.2007101139>.
- Takakura, A. *et al.* (2009) 'Renal injury is a third hit promoting rapid development of adult polycystic kidney disease', *Human Molecular Genetics*, 18(14), pp. 2523–2531. Available at: <https://doi.org/10.1093/hmg/ddp147>.
- Tan, A.Y. *et al.* (2018) 'Somatic Mutations in Renal Cyst Epithelium in Autosomal Dominant Polycystic Kidney Disease', *Journal of the American Society of Nephrology : JASN*, 29(8), pp. 2139–2156. Available at: <https://doi.org/10.1681/ASN.2017080878>.
- Tanner, G.A. *et al.* (1996) 'Role of obstruction in autosomal dominant polycystic kidney disease in rats', *Kidney International*, 50(3), pp. 873–886. Available at: <https://doi.org/10.1038/KI.1996.387>.
- Thi, M.M. *et al.* (2004) 'The role of the glycocalyx in reorganization of the actin cytoskeleton under fluid shear stress: a "bumper-car" model', *Proceedings of the National Academy of Sciences of the United States of America*, 101(47), pp. 16483–16488. Available at: <https://doi.org/10.1073/PNAS.0407474101>.
- Thivierge, C. *et al.* (2006) 'Overexpression of PKD1 causes polycystic kidney disease.', *Molecular and cellular biology*, 26(4), pp. 1538–48. Available at: <https://doi.org/10.1128/MCB.26.4.1538-1548.2006>.
- Tokuda, S. *et al.* (2009) 'Hydrostatic pressure regulates tight junctions, actin cytoskeleton and transcellular ion transport', *Biochemical and Biophysical Research Communications*, 390(4), pp. 1315–1321. Available at: <https://doi.org/10.1016/J.BBRC.2009.10.144>.
- Tourovskaja, A. *et al.* (2014) 'Brief Communication: Tissue-engineered Microenvironment Systems for Modeling Human Vasculature', *Experimental biology and medicine (Maywood, N.J.)*, 239(9), p. 1264. Available at: <https://doi.org/10.1177/1535370214539228>.

- Trudel, M., D'Agati, V. and Costantini, F. (1991) 'C-myc as an inducer of polycystic kidney disease in transgenic mice', *Kidney international*, 39(4), pp. 665–671. Available at: <https://doi.org/10.1038/KI.1991.80>.
- Vedula, E.M. *et al.* (2017) 'A microfluidic renal proximal tubule with active reabsorptive function', *PLoS ONE*, 12(10). Available at: <https://doi.org/10.1371/journal.pone.0184330>.
- Venzac, B. *et al.* (2018) 'Engineering small tubes with changes in diameter for the study of kidney cell organization', *Biomicrofluidics*, 12(2). Available at: <https://doi.org/10.1063/1.5025027>.
- Verhulsel, M. *et al.* (2021) 'Developing an advanced gut on chip model enabling the study of epithelial cell/fibroblast interactions', *Lab on a Chip*, 21(2), pp. 365–377. Available at: <https://doi.org/10.1039/D0LC00672F>.
- Viau, A. *et al.* (2020) 'Divergent function of polycystin 1 and polycystin 2 in cell size regulation', *Biochemical and Biophysical Research Communications*, 521(2), pp. 290–295. Available at: <https://doi.org/10.1016/j.bbrc.2019.10.074>.
- Wallace, D.P., Grantham, J.J. and Sullivan, L.P. (1996) 'Chloride and fluid secretion by cultured human polycystic kidney cells', *Kidney International*, 50(4), pp. 1327–1336. Available at: <https://doi.org/https://doi.org/10.1038/ki.1996.445>.
- Weber, E.J. *et al.* (2016) 'Development of a microphysiological model of human kidney proximal tubule function', *Kidney International*, 90(3), pp. 627–637. Available at: <https://doi.org/10.1016/j.kint.2016.06.011>.
- Weimbs, T. (2007) 'Polycystic kidney disease and renal injury repair: Common pathways, fluid flow, and the function of polycystin-1', *American Journal of Physiology - Renal Physiology*, 293(5), pp. 1423–1432. Available at: <https://doi.org/10.1152/AJPRENAL.00275.2007/ASSET/IMAGES/LARGE/ZH20110749340002.JPEG>.
- Westermann, L. *et al.* (2022) 'Wildtype heterogeneity contributes to clonal variability in genome edited cells', *Scientific Reports*, 12(1), p. 18211. Available at: <https://doi.org/10.1038/S41598-022-22885-8>.
- Wilkes, M. *et al.* (2017) 'Molecular insights into lipid-assisted Ca²⁺ regulation of the TRP channel Polycystin-2', *Nature Structural & Molecular Biology* 2017 24:2, 24(2), pp. 123–130. Available at: <https://doi.org/10.1038/nsmb.3357>.
- Wu, G. *et al.* (1998) 'Somatic inactivation of Pkd2 results in polycystic kidney disease', *Cell*, 93(2), pp. 177–188. Available at: [https://doi.org/10.1016/S0092-8674\(00\)81570-6](https://doi.org/10.1016/S0092-8674(00)81570-6).
- Wu, G. *et al.* (2000) 'Cardiac defects and renal failure in mice with targeted mutations in Pkd2'. Available at: <http://genetics.nature.com> (Accessed: 26 July 2023).
- Xi, W. *et al.* (2017) 'Emergent patterns of collective cell migration under tubular confinement', *Nature Communications*, 8(1), p. 1517. Available at: <https://doi.org/10.1038/s41467-017-01390-x>.
- Xu, G.M. *et al.* (2001a) 'Polycystin-1 Interacts with Intermediate Filaments', *Journal of Biological Chemistry*, 276(49), pp. 46544–46552. Available at: <https://doi.org/10.1074/JBC.M107828200>.
- Yamaguchi, T. *et al.* (2000) 'cAMP stimulates the in vitro proliferation of renal cyst epithelial cells by activating the extracellular signal-regulated kinase pathway', in *Kidney International*. Available at: <https://doi.org/10.1046/j.1523-1755.2000.00991.x>.
- Yamaguchi, T. *et al.* (2003) 'Cyclic AMP activates B-Raf and ERK in cyst epithelial cells from autosomal-dominant polycystic kidneys', *Kidney International*, 63(6), pp. 1983–1994. Available at: <https://doi.org/10.1046/j.1523-1755.2003.00023.x>.
- Yamaguchi, T. *et al.* (2004) 'Calcium restriction allows cAMP activation of the B-Raf/ERK pathway, switching cells to a cAMP-dependent growth-stimulated phenotype', *Journal of Biological Chemistry*, 279(39), pp. 40419–40430. Available at: <https://doi.org/10.1074/jbc.M405079200>.

- Yamaguchi, T. *et al.* (2006) 'Calcium restores a normal proliferation phenotype in human polycystic kidney disease epithelial cells.', *Journal of the American Society of Nephrology: JASN*, 17(1), pp. 178–87. Available at: <https://doi.org/10.1681/ASN.2005060645>.
- Yang, X. *et al.* (2011) 'Elevated pressure downregulates ZO-1 expression and disrupts cytoskeleton and focal adhesion in human trabecular meshwork cells', *Molecular Vision*, 17, p. 2978. Available at: [/pmc/articles/PMC3224831/](https://pubmed.ncbi.nlm.nih.gov/224831/) (Accessed: 21 September 2023).
- Yao, G. *et al.* (2013) 'The cytoplasmic protein Pacsin 2 in kidney development and injury repair', *Kidney international*, 83(3), pp. 426–437. Available at: <https://doi.org/10.1038/KI.2012.379>.
- Yao, G. *et al.* (2014) 'Polycystin-1 regulates actin cytoskeleton organization and directional cell migration through a novel PC1-Pacsin 2-N-Wasp complex', *Human molecular genetics*, 23(10), pp. 2769–2779. Available at: <https://doi.org/10.1093/HMG/DDT672>.
- Ye, M. *et al.* (1992) 'Cyst fluid from human autosomal dominant polycystic kidneys promotes cyst formation and expansion by renal epithelial cells in vitro', *Journal of the American Society of Nephrology*, 3(4), pp. 984–994.
- Yu, S.M. *et al.* (2018) 'Substrate curvature affects the shape, orientation, and polarization of renal epithelial cells', *Acta Biomaterialia*, 77, pp. 311–321. Available at: <https://doi.org/10.1016/j.actbio.2018.07.019>.
- Zhang, B., Tran, U. and Wessely, O. (2018) 'Polycystin 1 loss of function is directly linked to an imbalance in G-protein signaling in the kidney.', *Development (Cambridge, England)*, 145(6), pp. dev158931–dev158931. Available at: <https://doi.org/10.1242/DEV.158931>.
- Zhang, K. *et al.* (no date) 'PKD1 inhibits cancer cells migration and invasion via Wnt signaling pathway in vitro'. Available at: <https://doi.org/10.1002/cbf.1417>.
- Zhang, Y., Reif, G. and Wallace, D.P. (2020a) 'Extracellular matrix, integrins, and focal adhesion signaling in polycystic kidney disease', *Cellular signalling*, 72, p. 109646. Available at: <https://doi.org/10.1016/J.CELLSIG.2020.109646>.
- Zhao, B. *et al.* (2007) 'Inactivation of YAP oncoprotein by the Hippo pathway is involved in cell contact inhibition and tissue growth control', *Genes & development*, 21(21), pp. 2747–2761. Available at: <https://doi.org/10.1101/GAD.1602907>.
- Zhou, J., Li, Y.S. and Chien, S. (2014) 'Shear stress-initiated signaling and its regulation of endothelial function', *Arteriosclerosis, thrombosis, and vascular biology*, 34(10), p. 2191. Available at: <https://doi.org/10.1161/ATVBAHA.114.303422>.

Appendix

Matlab script for nuclei and Ki-67 segmentation

```
function [nuclei,nuclei_periphery,ki67,tissue,periphery,success,success_ki67]=Nuclei3D_ki67_density_periphery_v2(path)
%input is the path to the folder containing the images stacks for the actin and Nuclei probability and the 3D confocal stack for the Ki-67 staining
%output are 3D matrix of segmented nuclei, Ki-67 positive nuclei
    success=1;
    success_ki67=1;
    nuclei_periphery=[];
    tissue=[];
    periphery=[];

    %% READ 3D IMAGE
    %import actin

    [~,name] = fileparts(path);
    dir_actin=dir([char(path), '\', '*Probabilities____0.tif*']);

    if (~dir_actin.isdir) && (length(dir_actin)) == 1

        path_actin=append(dir_actin.folder, "\", dir_actin.name);
        info = imfinfo(path_actin);
        numberOfPages = length(info);
        tmp_IM = imread(path_actin);

        tmpIM = tmp_IM(:,:,1);

        [l m] = size(tmp_IM);

        IM_actin = zeros(l,m,numberOfPages);

        size(IM_actin)
        for k = 1 : numberOfPages
            % Read the kth image in this multipage tiff file.

            thisPage = imread(path_actin, k);
            IM_actin(:,:,k) = thisPage;
        end

        mini = min(IM_actin(:));
        maxi = max(IM_actin(:));
        if isa(tmpIM, 'single')
            IM_actin = uint8(2^16*(IM_actin-mini/(maxi-mini)));
        elseif isa(tmpIM, 'uint8')
            IM_actin = uint8(IM_actin);
        elseif isa(tmpIM, 'uint8')
            IM_actin = uint8(IM_actin);
        end
        else

            success=0;

    %import ki67

    if ~isempty(directory)

        nb_stacks=length(directory);
        tmpIM = imread([directory(1).folder '\', directory(1).name]);
        tmpIM = tmpIM(:,:,1);

        [l m] = size(tmpIM);

        IM_ki67 = zeros(l,m,nb_stacks);

        size(IM_ki67)

        success=0;
    end
    %import nuclei

    dir_nuclei=dir([char(path), '\', '*Probabilities____1.tif*']);

    if (~dir_nuclei.isdir) && (length(dir_nuclei)) == 1

        path_nuclei=append(dir_nuclei.folder, "\", dir_nuclei.name);
        info = imfinfo(path_nuclei);
        numberOfPages = length(info);
        tmp_IM = imread(path_nuclei);

        tmpIM = tmp_IM(:,:,1);

        [l m] = size(tmp_IM);

        IM_nuclei = zeros(l,m,numberOfPages);

        size(IM_nuclei)
        for k = 1 : numberOfPages
            % Read the kth image in this multipage tiff file.

            thisPage = imread(path_nuclei, k);
            IM_nuclei(:,:,k) = thisPage;
        end

        mini = min(IM_nuclei(:));
        maxi = max(IM_nuclei(:));
        if isa(tmpIM, 'single')
            IM_nuclei = uint8(2^16*(IM_nuclei-mini/(maxi-mini)));
        elseif isa(tmpIM, 'uint8')
            IM_nuclei = uint8(IM_nuclei);
        elseif isa(tmpIM, 'uint8')
            IM_nuclei = uint8(IM_nuclei);
        end
        else

            success=0;

    %import ki67

    if ~isempty(directory)

        nb_stacks=length(directory);
        tmpIM = imread([directory(1).folder '\', directory(1).name]);
        tmpIM = tmpIM(:,:,1);

        [l m] = size(tmpIM);

        IM_ki67 = zeros(l,m,nb_stacks);

        size(IM_ki67)
```

```

for i = 1:nb_stacks
    tmpIM =imread([directory(i).folder
'\ '
directory(i).name]);
    tmpIM = tmpIM(:,:,1);
    IM_ki67(:,:,i) = tmpIM;
end

mini = min(IM_ki67(:));
maxi = max(IM_ki67(:));
if isa(tmpIM,'single')
    IM_ki67 = uint8(2^16*(IM-mini/(maxi-
mini)));
elseif isa(tmpIM,'uint8')
    IM_ki67 = uint8(IM_ki67);
elseif isa(tmpIM,'uint8')
    IM_ki67 = uint8(IM_ki67);
end
else
    success_ki67=0;
end
if success==1&success_ki67==1
    if
        (size(IM_actin)==size(IM_nuclei)&size(
IM_ki67)==size(IM_nuclei))
            success=1
        else
            success=0
        end
    elseif success==1&success_ki67==0
        if
            (size(IM_actin)==size(IM_nuclei))
                success=1
            else
                success=0
            end
        end
    end

if success==1
% % Selecting the whole tissue

tissue=(IM_actin >
IM_nuclei)&(IM_actin >255-IM_actin-
IM_nuclei);
tissue=imerode(tissue,strel('sphere',1
));
L_tissue = bwlabeln(tissue);
R_0_tissue = regionprops3(L_tissue);
max_volume_tissue =
max(R_0_tissue.Volume(:));
idx_filter_small_tissue =
find(R_0_tissue.Volume >
0.1*max_volume_tissue);
Mask0_tissue =
ismember(L_tissue,idx_filter_small_tis
sue);
Mask0_visu_tissue =
uint8(Mask0_tissue)*255;

vqclose_tissue =
imclose(Mask0_tissue,strel('sphere',5
));
vqclose_tissue_visu=uint8(vqclose_tiss
ue)*255;
tissue=imfill(vqclose_tissue,'holes');

for i=1:size(tissue,3)
    tissue(:,:,i)=imfill(tissue(:,:,i),'ho
les');
end

periphery=zeros(size(tissue));

if size(tissue,2)>size(tissue,1)
for i=1:size(tissue,2)

L_periphery=bwlabeln(tissue(:,i,:));

R_0_periphery=regionprops(L_periphery
);
    [~,idx_filter_small_periphery]=
max(vertcat(R_0_periphery.Area));

Mask0_periphery=squeeze(ismember(L_per
iphery,idx_filter_small_periphery));

R_periphery=regionprops(Mask0_peripher
y,'Centroid','MajorAxisLength','Orient
ation');
    if
        ~isempty(vertcat(R_periphery.Centroid
))

periphery(:,i,:)=imclose(Mask0_periphe
ry,strel('line',R_periphery.MajorAxisL
ength*0.55,R_periphery.Orientation));

        end
    end
else
for i=1:size(tissue,1)

L_periphery=bwlabeln(tissue(i,:,:));

R_0_periphery=regionprops(L_periphery
);
    [~,idx_filter_small_periphery]=
max(vertcat(R_0_periphery.Area));

Mask0_periphery=squeeze(ismember(L_per
iphery,idx_filter_small_periphery));

R_periphery=regionprops(Mask0_peripher
y,'Centroid','MajorAxisLength','Orient
ation');
    if
        ~isempty(vertcat(R_periphery.Centroid
))

periphery(i,:,:)=imclose(Mask0_periphe
ry,strel('line',R_periphery.MajorAxisL
ength*0.55,R_periphery.Orientation));

        end
    end
for i=1:size(tissue,3)

R_periphery=regionprops(uint8(periphe
ry(:,:,i)),'Centroid','MinorAxisLength'
,'Orientation');

```

```

    if
~isempty(vertcat(R_periphery.Centroid)
)

periphery(:, :, i)=imclose(periphery(:, :
,i),strel('line',R_periphery.MinorAxis
Length*0.55,R_periphery.Orientation+90
));
    end
end

% Measuring the depth into the tissue
(distance inside the tissue from the
% outside
periphery=bwdist(~periphery);

%Filtering elements in the nuclei
stack that are outside of the tissue
or
%falling in the actin stack

IM_cut=IM_nuclei.*uint8(tissue);

IM_thresh = (IM_cut >
IM_actin)&(IM_cut >255-IM_actin-
IM_nuclei);

% %Filtering of small elements (noise,
artefacts, pieces of structures...)
L = bwlabeln(IM_thresh);
R_0 = regionprops3(L);
max_volume = max(R_0.Volume(:));
idx_filter_small = find(R_0.Volume >
50 );

Mask0 = ismember(L,idx_filter_small);
Mask0_visu = uint8(Mask0)*255;

%Morphological opening of the nuclei
elements to preseparate nuclei
%agglomerates and filter out small
elements attached to bigger structures

vq_open =
imopen(Mask0,strel('sphere',1));

D = bwdist(~vq_open);
D = -D;
D(~vq_open) = Inf;

hminparam = 1.5;%parameter made
smaller in case of undersegmentation
and inversely, to eventually adapt to
different type of cells
Htf = imhmin(D,hminparam);

W = watershed(Htf);
W(~vq_open)=0;
Wvisu = W;
Wvisu(Wvisu>120)=0;
%
R =
regionprops3(W, 'Volume', 'VoxelList', 'C
entroid');

%
%
```

```

% %Filtering of pieces of nuclei
mean_volume = mean(R.Volume(:));
median_volume = median(R.Volume(:));
W_corr = W;
idx_filter = find((R.Volume
>(0.125*mean_volume)));
Mask = ismember(W_corr,idx_filter);
W_corr = uint8(W_corr).*uint8(Mask);
R2 =
regionprops3(bwlabeln(W_corr), 'Volume'
, 'VoxelList', 'Centroid', 'PrincipalAxis
Length');
nuclei=R2;

tmpvisu = W_corr.*uint8((W_corr<125));
if success_ki67
IM_ki67=IM_ki67>(max(IM_ki67,[], 'all')
*0.75);
IM_ki67=uint8(IM_ki67).*uint8(W_corr>0
);
for z=(1:size(IM_ki67,3))

IM_ki67(:, :, z)=imgaussfilt(IM_ki67(:, :
,z),2);
end

%ki67 image treatment
L_ki67 = bwlabeln(IM_ki67);
R_0_ki67 = regionprops3(L_ki67);
max_volume_ki67 =
max(R_0_ki67.Volume(:));
idx_filter_small =
find(R_0_ki67.Volume >
0.1*(mean(nuclei.Volume)) );

Mask0_ki67 =
ismember(L_ki67,idx_filter_small);
Mask0_visu_ki67 =
uint8(Mask0_ki67)*255;

vqclose_ki67 =
imclose(Mask0_ki67,strel('sphere',4));
W_corr_ki67=vqclose_ki67.*Mask;

for i = 1:size(W_corr_ki67,3)
    W_corr_ki67(:, :, i) =
imfill(W_corr_ki67(:, :, i), 'holes');
end
W_corr_ki67=bwlabeln(W_corr_ki67);
R_ki67 =
regionprops3(W_corr_ki67, 'Volume', 'Vox
elList', 'Centroid');

idx_filter_ki67 = find(R_ki67.Volume >
0.25*(mean(nuclei.Volume)+median(nucle
i.Volume)) );
Mask_ki67 =
ismember(bwlabeln(W_corr_ki67),idx_fil
ter_ki67);
W_corr_ki67 =
uint8(W_corr_ki67).*uint8(Mask_ki67);

R2_ki67 =
regionprops3(bwlabeln(W_corr_ki67), 'Vo
lume', 'VoxelList', 'Centroid');
ki67=R2_ki67;
else
```

```

ki67=[];
end

[~,distance]=nearest_nuclei(nuclei.Cen
troid);

% Determining a ballpark approximation
of the mean cell height in the
% tissue
cell_height=max(mean(nuclei.PrincipalA
xisLength)+std(nuclei.PrincipalAxisLen
gth));

% Selecting the nuclei on the outside
layer of the tissue based on the
% estimation of the cell height

Mask_periphery=(periphery<cell_height*
1.75);
W_periphery=W_corr.*uint8(Mask_periphe
ry);
W_periphery=bwlabeln(W_periphery);
nuclei_periphery=regionprops3(W_periph
ery,'Volume','Centroid','VoxelList');
idx_filter_p1 =
find(ismember(nuclei_periphery.Centroi
d,nuclei.Centroid,'rows'));
Mask_periphery=
ismember(W_periphery,idx_filter_p1);
W_periphery=W_corr.*uint8(Mask_periphe
ry);
W_periphery=bwlabeln(W_periphery);
nuclei_periphery=regionprops3(W_periph
ery,'Volume','Centroid','VoxelList');

cd(path)

%% Sauvegarde des images segmentées

```

```

imwrite(W_corr(:,:,1),append(string(pa
th),'\nuclei_segmented.tif'));

imwrite(W_periphery(:,:,1),append(stri
ng(path),'\nuclei_periphery.tif'));
for i = 2:size(W_corr,3)

imwrite(W_corr(:,:,i),append(string(pa
th),
'\nuclei_segmented.tif'),'WriteMode','
append');

imwrite(W_periphery(:,:,i),append(stri
ng(path),
'\nuclei_periphery.tif'),'WriteMode','
append');
end
% cd(path)
if success_ki67
save(append(string(path),
'\Data.mat'),'IM_nuclei','IM_ki67','hm
inparam','W','W_corr','W_corr_ki67','W
_periphery','R','R_ki67','R2_ki67','nu
clei','nuclei_periphery','periphery','
tissue','Mask0_tissue');
else
save(append(string(path),
'\Data.mat'),'IM_nuclei','hminparam','
W','W_corr','R','tissue','Mask0_tissue
','nuclei','nuclei_periphery','periphe
ry','W_periphery');
end
else
ki67=[];
nuclei=[];
tissue=[];
nuclei_periphery=[];
end
end

```

Matlab script to compute the internuclei distance

```

function
[distances,result]=nearest_nucleiv3(co
ordinates)

coordinates=rmmissing(coordinates);
distances=pdist(coordinates);
distances=squareform(distances);
distances=sort(distances);
distances=distances(2:7,:);

```

```

CI = icdf('Normal',[0.25
0.75],mean(distances,'all'),std2(dista
nces));
filt1=CI(1);
filt2=CI(2);

result=distances;
result(~(distances>filt1&distances<fil
t2))=NaN;
result=nanmean(result);

```

Matlab script to segment GFP and mScarlet fluorescent cells

```

function [GFP,mSC,success]=mSCvsGFP(path)
    success=1;

    %% READ 3D IMAGE
    %import GFP

    [~,name] = fileparts(path);
    directory = dir([char(path),
    '\', '*.tif*']);

    if ~isempty(directory)
    nb_stacks=length(directory);
    tmpIM = imread([directory(1).folder
    '\' directory(1).name]);
    tmpIM = tmpIM(:,:,1);

    [l m] = size(tmpIM);

    IM_GFP = zeros(l,m,nb_stacks);

    for i = 1:nb_stacks
        tmpIM =imread([directory(i).folder
        '\' directory(i).name],2);
        tmpIM = tmpIM(:,:,1);
        IM_GFP(:,:,i) = tmpIM;
    end

    mini = min(IM_GFP(:));
    maxi = max(IM_GFP(:));
    if isa(tmpIM,'single')
    IM_GFP = uint8(2^16*(IM_GFP-
    mini/(maxi-mini)));
    elseif isa(tmpIM,'uint8')
    IM_GFP = uint8(IM_GFP);
    elseif isa(tmpIM,'uint8')
    IM_GFP = uint8(IM_GFP);
    end
    tmpIM_GFP=IM_GFP;
    else
        success=0;
    end
    %import mScarlett

    directory = dir([char(path),
    '\', '*.tif*']);

    if ~isempty(directory)

    nb_stacks=length(directory);
    tmpIM = imread([directory(1).folder
    '\' directory(1).name]);
    tmpIM = tmpIM(:,:,1);

    [l m] = size(tmpIM);

    IM_mSC = zeros(l,m,nb_stacks);

    for i = 1:nb_stacks
        tmpIM =imread([directory(i).folder
        '\' directory(i).name],1);
        tmpIM = tmpIM(:,:,1);

        IM_mSC(:,:,i) = tmpIM;
    end

    mini = min(IM_mSC(:));
    maxi = max(IM_mSC(:));
    if isa(tmpIM,'single')
    IM_mSC = uint8(2^16*(IM_mSC-
    mini/(maxi-mini)));
    elseif isa(tmpIM,'uint8')
    IM_mSC = uint8(IM_mSC);
    elseif isa(tmpIM,'uint8')
    IM_mSC = uint8(IM_mSC);
    end
    tmpIM_mSC=IM_mSC;
    else
        success=0;
    end

    %import background

    directory = dir([char(path),
    '\', '*.tif*']);

    if ~isempty(directory)

    nb_stacks=length(directory);
    tmpIM = imread([directory(1).folder
    '\' directory(1).name],3);
    tmpIM = tmpIM(:,:,1);

    [l m] = size(tmpIM);

    IM_background = zeros(l,m,nb_stacks);
    size(IM_background)

    for i = 1:nb_stacks
        tmpIM =imread([directory(i).folder
        '\' directory(i).name],3);
        tmpIM = tmpIM(:,:,1);
        IM_background(:,:,i) = tmpIM;
    end

    mini = min(IM_background(:));
    maxi = max(IM_background(:));
    if isa(tmpIM,'single')
    IM_background =
    uint8(2^16*(IM_background-mini/(maxi-
    mini)));
    elseif isa(tmpIM,'uint8')
    IM_background = uint8(IM_background);
    elseif isa(tmpIM,'uint8')
    IM_background = uint8(IM_background);
    end
    tmpIM_background=IM_background;
    else
        success=0;
    end

```

```

end

if success==1
    %proba de du GFP supérieure aux
    autres
    IM_GFP=IM_GFP.*uint8(IM_GFP>127);
    IM_GFP =
    imclose(IM_GFP,strel('sphere',1));

    L_GFP = bwlabeln(IM_GFP);
    R_0_GFP = regionprops3(L_GFP);
    mean_volume_GFP =
    mean(R_0_GFP.Volume(:));

    idx_filter_small = find(R_0_GFP.Volume
    > 0.005*mean_volume_GFP );

    Mask0_GFP =
    ismember(L_GFP,idx_filter_small);
    Mask0_GFP_visu = uint8(Mask0_GFP)*255;

    for i = 1:size(IM_GFP,3)
        GFP(:,:,i) =
        imfill(Mask0_GFP(:,:,i),'holes');
    end

    %proba de mSC supérieure aux autres
    IM_mSC=IM_mSC.*uint8(IM_mSC>127);
    IM_mSC =
    imclose(IM_mSC,strel('sphere',1));
    L_mSC = bwlabeln(IM_mSC);
    R_0_mSC = regionprops3(L_mSC);
    mean_volume_mSC =
    mean(R_0_mSC.Volume(:));

    idx_filter_small = find(R_0_mSC.Volume
    > 0.005*mean_volume_mSC );

    Mask0_mSC =
    ismember(L_mSC,idx_filter_small);

```

```

Mask0_mSC_visu = uint8(Mask0_mSC)*255;

for i = 1:size(IM_mSC,3)
    mSC(:,:,i) =
    imfill(Mask0_mSC(:,:,i),'holes');
end

GFP=GFP&~IM_mSC;
mSC=mSC&~IM_GFP;

L_GFP=bwlabeln(GFP);
L_mSC=bwlabeln(mSC);
R_GFP=regionprops3(GFP);
R_mSC=regionprops3(mSC);

if success
    save(append(string(path),
    '\Data.mat'),'R_GFP','R_mSC','GFP','mS
    C');
    mkdir(append(string(path), '\mSC'));
    mkdir(append(string(path), '\GFP'));
    for i = 1:size(mSC,3)

        imwrite(uint8(mSC(:,:,i)).*255,append(
        string(path), '\mSC\',
        num2str(i,'%04.f'), '.tif'));

        imwrite(uint8(GFP(:,:,i)).*255,append(
        string(path), '\GFP\',
        num2str(i,'%04.f'), '.tif'));
    end
end
else
    GFP=[];
    mSC=[];
end
end

```

Matlab script to segment basal and apical sides of the tubules

```

function
[apical,basal]=basalVSapical(tissue,thresho
ld)

tissue_filt=bwareaopen(tissue,threshold);
tissue_filt=double(tissue_filt);
[TH,R,Z]=cart2pol_centered(tissue_filt);
TH=round(TH,0);
apical=zeros(size(Z));
basal=zeros(size(Z));

for t=-180:1:179
    z=Z.*(TH==t);
    r=R.*z;
    r(r==0)=NaN;

    [~,r_apical]=min(r,[],'all','linear','omitn
an');

    [~,r_basal]=max(r,[],'all','linear','omitna
n');
    basal(r_basal)=1;
    apical(r_apical)=1;
end

```

```

function
[TH,R,Z]=cart2pol_centered(tissue)
[rr,cc]=meshgrid(1:size(tissue,2),1:si
ze(tissue,1));
tissueprop=regionprops(tissue);
if ~isempty(tissueprop)
    [TH,R,Z]=cart2pol(rr(:)-
tissueprop.Centroid(1),cc(:)-
tissueprop.Centroid(2),tissue(:));
else

[TH,R,Z]=cart2pol(rr(:),cc(:),tissue(:
));
end
TH=reshape(TH,size(rr));
R=reshape(R,size(rr));
Z=reshape(Z,size(rr));
TH=rad2deg(TH);
end

```

Résumé en Français

Les reins constituent une formidable machinerie dont le rôle est le maintien de l'homéostasie du plasma sanguin à travers des processus d'ultrafiltration et de réabsorption. Ils équilibrent la concentration ionique, le pH, éliminent les petites molécules potentiellement nocives par excrétion. Ces processus résultent de flux, pressions, réabsorptions et sécrétions étroitement régulés dans des unités tubulaires, appelées néphrons de géométries strictement contrôlées (Figures 1.1-1.5).

La polykystose rénale autosomale dominante (PKRAD), affectant environ 1 personne sur 1000, altère profondément la géométrie de ces unités tubulaires à travers des distensions en forme de ballon appelées kystes. Ces kystes entraînent une cascade de processus qui perturbent la géométrie et le flux dans les unités tubulaires, rendant éventuellement l'organe inefficace, nécessitant une dialyse ou une transplantation (Figure 1.8).

Bien que les gènes responsables de la PKRAD aient été identifiés il y a près de 30 ans, la pathogenèse reste floue. La maladie se développe lentement au stade initial, s'en suit une apparition rapide des kystes à un stade avancé. L'hypothèse la plus couramment acceptée pour sa pathogénèse suggère un mécanisme en trois étapes. A l'origine une mutation germinale hétérozygote sur le gène *PKD1* ou *PKD2* constitue la première étape. Dans un deuxième temps des mutations somatiques survenant aléatoirement entraînent une perte totale de l'expression de *PKD1/2* dans certaines cellules qui à leur tour peuvent former des premiers kystes. Enfin ces premiers kystes perturbent le microenvironnement rénal, favorisant la formation d'autres kystes dans leur proche voisinage, entraînant un effet « boule de neige ». (Figure 1.13) Ces perturbations peuvent être d'origine biomécanique : en se développant les kystes obstruent partiellement les néphrons environnant, et perturbent flux et pressions intraluminales. L'absence des gènes *PKD1/2* entrainerait alors une réponse aberrante pro-kystes de la part de cellules dormantes. En effet, *PKD1* et *PKD2* codent pour les protéines, polycystines 1 et 2 dont le rôle n'est pas encore clair mais que l'on pense être des mécanosenseurs liés justement au flux et à la pression (Figures 1.9-1.10).

Dans notre laboratoire, nous utilisons une approche innovante avec un rein sur puce pour étudier ces processus. Ces dispositifs microphysiologiques imitent in vitro l'environnement des unités tubulaires rénales, offrant une modularité et un contrôle similaires aux cultures cellulaires classiques, mais intégrant des éléments essentiels pour la fonction tubulaire. Le travail de ma thèse vise à développer une nouvelle puce rénale reproduisant fidèlement les géométries tubulaires dans une matrice biomimétique en collagène I tout en intégrant les contraintes hydrodynamiques physiologiques et pathologiques liées à la fonction rénale et à la présence de kystes en cultivant in vitro dans ces systèmes des cellules rénales modèle de la PKRAD.

La modélisation de maladie rénales de manière générale et plus précisément de polykystoses rénales a été peu explorée. Pour cette raison, les modèles préexistants dans la littérature se montrent particulièrement perfectibles au regard des problématiques géométriques et hydrodynamiques liées à la PKRAD (Figure 2.1-2.5). Nous avons donc dû concevoir nos propres modèles de puces microfluidiques pour répondre à nos questions : Quels phénomènes sont à l'origine de la formation des kystes ? Quels phénomènes alimentent l'effet boule de neige ? Quelle est l'importance des contraintes hydrodynamiques pour l'homéostasie des néphrons et comment la perte du gène *PKD1* altère la réponse des tissus à ces contraintes ?

Le premier objectif de cette thèse était de développer ce nouveau rein-sur-puce. Nous sommes partis d'une puce développée précédemment dans l'équipe qui permettait d'obtenir des tubules rénaux parallèles entre eux d'un diamètre de 80µm espacés de 100µm ou 200µm moulés dans du collagène I à l'aide de fil de tungstène eux-mêmes positionnés précisément grâce à la puce microfluidique (Figure 2.5). Cette puce ne permettant une perfusion stable et suffisamment contrôlée des tubules (Figure 2.7), nous sommes passés par plusieurs itérations de puces en PDMS (Figure 2.8-2.11). Nous nous sommes finalement arrêté sur une puce dont la géométrie reste aussi proche du néphron tout en permettant d'induire de manière découplé une pression et un flux intraluminal dans les tubules. Ceci nous permet par la suite d'étudier séparément l'influence de ces deux contraintes qui sont souvent indissociées. Nous avons opté pour un mode de perfusion utilisant la pression hydrostatique générée par la gravité, nous offrant un système versatile et à bas coût permettant la mise en parallèle d'un grand nombre d'expériences (Figure 2.12-2.14). De plus nous avons optimisé la procédure d'ensemencement de cellules dans la puce nous permettant d'obtenir un tube de cellules épithéliales confluent et en monocouche le jour suivant l'ensemencement (Figure 2.10).

Dans un premier temps nous avons étudié avec ce système l'importance du gène *Pkd1* pour le maintien de la géométrie tubulaire. La courbure du substrat influe grandement la prolifération, la migration, la différenciation et la morphologie des cellules épithéliales. Une régulation de ces phénomènes est cruciale pour le bon maintien d'une structure tubulaire fermée. Dans le contexte de la PKRAD, ces processus de régulation pourraient être impactés même si il reste de nombreuses zones d'ombre concernant la cascade de phénomènes menant à la formation d'un kyste. Notre étude utilise des structures tubulaires préformées et permettent un suivi en direct de l'évolution de la géométrie de ces structures. Ceci nous a permis dans un premier temps dans des conditions statiques d'examiner la manière dont la perte de *Pkd1* affecte la manière dont les cellules parviennent à maintenir où nous la structure tubulaire initiale, permettant de jeter une lumière nouvelles sur de possibles phénomènes à l'origine de la formation des kystes dans la PKRAD. Dans une étude précédente avec des cellules dérivées du tube proximal convolué de souris, les PCT, *Pkd1*^{-/-} et *Pkd1*^{+/-}, nous avons montré qu'une surprolifération des cellules dû à la perte de *Pkd1* entraînait une dilatation moyenne des canaux en quelques jours de plus de 50%.

Durant mes travaux de thèse, nous avons également travaillé avec une lignée cellulaire issue du canal collecteur de souris, les mIMCD-3 (abrégé ici IMCD) WT et *Pkd1*KO. De manière similaire aux PCT, une perte du gène *Pkd1* entraîne une dilatation de l'ordre de 50% des canaux. Cependant, ces dilations ne peuvent être attribuées à une prolifération accrue (Figure 3.1-3.2). En effet, les cellules *Pkd1*KO sont autant voir moins prolifératives que les cellules WT dans les tubules en condition statique. En revanche, en mesurant la distance internucléaire de ces tissus plusieurs jours après confluence, nous montrons que les cellules *Pkd1*KO sont plus étalées et moins cuboïdales que les cellules WT. Là où une prolifération des cellules WT se traduit par une augmentation de la densité du tissu, la prolifération de cellules *Pkd1*KO entraîne par effet stérique, une dilatation tubulaire (Figure 3.3-3.5). Cette dilatation est contrariée par une matrice extracellulaire plus dense. Le passage d'une matrice de 6mg/mL de collagène à une matrice de 9 mg/mL entraîne une augmentation du même ordre du module d'Young du collagène mais empêche toute dilatation significative des tubules *Pkd1*KO, montrant que ce mode de dilatation est très sensible aux propriétés mécaniques de la matrice extracellulaire.

Néanmoins nous avons constaté que l'absence de flux entraîne à moyen terme sur les cellules IMCD WT la formation de multicouches, un comportement non physiologique. Ainsi l'adjonction de flux paraît primordiale pour le modèle. Dans un second temps nous avons donc cultivé les IMCD dans nos puces avec un flux intraluminal de l'ordre de 1 dyn/cm² mais avec

une pression intraluminale négligeable. Le cisaillement du au flux préserve le lumen des tubules WT mais également la géométrie tubulaire des tubules *Pkd1KO*. En effet, nous n'observons plus de différence significative de dilatation tubulaire entre cellules WT et *Pkd1KO* dans cette configuration (Figure 4.1). Ceci se voit aussi au niveau de la morphologie des cellules qui semblent plus difficiles à distinguer entre WT et *Pkd1KO*, ce qui est confirmé au niveau quantitatif par un tissu aussi dense voire plus dense pour les *Pkd1KO* dans la configuration flux sans pression.

L'ajout d'une pression intraluminale d'ordre physiologique, de 10 mbar, à ce flux entraîne chez les cellules IMCD WT et *Pkd1KO* une importante dilation tubulaire. Néanmoins, là où le niveau de dilation pour les cellules WT a tendance à stagner, pour les cellules *Pkd1KO* la dilation devient significativement plus importante au fil du temps pour atteindre l'ordre de 200% dans les cas les plus extrêmes. Là encore, les cellules *Pkd1KO* ne se montrent pas plus prolifératives que les cellules WT et l'origine de cette dilatation plus importantes ce trouverait également au niveau d'une différence de morphologie cellulaire. La pression intraluminale rétablit en quelque sorte la différence d'étalement des cellules et de densité cellulaire que l'on voyait dans les conditions statiques. (Figure 4.2) Ces résultats suggèrent que des effets protecteur du flux sur les cellules seraient contrebalancés par des effets délétères de la pression intraluminale. Ici également, la dilatation est contrariée par une augmentation de la densité en collagène I de la matrice extracellulaire de 6 à 9mg/mL (Figure 4.4). Au vu de la faible augmentation de module d'Young que cela engendre, il ne nous paraît peu probable que cette observation soit due à une simple augmentation de rigidité de la matrice. De plus des résultats préliminaires indiquent que la réponse à court terme à la pression différerait significativement entre WT et *Pkd1KO* après 1 jour de culture sous flux et pression. En effet, le tubule se montrerait plus rigide pour les cellules WT que pour les cellules *Pkd1KO* (Figure 4.3). Ce phénomène, si confirmé, pourrait être attribué soit à une différence de rigidité des cellules elles-mêmes ou alors par une différence de modification de la matrice extracellulaire qu'elles engendreraient, possiblement au niveau d'une membrane basale. Ceci ferait écho à l'observation in vivo que les propriétés mécaniques des tubules rénaux sont majoritairement dictées par la membrane basale.

Nos résultats montrent que les contraintes de flux et de pression sont nécessaires pour maintenir un épithélium monocouche proche du cas physiologique et à approcher ce qu'il se passe dans la PKRAD. Cependant, ils suggèrent également qu'il serait grandement bénéfique de s'intéresser à la formation d'une matrice extracellulaire aux propriétés mécaniques plus proches de la membrane basale du rein pour résister à une pression intraluminale physiologique sans distension tubulaire. En effet, les propriétés de la matrice extracellulaire et la capacité des cellules à les moduler sont au cœur des distensions tubulaires induites par le stress mécanique dans la PKRAD. Ces résultats s'inscrivent également dans le débat sur le rôle de la prolifération dans la kystogenèse, suggérant qu'elle n'est pas nécessaire dans les premières étapes de la formation du kyste pour certains types cellulaires et que son rôle pourrait dépendre du segment du néphron.

Nous avons également menées des expériences similaires de culture sous flux uniquement et sous flux plus pression de tubules PCT *Pkd1^{+/-}* et PCT *Pkd1^{-/-}* (Figure 4.5). Celles-ci ont montré de nouveau que les PCT *Pkd1^{-/-}* suivaient un mode de dilatation différent des IMCD *Pkd1KO*, qui serait lui dominé par une augmentation de leur prolifération. Contrairement aux IMCD, sous flux les PCT *Pkd1^{-/-}* dilatent encore de manière importante les tubules dû à une surprolifération de celles-ci, ce qui est de nouveau constaté après l'ajout de pression.

Enfin, parallèlement à ces expériences de dilatations tubulaires, nous nous sommes intéressés à des cocultures de cellules parentales avec des cellules *Pkd1^{-/-}* pour mimer la situation suivant les mutations somatiques observées in vivo à l'origine des premiers kystes. Dans un premier temps, avec les PCT, nous avons montré sans flux que les PCT *Pkd1^{-/-}* ensemencées en faible minorité avec PCT parentales finissaient par remplacer totalement les parentales dans le tissu, entraînant des dilatations homogènes du tubules. Nous attribuons ici encore ce comportement à une surprolifération de ces cellules (Figure 5.3-5.5). L'adjonction d'un flux et d'une pression intraluminal ont tendance à protéger les cellules parentales et favoriser leur maintien dans le tissu à plus long terme (Figure 5.6).

En ce qui concerne les mélange de cellules IMCD, ils montrent un comportement quasi diamétralement opposé aux PCT. Ici les cellules *Pkd1KO* semblent extrudées par les cellules parentales du tissu même si initialement présentes en faible majorité (Figure 5.8). Cultiver ces tubes mosaïques sous flux stabilise encore une fois les types cellulaires en présence, en protégeant cette fois-ci les cellules *Pkd1KO* (Figure 5.9-5.10). Dans l'ensemble un ensemencement mosaïque de cellules *Pkd1KO* avec des cellules exprimant le gène *Pkd1* n'aboutit pas à des dilatations localisées faisant penser à des kystes dans les conditions testées et avec nos modèles cellulaires. Nous pensons que ceci est dû à l'absence de persistance suffisamment longue de cluster de cellules *Pkd1^{-/-}* avec une taille idéale. Les contraintes hydrodynamiques de flux et de pression qui apparaissent stabiliser les différents types cellulaires en présence pourraient être une première étape vers un modèle de kyste sur puce.

En conclusion, nous sommes convaincus que les microenvironnements 3D conçus comme les reins-sur-puces sont d'une importance capitale pour décrypter les mécanismes de la maladie rénale polykystique. Ils offrent une large gamme de paramètres contrôlables qui semblent au cœur de la kystogenèse : propriétés de la matrice extracellulaire, géométrie et fluïdique. Grâce à notre capacité à moduler facilement ces paramètres avec notre rein-sur-puce, nous avons pu les étudier spécifiquement in vitro, ce qui semble être une tâche beaucoup plus complexe in vivo et impossible avec la plupart des modèles in vitro actuellement décrits

RÉSUMÉ

La PKRAD est une néphropathie héréditaire qui atteint une personne sur 1000, dans laquelle le développement de nombreux kystes rénaux entraîne une insuffisance rénale à l'âge adulte. 80% des PKRAD sont dues à une mutation hétérozygote sur le gène *PKD1*, codant pour une protéine du cil primaire qui serait impliquée dans la détection de flux et de pression luminale dans les néphrons. Elle participerait ainsi au maintien de la géométrie fonctionnelle des néphrons. Des mutations somatiques localisées entraînent la disparition de la protéine fonctionnelle dans quelques cellules et rompent localement cet équilibre. Des mécanismes mal identifiés, possiblement liés à des obstructions de canaux encore sains par des kystes voisins, participent ensuite à la propagation des kystes dans le rein et entraînent une progression exponentielle de la maladie après une longue phase de dormance. Pour mieux comprendre la dynamique de la kystogénèse, nous avons développé un rein-sur-puce reproduisant avec des tubes dans du collagène la géométrie de sections de néphrons empoussés. Ces tubes sont de plus perfusables, permettant de mimer les contraintes luminales d'ordre hydrodynamique des néphrons, nous offrant ainsi un des modèles *in vitro* les plus fidèles du rein. Après avoirensemencé ce dispositif de lignées cellulaires modèle de la PKRAD issues du tube proximal et du canal collecteur, cette puce permet d'étudier des phénomènes de dilatations et de compétition ayant lieu lors de la formation des kystes. C'est ainsi que nous avons observé une dilatation significative du tube avec des cellules dépourvues de *Pkd1* comparativement à celles qui expriment encore ce gène. Par ailleurs, mises en compétition dans les tubes, les premières tendent à prendre le dessus sur les secondes, comme cela a pu être décrit *in vivo*. Nous nous sommes par la suite intéressés à l'impact de flux et pressions physiologique intraluminales sur ces phénomènes de dilation et de compétition cellulaire. Ces expériences pourraient permettre d'éclaircir l'impact de telles contraintes mécaniques sur la formation des kystes.

MOTS CLÉS

Comportement collectif ; organe sur puce ; biomimétique ; microfluidique ; PKRAD ; mecanotransduction

ABSTRACT

ADPKD (Autosomal dominant polycystic kidney disease) is a hereditary nephropathy that affects one person out of every 1000, wherein the development of numerous kidney cysts leads to renal failure in adulthood. 80% of PKRAD cases are due to a heterozygous mutation in the *PKD1* gene, which encodes a protein in the primary cilium believed to be involved in the sensing of flow and light pressure within the nephrons. It is thought to contribute to the maintenance of the functional geometry of the nephrons. Somatic mutations localized in specific cells result in the loss of functional protein and disrupt this balance locally. Poorly understood mechanisms, possibly related to obstructions of still healthy channels by neighboring cysts, then contribute to the propagation of cysts in the kidney and lead to an exponential progression of the disease after a long dormant phase. In order to better understand the dynamics of cystogenesis, we have developed a kidney-on-a-chip that replicates the geometry of packed nephron sections using tubes embedded in collagen. These tubes are also perfusable, allowing us to mimic the luminal hydrodynamic stresses of the nephrons, thus providing one of the most faithful *in vitro* models of the kidney. After seeding this device with ADPKD model cell lines derived from the proximal tube and collecting duct, this chip allows us to study phenomena of dilation and competition that occur during cyst formation. It was thus observed that the tube significantly dilated with cells lacking *Pkd1* compared to those still expressing this gene. Furthermore, when in competition within the tubes, the former tend to outcompete the latter, as has been described *in vivo*. Subsequently, we investigated the impact of physiological intraluminal flows and pressures on these phenomena of cell dilation and competition. These experiments may provide insights into the role of mechanical constraints in cyst formation.

KEYWORDS

Collective behavior ; microfluidics ; biomimetics ; ADPKD ; organ-on-chip ; mechanotransduction